THE BAUSCHINGER EFFECT AND THE WORK HARDENING OF ALUMINUM COPPER ALLOYS

THE BAUSCHINGER EFFECT AND THE WORK HARDENING OF ALUMINUM COPPER ALLOYS

BY

GERARD DESMOND MOAN M.A.

A THESIS

SUBMITTED TO THE SCHOOL OF GRADUATE STUDIES

IN PARTIAL FULFILLMENT OF THE REQUIREMENTS

FOR THE DEGREE

DOCTOR OF PHILOSOPHY

McMASTER UNIVERSITY

FEBRUARY 1977

ACKNOWLEDGEMENTS

The author would like to record his indebtedness to Professor J.D. Embury for advice and guidance during the course of this work. Thanks are also expressed to the members of the Mechanical Metallurgy Research Group for frequent discussions and other help. Special mention is made of the assistance received from Professor C.M. Sargent and Dr. L.M. Brown.

The work carried out by M. van Oosten, T. Bryner and H. Neumayer is appreciated. The typing skill of Ms. Joanne Lemon is also acknowledged.

The research was supported by the National Research Council of Canada. Thanks are also due to Alcan International Ltd. for providing the alloys used in the study.

Many thanks are due to my wife for her patience. I would like to dedicate the work to my parents to acknowledge their help and encouragement.

DOCTOR OF PHILOSOPHY (1977) McMASTER UNIVERSITY
(Metallurgy and Materials Science) Hamilton, Ontario.

TITLE: The Bauschinger Effect and The Work Hardening of Aluminum Copper Alloys

AUTHOR: Gerard Desmond Moan, M.A. (University of Cambridge)

SUPERVISOR: Professor J.D. Embury

NUMBER OF PAGES: xv, 303.

ABSTRACT:

Several conflicting models have been proposed to describe the work hardening behaviour of alloys composed of a hard second phase in a plastically deforming matrix. Good agreement is reported when the models are compared with the results of unidirectional tests. To distinguish between the models, it is necessary to use tests which include deformation in both the forward and reverse directions.

In this study the work hardening behaviour in aluminum copper alloys has been studied using deformation in compression immediately after deformation in tension. The large Bauschinger Effect obtained has been analysed to give the magnitude of the long range back stress present in the alloy due to the elastic deformation of the θ' particles in the plastically deforming matrix. Experiments were carried out on polycrystals, and on single crystal test pieces oriented for single and multiple slip over a wide range of temperatures. The results give excellent agreement with a

model which calculates the long range back stress. The reported good agreement of other experimental work with an opposing model has been critically examined.

The behaviour at large strains has been studied to determine the processes leading to plastic relaxation. The conditions at the onset of necking of the single crystal test pieces have been examined, and the formation of coarse shear bands and final fracture correlated with the work hardening rate.

TABLE OF CONTENTS

LIST OF FIGURES

LIST OF TABLES

CHAPTER I

INTRODUCTION

In the study of the plastic deformation of two phase alloys containing hard non-deforming precipitate particles in a plastically deforming matrix, there are three areas of considerable theoretical interest and great industrial importance. These are:

a) the description of the initial yielding of the material,

b) the description of the work hardening rates during the initial plastic deformation, and

c) at greater plastic strains, the determination of the competing processes which result in either continued uniform plastic deformation or in the onset of strain localisation and/or fracture.

In the past three decades the first of these areas, the description of the initial yielding, has seen considerable progress towards the formulation of an adequate theory. There is now a reasonably complete description of the yielding process in terms of the size and distribution of the second phase particles and the angle through which the dislocations must be bent in order to pass them. The yield

stresses have been calculated for many different alloy systems and the results compare favourably with those obtained in careful experiments on well characterised single crystals.

The description of the work hardening at small strains and the competitive processes occurring at large strains demand a more detailed understanding of the behaviour of plastically inhomogeneous materials from both a macroscopic and mechanistic viewpoint. A variety of comprehensive theories have been advanced and these will be examined. It is important to consider

(a) the assumptions on which they are based, and

(b) their comparison with experimental observations

before attempting to judge the veracity or completeness of any given model.

One possible description is that the work hardening is due to the accumulation of dislocations close to the particles. This causes the matrix to become harder locally, and an increased stress must then be applied to continue the plastic deformation. These harder regions increase in size and also increase in dislocation density as the strain increases, so that the material is expected to work harden. An alternative description is that the hardening is due to large long range back stresses which result when the matrix deforms plastically and the particles deform elastically

only. These back stresses inhibit the continued forward deformation, and the increased applied stress necessary to overcome them is equated to the work hardening. The model is a continuum one, and makes no use of dislocations or slip line spacing, although equivalent models can be developed in terms of dislocations.

These two types of models as formulated lead to a problem. Since they are designed to give an adequate description of the forward work hardening it is not possible to distinguish between them on the basis of experiments using monotonic loading. Additional information from reverse loading experiments is needed.

In the examination of the models it is needed also to relate the macroscopic and mechanistic aspects so that a comprehensive description can be found to distinguish the important parameters which control the behaviour. For example, it is of value to be able to relate the behaviour of polycrystals and single crystals, to define the role of the volume fraction of the second phase, and to clearly elucidate when the behaviour is dependent upon the detailed geometry and distribution of slip or when it is determined by the competition between local events such as those which occur at the particle-matrix interface.

The present work is an attempt to study the work hardening of a well characterised two phase alloy system

containing hard particles, using both forward and reverse deformation and using both single crystals of different orientations and polycrystals, in order to define the ranges of applicability of the recent models proposed to describe the work hardening of these alloys.

In a description of work hardening processes it is important to indicate, both theoretically and experimentally, the limitations of a given process. It is of value to indicate the nature of the competition between continuing uniform plasticity and the localisation of the plastic strain in terms of the different components of the microstructure. Hence, in this work, experiments were also carried out at large strains to study the onset of the alternative processes in the vicinity of the second phase particles, and to determine their effect on the macroscopic behaviour of the two phase materials. In this part of the study, single crystals were again used, oriented for single and multiple slip.

In summary, the objectives of the study were to determine the local processes which operate in the vicinity of the particles at different levels of strain, and to show how these affect the overall plastic response of the material. At small strains their effect on the work hardening rate is of most interest, whilst at larger strains it is their effect on the instability leading to failure that is emphasised.

The work contains an attempt to construct a model to

describe the forward and reverse deformation of the alloy system. This is mainly a microscopic model based on the interaction of dislocations on a given slip plane with particles intersecting that plane. Electron metallographic and X-ray evidence is presented in support of the model, but there are always problems in extrapolating these local interactions from the scale of the slip plane model to the total volume of the test piece. The model is also described in terms of a macroscopic continuum model which can be stated in an empirical form of more general applicability to more complex multi phase systems.

CHAPTER II

LITERATURE REVIEW

Introduction

In the first part of this chapter, a short description of the Bauschinger Effect will be given. It will include a discussion of the important features of the reverse deformation of materials. The second part will be devoted to a review of the principal models proposed in the literature to describe the unidirectional work hardening processes in two phase alloys. The models will be examined critically to determine if they can account for the occurrence and magnitude of the Bauschinger Effect. In the third section, previous studies of the Bauschinger Effect and of the reverse deformation of alloys reported in the literature will be discussed.

2.1 The Bauschinger Effect

There has been extensive interest in recent years in the Bauschinger Effect. Some of this interest has arisen because theoretical and experimental studies have shown that some information about the work hardening processes in two

phase alloys can be obtained from an examination of the Bauschinger Effect. Other work of great industrial importance has been concerned with the characterisation and possible elimination of the effect, especially in those industrial materials which rely on a combination of second phase particles and work hardening to achieve the required strength levels.

The Bauschinger Effect, first reported in 1886, can be described by reference to the schematic diagram, figure 2.1. Consider a test piece subjected to deformation in a forward sense. As the imposed strain increases, the material undergoes elastic deformation until at A, at a stress σ_o, it yields and undergoes plastic deformation. With increasing strain, the stress-strain curve follows the curve ABC. If the test were repeated on another test piece to the point B, and unloaded to zero load at D then reloaded in the original direction, the new part of the curve will follow the line DBC. Usually the yielding at B is well defined but it sometimes becomes increasingly rounded, as for example DGC, if the test piece is allowed to rest for longer periods of time at higher temperatures. However, the stress-strain curve will usually follow the loading path BC.

If a third test is carried out to the point B again and unloaded to D and then immediately deformed in the reverse direction, a curve similar to BDE is obtained. This

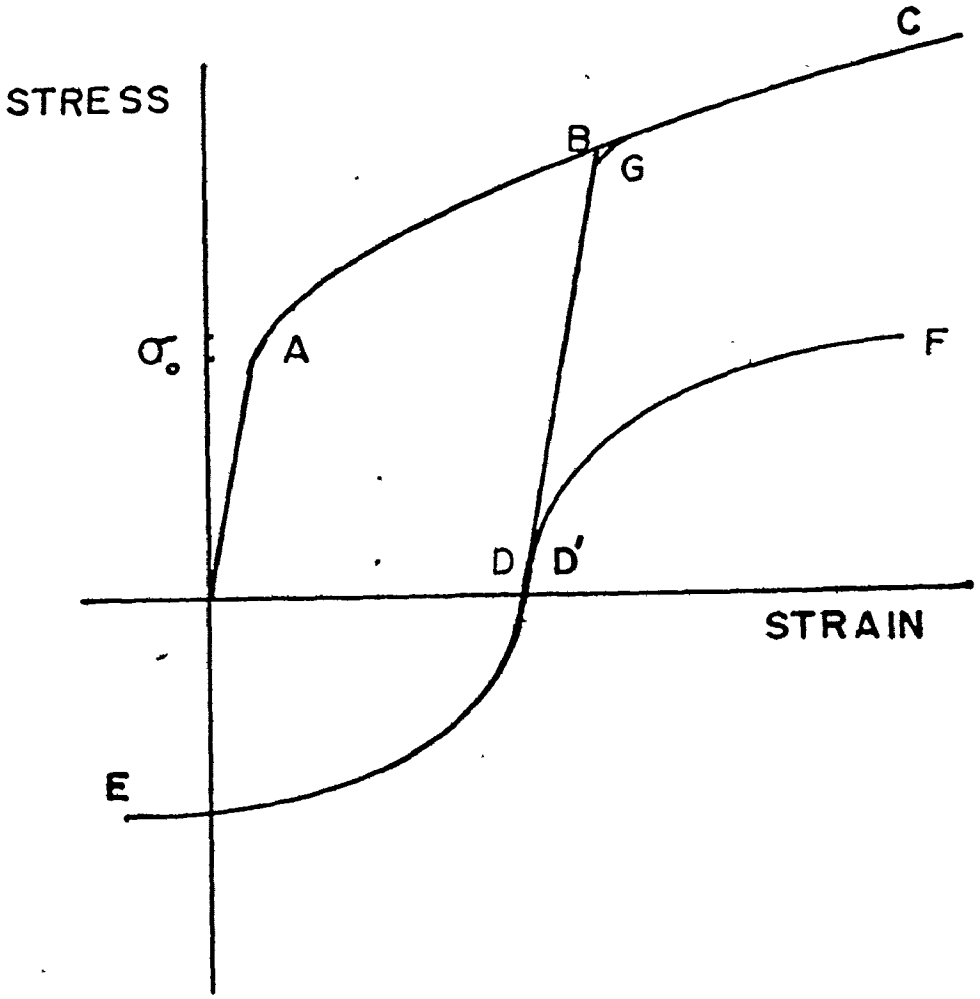

FIG 2.1 SCHEMATIC DIAGRAM OF BAUSCHINGER EFFECT

response in compression can be redrawn in the positive stress quadrant as the curve D'F. There are several differences to be pointed out between the curves DBC representing the continued forward deformation, and D'F representing the reverse deformation.

The continued yielding in the forward sense at B or G takes place at a stress approximately equal to that from which the test piece was unloaded. The subsequent work hardening curve follows BC, the original curve. In contrast, the reverse deformation does not have a well defined yield stress, the curve is very rounded, and plastic deformation in the reverse sense proceeds at stresses much smaller than those needed for the continued forward deformation; the curve D'F lies well below the curve BC initially. The exact shape of the curve D'F depends on the material tested; in some cases, for example Cu-SiO_2, it seems to have a linear portion which is parallel to and below BC, whilst in other cases the curve D'F joins BC after some reverse deformation.

The reverse deformation can also be considered in terms of the magnitude of the reverse strain. It can be seen that as the reverse flow stress approaches the magnitude of the original prestress at B, the reverse strain obtained is very large. This large plastic strain has to be compared with the zero plastic deformation that would have

been obtained if the test had been carried out in the forward direction from D.

These two different ways of considering the reverse deformation have led to two different methods of studying the Bauschinger Effect. In one of these methods, attention is focussed on the stress at which reverse yielding takes place; this occurs at a stress much smaller than that required for continued forward deformation. The definition of the Bauschinger Effect using the comparison of the yield stresses leads to the development of Bauschinger Effect Parameters defined in terms of stress. The other method, using strains, leads to a Bauschinger Effect Parameter defined in terms of strains. In general, materials with a large Bauschinger Effect Parameter (BEP) measured in terms of stresses will also have a large BEP if measured in terms of strain. However, in the comparison of some materials, different rankings are obtained depending on which BEP is used (Abel and Muir, 1972).

As indicated, the shape of the reverse stress-strain curve is complex. It is very rounded and the extent of its roundedness depends on the alloy being tested and on the conditions under which the test is conducted. In the forward deformation the yield stress could be determined readily; for the reverse strain it is more difficult to specify when the transition from elastic to plastic deformation

takes place. Sometimes it seems that this reverse plastic deformation commences whilst the material is still loaded in a forward sense. Also, the work hardening rate in the early stages of the reverse deformation is very high, much higher than that at the same cumulative forward strain.

In this work, the Bauschinger Effect has been studied in a material which contains hard particles in a soft matrix. The aim was to gain a better understanding of the processes involved in the high work hardening rates of these materials. Several models have been proposed in the literature to describe the unidirectional processes and these will be discussed in the next section. It is hoped that the results of this study will permit distinctions to be made between some of these models, and lead to consideration of how the competition between deformation processes at larger strains affects the stability of the deformation.

It is appropriate to review here the major models proposed to account for the work hardening in two phase alloys. It will be pointed out how some of these models can predict a large Bauschinger Effect and also how some of them are modified to describe materials containing a variety of shapes of second phase particles by considering the elastic and plastic compatability conditions of the particle and the matrix.

2.2 Work Hardening Models

In this section the principal theories developed to describe the work hardening of two phase alloys will be examined. These alloys are made up from a hard non deforming second phase in a plastically deforming matrix. It is necessary to consider the premises on which the models are based and to discuss their applicability to materials containing large particles. In particular, it is important to learn if the models can predict the large Bauschinger Effect observed in these alloys. It is also necessary to examine carefully those models which do not predict a Bauschinger Effect, but which are still in reasonable agreement with other experimental data, especially the unidirectional work hardening behaviour.

There are two principal approaches to work hardening; these are represented by the microstructural approach and by the continuum approach. In the microstructural models, the emphasis is on the calculation, using dislocation theory, of the local stresses inside the material, and on the determination of their contribution to the work hardening process. The microstructural models are of two extreme types

a) unrelaxed, in which the only dislocations have primary Burgers vectors and no mechanism is allowed to reduce the number of Orowan loops on each of the particles.

b) relaxed, in which one of several possible mechanisms is allowed to reduce the number of Orowan loops on the particles and to give rise to dislocations with secondary Burgers vectors.

In the continuum approach there are two ways to include the idea of work hardening:

a) isotropic hardening in which the yield surface is considered to expand isotropically in all directions during plastic deformation. This leads to the material having equal yield stresses in tension and compression after plastic deformation.

b) kinematic hardening in which the yield surface is considered to not change its shape, but to translate in stress space very much like a rigid body.

It is possible to consider models which include parts of these two ideas, so that the yield surface is enlarged and translated, and a further refinement permits the distortion of the surface. These models are very complicated for real materials, and although they can be made to be exact, they do require some additional input from experiment before the exactness is realised. Only one continuum model will be examined in this section, after the dislocation models.

A Dislocation Models

The hard second phase particles have an effect on the yield process in the alloys. This process has been examined by Orowan (1948); the work of Ashby (1966a) and the review of Brown and Ham (1971) give a good description of the yielding. When a dislocation moving on a slip plane encounters the hard particles, it is hindered, and unless the applied stress is sufficiently large the dislocation is arrested. Under the action of the applied stress, it will bow between the particles; if the stress is increased the extent of the bowing will increase. Depending on the size of the obstacle and the interaction between it and the dislocation there will be a critical stress at which the obstacle breaks and dislocation advances to the next part of the obstacle array. If the obstacle is very strong so that it does not break even when the dislocation has almost completely bowed around it, the dislocation will reach an unstable semicircular configuration. It will then act as a Frank-Read source, leaving an Orowan loop on each particle bypassed. The critical shear stress τ can be written as

$$\tau \approx \frac{\mu b}{L}$$

where μ is the matrix shear modulus, b the Burgers vector and L the interparticle spacing.

As the plastic deformation increases, the number of Orowan loops on the particles increases, and their interaction energy will be great. If all the loops are maintained there will be a large hardening effect; if some process occurs near the particles to reduce the number of the loops, the stored energy will be smaller. The energy or the number of Orowan loops can be reduced by several possible mechanisms, including the conversion of the shear loops to prismatic loops, the fracture of the particles, the cutting of the particles, the decohesion of the particle matrix interface, and the cross slip or climb of the dislocations. When such a process takes place to reduce the number of Orowan loops, the model is said to be relaxed, to distinguish it from the unrelaxed ones in which all the Orowan loops are maintained.

The dislocation models will be examined in sequence. The model proposed by Fisher, Hart and Pry (1953) attempted to calculate the hardening caused by particles present in a volume fraction f. This hardening was to be in addition to the hardening which the pure matrix would have undergone at the same total strain. They considered a single crystal, oriented for single slip, containing spherical particles, and calculated the interaction between mobile dislocations and a coplanar set of Orowan loops surrounding each particle. It was argued that this interaction, being repulsive, would

stop the operation of the Frank-Read sources on the same slip plane and that an additional stress $\Delta\tau_h$ would have to be applied for further plastic deformation. This stress was calculated as

$$\Delta\tau_h = 3\ f^{3/2}\ \frac{N\mu b}{r}$$

where the particles of radius r are surrounded by N Orowan loops.

There was a maximum value for $\Delta\tau_h$; this was controlled by those processes which could compete with dislocation loop accumulation at the particles. The maximum would be reached when the local stresses from the dislocation pile-up close to the particles exceeded the yield strength of the particles, or of the matrix, or of the particle matrix interface. Then the number of loops was expected to remain constant and the maximum hardening increment given by

$$\Delta\tau_{max} = 3\ f^{3/2}\ \tau_c$$

where τ_c is the critical local stress.

The model has no further increment in hardening beyond the strain necessary to reach the critical stress τ_c at the particles. The value of this strain is small, of the order of 0.01, so that the model has only a limited usefulness, and provides little information at larger strains.

At these large strains one of the other models must be used. There is no provision in the model for the effect of particle shape and size on the hardening increment, and the volume fraction dependence is at variance with that obtained from later experimental work.

The authors did not consider if there would be a Bauschinger Effect, but it can be argued that the repulsive interactions, leading to long range stresses, between the Orowan loops and mobile dislocations would cause a Bauschinger Effect at small strains. At larger strains it is not possible to make any prediction because the nature of the process responsible for the saturation of the hardening increment was not known.

Ashby examined the work hardening process in a series of papers (1966a, 1966b, 1969, 1970, 1971). He accepted the Fisher, Hart and Pry (1953) idea that the early part of the work hardening is due to long range back stresses resulting from Orowan loop accumulation at the particles. He calculated the number N of such loops as a function of shear strain γ for particles whose diameter was d,

$$N = \gamma \, d/b$$

making the assumption that the back stress from the N loops could be added linearly, the hardening was calculated as

$$\Delta\tau = 6 \, \mu \, \gamma \, f^{3/2}$$

This result differed from the Fisher et al. result in that it calculated the increment of shear stress over the initial yield stress, not the increment over the flow stress of a single phase material at the same strain. It is a stress-strain relationship.

It can be seen that the model predicts a linear work hardening rate, and that the important parameter is not the size or spacing of the particles, but their volume fraction f. The model leads to large elastic stresses on the particles, and led Ashby to predict a large Bauschinger Effect. However he did not actually define how the effect would be measured, nor did he indicate the conditions under which reverse yielding would occur. This model is subject to the same criticism as that of Fisher et al. in that it can be used only at small strains.

At a shear strain of γ the stress exerted on the particles and on the immediate matrix is close to $G\gamma$. The array of shear loops will be stable only as long as the local stress is smaller than that needed to activate the relaxation mechanisms which restrict the range of application of the model of Fisher et al. However as the strain increases, the local stress exceeds that required to activate a relaxation mechanism. It was felt, on the basis of the work of Hirsch and Humphreys, that the process would be cross slip, as this would take place before the generation

of new dislocations from the interface. It had been shown for $Cu\text{-}SiO_2$ alloys with particles 1000 Å diameter that a stress of approximately 0.01μ could lead to cross slip. Then the shear array could be expected to break down at strains of the order of 1%. The figure may differ for other alloy systems but it does indicate that only a small strain is required to cause the breakdown of the array of shear loops at spherical particles.

Above this strain, secondary dislocation loops are formed to accommodate the plastic strain gradient between the particle and the matrix. Ashby calculated their density

$$\rho_G = \frac{1}{\lambda_G} \frac{4\gamma}{b}$$

He gave the title "geometric dislocations" to them since their presence was required to maintain compatability between the matrix and the precipitates. They were thus different from those dislocations which were present in the material for other reasons. In the microstructure, however, it is not possible to distinguish between the two types of dislocations. The parameter λ_G was the geometric slip distance, and was a characteristic of the structure. It was compared with the parameter λ_S for the statistical storage of dislocations (as used by Mader 1963) which is a function of strain. For alloys containing particles, λ_G was the interparticle spacing on the slip plane in the slip direction.

In this model there were two components in the hardening:

a) the long range back stress as calculated for the earlier model

b) the secondary dislocation or frictional type hardening.

However it was not clear how the long range back stresses should have been included and Ashby excluded them, arguing that they

(i) were limited to applicability at small strains ($\lesssim$ 1%)

(ii) represented a minor contribution to the work hardening in alloys with a small volume fraction of particles.

The model was then developed to describe the work hardening in terms of the total dislocation density ρ_T, along the lines of the model used by Nabarro, Basinski and Holt (1964)

$$\tau = \tau_o + C\mu b\sqrt{\rho_T}$$

where τ_o was the initial yield stress and C a constant.

The total dislocation density was considered as the sum of the statistically stored dislocations and the geometrically necessary dislocations. When the geometrically necessary contribution dominates at small strains the dislocation density is

$$\rho_T = \rho_G = 4\gamma/\lambda_G b$$

and then

$$\tau = \tau_o + 2C\mu \sqrt{b\gamma/\lambda_G}$$

Since λ_G is strain independent, the formulation of the work hardening, based on dislocation density, shows a parabolic dependence on strain.

It is of interest to point out:

a) this is quite a different equation from the earlier one

$$\tau = \tau_o + 6\mu\gamma f^{3/2}$$

b) for spherical particles it reduces to

$$\tau = \tau_o + 2C\mu \sqrt{\frac{fb\gamma}{r}}$$

in which there is a parabolic dependence on strain and the important particle parameters are $\sqrt{f/r}$.

c) for plate shaped particles, with $\lambda_G = L$ = particle spacing

$$\tau = \tau_o + 2C\mu \sqrt{\frac{b\gamma}{L}}$$

which again has a parabolic dependence on strain; the volume fraction does not directly enter the equation.

d) at large strains the statistically stored dislocations will dominate the hardening, as shown in Figure 2.2.

This model does include a Bauschinger Effect, but only because it arises from the shear loops accumulated during the early part of the deformation. The number of these loops is expected to remain constant during the deformation, but the forest hardening, due mainly to the

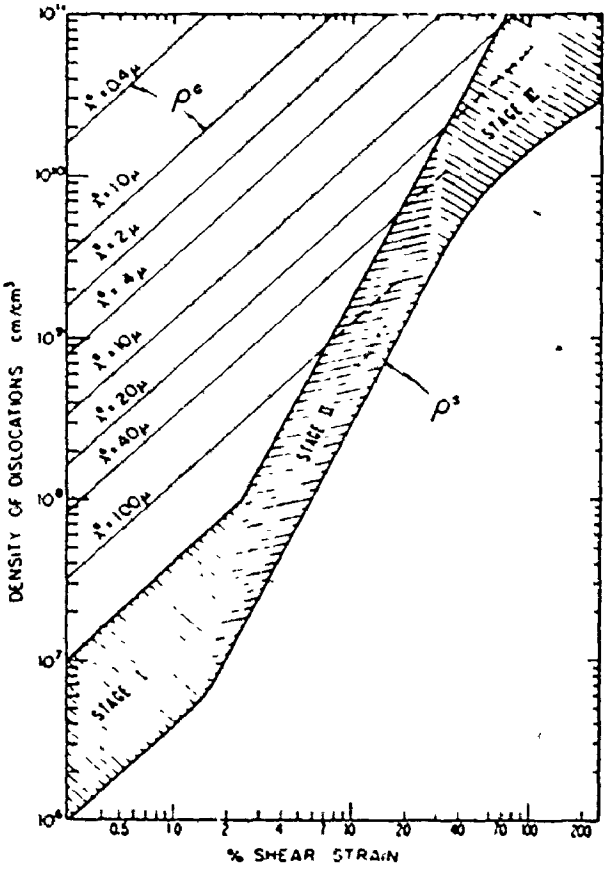

The statistically stored (shaded band) and geometrically necessary dislocation density, plotted against strain. Note that ρ^G can dominate the total density at small strains but be swamped by the statistically stored dislocations at larger strains.

Fig. 2.2. Figure to show that the dislocation density, geometric and statistical, depends on strain. (After Ashby 1971)

secondary loops, will increase. The forest hardening always hinders the dislocation motion, so that, as it increases, the Bauschinger Effect will be expected to decrease. However, although Ashby recognised that some materials had been shown to have a large Bauschinger Effect, he did not include the long range back stress hardening in the final formulation of his model. The large Bauschinger Effect obtained in some materials must then raise doubts as to the applicability of Ashby's equation to them. Perhaps of greater importance is the objection that, in the model, Ashby used the average dislocation density, which is a scalar quantity, to describe a work hardening process which is known from the Bauschinger Effect to possess a definite directionality.

The applicability of the Ashby model was examined in considerable detail by Russell and Ashby (1970). In this study, the work hardening and slip characteristics of the aluminum-copper alloys containing 2, 3 and 4% copper and aged to θ' were examined by subjecting single crystal test pieces to compressive strains. In this alloy, the interparticle spacing L sets an upper limit for the geometric slip distance λ_G, and for all the alloys it was considered that the particles dominated the work hardening

since

$$\lambda_G < \lambda_S$$

At a shear strain γ, the density of dislocations was calculated to be

$$\rho = 4\gamma/bL$$

and the dislocations were to be stored at the particles in such a way that, on one side of a particle, all the dislocations had the same sign; this sign was opposite to that of the dislocations on the other side of the particle. The result was that the particle and the matrix adjacent to it were rotated through an angle $\phi = \gamma$ for shear strains $\gamma \lesssim 0.20$. Such a rotation would be expected to give rise to extensive X-ray asterism and differences in contrast at the particles during TEM studies.

The large X-ray asterism was established in the materials containing the platelets. Comparison tests on identical but quenched single phase solid solution alloys of the same composition at the same strains showed asterism, but it was not as extensively developed. From a study of the asterism it was possible to show that the roller axis for the deformation was $[\bar{1}21]$. The electron microscopy also confirmed the presence of the dislocations with primary Burgers vector stored close to the particles. Further work involving the study of the shape change showed that the deformation took place by slip on a single slip system,

and not, as many had earlier expected, by multiple slip.

Measurements of the dislocation density with strain showed that the storage rate was much higher when the particles were closer together. The authors then attempted to establish a relationship between the dislocation density and the shear strain, and between the dislocation density and the work hardening increment; it is unfortunate that only two points were available for each of these possible relationships. It was argued that the dislocation density measurements showed that the flow stress of the alloy depended simply on the square root of the dislocation density, which led to a parabolic relationship between the shear stress τ and the shear strain γ, for all volume fractions

$$\tau = \tau_o + 0.35\mu \sqrt{\rho}$$

$$= \tau_o + 0.35\mu \sqrt{\frac{b\gamma}{L}}$$

By comparing the data from their own experiments and also that of Dew-Hughes and Robertson with the above equation, Russell and Ashby were able to obtain good agreement between theory and experiment, and argued that the work hardening in the Al-Cu alloy aged to θ' could be accounted for by their simple model.

The implications of this model will have to be discussed in greater detail later. Here it is sufficient to indicate again that it does not include a contribution from the long range back stress hardening, (and no Bauschinger Effect) because it was considered that this contribution would be very small.

Hirsch and Humphreys attempted to give an account of the uniaxial work hardening in two phase alloys at strains larger than that necessary to cause cross slip. The basis of the model was that the hard particles were bypassed by the cross slip mechanism proposed by Hirsch (1957, 1962). In this mechanism the particles were bypassed by the screw component of the mobile dislocation undergoing cross slip and leaving at the particle a prismatic loop. There was considerable microstructural evidence for this mechanism in the work of Hirsch and Humphreys (1969, 1970) on Cu-SiO_2, Cu-Al_2O_3 and other two phase alloys. Their micrographs showed many prismatic loops arranged close to the particles, the rows of loops suggesting the type of mechanism which took place at the particles. Occasional Orowan loops in the arrays show that the dislocation processes are complex.

The model was based on the premise that the flow stress of a work hardened material depended not only on the density of the dislocations, but also on their type and

distribution. The dislocations of most interest were the arrays of prismatic loops with primary Burgers vector, left close to the particles. There were essentially two steps in the calculation of the hardening:

a) an estimate of the number N of loops on each particle as a function of strain

b) the calculation of the hardening due to those loops.

To estimate the number of loops it was considered that each Orowan loop gave rise to one prismatic loop as a result of cross slip, so that if no recovery takes place, at a plastic strain ε_p,

$$N = 2 r \varepsilon_p / b$$

In the calculation of the hardening it was argued that the screw dislocations will interact with the arrays to form the commonly observed helices, and that the dislocation will bow between the end of the helix and the neighbouring particle. As the applied stress increases, the dislocation will have a greater tendency to pass because its loop radius will decrease, and also the pitch of the helix will decrease. The effect of the array was to convert the spherical obstacle into a cylindrical one, so that its length was expected to increase with increasing strain, subject to the array being stable.

The average spacing of the obstacles changed, and a new criterion for bypass was established. This was that the mobile dislocations would bow until they touched a nearby array, after which the dislocation would continue to propagate as a double kink. Then, using equations derived from the geometry of the arrays and an equation derived earlier to give the yield strength of a material containing N_S obstacles per unit area on the slip plane,

$$\tau = \frac{.81\ \mu\ b\ N^{1/2}}{2\pi\ (1-\nu)}\ \ell n\ \frac{2r}{r_o}$$

where r_o is the dislocation core size, and ν is Poisson's Ratio, the following equation was derived for the hardening:

$$\Delta\tau = \frac{\mu b}{2\pi\,(1-\nu)^{1/2}}\ \frac{S}{2D^2}\ \ell n\ \frac{2r}{r_o}$$

in which S was the array size and D the distance between the end of the array and a nearby particle.

The equation was simplified using the assumptions that all the loops were pressed against the particles and that their spacing was approximately equal to the particle radius. Then

$$\Delta\tau = \frac{0.10\ \mu}{(1-\nu)^{1/2}}\ \ell n\ \left(\frac{2r}{r_o}\right)\ .\ f\ .\ \varepsilon_p$$

This equation shows a linear dependence on strain and volume fraction and slight dependence on the particle radius.

The model and calculations must be expected to hold only at small strains. At larger strains the prismatic loops do not lie in neat arrays; some of them are secondary loops, some are swept away by mobile dislocations on adjacent slip planes, and as the strain increases, a greater proportion of the loops is expected to be randomly distributed. The work hardening rate will be reduced.

To ascertain if the model can predict a Bauschinger Effect, it is necessary to consider it in three parts:

a) small strains (<0.01): at which the only loops are Orowan loops. These will give rise to a long range back stress and a Bauschinger Effect. This point was not discussed in the paper by Hirsch and Humphreys, but the result should be similar to that of Fisher, Hart and Pry.

b) larger strains (<0.1): at which the primary prismatic loops are present. The arrays contributed to the hardening, principally by reducing the separation of the particles. This does not lead to a Bauschinger Effect. However, the contribution due to the few Orowan loops will still exist, but its relative magnitude will be reduced.

c) large strains: the random prismatic loops which dominate the hardening will have no long range back stress, and no Bauschinger Effect.

Thus the earlier papers by Hirsch and his co-workers do not predict a Bauschinger Effect comparable to that observed in many materials. Their model is applicable to materials containing small particles, and can not readily be extended to those with large precipitates or with precipitates not spherical in shape. The reason is that, in materials with large precipitates, the dislocations are not arranged as observed by Hirsch and Humphreys. As stated in their work, prismatic loops with primary Burgers vector were generated by cross slip at and on one side of the particles. This is not the common observation if large particles are used (Brown and Stobbs 1971, Atkinson et al. 1973, 1974); then there are large numbers of dipoles and/or secondary slip occurs.

In two important papers, Brown and Stobbs (1971) attempted to describe the work hardening of copper alloys containing a small volume fraction of silica particles. In their microstructural examination of the deformed alloy, they observed many secondary dislocations, with some primary ones. The secondary dislocations they considered to have been formed as a result of plastic relaxation processes near the silica particles. Before attempting to develop a model to include their microstructural observations, they examined a model in which no relaxation took place. It was realised that such a model was unrealistic

for their alloy, but its development has led to some clarification of a difficult problem.

The particles were considered to be spherical; the dislocations trapped by them were smeared out as in a continuum model so that they did not consider the slip line spacing. They sought first the solution to the problem of the resulting stresses and strains in a finite body (containing a volume fraction f of particles radius r) if it were given a uniform shear strain ϵ_p. They used Eshelby's model (1957) and calculated the displacements in the matrix and in the particles; the results were complicated, but they did show

a) there were long range and short range stresses in the matrix

b) these stresses had a mean value of zero, so that they were as likely to aid a moving dislocation as to oppose it

c) for the particles there were stresses inside, whose magnitude was given by

$$\sigma_{xz} = \sigma_{zx} = 2 \gamma \mu \epsilon_p$$

where γ is an Eshelby constraint factor. All other $\sigma_{ij} = 0$.

These stresses were independent of position and of the size of the particles. The important point in this

model is that, since all the stress components in the matrix σ_{ij} have mean values of zero and there still exists the σ_{xz} in the particles, this σ_{xz} can be averaged over the whole test piece giving a value

$$\overline{\sigma_{xz}} = 2\gamma f \mu \varepsilon_p$$

In paper I (1971) this is called the image stress, but in later papers the term "mean stress in the matrix" is used. It is the average stress exerted by the particles in the matrix at a strain ε_p. This stress acts to oppose continued forward deformation in the matrix and to aid deformation in the reverse sense. Further modification of the elastic constant μ is required if the particles are not elastically identical to the matrix.

In paper II the possible processes of plastic relaxation were discussed. In these processes the primary shear loops (Orowan loops) interacted with each other and with approaching dislocations to give different types of dislocation configurations, with primary and secondary Burgers vectors. For small particles only primary dislocations were observed, and the process was similar to that proposed by Hirsch (1957). For larger particles, at larger strains, relaxation occurred and the formation of secondary dislocations took place. The formation of these secondary dislocations had important consequences in that it

a) led to the local hardening of the matrix adjacent to the particles and thus it

b) made further plastic relaxation more difficult.

The plastic relaxation reduced the unrelaxed strain and this caused a reduction in the mean stress in the matrix. The total strain was ε_p and it was equal to the sum of the relaxed strain and the unrelaxed strain ε_p^*. The size of the secondary dislocation zone at the particles increased slowly with strain. The work hardening was considered as the sum of the hardening resulting from the mean stress in the matrix, and that caused by the increase in the dislocation density adjacent to the particles. The formula used by Ashby (1971) and by Nabarro et al. (1964) was applied to calculate the hardening resulting from the secondary dislocations

$$\Delta\tau = \alpha \mu b \sqrt{\rho_{sec}}$$

Detailed consideration of the relaxation processes has shown that: -

a) the unrelaxed strain $\varepsilon_p^* = \left(\frac{8\pi b}{\alpha^2 \varepsilon_p r_o}\right)^{1/8} . \alpha . \left(\frac{8 \varepsilon_p b}{\pi r_o}\right)^{1/2}$

This shows almost a quadratic dependence on the imposed strain. There is an inverse dependence on particle size.

b) the contribution from the secondary dislocations (or

forest) is calculated as

$$f_p^{1/2}\sigma_{local}$$

Here f_p is the volume fraction of the regions containing secondary dislocations, and are called "plastic zones". σ_{local} is the local flow stress in the plastic zone.

c) the mean stress in the matrix is $f\ \mu\ \varepsilon_p^*$.

d) since the volume fraction of the plastic zone depends linearly on the volume fraction of the particles the two hardening contributions have a volume fraction dependence, such that

$$\frac{\text{mean matrix stress contribution}}{\text{forest contribution}} \propto f^{1/2}$$

This is important since it predicts the origin of some of the volume fraction dependence of the Bauschinger Effect.

e) the forest hardening term is similar to that of Ashby (1966, 1970). The back stress term is smaller by a factor of $f^{1/2}$ and so for small volume fractions the back stress makes a very small contribution to the work hardening,

for example, at f = 1%, $f^{1/2} = 0.1$

and Ashby was correct in not including the back stress hardening in his model. However the Brown and Stobbs' theory of the work hardening given above is dependent on there being a large plastic relaxation so that forest

hardening dominates. In materials in which there is little forest hardening, as for example in those tested in this present work and in fibre composite materials, the conditions imposed by Brown and Stobbs are not obeyed, the volume fraction $f^{1/2}$ dependence indicated above is not valid and Ashby's assumption that the back stress hardening is negligible is not correct. This last point is very important and will be developed in a later discussion.

f) The model also predicts a Bauschinger Effect with the difference in the yield stresses being predicted reasonably well. This is better than most other theories which do not include a Bauschinger Effect. The origin of the effect is in the back stress (or mean matrix stress) which opposes the continued forward deformation and aids the reverse deformation. The authors point to the evidence from the work of Wilson and Konnen (1964) and Wilson (1965) in support of their belief that the long range back stresses are responsible for the Bauschinger Effect. The work of Wilson will be examined in the next section.

Tanaka and Mori (1970, 1973) considered the work hardening from a continuum approach in which they ignored any effect of slip line spacing and were interested in the effect of the particles on the free energy of the system.

The particles were allowed to deform only elastically and the plastic deformation was considered to take place by multiple slip since it was argued that this process gave a more energetically favourable deformation mechanism than single slip. The deformation was ε in a tensile direction and $-\frac{\varepsilon}{2}$ in the transverse directions.

The free energy change was calculated for a material containing N non deforming particles, after a plastic strain ε at which the applied tensile stress was σ_A. The result was

$$G = N[E_{el} + E_{int} + E_{inh}] - \frac{1}{2} E \sigma_A^2 V_o + \sigma_o \varepsilon V_o - \sigma_A \varepsilon V_o$$

The individual terms were explained as follows:

1. E_{el} is the elastic strain energy in and close to the inclusions due to the particle deforming elastically whilst the matrix is deformed plastically.
2. E_{int} is the interaction energy of the internal stress field under the applied stress.
3. E_{inh} is the energy due to the disturbance of the external stress due to the differing elastic constants.
4. $\frac{1}{2} E \sigma_A^2 V_o$ is said to be the elastic strain energy the body would have at the applied stress σ_A if it had no inclusions. It is not clear that this is so, since the product $E \sigma_A^2$ is not an energy.

5. $\sigma_o \varepsilon V_o$ is the energy dissipated by friction during the plastic flow of the body.
6. $\sigma_A \varepsilon V_o$ is the change in the external potential energy due to the occurrence of plastic flow.

The conditions for stable deformation were given as

$$\frac{\partial G}{\partial \varepsilon} = 0 \quad \text{and} \quad \frac{\partial^2 G}{\partial \varepsilon^2} > \text{for } \sigma \text{ constant.}$$

Then, using values for terms 1, 2 and 3 above, derived earlier in their work, it was shown that the stress-strain relation for a body containing spherical particles was of the form

$$\sigma = \sigma_o/(1-B) + AE\varepsilon/(1-B)$$

where A and B are constants for a given alloy system and depend on the Elastic Moduli, Poisson's Ratios and the volume fraction of the particles and matrix.

Similar calculations for other alloy systems containing disc-shaped and needle-shaped particles showed that the same formula could be used, but with different values of the constants A and B. These constants also depended on the particle orientation.

The derived equation predicted a linear hardening rate $AE/(1-B)$ and a yield stress of $\sigma_o/(1-B)$, but the authors acknowledged that the initial yielding might be governed by the yielding of the matrix at its own yield stress σ_o, and

that there could then be a small strain in which the work hardening rate was high. This agrees with many experimental results. Beyond this small strain, the hardening rate would be AE/1-B.

Further work has shown that the hardening rate is almost linearly proportional to the volume fraction at small volume fractions and closely similar elastic moduli. The effect of the difference in elastic moduli also seems to saturate.

The work hardening behaviour depended on the shape and orientation of the particles and it was shown clearly that the effect was greatest for disc shaped particles parallel to the tensile axis. The spherical particles had the smallest contribution. The effect of particles at random orientations to the tensile axis, as for example in a polycrystalline material, was given as a weighted average of the effects of the particles parallel to and perpendicular to the tensile axis.

The authors also considered the breakdown of linear hardening and its resultant parabolic form. They can be considered to have approached the work hardening behaviour in a way similar to that of Brown and Stobbs. At small strains the deformation was unrelaxed; at larger strains it was relaxed. For Tanaka and Mori the relaxation process was the onset of prismatic punching or the cross slip

of dislocations. They attempted to calculate the strain necessary for this, arguing that the relaxation process will take place when the shear stress in the particle matrix interface exceeds the theoretical shear strength (approximately $\mu/30$). Their results indicate that for many different materials the critical strains are less than 5% tensile strain.

It must be pointed out that, because of effects not included in the model, the work hardening calculated is a lower bound. It was assumed that all the work done by the extra applied stress over the initial yield stress was stored as internal elastic energy. Any additional work used to produce heat was not included and as such must cause the correct flow stress to be higher than that calculated. An example of the processes dissipating energy is dislocation bowing due to non uniform stress fields in the body. These local differences in the stress field are due to the elastic moduli differences.

Brown (1973) has shown that the hardening calculated by Tanaka and Mori is the same as that calculated in the papers by Brown and Stobbs and called "image" stress, or later "mean stress in the matrix". Since the hardening calculated by Tanaka and Mori is not frictional, but rather a back stress type hardening, it must readily account for the large Bauschinger Effect observed in materials containing

hard particles. However, they did not indicate the conditions for reverse yielding.

In an attempt to extend the work of Fisher, Hart and Pry (1953), Hart (1972) was concerned with avoiding the principal defect of the earlier theory. He assumed that the Orowan stress was simply additive to the matrix flow stress, and that the effect of the back stress from the trapped loops raised the critical stress for bowing additional dislocations between the particles. He recognised that the Orowan process was a critical step, and attempted to calculate the strain hardening increment τ_h where

$$\tau_h = \tau - \tau_m$$

with τ = flow stress of the alloy, and τ_m the flow stress of the single phase material at the same strain. There is here the important assumption, also made by Fisher et al. (1953), that the matrix work hardens as if the second phase were absent. This assumption can be readily disputed on the basis of the microstructural evidence obtained by Brown and Stobbs (1971).

Hart equated the work hardening to the additional stress necessary to force a dislocation between two particles each of which is surrounded by several Orowan loops. It is important to realise he not only calculated the effect

of source shortening. Rather, by considering the interaction between the glide dislocation and the existing loops as a dipole he calculated the forces between them. The result, assuming single slip is that

$$\tau_h = \tau_o[1 + A\gamma^{*1/2}f^{3/4} + B\gamma^{*}f^{3/2}]$$

where τ_o is the Orowan stress, and γ^* the unrelaxed strain, such that

$$\gamma^* = Nb/2r$$

where N is the number of loops on the particles. Here A and B are constants including the modulus, line tension, particle radius and number of loops. Since some relaxation took place $\gamma^* < \gamma$ the imposed strain. However, the hardening resulting from the relaxation debris was considered negligible and was not included. The work hardening had a maximum value determined by γ^*;

a) $\gamma < \gamma^*$ hardening is parabolic in strain.

b) $\gamma > \gamma^*$ hardening is constant.

According to Hart, the model predicts a large Bauschinger Effect on stress reversal, but not upon simple stress removal. He explained how the calculated back stress aids the reverse motion of the dislocations and how the dislocation loops on the particles provide no resistance to this motion. Even if the reverse motion of the dislocations

was not on the same slip plane as the dislocation loops, the short range interaction could be expected to lead to the annihilation of the loops, with perhaps some debris left behind. The particles with loops were not then expected to resist slip in the reverse direction. However, he seems to have ignored the effect of the friction stress in the matrix.

It was predicted that for a prestrain of γ the stress increment τ_h on stress reversal would be substantially zero (or even negative) for a strain interval approximately equal to γ or γ^*, whichever was smaller. After this reverse strain, the stress increment would rapidly rise to the value τ_o and hardening would continue again, being given by the equation derived, but with γ now measured to start from the sudden increase at τ_o.

This model considered only the hardening arising from the interaction of the dislocation loops with the bowing dislocations. The hardening mechanism used above by Hirsch and Humphreys was not included. Hart considered that this type of hardening - resulting from the interaction of glide dislocations with dislocation debris left over from cross slip processes - was much less than the contribution calculated in his model. The debris hardening is a friction type hardening: it affects dislocation motion in both the forward and reverse directions and as such it has the

effect of reducing the Bauschinger Effect.

Likewise Hart did not calculate the long range back stress hardening due to the elastic deformation of the particles. This stress would have to be added to that calculated as τ_h and, since there is no forest hardening associated with it, the magnitude of the Bauschinger Effect would be increased. He does not give any criteria to determine the onset of reverse yielding, except to say that it will not take place during unloading, and that some reverse stress is necessary. The reasons for this reverse stress are not given, but the inclusion of a back stress due to the particles must reduce the reverse yield stress. This is hinted at in an appendix to the paper.

It seems appropriate here to point out that the curve shown by Figure 1 in Brown (1973), here Figure 2.3 labelled "Hart", used to compare experiment with theory should really be called "Hart and Brown and Stobbs". It represents the combined back stress theory of Brown and Stobbs and the theory proposed by Hart. When the Brown and Stobbs forward curve is compared with that of "Hart, Brown and Stobbs" it is easy to see that the Hart contribution is a smaller one. It does, however, have a great effect on the reverse curve, but, as explained above, it is not clear how Hart arrived at his reverse yield criterion.

Brown and Clarke (1975) attempted to calculate the

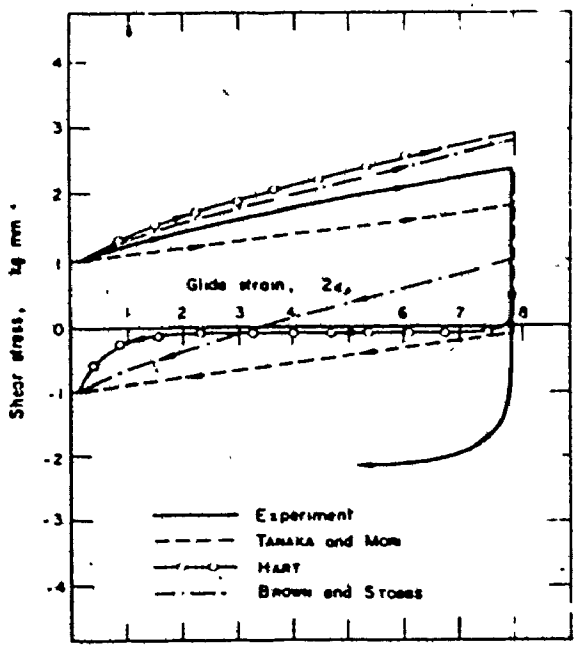

Comparison of theories for the PMS with experimental observation

The experimental stress strain curve is taken from Brown and Stobbs.[4] For this material (Cu SiO_2),

$$f = 0.54\%; \qquad \mu = 4.8 \times 10^3 \text{ Kg mm}^{-2};$$

$$\nu = 0.4; \quad \frac{\mu^*}{\mu^* - \gamma(\mu^* - \mu)} = 0.8;$$

and mean volumetric particle radius = 650 Å.

The curve labelled Tanaka and Mori is constructed from equation (3). The unloading behaviour is determined by the assumption that the Orowan stress acts as a friction stress, so that no reverse flow occurs until the stress drops by $2\sigma_0$.

The curve labelled Hart is taken from reference (2), equation (22) as corrected in the appendix of that paper. In Hart's notation, α^* is the unrelaxed glide strain and is equal to $2\varepsilon_p$. The unloading curve is constructed according to Hart's prescription.

The curve labelled Brown and Stobbs is constructed from reference (4). The unloading behaviour has been constructed as follows: assume that the fluctuating stresses with zero mean value act essentially as a friction stress, so that they play the role of σ_0 in Tanaka and Mori's theory. Then the stress must be lowered by twice the amount by which Brown and Stobbs' curve exceeds Tanaka and Mori's curve before reverse flow starts, and thereafter the reverse flow follows a curve which is simply the forward work-hardening curve, displaced downwards by a constant amount.

This figure replaces and improves upon Fig. 5 of reference (4), which is erroneously drawn.

Fig. 2.3. Comparison of different work hardening models, including the Bauschinger Effect, for Cu-SiO_2 (After Brown 1973)

work hardening in two phase materials by considering that the resistance to plastic deformation in these materials was made up from five contributions:

a) friction stress of the matrix

b) Orowan Stress

c) mean stress in the matrix. It is equal to the differential of the total elastic energy with respect to strain

d) local fluctuating stresses of mean zero value which are heat producing

e) forest contributions - due to the interaction of the glide dislocations with the increasing density of secondary or forest dislocations as plastic relaxation takes place.

In the model, Brown and Clarke examined the work hardening under conditions where no plastic relaxation occurred, and attempted to calculate the work hardening increment arising from the mean stress in the matrix. Then differences between the calculated increments and the experimental values were attributed to other forms of hardening, for example source shortening.

The determination of the mean matrix stresses makes use of the work of Eshelby which attempts to calculate the stresses and strains produced in the matrix when an inclusion changed its shape due to a transformation. The inverse is used in the model. The material undergoes plastic

deformation under the action of the external stresses, but the changes in shape of the inclusion are elastic and the interaction of this elastic deformation of the inclusion with the matrix leads to the development of the mean matrix stress. It was assumed that the plastic deformation was uniform, so that the slip line spacing was much smaller than the particle size. The model attempted to calculate two quantities:

a) the mean stress in the matrix following a plastic deformation by single slip.

b) the stress needed to continue plastic deformation in a material oriented for multiple slip.

The model used as its starting point Eshelby's equation for the mean strain in the matrix $\langle \varepsilon_{ij}^{F} \rangle_{M}$ (in a Finite material) in terms of the transformation strain ε_{ij}^{T}, the Eshelby coefficient S_{ijkl} and the volume fraction f,

$$\langle \varepsilon_{ij}^{F} \rangle_{M} = f(\varepsilon_{ij}^{T} - S_{ijkl}\ \varepsilon_{kl}^{T}).$$

Brown and Clarke simplified this

$$= f\ \gamma_{ij}\ \varepsilon_{p}$$

where ε_{p} was the fractional tensile strain and γ_{ij} was a second rank accommodation tensor, which can be defined in terms of S_{ijkl}. Also defined were the stress accommodation coefficients Σ_{ij} such that

$$\langle \sigma^{F}_{ij} \rangle_{M} = 2\mu \, \Sigma_{ij} \, f \, \varepsilon_{p}$$

with

$$\Sigma_{ij} = \gamma_{ij} + \left(\frac{\nu}{1-2\nu}\right)\gamma_{mm}\delta_{ij}$$

The authors calculated S_{ijkl} for ellipsoidal inclusions of different types, including ribbons, fibres, discs and spheres, and they also treated three cases of importance for this study in which the inclusions were on cube planes. The calculated S_{ijkl} gave the values of γ_{ij} needed for the determination of the contribution from fibres and discs parallel to or perpendicular to the tensile axis.

The table giving the stress accommodation coefficients showed that in all except the most symmetric case there are hydrostatic stress components. These caused a need to decide on a criterion for plastic flow before the work hardening could be calculated. The choice was the Tresca criterion which made use of the difference between the maximum and minimum principal stresses being equal to twice the resolved shear stress for plastic flow. Then the critical resolved shear stress required to overcome the mean shear stress in the matrix was written

$$\sigma_{SHEAR} = 2\gamma\mu f \varepsilon_{p}$$

where γ was the accommodation factor given for single slip and multiple slip in table 2BC.

The analysis was extended to include the effects of elastic inhomogeneity. Again using Eshelby's approach and the Tresca criterion, it was shown that

$$\sigma_{SHEAR} = 2\gamma\mu f \varepsilon_p D$$

where D is the modulus correction factor. Values for D, for discs and other shapes, were presented in graphical form to show the dependence on modulus and orientation. The result that discs parallel to the tensile axis had a greater effect than fibres parallel to the axis, with spheres having a small effect, supported the work of Tanaka and Mori.

The authors compared their equations with the experimental results for many different alloy systems. The calculated hardening rate was always smaller than the observed rate. This difference was expected, because the model ignored the locally fluctuating stresses which caused the required applied stress to be greater than the calculated stress.

The stress calculated in this model was the mean stress in the matrix; it has the same effect in the work hardening as the back stress. This means that the Bauschinger Effect is expected, and the stress calculated will aid the reverse deformation. The authors do not, however, consider the conditions for reverse yielding.

Since this model attempted to include the Bauschinger

Effect, and to consider the effect of particle shape on the work hardening process, it will be examined later and a comparison will be made between it and this experimental work.

Hazzledine and Hirsch (1974) were concerned to calculate the effect of Orowan loops on the flow stress, work hardening and Bauschinger Effect in Cu-Al_2O_3, and to combine the different hardening mechanisms to derive a stress strain curve. In the model they considered the deformation to take place in such a way that each particle was intersected by only one active slip plane (particle diameter <500 Å); in this they differed from earlier authors who assumed that the deformation was uniform. The single slip plane intersecting each particle resulted in a pile up of circular, concentric and coplanar Orowan loops. The slip plane spacing was an independent parameter which had to be determined in order to derive the work hardening curve. At small strains the loops were stable, but at large strains other dislocation arrangements were obtained, in a manner discussed by Hirsch and Humphreys (1970) and Brown and Stobbs (1971). The accumulated loops stood off from the particles, the innermost hugging the interface, the succeeding ones being at a distance controlled by the interactions and applied stress.

The model considered the work hardening to be made

up from three principal components:

$$\text{work hardening} = \text{image stress} + \text{long range back stress} + \text{bowing stress}$$

The image stress and the long range back were two long range back stresses which opposed continued deformation in a forward sense and aided the deformation in the reverse sense. The long range back stress was calculated, assuming an infinite solid, using a method based on the work of Kroupa (1962); only the loops on the active slip plane had any contribution to this back stress. The back stress on all other parallel planes averaged out to zero.

The image stress was the same as that calculated by Brown and Stobbs (1971); but in this case the shear strain had to be reconsidered. As stated Brown and Stobbs assumed a uniform shear, whereas Hazzledine and Hirsch allowed slip on only some planes so that the particles were intersected by only one active slip plane. The term in the Brown and Stobbs formula had to be replaced by an expression which included the slip line spacing, and a correction for the mean area enclosed by the loops.

The bowing stress was based on the stress required to bow glide dislocations between two particles whose centres were at some distance apart, and which had some Orowan loops. These Orowan loops stood off and reduced the critical length of glide dislocation which could bow. As this

length was reduced the applied stress had to increase.

Although the slip line spacing was assumed constant, it was realised that it could vary with strain. This would have had a profound effect on the nature of the stress strain curve. The authors decided to minimise the flow stress at a given strain to determine the slip line spacing. The need for uniformity of deformation would lead to a reduction of the slip plane spacing, but there was an interaction between dislocations moving on parallel slip planes which tended to increase the spacing.

The reverse deformation could be considered to take place on the same slip planes as used for the forward deformation. However this has been found by Hazzledine and Hirsch and by Brown (1973) to lead to a reverse stress strain curve for which the stress level is too small when compared with experiments. When Hazzledine and Hirsch introduced the interaction stress between dislocations moving on parallel slip planes the reverse curve was better, but the work hardening rate and Bauschinger Effect were too large. The third possibility considered was that of storing about 4-5 Orowan loops on the particles and converting additional loops into prismatic loops. This process would still lead to an increasing bowing stress with increasing strain. This gave a reasonable agreement with the forward and reverse curves, even though it was acknowledged that

the reverse calculation required some arbitrary assumptions.

The good agreement of the "hybrid model" with the forward and reverse stress strain curves does not readily lead to the model being accepted. One reason for this is the slip plane spacing. The authors did not clearly state which slip plane spacing was being used. In a model of this kind, the value which should be used is the current slip plane spacing; that is, the spacing between those slip planes which were active for a given infinitesimal strain increment. It is unlikely to be the slip plane spacing obtained from surface measurements on the test piece after a small strain. The value obtained in an experiment like this would be a lower bound on the spacing.

Brown and Stobbs in Paper V (1976-7) have argued against the use of the slip plane spacing as found in this model of Hazzledine and Hirsch. The slip plane spacing was considered a means of introducing the term for the interaction hardening due to dislocations gliding on parallel slip planes. It was important to Brown and Stobbs that the interaction hardening was necessary in the Hazzledine and Hirsch model to produce the good agreement between the experimental results, and to avoid having a slip plane spacing which was indefinitely small. In their view the slip plane spacing will be as small as the number of active sources allows. They asserted that it will be small enough

so that the continuum model as used by them (in which the dislocations were smeared out) will give a reasonable estimate of the internal stress. The need to invoke the interaction hardening is considered unjustified as the data of Gould et al. (1974) can be satisfactorily explained by other models. It was the experiments of Gould et al. which the model of Hazzledine and Hirsch was trying to describe.

B Continuum Models

The models discussed so far have been dislocation models; it seems appropriate to conclude this section with a description of some continuum models which have recently been discussed by Asaro (1975). The first of these models was proposed by Masing (1927), and in it the material was considered to be made up from many elastic-plastic elements, each with a different yield strength. The elements were perfectly plastic so that no work hardening occurred during their plastic deformation. They were also identical in size and had equal yield strengths in tension and compression.

The stress-strain history of a material composed of elements bound in parallel like this can be examined. For the first part of the deformation all the elements will deform elastically until the stress σ_1 is reached at which element 1 undergoes yielding. If this happens at a strain

ε_1 the stress is σ_1. As the load increases, element 1 makes no further contribution to the load carrying ability and the stress on the other element increases faster. At a stress σ_2 element 2 undergoes plastic deformation; the strain is ε_2. Again increasing the load causes further yielding of additional elements to take place, and the mean stress in the structure at the time when the last element yields can be calculated from

$$\bar{\sigma} = (\sigma_1 + \sigma_2 + \sigma_3 + \ldots . \sigma_n)/n$$

When this model undergoes reverse deformation after a prestrain the elastic unloading occurs over a strain range of $2\varepsilon_1$ and a stress amplitude of $2\sigma_1$. Then element 1 yields in compression, and the stress is

$$\sigma_{rev} = \bar{\sigma} - 2\sigma_1.$$

Increased reverse loading leads to element 2 yielding in reverse at a reverse strain of $2\varepsilon_2$, and the reverse stress could be calculated. A two element model is shown in Figure 2.4.

It can be shown that the reverse loading curve is the same as that in the forward direction, except that the strain values in reverse are doubled when compared with the forward curve. As the number of elements increases this is still true, but the curves become more rounded. If the elements are considered as work hardening, the pattern

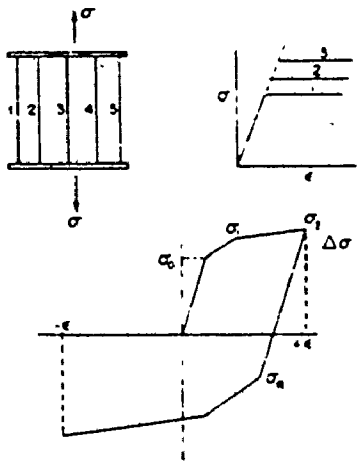

FIG 2 (a) Model structure composed of elastic rigid plastic elements (b) Stress-strain behavior for model elements in (a) (c) Composite stress-strain behavior for structure shown in (a).

Fig. 2.4. Two element model used to explain the Bauschinger Effect. (After Asaro 1975)

changes; the factor of 2 is no longer maintained between reverse and forward strains; however, the work hardening of the elements itself presents complications. It has to be decided what type of hardening occurs in the elements: frictional or back stress?

Several other continuum models exist to describe the work hardening of materials in unidirectional deformation. These include the combined kinematic and isotropic hardening model, and models based on the translation, expansion and distortion of the yield surface. They are all complex and this complexity has hindered their application to real materials. It is accepted that these models can be made very exact, but they need considerable input from the material in order to determine the many constants in the equations.

2.3 Studies of the Bauschinger Effect and Reverse Deformation

In this section an account will be given of those studies reported in the literature which examined the Bauschinger Effect and the reverse deformation of materials. Of interest here is an examination of the techniques used to measure the Bauschinger Effect and how the relevant information was obtained. The difficulties involved in these measurements will be briefly discussed, and the significance

of the results will be examined.

A Problems

It was indicated earlier that the shape of the reverse stress-strain curve is very rounded and that reverse yielding takes place at a lower stress than the flow stress in the forward direction. Problems arise if the Bauschinger Effect is considered as a reduction of the yield stress in the reverse deformation: the chief problem is that the roundedness makes the definition of the yielding very difficult. Also the work hardening rate at small reverse strains is very high so that any uncertainty in determining the onset of reverse yielding will cause a large error in the measured reverse yield stress. These problems have been realised for some time, and they have affected the approach taken to the analysis of the stress-strain curves in reverse.

For example, Woolley (1953) in his study of the Bauschinger Effect in pure polycrystalline materials defined the effect in terms of stress, but then explained the problems involved in measuring the stresses and strains in uniaxial tests and opted for torsion tests. Here he did not use his original definition. Rather he considered the Bauschinger Effect as the existence of a large reverse strain that is necessary to bring the reverse flow stress

up to the same level as the original forward flow stress at the end of the prestrain. Then the problems of deciding on a yield criterion and of measuring stresses and strains at small reverse strains have been replaced by an easier one - that of determining the reverse strain required to make the reverse flow stress equal to the forward flow stress.

For some processes the Bauschinger Strain is an important parameter, but for much of the recent work the main interest is in using the Bauschinger Effect to study the work hardening process in alloys containing hard particles. This requires that the local stresses inside the alloys be determined so that the processes can be identified. As explained earlier, it is considered that the long range back stresses responsible for the Bauschinger Effect are built up in the materials during the forward plastic deformation. The magnitude of these back stresses is of great interest and many different approaches have been used in their determination.

Before giving an account of some of the experimental methods, some mention should be made of the contribution by Orowan (1959). He considered the behaviour of a plastic material on stress reversal. There were two separate parts of the reverse curve of interest to Orowan.

a) at large reverse strains one part showed a constant stress difference between the forward and reverse

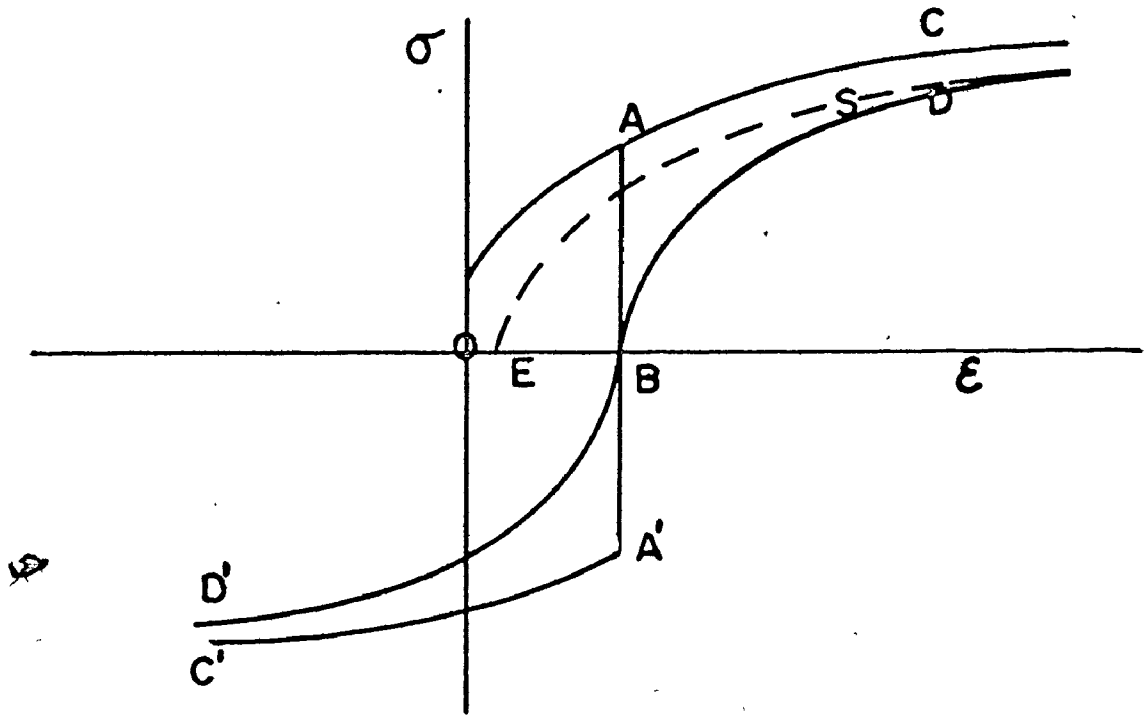

OROWAN'S DEFINITION OF THE BAUSCHINGER EFFECT

1. PERMANENT SOFTENING AT LARGE STRAINS.
2. RAPID DECREASE IN DIFFERENCE BETWEEN FORWARD & REVERSE CURVES.
3. TRANSLATION OF FORWARD CURVE TO GIVE REVERSE CURVE.

FIG 2.5

curves, SD

b) at small reverse strains the curve was very rounded and showed a rapidly decreasing difference between the two curves.

For Orowan this transient softening was the Bauschinger Effect; on the basis of the data he had examined, he predicted that the rounded part of the stress-strain curve would "extend over a strain of the range 1-3%" if the prestrain "was more than a few percent". He also considered that the parallel curves SD, could be obtained by moving the forward curve OAC to a position such as ESD.

It is unfortunate that Orowan did not see a wide range of materials when making his prediction. The 1-3% prediction holds for some single phase materials, as does the permanent softening, but materials which exhibit a large Bauschinger Effect will be shown to not follow the prediction. Examples are those materials which contain a hard second phase. The work of Wilson (1965) showed that the single phase materials followed the Orowan prediction, but the two phase alloys did not.

B Studies

Wilson (1965) carried out a series of tests on several cubic materials to study the long range back stresses

set up during plastic deformation. He used mechanical tests, but the more important part of the work was the use of X-ray techniques, described in Wilson and Konnan (1964), to determine the long range back stress from lattice strains. The work established that long range back stresses did exist and that they were responsible for the Bauschinger Effect.

In the experimental work, Wilson used thin tubes of material and deformed them in torsion, first in a forward sense to 9% shear strain, then immediately in a reverse sense; others were given a forward strain of some 15%. From these curves it was possible to study how the ratio τ_r/τ_f (where τ_f is the flow stress in the forward sense, τ_r is the flow stress in reverse at the same cumulative strain) depended on reverse plastic strain. The many materials tested fell into two groups:

a) principally pure single phase materials showed a rapid increase to a ratio greater than 0.8 in the first 1% reverse strain, and then saturated at $\tau_r/\tau_f = 0.9$ after 2%. These materials showed a permanent softening, whose magnitude was small, about $\tau_f/10$.

b) the second group composed of materials containing hard particles did not show the same tendency to reach a constant value of τ_r/τ_f - in fact several of them do not remotely approach such a state. The ratio is always increasing. There is thus some problem in attempting

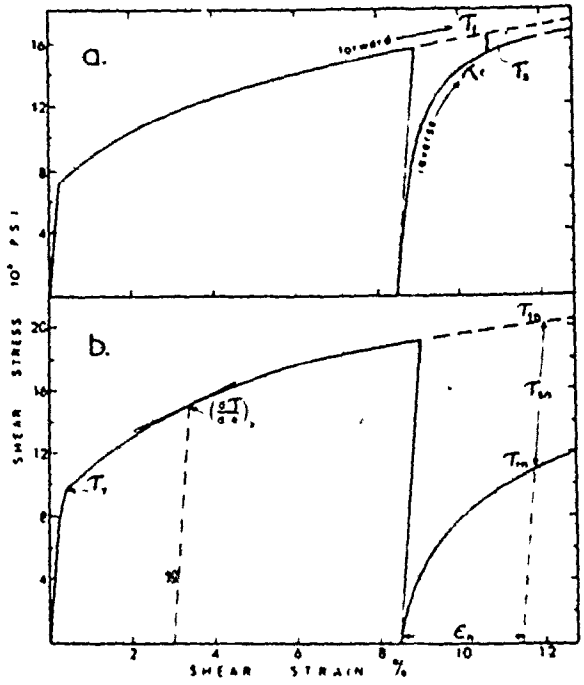

FIG. 1. The effect of precipitation on the Bauschinger Effect in alloy 7 (Al 4% Cu) quenched from 525 C and aged at 190 C for (a) 5 hr and (b) 110 hr before straining (Fig. 1b is also used to define τ_{ss}).

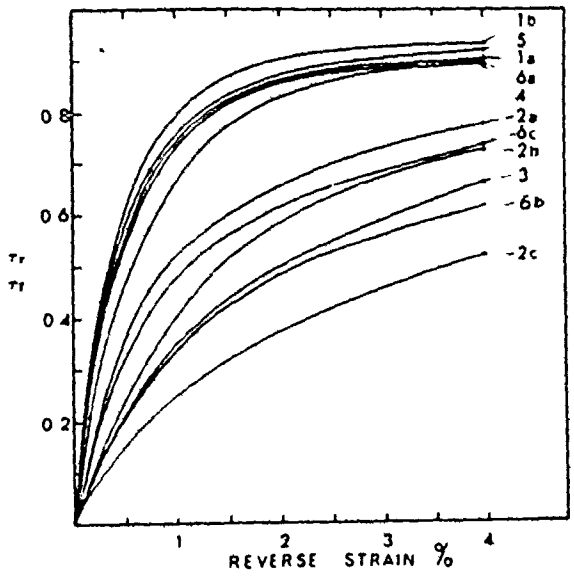

FIG. 2. The ratio of flow strength in reversed deformation to that in continued forward deformation, measured at the same total strain. The curves are identified with the alloy designations used in Table 1.

Fig. 2.6. Experimental curves reported by Wilson (1965)

to describe these tests as showing "permanent softening". Wilson summarised this work by correlating the relative magnitudes of the "permanent softening" effects with the types of dislocation barriers expected in the materials. The weak barriers gave rise to small permanent softening, whilst the harder obstacles had a much greater effect.

He also demonstrated that the long range stresses built up by the prestrain could be removed by the reverse straining. Specimens were deformed to 9% in torsion, unloaded and carefully sectioned with two mutually perpendicular cuts at 45° to the axis of the test piece. After polishing to remove the damaged material, the surfaces were examined using X-ray diffraction to measure the lattice strains. The angular difference, $\Delta 2\theta$ between the positions of diffraction line peaks was measured. Other tests were carried out in which the test piece was given a reverse strain after the 9% forward strain. The results were plotted as $\Delta 2\theta$ against reverse strain. At some reverse strain, ε_N, the sign of $\Delta 2\theta$ changed. This was taken to be the reverse strain necessary to reduce to zero the average value of the back stress from the prestrain. This work was carried out for many of the materials and the results are

a) single phase materials $\varepsilon_N \gtrsim 1.6\%$.

b) two phase materials with a hard second phase $\varepsilon_N \gtrsim 4.7\%$.

The value of ε_N was then used to calculate the "permanent softening" τ_{SN} at N% reverse strain after 9% forward strain, as the difference between the forward and reverse curves.

A further X-ray study was made to determine the lattice strains in the material after 9% forward strain. Again the relative positions of two peaks were compared, the strain ε_{XRAY} calculated, and the average basic stress determined for the constrained deformation as

$$\tau_{XRAY} = \varepsilon_{XRAY} E/(1 + \nu)$$

Results for several materials were obtained using different radiation and a plot was made showing that

$$\tau_{XRAY}/\tau_{SN} = .53$$

This is an important result; it shows that the average back stress in the material is proportional to the "permanent softening" measured at N% reverse strain. Wilson pointed out, however, that τ_{XRAY} must underestimate the back stresses because of the relaxation processes likely to occur when the test pieces are cut and polished. To reduce this, strain ageing was carried out.

Wilson's work also shows that the back stress hardening is increased by

a) a larger volume fraction of precipitates

b) a finer precipitate size

c) a higher matrix elastic modulus.

He was also able to show from measurement of τ_{XRAY} that the back stress hardening was probably responsible for 0.25-0.5 of the total flow strength at 9% prestrain. These results are important, but of greater significance is the calculation of the fraction of the work hardening that was due to the back stress. This fraction depends critically on the initial yield stress and Wilson had to use log-log plots to estimate the yield stress of some of the steels. It is sufficient to indicate here that the results of these measurements show that the materials separate into three groups:

	$\frac{\tau_{XRAY}}{\tau_{WKHDG}}$
a) little permanent softening - single phase materials	$\lesssim$ 20%
b) more "permanent softening" - higher carbon steels	~ 50%
c) greatest "permanent softening" - Duralumin (Al - 3.5 - 4.5 % Cu)	~ 80%

Further calculations will be made as necessary to show that the method used in this present work to determine the back stress from the stress strain curves leads to results that are consistent with those from Wilson's X-ray studies. These calculations will be given in the chapter containing the experimental results.

Abel (1965) and Abel and Ham (1966) studied the

Bauschinger Effect in single crystals of aluminum - 4% copper alloys aged to contain the different precipitates: GP zones, θ", θ' and θ. They carried out the deformation in tension and compression at different temperatures 293°K and 80°K. The strain ranges used for most of the tests were small $\lesssim .01$.

The chief interest in this work was in the stress measurements. The departure from elastic loading in the forward sense was taken as the initial yield stress σ_0; in the reverse sense the departure gave $\sigma_{reverse}$. Their parameter to describe the Bauschinger Effect was the ratio

$$\sigma_{back}/\sigma_{forward}$$

where $\sigma_{forward}$ is the flow stress at the end of the pre-strain, and

$$\sigma_{back} = \frac{1}{2}(\sigma_{forward} - |\sigma_{reverse}|)$$

The results can be summarised as follows:

a) for small coherent, easily cut, precipitates the Bauschinger Effect is small and similar to that obtained in pure aluminum.

b) as the particles increase in size and the strengthening mechanism depends on the Orowan bypassing mechanism rather than precipitate cutting, the Bauschinger Effect increases.

c) the Bauschinger Effect is greatest for the θ' condition.

d) the Bauschinger Effect is increased at low temperatures, especially in the θ' alloy.

It was considered that the Bauschinger Effect was due to the disordering of the small cutable precipitates when they were sheared and to the large back stress in the materials containing θ' and θ particles. It was hinted that the back stress developed as the dislocations accumulated around the particles, but no details were given.

It is interesting to see in their work that the reverse yield stress was always compressive when the cutable precipitates were used. However the θ' precipitates gave rise to reverse yielding when the test piece was still in tension. It is not clear from their analysis if they accepted that this reverse plastic deformation could occur whilst the system was in tension. Their reverse deformation curves were all convex.

Abel and Muir (1972) developed the understanding of the Bauschinger Effect beyond that of Abel and Ham (1966) with the realisation that the effect is associated with the nature of plastic deformation, so that not only the reverse yielding process was affected but also the whole of the reverse stress strain curve. They accepted the fact that reverse yielding can, under some circumstances, occur during unloading when the material is still loaded in the forward sense. The idea of permanent softening was introduced, but

not really proven.

Because of the difficulties encountered in characterising the Bauschinger Effect, three new parameters were suggested. It was hoped that there then would be some uniformity in the parameters in use. The ones suggested by Abel and Muir are best introduced with the help of a sketch. In Figure 2.7 the reverse deformation is drawn in the positive stress quadrant and the cumulative strain is plotted.

1. The Bauschinger Strain Parameter, $\beta(\varepsilon)$

This is the ratio of the Bauschinger Strain (the reverse strain required to bring the reverse flow stress to the same magnitude as the forward flow stress) to the prestrain

$$\beta(\varepsilon) = \text{Bauschinger strain/prestrain}$$
$$= \beta/\varepsilon_p.$$

With this parameter, materials with no Bauschinger Effect have

$$\beta = 0$$
$$\therefore \beta(\varepsilon) = 0.$$

Abel and Muir considered that $\beta(\varepsilon)$ will usually be less than 1.0, and the possibility exists that it may have a value of 2.0. They do not explain the conditions for this value of

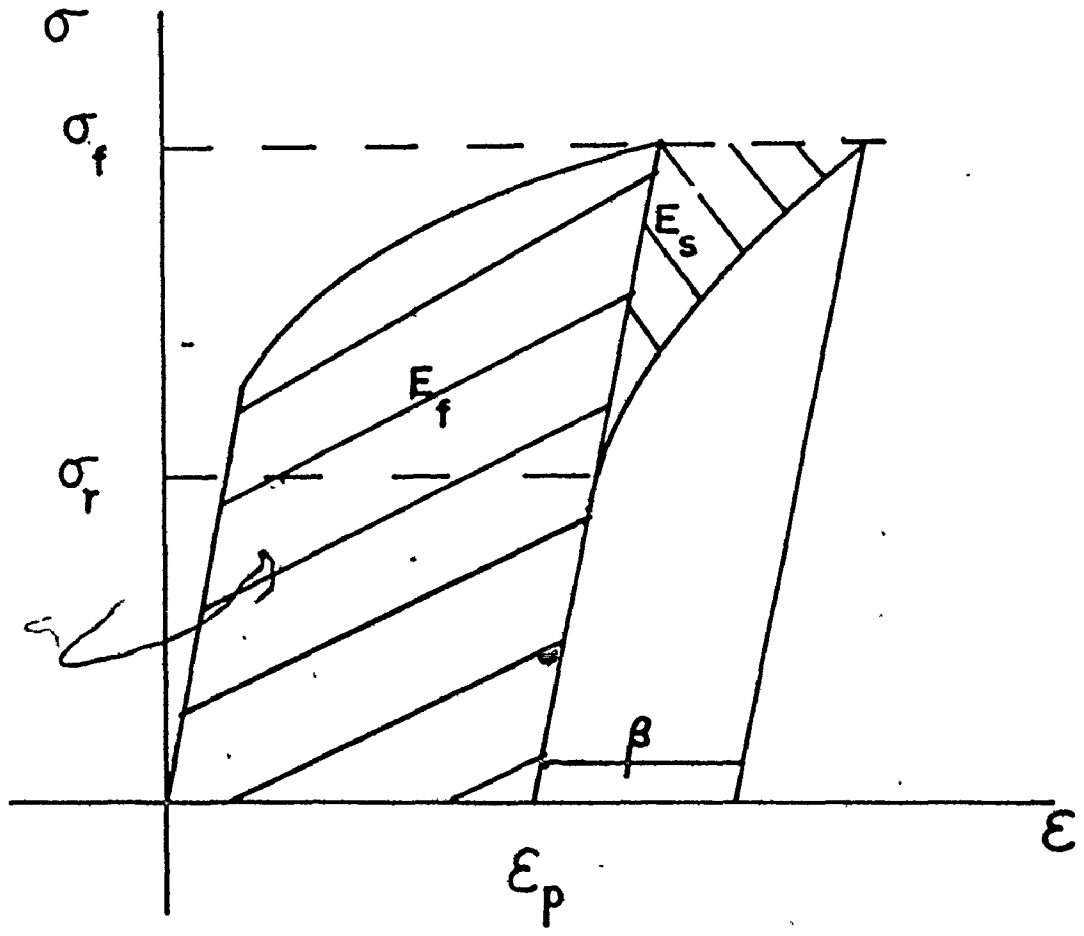

1. $\beta(\varepsilon) = \beta/\varepsilon_p$

2. $\beta(\sigma) = (\sigma_f - \sigma_r)/\sigma_f$

3. $\beta(E) = E_s/E_f$

FIG 2.7 PARAMETERS USED BY ABEL AND MUIR.

2.0, but it is possible to have processes which would lead to a result greatly in excess of 2.0.

2. The Bauschinger Stress Parameter $\beta(\sigma)$

This relates the decrease in yield stress to the flow stress at the end of the prestrain. The notation used by Abel and Muir conflicted with that used most commonly.

$$\beta(\sigma) = (\sigma_f - \sigma_r)/\sigma_f$$

The magnitudes of $\beta(\sigma)$ were not considered by the authors. However, the maximum and minimum values can be set.

a) if the material does not show a Bauschinger Effect

$$\sigma_f = \sigma_r$$

and $\beta(\sigma) = 0.$

b) if the Bauschinger Effect is very great so that reverse yielding takes place immediately the unloading commences

$$\sigma_f = -\sigma_r$$

and $\beta(\sigma) = 2.$

3. The Bauschinger Energy Parameter

It was argued that the energy parameter related the

stress and strain parameters, and that it was the best one to use.

$$\beta(E) = E_s/E_f$$

where E_s is the energy saved during the reverse deformation in bringing the stress up to the same level as the prestress. It represents the area outside the reverse stress strain curve. E_f is the energy stored during the prestrain. Abel and Muir consider that E_s is always small and that $\beta(E)$ must then be less than 1.0. However conditions can be examined in which this ratio easily exceeds 1.0.

These parameters were applied to two sets of data obtained from experiments carried out by Abel and Muir:

a) For low Carbon Steel it was found that the parameters $\beta(E)$ and $\beta(\varepsilon)$ decreased with increasing prestrain, whilst $\beta(\sigma)$ increased.

b) For the Cu-Al alloys examined, the tests were carried out to the same strain on different alloy compositions. These alloys were designed to have lower stacking fault energies and thus a greater tendency to planar slip as the aluminum content increased. At the small strain used, 10^{-4}, all the parameters increased.

Two points of interest in these results are found in the data for the alloy containing Cu - 8% Al, with a very low stacking fault energy.

(i) The Parameter

$$\beta(\sigma) = 1.6$$

is very large;

(ii) It can be seen very easily that the stress strain curves in tension compression do not show a permanent softening. In fact the gradient of the reverse deformation curve is very steep and indicates that the forward and reverse curves would cross at a strain just greater than 10^{-4} in reverse. This is important considering that many authors draw the diagram for the Bauschinger Effect showing "permanent softening".

None of the Bauschinger Effect parameters proposed by Abel and Muir have been adopted in this present study. The chief object of this work is to determine the contributions to the work hardening arising from the long range back stresses of the type investigated by Wilson. None of the parameters provides any information on these stresses.

Atkinson, Brown and Stobbs (1973, 1974) studied the Bauschinger Effect in the copper-silica system to test the earlier theory of Brown and Stobbs (1971). Copper-silica single crystals oriented for single slip were tested in tension-compression at different temperatures 77°K - 473°K, to different prestrains. The compression part of the curve was compared with a previously obtained tensile curve at the

same cumulative strain and they were able to measure the stress difference

$$\sigma_f - \sigma_r$$

where σ_f is the forward flow stress at a given cumulative strain and σ_r is the flow stress in reverse at the same cumulative strain. It was shown that this stress decreased rapidly in the first 2% reverse strain, but that at larger reverse strains it was constant. This constant value, which depended on the prestrain, temperature and volume fraction of the particles, was called the "permanent softening". It should be realised that this is the same effect as that obtained by Wilson for some materials, and considered by Orowan. When the permanent softening was compared with Wilson's work it was shown that there was a relationship between their work and Wilson's X-ray work. This gave a method to determine the back stresses in the material (or "the mean stress in the matrix" as they termed it) from

$$\sigma_{XRAY} = .53\ \sigma_{PERMANENT\ SOFTENING}$$

This result is important. The quantity sought after is the long range back stress in the material as measured by X-ray techniques. These techniques can not always be applied and it is desirable to be able to determine the back stresses from the more readily available stress strain curves. The

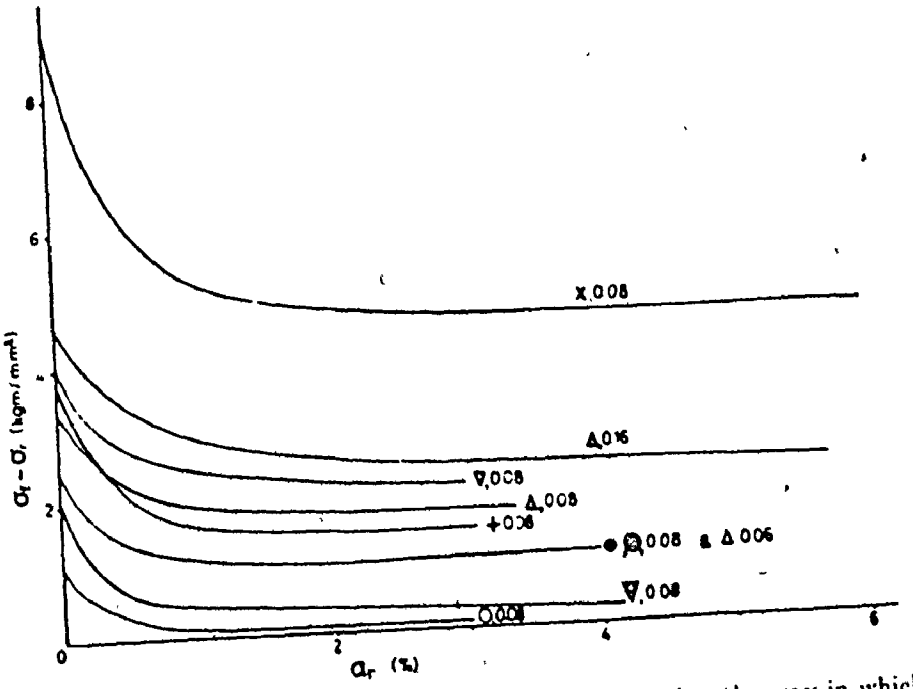

$\sigma_f - \sigma_r$ as a function of the resolved reverse strain, α_r, showing the way in which the 'permanent softening' is approached. The individual graphs are marked with the resolved forward applied strain and data symbols which are listed with the alloy and testing conditions to which they refer in table 2.

Fig. 2.8. Permanent softening in Cu-SiO_2 alloys.
(After Atkinson et al., 1974)

material, Cu-SiO_2, gave a permanent softening and the back stress was then determined.

A second approach enabled them to calibrate the very rounded part of the stress strain curve in terms of the mean stress in the matrix. They were able to show empirically that

$$\sigma_r/\sigma_f = \beta\ \varepsilon_r^{1/2}$$

at a reverse strain of ε_r measured from $\sigma = 0$. Then using their own data with that of Wilson they were able to show that

$$\beta \propto (\sigma_{XRAY})^{-1}$$

This result means that the internal stresses as measured by X-rays at a given prestrain were correlated with the shape of the reverse curve. Of interest here was that their own results fitted the master curve obtained from Wilson's work if they used

$$.53\ \sigma_{PERMANENT\ SOFTENING}$$

instead of σ_{XRAY}. A plot of β v back stress was obtained and by determining β in a given test they were able to arrive at the values of the back stress. This method works for the materials which showed a permanent softening, but it was not expected to work for those which did not show a permanent softening.

Having established that the permanent softening was equal to twice the mean stress in the matrix, the authors used it to investigate how the mean stress depended on pre-strain, temperature, volume fraction and particle size. In this work they were checking on the validity of the formula derived earlier (Brown, 1973)

$$\sigma_{MEAN} = 2\mu\gamma f \varepsilon_p^* \frac{\mu^*}{\mu^* - \gamma(\mu^* - \mu)}$$

where ε_p^* is the unrelaxed plastic strain, μ and μ^* are the moduli of the matrix and particles and γ is the accommodation factor derived by Brown from the work of Eshelby (1957). For equiaxed particles $\gamma = 0.5$. They were able to show that there is a linear dependence on volume fraction but not particle size. By calculating ε_p^* from their measured σ_{MEAN} they showed that

$$\varepsilon_p^* = \varepsilon_p$$

at small strains and low temperatures. This indicated that their formalism was reasonably correct.

The same plot of calculated ε_p^* v imposed plastic strain showed that at 77°K

$$\varepsilon_p^* = \varepsilon_p$$

up to a resolved shear strain of .06, and at 293°K this was true up to a strain of about .015. This equality means that no plastic relaxation had occurred and only Orowan loops

would be found on the particles. There would be no secondary prismatic loops. Beyond these strains, the value of ε_p^* increased more slowly, approximately parabolically, with ε_p. Then plastic relaxation was taking place by the production of secondary dislocations at the particles. The stress to cause production of secondary loops calculated from

$$2\mu\,\varepsilon_p^*$$

is close to that obtained by Ashby et al. (1969) - $\frac{7\mu}{100}$ at 77°K and $\frac{\mu}{100}$ at 293°K.

In the second part of the work, the softening at room temperature is discussed. By this is meant the time dependent decrease in the work hardening increment. It is considered to occur by the material relieving the internal stresses in such a way that it may lose its ability to recover. This softening occurs by the removal of Orowan loops by plastic relaxation and is accompanied by a small shape change in the direction of increasing deformation. They investigated the effect of the softening on the measured Bauschinger Effect.

The experiments to study this softening were carried out on materials with small particles. The specimens were deformed in tension to some prestrain at 77°K and then unloaded and left at 293°K for several days. On retesting in tension the yield stress was lower than the previous flow

stress. The softenable fraction of the work hardening increased rapidly with strain beyond a resolved strain of 0.02, reaching a constant value of about 30% at a strain of 0.08. The magnitude of the softening at any strain was equal to the sum of the magnitudes of the softening found when a crystal was softened at a series of strains up to the given strain. This result showed that the fully softened strength is a unique function of strain. Little or no softening was found in materials with large particles.

When the softening delay preceded the compression part of the Bauschinger test, it was found that an increase in the compressive yield strength resulted. Thus the softening caused a reduction in the Bauschinger Effect; the permanent softening and the roundedness of the reverse curve were both reduced. When the softening took place after increasing reverse strains it was found that the softening decreased as the reverse strain increased. For 8% forward strain the softening was zero at a reverse strain of 4%. This result confirmed the work of Wilson who showed that reverse strain reduced the internal stresses and at approximately 3% reverse strain in torsion the back stress resulting from a 9% torsion prestrain had been reduced to zero.

Gould et al. (1973, 1974) considered the work hardening process in copper alloys. As already explained in the papers by Hirsch et al. (1971) the accumulation of

Orowan loops on a slip plane surrounding a particle are stable to some small strain. For larger strains, new Orowan loops lead to the formation of prismatic loops by a cross slip mechanism. Both the shear Orowan loops and the new prismatic loops are responsible for the continued work hardening, until, as shown by Atkinson et al. (1974) and Palmer and Smith (1968), voiding takes place at the particle matrix interface. Gould et al. were interested in determining the contribution of the Orowan and prismatic loops to the work hardening process, in materials with small hard particles. To do this they carried out tests at 77°K to study the Bauschinger Effect. In many of the tests they carried out anneals at 293°K (with the specimen in the unstressed condition after the prestrain), before completing the test at 77°K.

The materials studied were Cu-Al_2O_3 produced by internal oxidation to have very small volume fractions <.05% of small particles ($\lesssim$ .05μ) with interparticle spacing ~ 0.5μ. After the annealing treatment at 293°K, it was found that the flow stress for continued deformation had been reduced. During the compression an initial high work hardening rate was obtained after a lower yield stress, and after a strain in reverse, called by them the Bauschinger Strain, the work hardening became nearly linear. The reverse yield stress τ_B was obtained by back extrapolating

the linear work hardening curve to zero reverse plastic strain; Figure 2.9. It was found that τ_B after annealing was significantly different from the same quantity obtained if no annealing were carried out. A strain dependence of the amount of recovery was observed; it was very small for small strains (< 2%) but increased to more than 30% of the work hardening increment at larger strains. This result is similar to that of Atkinson et al..

The hardening contribution from the Orowan loops was considered to be the sum of three terms,

a) a bowing term τ_b

b) a long range stress term τ_ℓ due to loops on the same slip plane

c) an image stress τ_i of the type calculated by Brown and Stobbs.

The term τ_ℓ due to loops on parallel planes was assumed to be zero.

The flow stress τ_M at some strain is then

$$\tau_M = \tau_o + \tau_b + \tau_\ell + \tau_i.$$

It was considered that τ_ℓ and τ_i would aid the reverse deformation and reverse yielding occurred at τ_B^1, when

$$\tau_B^1 = \tau_o - (\tau_\ell + \tau_i)$$

so that $\tau_M - \tau_B^1 = \tau_b + 2(\tau_\ell + \tau_i)$

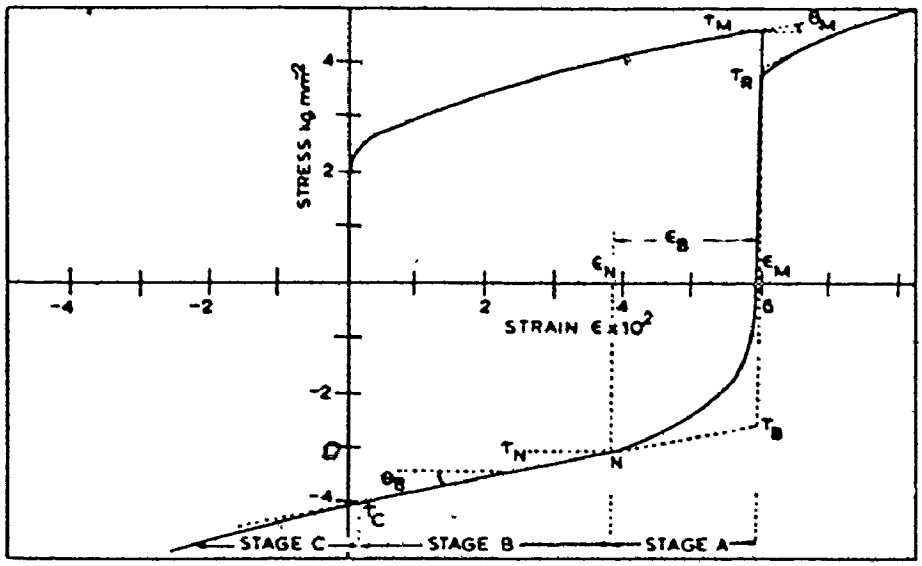

Typical experimental reverse stress/strain curve at 77°K and the measured parameters.

Fig. 2.9. Reverse Stress Strain Curve for Cu-Al_2O_3, after Gould et al. (1974).

Similarly, after recovery, the forward and reverse yield stresses differed by

$$\tau_R^1 - \tau_{BR}^1 = (\tau_b + 2\tau_\ell + 2\tau_i)_R$$

Use was made of these equations, together with theoretical estimates of τ_b, τ_ℓ and τ_i to evaluate the number of Orowan loops on the particles before and after recovery:

	number of loops	equivalent strain
Before Recovery	4 - 5	1.8%
After Recovery	1 - 2	<1%

Several methods were employed to cross check these results, but in general they all depended on equating stress differences found between the forward and reverse curves, with and without delays for recovery.

The hardening contributions from individual Orowan and prismatic loops were also calculated. One example, at 8.5% showed 5 Orowan loops and 20 prismatic loops on the particles. The work showed that about 30% of the work hardening results from the combined image and long range stress. Whilst it is not clear that all the hardening terms are linearly additive, the image stress and long range stress are considered to be additive to the hardening resulting from prismatic loops and matrix dislocations. This 30% of the hardening resulting from image and long range stresses

led to

$$\frac{\text{hardening per individual Orowan loop}}{\text{hardening per individual prismatic loop}} \geq \frac{12}{7} \sim 1.7$$

In a second theoretical calculating using the work of Hirsch and Humphreys, the value of 1.7 was obtained again. However the value was expected to depend critically on the slip line spacing.

Ibrahim (1974) has studied the Bauschinger Effect in single phase body centred cubic materials. The flow stress σ_F at a prestrain was expressed as the sum of three terms, the initial flow stress of the material σ_o, a forest hardening contribution σ_{for} and the long range elastic back stress σ_B. The elastic back stress opposed continued forward deformation and aided the reverse deformation so that

$$\sigma_F = \sigma_o + \sigma_{for} + \sigma_B$$

The reverse yield stress was given by

$$\sigma_R = \sigma_o + \sigma_{for} - \sigma_B$$

so that a Bauschinger Effect parameter could be defined as

$$B.E.P. = 2\sigma_B/(\sigma_F - \sigma_o)$$

This parameter is a measure of the fraction of the total work hardening caused by the long range back stress.

The results obtained for the B.E.P. as a function of strain at 298°K and 195°K for niobium and for Armco Iron

show that the B.E.P. is to a first approximation independent of strain and temperature, and also of the material. The most probable explanation for the constancy of the B.E.P. is that the back stress and forest contributions to the work hardening are proportional to each other and independent of the dislocation arrangement. This interpretation agrees with the Brown and Stobbs model in which both the forest and back stress contributions increase with strain.

Lasalmonie and Martin (1974, 1975) studied the Bauschinger Effect in the unidirectionally solidified Al-Al_3Ni alloy system, and discussed their results in terms of the conventional fibre composite models. In these models, some of the load is carried by the plastically deforming matrix, and part by the elastically deforming fibres. The stresses in the matrix and fibres can be calculated using these models. The authors attempted to do this and to thus explain the origin of the large Bauschinger Effect observed. They considered that the plastic deformation of the composite took place by the elastic deformation of the fibres; the matrix deformed plastically. The matrix dislocations did not cut or break the fibres, and must accumulate around them as Orowan loops. The number of these loops increases as the strain increases.

The stress to be applied to continue the forward plastic deformation is called "the flow stress of the material" by many people; unfortunately in the Lasalmonie and

Martin papers the term "back stress" is used instead. This leads to confusion as "back stress" is used differently by many other authors. This forward flow stress is considered to be made up from two parts

a) a frictional type stress, which opposes <u>all</u> dislocation motion, both forward and reverse, and hence all plastic deformation (their σ_r reversible)

b) a stress which opposes continued forward deformation, and aids reverse deformation (their σ_i, our σ_b and the $\langle\sigma\rangle_M$ of Brown (1973)).

In the first paper, fibre composite theory is used to determine σ_i in the matrix, which they called σ_{im}. The values calculated are very small and it seems they calculated only a small part of the stress which aids the reverse deformation. They should really be interested in the stress which aids the reverse deformation in the composite, not merely in the matrix. Other work in single phase materials shows that this quantity is very small when compared with that in the composite material.

One possible reason for the authors' preoccupation with their stress σ_{im} in the matrix is that plastic deformation takes place by matrix dislocations moving until they are stopped by obstacles. The dislocations move only in the matrix, and the interaction stopping them is in the matrix; however, the particles or fibres are responsible for

this interaction.

Their evaluation of the stress σ_{im} in the matrix is very involved and relies heavily on fibre composite theory, with its approximations, for example the modulus of the composite is

$$E_c = E_f V_f + E_m V_m.$$

The values of σ_{im} arrived at are small, an order of magnitude smaller than their theoretical values, determined from the models proposed by Hazzledine and Hirsch (1974) and Brown and Stobbs (1971). Clarke and Lilholt (1975) pointed out that a wrong formula was used to calculate σ_{im}. However, from the way the authors separate the contributions to the load carrying ability into those from the fibre and matrix, it is not clear they should be using the Brown and Stobbs formulation. Nor is it clear if they understand the image stress (later called mean stress) in the sense in which it was used by Brown and Stobbs (1971) and by Brown (1973).

In the second paper, Lasalmonie and Martin (1975) were prompted to calculate a different quantity again using fibre composite theory. This is the difference $\Delta\sigma$ between the flow stress in the forward direction and the yield stress for reverse deformation after the forward prestrain. Again this calculation is subject to the same approximations

as the fibre composite theories, but the stress differences calculated are close to those evaluated by Clarke and Lilholt from the published curves of Lasalmonie and Martin (1974).

Clarke and Lilholt evaluated the stress differences by extrapolating the almost linear portions of the reverse plastic deformation curves to the elastic unloading line. They obtained results that showed that the stress differences $\Delta\sigma$ depend on the forward plastic prestrain. The shape of the curve $\Delta\sigma$ v prestrain shows the following important characteristics:

a) it is linear at small strains

b) at larger strains it departs from linearity with the stress difference increasing more slowly

c) the gradient of the linear portion agrees well with that expected if the formula given by Brown and Stobbs (1971) is used

d) the departure from linearity agrees with the experimental evidence of Hertzberg (1965) that the matrix dislocations are beginning to penetrate and cut the fibres at plastic strains of order .015.

Clarke and Lilholt then concluded that the Al-Al_3Ni composite system deformed by the Orowan process with the accumulation of shear loops around the fibres until the fibres were cut. Until this happened there was no relaxation of the Orowan loops.

These three papers can be summarised as follows:

1. Lasalmonie and Martin (1974) published some reverse deformation curves for the Al-Al_3Ni alloy system, but made an error in calculating their image stress.
2. Clarke and Lilholt (1975) showed how the curves could be analysed to give a stress difference of $\Delta\sigma$, which agreed with the value of $\Delta\sigma$ calculated for the system using the Brown and Stobbs theory.
3. Lasalmonie and Martin (1975) used standard fibre composite theory to calculate the same $\Delta\sigma$ as Clarke and Lilholt. It is not clear, however, that they look on this $\Delta\sigma$ in the same way as Clarke and Lilholt.
4. There seems to be a considerable contradiction between the conclusions of Lasalmonie and Martin (1974) and the first paragraph of Lasalmonie and Martin (1975).

The results of two other studies will be briefly presented. These represent attempts made to examine from a continuum mechanics approach the relation between prestrain and the magnitude of the Bauschinger Effect. In the work the area of interest is the consideration of how the increments in work hardening are partitioned between the back stress and the other contributions. The back stress is the stress responsible for the large Bauschinger Effect.

Kishi and Tanabe (1973) consider that the work hardening has three contributions

a) isotropic hardening, which could be represented by an expansion of the yield locus.

b) anisotropic hardening, in which the shape of the yield locus changes, as represented by Hill.

c) kinematic hardening in which the yield locus is translated, and is the hardening responsible for the Bauschinger Effect. This is the quantity of interest in the study.

The experiments were carried out in torsion on many materials, and different reverse offsets were used to determine the yield stress in reverse; the 0.001 was finally chosen. The Bauschinger stress was defined as

$$\tau_B = \tau_F - |\tau_R|$$

where τ_F and τ_R are the flow stress in forward sense and yield stress in reverse. The relationship

$$\tau_B = K \gamma_F^m$$

was established empirically, where γ_F is the forward prestrain, m a constant called the Bauschinger Effect exponent, and K the Bauschinger Effect constant.

The magnitude of the Bauschinger Effect depends on K and m, and the variation of these for different materials was investigated.

The work suggests that the reverse yield stress τ_R for materials deforming by a strain γ_F can be written as

$$\tau_R = \tau_F - \tau_B$$

$$= \alpha_o \gamma_F^n - K\gamma_F^m$$

in which use has been made of the relationship between forward flow stress and prestrain. The indication is that the reverse flow stress can then be described in a way similar to that used for the forward flow stress. However, the authors did not make any correlation between K and m and the microstructural parameters of the alloy. Only the grain size is given, but here the correlation is not a simple one, as the variation of grain size seems to have opposite effects in different materials.

In a recent paper, an attempt has been made by Gupta and Kodali (1976) to establish a relationship between the Bauschinger Stress and the prestrain for a wide range of materials. It is not clear how the Bauschinger stress σ_B was obtained, but it seems to have been calculated from

$$\sigma_B = \sigma_F - \sigma_R$$

where σ_F and σ_R are the flow stress at a prestrain in the forward sense and the yield stress in reverse.

The data obtained by Gupta and Kodali indicate a relationship of the form

$$\sigma_B = m \ln \varepsilon_p + K$$

which is a semi log dependence, whereas the relationship

favoured by Kishi and Tanabe was log, log. The constants m and K are different from those of Kishi and Tanabe. Since both expressions are empirical, it can be seen that the experimental results can be plotted in different ways.

The saturation of the Bauschinger stress with prestrain is at variance with the Kishi and Tanabe formula, and Gupta and Kodali argue that their formulation is the better. However, it should be pointed out that the strain range used by Gupta and Kodali to investigate the semi log dependence was not as large as their experimental strain range. For example, some of their data for steel and aluminum-copper are not plotted, and their inclusion causes the resulting plot to change from linear to non-linear. This must cause some objection to be raised about the validity of the semi log formula. At best it is valid over a much smaller strain range than that indicated.

There is one further point to be made about this paper. Gupta and Kodali were interested in possible differences in the Bauschinger Stress when measured in tension-compression (TC) and compression-tension (CT). There has been some experimental evidence that the Bauschinger stress is greater for CT than for TC. This result was confirmed for the Al-Cu alloy it was claimed to be observed only at small strains. However, their figure 2 shows that the curves drawn through the data points are identical at all

strains up to 8%, after which there is some small difference, with CT being slightly higher. It is not clear, however, that any significance can be attached to this as the difference is small.

SUMMARY OF LITERATURE REVIEW

The principal features of the work hardening models and reverse deformation studies can be summarised as follows:

The work carried out by Wilson has indicated that there are long range back stresses produced during the plastic deformation of materials. The back stresses were shown to be responsible for the Bauschinger Effect. Alloys with a hard second phase were shown to have a large back stress and a large Bauschinger Effect, whilst single phase alloys had small back stresses and Bauschinger Effects. However, Wilson did not indicate in detail the origin of the back stress in the alloys, beyond showing the correlation with the strength of the second phase.

Later models have attempted to explain the origin of the work hardening. The principal contributions to the work hardening in two phase alloys are:

1. the long range back stress arising from the elastic deformation of the particles in a plastically deforming

matrix. The calculation of this quantity was carried out by Brown and Stobbs, by Brown and Clarke, and by Tanaka and Mori, all using the results of Eshelby. The elastic deformation of the particles is directly dependent on the number of Orowan loops accumulated at them. If plastic relaxation occurs, the rate of accumulation of Orowan loops is decreased, prismatic loops are formed and the displacement at the particles increases less rapidly. Then the long range back stress does not increase linearly with the imposed strain.

2. long range back stresses arising from the interaction of mobile dislocations with coplanar Orowan loops on the particles. This contribution was included in the model of Hazzledine and Hirsch, but it only affects the dislocation source giving rise to the coplanar loops. Averaged over the test piece, the contribution to the total back stress is zero.

3. interaction of mobile dislocations with secondary dislocations. This type of hardening is that found in single phase materials and in two phase materials at large strains. The interaction is over a short range and can not make a large contribution to the long range back stress until the secondary dislocations have produced tangles etc. which cause them to behave almost like particles. The hardening is predominantly

frictional in nature in that it affects all dislocations independently of the direction in which they move.

4. Source shortening, arising from the Orowan loops standing off from the particles and reducing the critical radius to which the mobile dislocations must bow in order to pass between the particles. This hardening does not lead to a long range back stress, and the work used in bowing the dislocation between the particles is dissipated.

The relative importance of these contributions depends on the details of the deformation processes. In alloys in which the long range back stress is the dominant hardening process, the Bauschinger Effect will be large. If the work hardening arises entirely from the interaction between glide and forest dislocations, the Bauschinger Effect will be small. Because of the way that plastic relaxation occurs at the particles it is possible to have the deformation dominated by back stresses at small strains, whilst at larger strains the forest hardening dominates. Then the magnitude of the Bauschinger Effect will depend on the imposed strain.

CHAPTER III

EXPERIMENTAL PROCEDURES

The principal part of the experimental work described in this thesis concerns a study of the Bauschinger Effect in an aluminum-copper alloy. The work required the growth and characterization of single crystals of the material, and the production of suitable test pieces for use in tension compression tests, at strains up to 0.1. It was also necessary to examine the test pieces by X-ray and TEM techniques, to determine the structural parameters responsible for the tensile work hardening and the structural changes occurring during reverse deformation. The details of the procedures will be described below.

3.1 Preparation of Single Crystals

The material used in this work was supplied by Alcan International Ltd. in the form of hot rolled plate. The chemical analysis carried out on the metal using spark analysis techniques gave, in weight per cent: 3.62 Cu, 0.002 Fe, <0.001 Mg, 0.002 Si, remainder Al.

The production of single crystals was carried out by directional solidification using a modified Bridgman

technique. A rod of the material was melted in a graphite mold surrounded by an argon atmosphere, using a moving furnace. The plate, 0.5" (12.7 mm) thick was cut into sections and machined to rods approximately 0.40" (10 mm) diameter, 12" (30 cm) long, pointed at one end. The pointed end was fitted into the pointed bottom of a split graphite mold, and the two parts of the mold carefully bound together to minimise the formation of fins and to reduce the tendency for the alloy to leak out of the mold. The material found most satisfactory for the binding was chromel alumel thermocouple wire. It had good oxidation resistance and did not expand too much during heating in the furnace.

The mold was inserted into a vertical Inconel Furnace tube and supported on a piece of graphite rod. A steady stream of Argon was passed through the Inconel tube. The furnace temperature was set for 760°C and after about 1 hour the motor drive to raise the furnace was switched on. The motor drive passed through a gear reducer to give a speed of about 1 inch per hour. The motor did not actually lift the furnace - it merely moved a pair of balance weights which were attached to the furnace. It took approximately 36 hours for the furnace to traverse the length of the Inconel tube, prior to operating a microswitch to shut off the power to both the motor and the furnace. There was water cooling at the top and bottom of the Inconel tube.

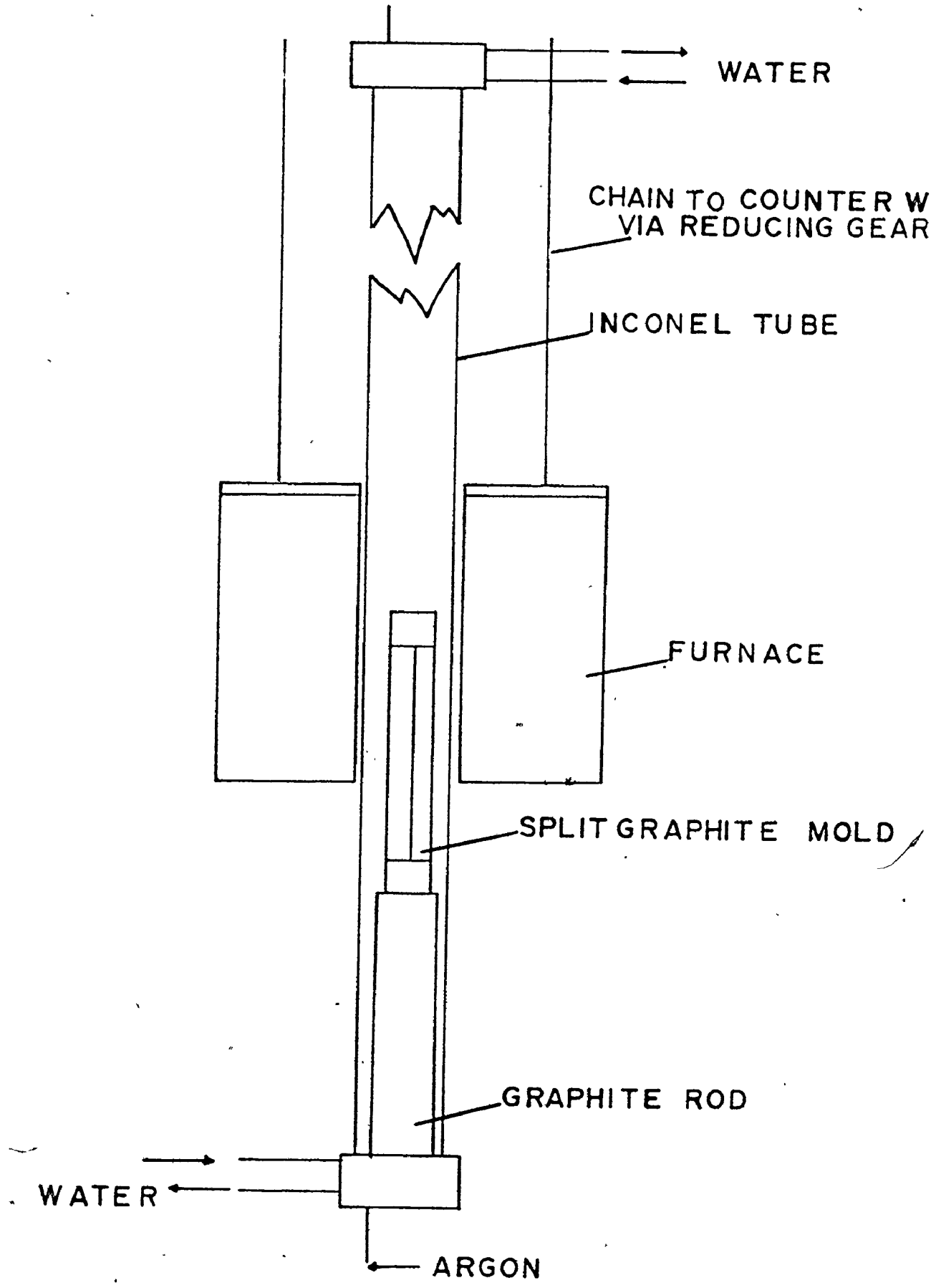

FIG. 3.1 CRYST L G 'ING T IS

The water cooling at the bottom was necessary as it provided a vertical temperature gradient in the mold. A schematic diagram of the apparatus is shown in Figure 3.1.

Some 4 hours after the furnace was switched off, the graphite mold could be removed from the Inconel tube. There were occasional fins on the rod and the top was very irregular. In later melts a short rod of graphite, diameter just less than 0.4" (1 cm), was placed on top of the alloy rod. It was found in these melts that the weight of the short graphite rod was sufficient to reduce much of the waste at the top of the alloy rod.

The end pieces, top and bottom 3/4" (2 cm), were cut from the rod with a jeweller's saw and their flat surfaces mechanically polished on silicon carbide paper to #600, and then on diamond paste to 1 μ. Etching these polished end pieces in Keller's Reagent showed that there were small grains at the perimeter of the bottom piece, but none were seen at the top piece. Further slices approximately 1/4" (6 mm) thick were removed and subjected to chemical analysis for copper content to check on the possibility of segregation effects. The results of the analysis showed that there were slightly different amounts of copper in the top and bottom. The results of 10 tops and bottoms show

TOPS: 2.96 $\pm$0.10 wt% Cu

BOTTOMS: 3.08 $\pm$0.15 wt% Cu.

There is thus a net loss of copper during the solidification. This has been observed by others (Brown, private communication). The cutting of the different pieces from the solidified rod left some 10" (25 cm) available for the production of test pieces.

The orientation of the top and bottom of the remaining solidified rod were determined from the analysis of back reflection Laue X-ray photographs. Three or more Laue photographs were taken from different places on the top and bottom, and their identity was considered to be confirmation of the etching study that the rods were single crystals. The as-grown structure showed some coring and lateral segregation. To reduce this segregation the single crystal rods were annealed for 10 days at 530 $\pm$ 10°C. Optical micrographs of the etched surfaces taken before and after the anneal showed that it was sufficient to remove the segregation on a horizontal section, but an order of magnitude calculation showed it would have little effect on the vertical segregation. Electron microprobe analysis of the etched surfaces showed the segregation before the anneal, but did not detect it in the quenched material after the anneal. The orientations of the crystals are shown in Figure 3.2.

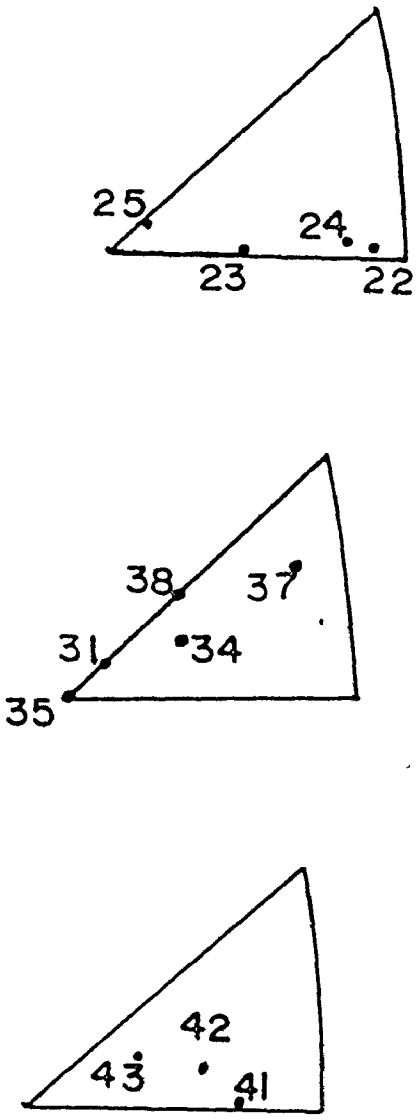

FIG. 3.2 SINGLE CRYSTAL ORIENTATIONS

CRYSTAL SX	SCHMID FACTOR
22	.45
23	.49
24	.45
25	.43
31	.45
34	.50
35	.40
37	.43
38	.45
41	.48
42	.50
43	.50
100	.40

TABLE 3.1 SCHMID FACTORS FOR SINGLE CRYSTALS

3.2 Preparation of the Test Pieces

It was decided to use test pieces with square cross sections for the mechanical testing. There were two reasons for this choice:

(i) it is easier to take Laue Photographs from flat faces than from cylindrical test pieces;

(ii) it was desired to carry out some slip plane trace analysis to determine the planes on which slip was taking place.

Attempts to produce these square cross sections by using a U-shaped tool in a Servomet Spark cutting machine were not successful. Two parallel faces could be cut using this tool, but when the attempt was made to rotate the test piece through 90° to make the second set of cuts the axis of rotation could not always be made to coincide with the axis of the test piece. The resulting shape was usually skew and not suited for mechanical testing. There was a small amount of wobble in the goniometer; it was responsible for the difficulty experienced. A further objection to the use of this technique is its speed. It took approximately one day to make each cut and a brass U-shaped tool was worn out in the process.

The crystals were hard and it was decided to have them machined in the workshop by a skilled machinist. This

machining raised the problem of defining the amount of damage in the surface layers. In all cases the test pieces were made to specification and the gage length was carefully finished by hand with #600 silicon carbide paper before an electropolish. The final width was at least .005" smaller than that obtained from the machine shop. That the final surface layers were not severely damaged was confirmed by the Laue photographs. These showed extensive asterism before and after the silicon carbide polishing, but it was removed as the electropolishing progressed. The Laue photographs at zero strain in Figures 4.20-4.22 indicate the surface quality, but are not to be interpreted as standards of that quality. The type of finish on #600 paper followed by electropolishing was used in thin foil preparation for transmission electron microscopy. No evidence of damage was detected in this work and it is assumed that the test pieces were aged to the θ' condition after the completion of the electropolish. This procedure included heating to 550°C, which is equivalent to an annealing process.

The specifications of the test pieces were:

a) gage length 0.55" (1.27 cm)

b) gage width, square, some 0.18" x 0.18" (.46 cm x .46 cm)
most 0.25" x 0.25" (.64 cm x .64 cm)

c) shoulders, cylindrical, diameter 0.44" (1.12 cm)
length 0.75" (1.9 cm).

The ratio of gage length to diameter was kept as small as possible to reduce the tendency for elastic buckling during the compression part of the tests. Any elastic buckling would lead to plastic buckling and a localisation of the strain. There were a maximum of 4 test pieces available from any one single crystal.

When the gage length had been polished with #600 silicon carbide paper the shoulders were laquered with "Microstop" and the gage lengths electropolished in methyl alcohol/nitric acid (3:1) solution at (-10-0)°C. This electropolish removed the silicon carbide marks and produced a clean surface. The test pieces were then aged to θ' using the following heat treatment sequence:

a) 2 hours at 550 ±5°C, air furnace
b) quench into cold water
c) 3 hours at 300 ±2°C, air furnace, followed by air cooling

After the heat treatment was completed, the gage lengths were subjected to a further electropolish in the methyl alcohol/nitric acid solution. Laue photographs were obtained from the sides of those test pieces which were used in the study of the development of asterism.

3.3 Mechanical Testing

The majority of the mechanical tests were carried out on an Instron TTC floor model testing machine, with an FR cell, which could be used up to 10,000 pounds load for tests in tension and compression. To perform the tension-compression tests it was necessary to use a special rig, mounted on the underside of the crosshead. This rig had been designed by Watt (1967) for use in the study of the fatigue of copper single crystals. It was designed carefully:

a) to be rigid

b) to allow no back lash and no pause on going from tension into compression

c) to allow no lateral displacement

d) to have a very small friction; less than 2 pounds (1 kg)

e) to be suitable for tests at temperatures from 77°K to over 373°K

f) to be capable of being aligned such that the tension-compression axis coincided with the axis of the rig

g) to have conical specimen grips such that the test piece could be aligned in these grips and then inserted into the rig. Then it was known that the specimen axis coincided with the tension-compression axis. This design feature is of great importance during compression

tests, as any non alignment of the axes will lead to elastic/plastic buckling.

The setting-up of the rig and its alignment on the Instron testing machine took the major part of a day, because of the detailed alignment procedure. This procedure is described in great detail by Watt (1967). The removal of the rig from the testing machine could be carried out in a few minutes. The rig is shown in Figure 3.3.

When the rig was satisfactorily aligned it was necessary to fit the test piece into the conical specimen grips such that its axis coincided with the axis of the grips. This step was carried out with the help of a gallows type rig, on which a rod, diameter 0.440 inches, was arranged so that its axis coincided with the axis of a male specimen grip when both the rod and grip were securely fixed. The specimen was inserted into the grip and its free end kept close to the lower end of the 0.440 inch diameter rod. Eight set screws were tightened so that the top of the specimen and the bottom of the rod showed no lateral displacement. The set screws were tightly fixed in position and it was found that they were impressed into the specimen shoulder. The alignment was checked further by rotating the grip in its seating, making sure that the zero lateral displacement was still maintained.

The specimen and grip were then removed from the

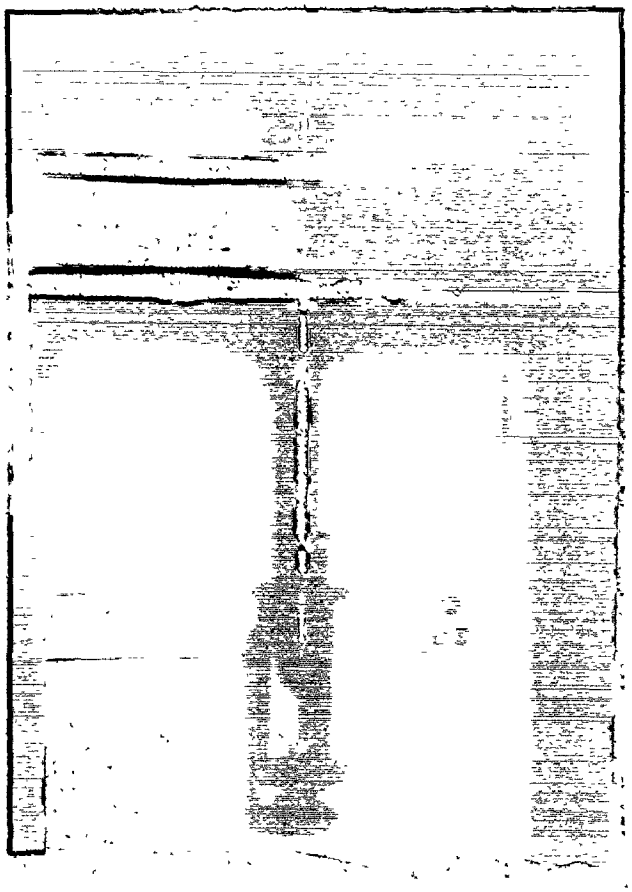

Fig. 3.3. Tension-compression rig on Instron Testing Machine. Male specimen grips not shown.

rig and the second male grip fitted to gallows rig. The free end of the specimen was fitted into it and the conical end of the other grip was aligned with a second rod. Again 8 set screws were tightened onto the specimen shoulder and the alignment checked by rotating the male grip about its axis. This procedure arranged the specimen axis to coincide with male grip axes. It was already arranged to have the testing rig arranged so that the axes of the female grips on the rig were coincident with the axis of the rig. Then when the specimen and male grips were fixed into the female grips the axis of the test piece would coincide with the axis of the testing rig.

The test piece and grips were carefully set into the testing rig. It had been determined that 4 turns were sufficient to tighten down the nut on the bottom male grip. The top grip was set in place first and tightened, then the crosshead raised to insert the lower grip. Strict control was kept over this part of the procedure; the applied loads were kept at values less than 40 pounds, which represents an applied stress of about 1 ksi (7 MPa). This stress is much smaller than the yield stress of the material (~5 ksi, 34 MPa). This care was necessary for two reasons:

a) to know the initial yield stress so that the work hardening could be determined. Any overloading in tension

will lead to an erroneously large yield stress, whilst any compressive overload will cause an erroneously small yield stress in tension.

b) to maintain control over the strain history of the specimen.

The crosshead was raised manually until the 4 tightening turhs were obtained on the lower grip. Here care was also necessary to prevent the test piece being twisted whilst the nut was being tightened.

In the tests the loads were recorded on the chart recorder; the load cell and load amplifier had previously been calibrated. An Instron tensile strain gage extensometer (.50" $\pm$50%) and amplifier were used to measure the elongation. They also had to be calibrated. The usual calibration was that, on Range #1, 10" of chart were equivalent to a tensile elongation of 0.02". Thus, this most sensitive range was such that each inch of chart represented a tensile strain of 0.4%.

The extensometer was carefully fitted to the gage of the test piece, taking care that the knife edges and clips were securely seated. This led to some little scratching of the specimen surface. The range and zero point for the extensometer were selected. It was usual to start the test with the pen some 2" above the chart zero, leaving about 8" of chart to contain the forward prestrain. This

starting position was chosen to prevent the extensometer exceeding its allowed chart travel during the reverse deformation back to zero strain. The zero control of the load amplifier was adjusted to give zero load at the 4 or 5 position on the 10 "inch" scale. The Instron amplifiers were known from calibration to be linear. The fitting of a test piece into the testing rig required some two hours.

Here the significance of an operation carried out at the start of the rig alignment procedure can be mentioned. Two large nuts on the underside of the crosshead on the main drive screws were tightened hand tight. Then the crosshead could not move with respect to the screw threads when the machine went from tension into compression. If this operation is not carried out there is a slight pause at approximately 400 pounds in compression, in each direction.

The crosshead was moved down at 0.01 inches per minute (.25 mm/minute) until the chart showed that the desired elongation had been reached. The crosshead motion was reversed, so that the test piece was unloaded and then compressed. The only stop occurred at the end of the prestrain when the crosshead motion was reversed. On the Instron machine this reversal happens without delay. The reverse deformation was stopped at a point which indicated that the test piece had a zero net strain. This required

some guesswork; it was important to have zero net strain in only a few of the tests - those in which the asterism was studied.

On completion of the deformation in tension-compression the test piece was examined for buckling by the cathetometer used in the alignment of the rig. If no buckling took place the reflections in the test piece and cage were all parallel. In those tests which buckled the reflections in the specimen were not parallel to those in the cage. The results from such tests were not used.

The majority of the tests were carried out at 25°C (298°K), with some at 77°K and 373°K. These tests at 77°K and 373°K required much more care than those at 25°C. There were two main problems encountered at 77°K:

(a) when the Dewar of liquid nitrogen was being raised around the cage, the stainless steel (used in the cage construction) and the test piece cooled and contracted at different rates. The crosshead had to be moved using manual control to keep the applied load within the set limits.

(b) there was a necessary delay as the apparatus cooled down to 77°K. The reduction of the boiling rate was one indication; a second and better one was the constancy of the small tensile load on the specimen due to the contraction of the long rod connecting the test

piece to the load cell. This load was always tensile after a few minutes. It was necessary to wait until it was constant and could be removed by a careful adjustment of the crosshead position. The delay for this part of the procedure was some 30 minutes.

The tests at 373°K had corresponding problems.

3.4 Laue Photographs

In some tests the development of asterism was studied during the deformation history. Two Laue photographs were taken of adjacent side faces of the test piece before testing. The X-ray tube used had a Tungsten target; the operating conditions were 50 KV, and 12 mA, white radiation; the exposure time was 6 minutes with a collimater .5 mm, and specimen-camera distance 3 cm.

The test piece and grips were fixed into the testing rig and a predetermined strain imposed, the specimen unloaded and removed from the rig. The Laue photographs were repeated. A rig was designed to hold the test piece and grips during the photography so that the same area was photographed each time. The test piece and grips were inserted into the testing rig, the compression carried out to zero net strain and unloaded. The Laue photographs were repeated. Some of the tests then required a further

compressive deformation and were then rephotographed. The inserting and removing of the test piece was a tedious process, and made this part of the experimental work very time consuming.

3.5 Transmission Electron Microscopy

The transmission electron microscopy was carried out on a Philips EM300 at 100 KV using a single tilt or a tilt-rotation specimen holder. Foil preparation from the test pieces involved the following steps:

i) Cutting of slices, at a predetermined angle to the tensile axis, using a Servomet Spark Cutting Machine. The cutting tool was a slowly moving continuous Molybdenum wire, 0.003" diameter. The slices were cut to be 0.02" (0.5 mm) thick, using control #6. Most cuts required at least 1 hour.

ii) Discs 3 mm diameter were cut from these slices using a thin walled copper tube 3.3 mm internal diameter as a cutting tool in the Servomet.

iii) Careful mechanical polishing to reduce the thickness to 0.005 - 0.007" required a special jig. A stainless steel cylinder, 1" diameter, 1" high, was drilled and tapped with a hole 3 mm diameter. A screw was inserted from the top and the 3 mm disc was placed in the bottom. The surface

tension of the water used to lubricate the #600 silicon carbide paper was sufficient to keep the disc in position. The screw was turned to expose the disc to the paper and the process continued until both sides of the disc were polished and its thickness was in the range 5-7 x 10^{-3} inches.

iv) The electropolishing was carried out in a jet polishing rig, gravity fed from a height of about 3 feet (1 metre). The electrolyte was the mixed acids:

40 parts phosphoric acid

30 parts acetic acid

20 parts nitric acid

10 parts water

cooled before use to (-10-0)°C. The electrolyte was delivered via Tygon tubing and #18 stainless steel hypodermic needles about 1 cm from the specimen. The 3 mm specimen disc was contained in a Teflon holder, described by Morrison (1975), so that a platinum wire could be kept in electrical contact. A DC power supply to 100 volts, 1 amp was arranged so that the specimen and platinum wire were positive, and the stainless steel needles were negative. During the polishing the voltage was kept at 70-80 V and the current at 0.2 amps. Maintaining good contact between the platinum wire and the specimen was often difficult owing to preferential attack at the point of contact on the disc. The

polishing continued until the specimen was just perforated. The onset of perforation is difficult to detect unless there is some back lighting. A light source was attached to a 0.5" diameter Perspex rod and the free end of the rod positioned close to one side of the specimen. The light coming through the perforation was the signal for manually switching off the power supply and the rapid washing of the Teflon holder and specimen in methyl alcohol.

This polishing technique sometimes gave foils which were heavily etched and could not be used. Attempts were made to improve the polish by using the above technique to produce dimples on the faces of the sample. The thin disc was then removed and the electropolishing continued in methyl alcohol/nitric acid mixture (3:1) at about -60°C, using a stainless steel cathode and holding the thin disc in fine stainless steel tweezers (anode) at 10-15 volts. The polishing was stopped at the first perforation and the disc washed in methanol.

The foils obtained were examined in the EM300 using both bright and dark field microscopy. The dark field work made use of both matrix and precipitate reflections. The techniques employed are described in more detail by Hirsch et al. (1965).

3.6 Material Used

The material used in this study is the aluminum copper alloy, containing 3.6 wt% copper. It has been shown that on remelting to produce single crystals the copper content reduced to 3.0%. The heat treatment available for the alloy can produce a variety of different metastable precipitates. The review by Kelly and Nicholson (1963) discusses them in detail. It is sufficient to indicate here that ageing process used leads to the precipitate sequence:

$$\text{GP zones} \rightarrow \theta' \rightarrow \theta$$

with the result that after 3 hours at 300°C the single crystals contain θ', whilst the polycrystalline material contains θ' in the middle of the grains and some θ in the grain boundary.

Much work has been carried out,(Kelly and Nicholson (1963)),on the nature of the precipitates. The θ' particles are ordered arrangements of the aluminum and copper atoms, formula $CuAl_{1.8}$, with a tetragonal unit cell, being a distorted CaF_2 structure with:

$$a = 4.04 \text{ Å}$$
$$c = 5.8 \text{ Å}$$

The precipitates are thin discs, the c axis of the cell being perpendicular to the habit plane. There is an orientation

relationship for θ' with respect to the matrix α,

$$\{100\}_{\theta'} \; //\{100\}_{\alpha}$$

It can be shown that there is a misfit of about 8% between the θ' and α normal to the habit plane (Weatherly and Sargent, 1971). This misfit causes the c dimension to remain small, and coarsening takes place principally by the increase in plate diameter. This misfit also causes the particles to be coherent on the flat faces, but incoherent in the c direction. It is then classed as semicoherent (Park et al., 1970).

In this study the principal precipitate was θ', obtained by ageing at 300°C for 3 hours after solid solution treatment at 550°C for 1-2 hours. The ageing to θ' leads to an increased work hardening rate over that of the solid solution single phase material of the same composition. However, the yield strength of the alloy aged to θ' is close to that obtained for the single phase alloy of the same composition as the matrix in the θ' alloy. Russell and Ashby (1970) carried out such tests at room temperature; the yield stresses are given as:

	τ_o kg/mm^2	τ_o ksi	τ_o MPa
Al - .45% Cu 2 hours/550°C	.4	.6	3.9
Al - 2% Cu 50 hours at 300°C	1.2	1.7	11.8
Al - 3% Cu 12 hours at 300°C	.4	.6	3.9
Al - 4% Cu 4 hours at 300°C	1.2	1.7	11.8

Weatherly (1970) has studied the defects found in the θ' particles in the Al-Cu alloy. Since the structure of θ' is made up from alternate layers of copper and aluminum atoms, with the copper planes not being close packed there are three possible antiphase boundary (APB) vectors $\underline{R}$:

$$[\tfrac{a}{2},\tfrac{a}{2},0],\ [\tfrac{a}{2},0,\tfrac{c}{4}],\ [0,0,\tfrac{c}{4}]$$

The permitted (h k ℓ) reflections in θ' are given by

$$h + k + \ell = 2n$$

and using the condition that APB's are visible for a given reflection, $\underline{g}$, when:

$$\underline{g} \cdot \underline{R} \neq \text{INTEGER},$$

it was shown that the best reflection to use was of the type [101] for θ'.

By using other precipitate reflections it was shown

that the more common fault vectors are

$$[\tfrac{a}{2},\tfrac{a}{2},0] \quad \text{or} \quad [0,0,\tfrac{c}{2}]$$

which give a lower energy fault than the $[\frac{a}{2},0,\frac{c}{4}]$ vector. The boundaries were parallel to $[100]_{\theta'}$ and $[010]$, parallel to $\langle 100\rangle_{A\ell}$ and must lie on $\{10\ \ell\}_{\theta'}$ planes. The most probable value for ℓ in the thin platelets is zero.

Some work was also carried out on material which had been given a 5% deformation by rolling. After a low temperature recovery anneal the APB's were identified. Analysis showed that they had vectors $[\frac{a}{2},\frac{a}{2},0]$, and that their number had increased by an order of magnitude over that in the material before deformation. Their presence indicated that the particles had been cut by matrix dislocations.

The volume fraction of θ' present in the aged alloy was determined by calculation. The method followed that used by Boyd (1966) in a study of the calorimetry of the ageing process the alloy, and for which the volume fraction had to be established. The value was calculated from the phase diagram as modified by Beton and Borelius:

$$V_f = V_{\theta'} \cdot c \cdot n \,/\, V_\alpha \cdot c_{\theta'} \cdot n_{\theta'}$$

where $V_{\theta'}$ is the volume of θ' unit cell $= 95.1 \times 10^{-24}$ cm^3

V_α is the volume of matrix unit cell $= 66.5 \times 10^{-24}$ cm^3

n is number of atoms per matrix unit cell = 4

n_θ, is number of atoms per θ' unit cell = 6

c_θ, is atomic concentration of copper in θ'($CuAl_{1.8}$) = .36

c is atomic concentration of copper which precipitates as θ'

This last quantity must be determined from the phase diagram at the ageing temperature. At 300°C the solubility of Cu in α is .45 wt%, and this must be subtracted from the copper content of the alloy.

CHAPTER IV

EXPERIMENTAL RESULTS

In this chapter the experimental results from the study of the Bauschinger Effect will be presented in three sections to cover the mechanical testing, the Laue X-ray photography and the transmission electron microscopy. With respect to the mechanical tests, it will be shown that the method used to measure the Bauschinger Effect has led to results which are internally consistent and almost identical to those obtained by Wilson using X-ray techniques.

4.1 The Mechanical Tests

In the study of the Bauschinger Effect, the quantity of greatest interest was the long range back stress, σ_b, or the mean stress in the matrix (as called by Brown and Clarke, (1975)). This is the stress which is developed in the material during its forward plastic deformation and which both opposes the continued forward deformation and aids the reverse deformation. It is a back stress of the same type as studied by Wilson (1965) and by Wilson and Konnen (1964). A second quantity σ_b/work hardening increment also was determined. It represents the fraction of the work

hardening which can be ascribed to the long range back stresses.

The basis for the method used to determine the back stress was to consider the flow stress, σ_f, at some pre-strain, ϵ_p, to be made up from the sum of three contributions

$$\sigma_f = \sigma_o + \sigma_b + \sigma_d$$

where σ_o is the initial yield stress of the alloy; in some alloy systems this is the Orowan stress, but in this alloy, with an overaged second phase, the particles are large and not closely spaced. The yield stress of the material is then controlled by the solid solution hardening. There are three pieces of evidence for this claim:

a) a test reported later, carried out on the single phase material obtained after quenching from 550°C, has a yield stress greater than that of the overaged material. It is appreciated here that the solid solution content in the two alloys is not the same.

b) Russell and Ashby (1970) carried out a compression test on averaged alloys and also on an alloy containing 0.45 wt% copper in aluminum. This had a yield stress very similar to that of the Al-3% Cu overaged alloy.

c) the estimated Orowan stress for the alloy, $\sigma_{OR} \approx 2$ ksi (14 MPa), smaller than σ_o (9 ksi).

The second term, σ_b, in the above equation is the long range back stress. The last term, σ_d, is the contribution to the hardening resulting from the necessary interaction of the glide dislocations with the forest dislocations present in the material during the test. Both the matrix yield stress σ_o and the forest term σ_d are considered as friction type hardening, because, to maintain dislocation motion in any direction, the stress on the dislocation must exceed the sum of these terms. The other term, σ_b, is considered to oppose only the increase of the deformation that has caused σ_b to develop, and to aid the deformation in the reverse sense.

Yielding in the reverse sense can be considered to take place at a stress σ_r given by

$$\sigma_r = \sigma_o + \sigma_d - \sigma_b$$

so that $\sigma_b = \frac{1}{2}[\sigma_f - \sigma_r]$

and σ_b/work hardening increment $= \dfrac{\sigma_f - \sigma_r}{2(\sigma_f - \sigma_o)} = \sigma_b$/wk hdg

There are important assumptions in this formulation:

a) the additivity of the three contributions to the flow stress;

b) the need for σ_d to remain unchanged as the test piece is unloaded and then subjected to reverse deformation;

c) the term σ_o behaves entirely as a friction stress during both the forward and reverse deformation.

More discussion of these assumptions will be given in Chapter VI.

The long range back stress is obtained from a knowledge of σ_f and σ_r. The value of σ_f is readily determined, but the value of σ_r has caused some problem to earlier authors, as discussed in the Literature Review in Chapter II. Many have investigated other techniques to avoid its measurement. In this study the reverse yield stress was measured for each test using three reverse offsets; these are zero, 0.001, 0.002. The back stress σ_b was calculated from each of them and the results tabulated and plotted against the prestrain ε_p.

Results are given in the tables for the following tests:

(i) many polycrystalline test pieces, square cross section, approximately 0.25" x 0.25"

(ii) tests on single crystal test pieces oriented for
   a) single slip
   b) double slip
   c) multiple slip, all with square cross sections.

(iii) most tests were carried out at 298°K, others at 373°K, and 77°K

(iv) in nearly all cases the alloy was aged to θ' condition.

TEST PX	ε_p $X10^{-2}$	σ_o ksi	σ_f ksi	$-\sigma_{r0}$ ksi	$-\sigma_{r.1}$ ksi	$-\sigma_{r.2}$ ksi	wk. hdg. ksi	σ_{b0} ksi	$\sigma_{b.1}$ ksi	$\sigma_{b.2}$ ksi	$\frac{\sigma_{b0}}{wk.hdg.}$	$\frac{\sigma_{b.1}}{wk.hdg.}$	$\frac{\sigma_{b.2}}{wk.hdg.}$
221	2.9	9.60	28.00	-2.40	4.80	8.00	18.40	15.20	11.60	10.00	.83	.63	.54
2191	1.0	8.80	19.20	0.00	4.80	7.60	10.40	9.60	7.20	5.80	.92	.69	.56
2198	0.8	8.80	16.80	-1.60	5.20	8.00	8.00	9.20	5.80	4.40	1.15	.73	.55
312	7.0	9.60	32.64	1.60	4.80	8.40	23.04	15.02	13.92	12.12	.65	.60	.53
314	9.25	9.60	33.20	0.00	5.60	10.40	23.60	16.60	13.30	11.40	.70	.56	.48
318	0.6	8.64	16.48	-1.92	4.80	7.36	7.84	9.20	5.84	4.56	1.17	.74	.58
319	0.8	8.64	16.48	-1.60	5.12	7.52	7.84	9.04	5.68	4.48	1.15	.72	.57
310	1.1	8.32	19.20	-2.56	3.52	5.76	10.88	10.88	7.84	6.72	1.0	.72	.62
311	5.0	9.60	31.60	0.00	5.40	10.80	22.00	15.80	13.10	10.40	.72	.60	.47
721	2.1	11.20	25.60	0.00	5.20	7.60	14.40	12.80	10.20	9.00	.89	.71	.63
316	10.0	10.40	33.20	4.00	7.00	10.00	22.80	14.60	13.10	11.60	.64	.57	.51
332	8.0	9.20	30.08	1.60	5.60	8.48	20.88	14.24	12.24	10.80	.68	.59	.52
333	6.8	9.60	32.40	0.00	8.00	11.20	22.80	16.20	12.20	10.60	.71	.54	.46
334	3.6	8.96	28.96	-1.60	5.20	7.52	20.00	15.33	11.88	10.72	.77	.59	.54
505	0.6	8.00	15.36	0.80	4.80	7.04	7.36	7.28	5.28	4.16	.99	.72	.57
502	0.15	7.36	11.68	3.20	7.36	9.92	4.32	4.24	2.16	0.88	.98	.50	.20
72Q Quench	3.2	11.20	24.48	8.00	18.08	21.20	13.28	8.24	3.20	1.64	.62	.24	.12

Because of the amount of data in the tables, stresses are given only in *ksi*. In the text *SI* equivalents are provided. *1ksi = 6.89 MPa.*

TABLE 4.1

RESULTS FOR POLYCRYSTALLINE TESTS, θ^1 AND UNAGED, 298°K

TEST SX	ε_p x 10^{-2}	σ_o ksi	σ_f ksi	$-\sigma_{r0}$ ksi	$-\sigma_{r.1}$ ksi	$-\sigma_{r.2}$ ksi	wk. hdg. ksi	σ_{b0} ksi	$\sigma_{b.1}$ ksi	$\sigma_{b.2}$ ksi	$\frac{\sigma_{b0}}{wk.hdg.}$	$\frac{\sigma_{b.1}}{wk.hdg.}$	$\frac{\sigma_{b.2}}{wk.hdg.}$
312	1.1	8.80	15.36	3.52	6.24	7.68	6.56	5.92	4.56	3.84	.90	.70	.60
313	2.0	8.80	20.00	0.00	4.96	7.36	11.20	10.00	7.52	6.32	.93	.68	.56
314	5.0	8.80	25.20	0.00	4.32	6.72	16.40	12.60	10.44	9.24	.77	.64	.56
383	2.0	6.50	16.00	-2.50	3.00	5.00	9.50	6.75	6.50	5.50	.71	.68	.58
342	4.0	7.72	23.61	0.00	1.54	3.70	15.89	11.81	11.04	9.96	.74	.69	.63
343	2.0	6.80	17.44	1.56	1.10	3.09	10.64	9.50	8.17	7.18	.89	.77	.67
351	3.8	5.75	18.25	0.25	6.00	7.88	12.50	9.00	6.13	5.18	.72	.49	.41
352	0.7	6.50	11.38	0.00	4.25	5.87	4.88	5.69	3.66	2.76	1.17	.75	.57
353	7.5	6.75	22.50	4.00	7.75	9.50	15.75	9.25	7.38	6.50	.59	.47	.41
354	2.0	6.75	17.50	1.50	5.63	7.50	10.75	8.00	5.94	5.00	.74	.55	.47
373	1.6	9.15	18.62	-6.30	3.63	5.21	9.47	9.63	7.50	6.71	1.02	.79	.71
374	3.2	8.82	24.54	-2.94	3.53	5.88	15.72	13.74	10.51	9.33	.87	.67	.59
371	0.8	6.17	11.11	-0.93	2.47	3.86	4.94	6.02	4.32	3.63	1.22	.87	.73

TABLE 4.2 -

RESULTS FOR SINGLE CRYSTALS, θ^1, 298°K

TEST SX	TEMP °K	ε_p 10^{-2}	σ_o ksi	σ_f ksi	$-\sigma_{r0}$ ksi	$-\sigma_{r.1}$ ksi	$-\sigma_{r.2}$ ksi	σ_{b0} ksi	$\sigma_{b.1}$ ksi	$\sigma_{b.2}$ ksi	wk. hdg. ksi	$\frac{\sigma_{b0}}{wk.hdg.}$	$\frac{\sigma_{b.1}}{wk.hdg.}$	$\frac{\sigma_{b.2}}{wk.hdg.}$
244	298	1.1	8.38	15.03	-2.31	2.31	4.19	8.67	6.36	5.42	6.65	1.30	.96	.82
241	298	1.2	8.67	17.34	-2.89	0.58	1.45	10.12	8.38	7.95	8.67	1.17	.97	.92
253	373	1.2	9.53	17.92	0.00	6.50	8.38	8.96	5.71	4.77	8.39	1.07	.68	.57
251	298	1.2	9.83	17.92	1.16	6.07	7.80	8.38	5.93	5.06	8.09	1.04	.73	.63
252	77	1.2	10.99	19.66	-1.16	3.76	6.07	10.41	7.08	5.93	8.67	1.20	.82	.68
231	298	1.1	8.67	16.19	-2.89	1.73	3.76	9.54	7.23	6.22	7.52	1.27	.96	.83
233	373	1.1	8.09	14.16	1.73	2.75	4.34	7.96	5.71	4.91	6.07	1.31	.94	.81
224	298	1.0	8.09	15.61	0.00	4.91	6.65	7.81	5.35	4.48	7.52	1.04	.71	.60
221	77	1.0	9.83	18.21	0.00	4.91	6.94	9.11	6.65	5.64	8.38	1.09	.79	.67

TABLE 4.3

SINGLE CRYSTAL RESULTS AT DIFFERENT TEMPERATURES

In some tests the as-quenched (unaged or solid solution) condition was used.

(v) other tests on 2024-T6 and pure aluminum were carried out for purposes of comparison.

Stress strain curves are shown in Figures 4.1-4.6 to illustrate how the yielding behaviour in reverse depended on the prestrain, the alloy ageing condition, the test temperature and the orientation of the test piece.

It has been explained earlier that some of the test pieces were found to be buckled at the end of the compressive strain; the data from these tests were not used. The results for σ_b v ε_p and σ_b/wk hdg v ε_p are plotted for the polycrystalline and single crystal materials in Figures 4.7-4.16. The trends established by the many tests with the polycrystalline materials were used on occasion in the drawing of the curves through the few points available for some of the single crystal materials.

The shape of these curves will be discussed in Chapter VI; here the characteristics common to all the curves will be indicated:

a) the back stress σ_b increases rapidly with prestrain, reaching a saturation value at a prestrain of the order of .03-.04.

b) over the same strain σ_b/wk hdg decreases to a constant value.

Choice of Reverse Offset for Reverse Yield Stress

There are two types of evidence which point to the

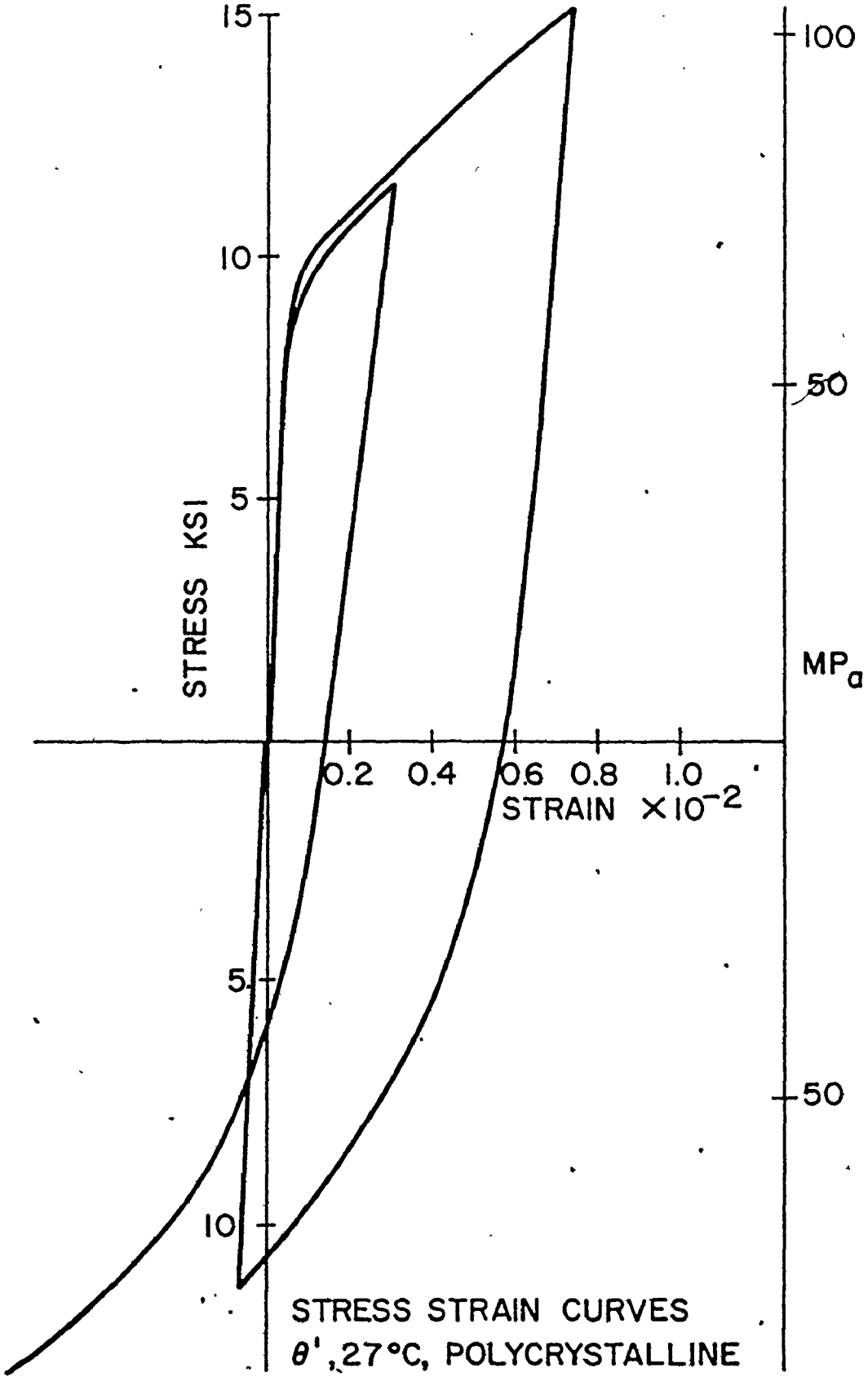
15
10
5
5
10
100
50
50
STRESS KSI
MPa
0.2
0.4
0.6
0.8
1.0
STRAIN ×10⁻²
STRESS STRAIN CURVES
θ', 27°C, POLYCRYSTALLINE

FIG 4.1

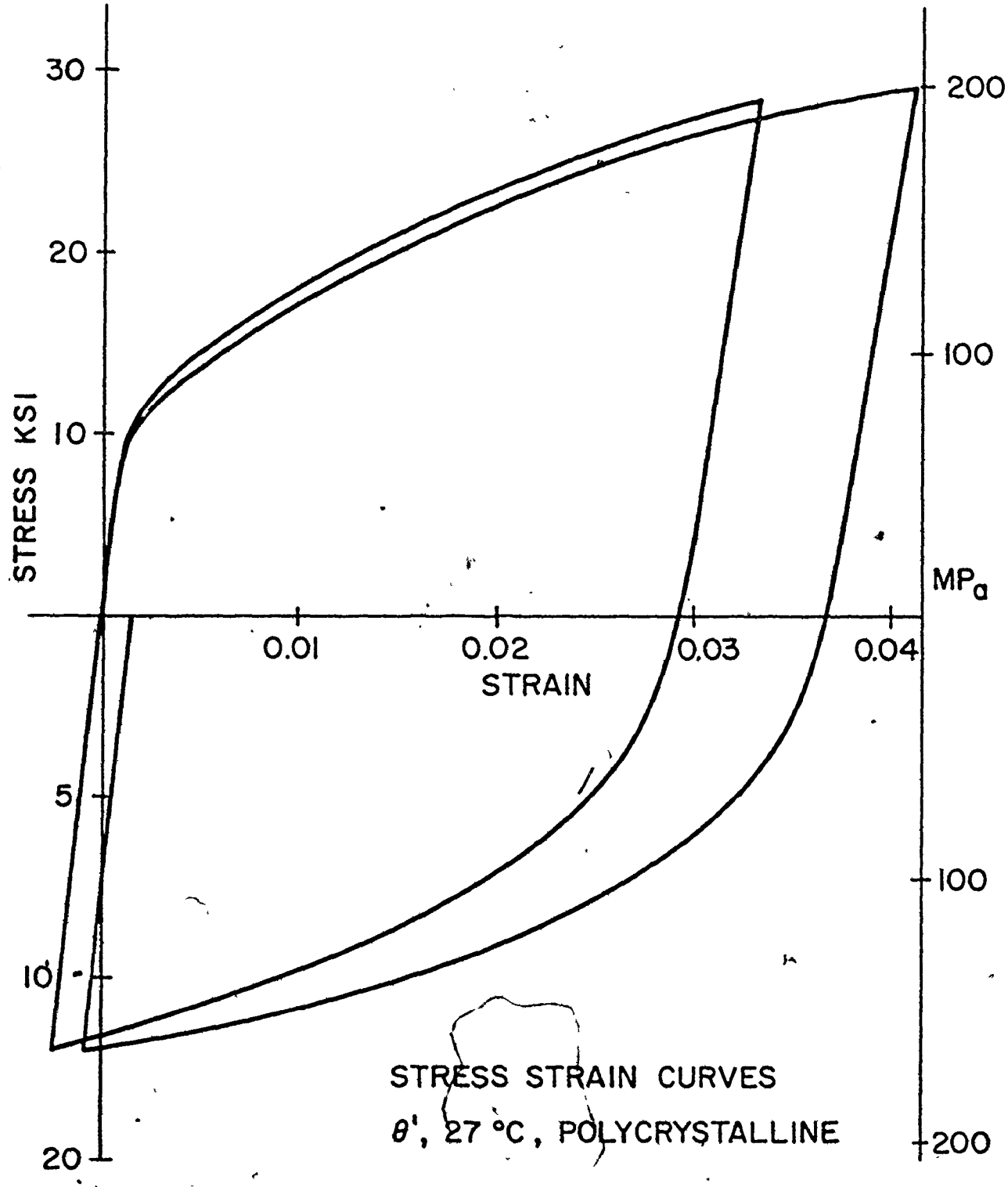
30
20
10
5
10
20
STRESS KSI
200
100
100
200
MPa
0.01
0.02
0.03
0.04
STRAIN
STRESS STRAIN CURVES
θ', 27 °C, POLYCRYSTALLINE

FIG 4.2

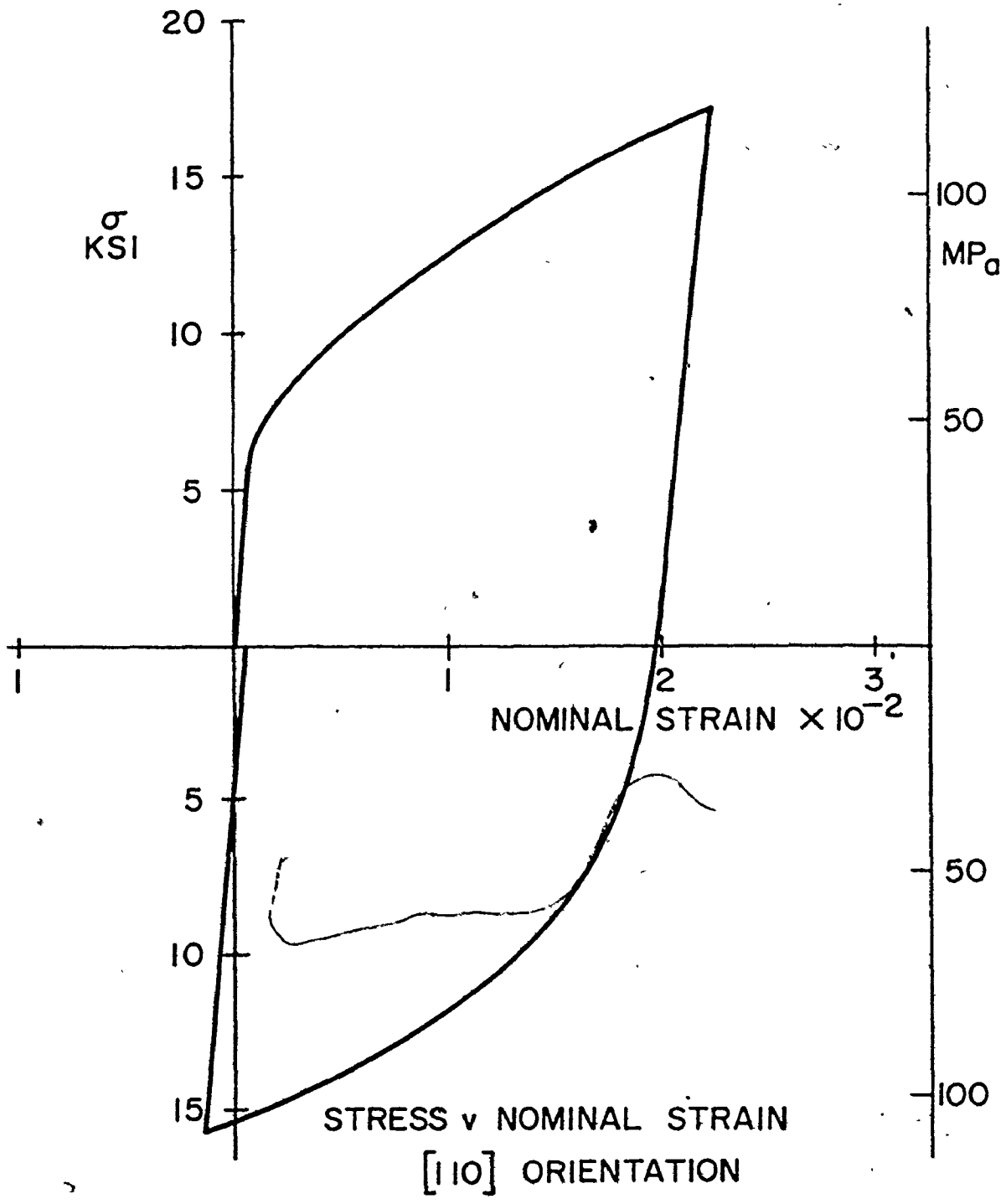
20
15
10
5
σ
KSI
100
MPa
50
1
1
2
3
NOMINAL STRAIN X 10⁻²
5
10
15
50
100
STRESS v NOMINAL STRAIN
[110] ORIENTATION

FIG 4.3

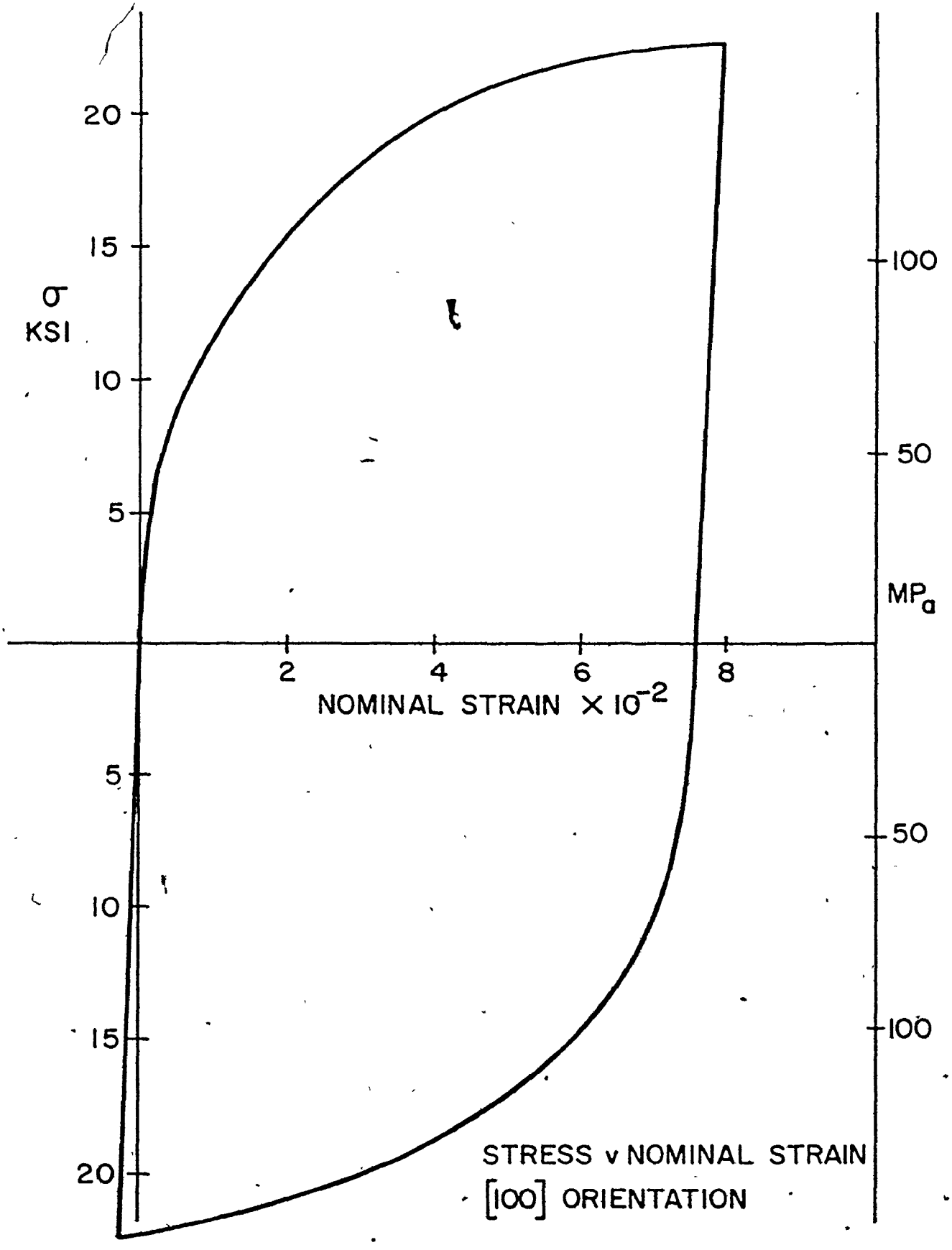
σ
KSI
20
15
10
5
5
10
15
20
2
4
6
8
NOMINAL STRAIN X 10⁻²
100
50
MPa
50
100
STRESS v NOMINAL STRAIN
[100] ORIENTATION

FIG 4:4

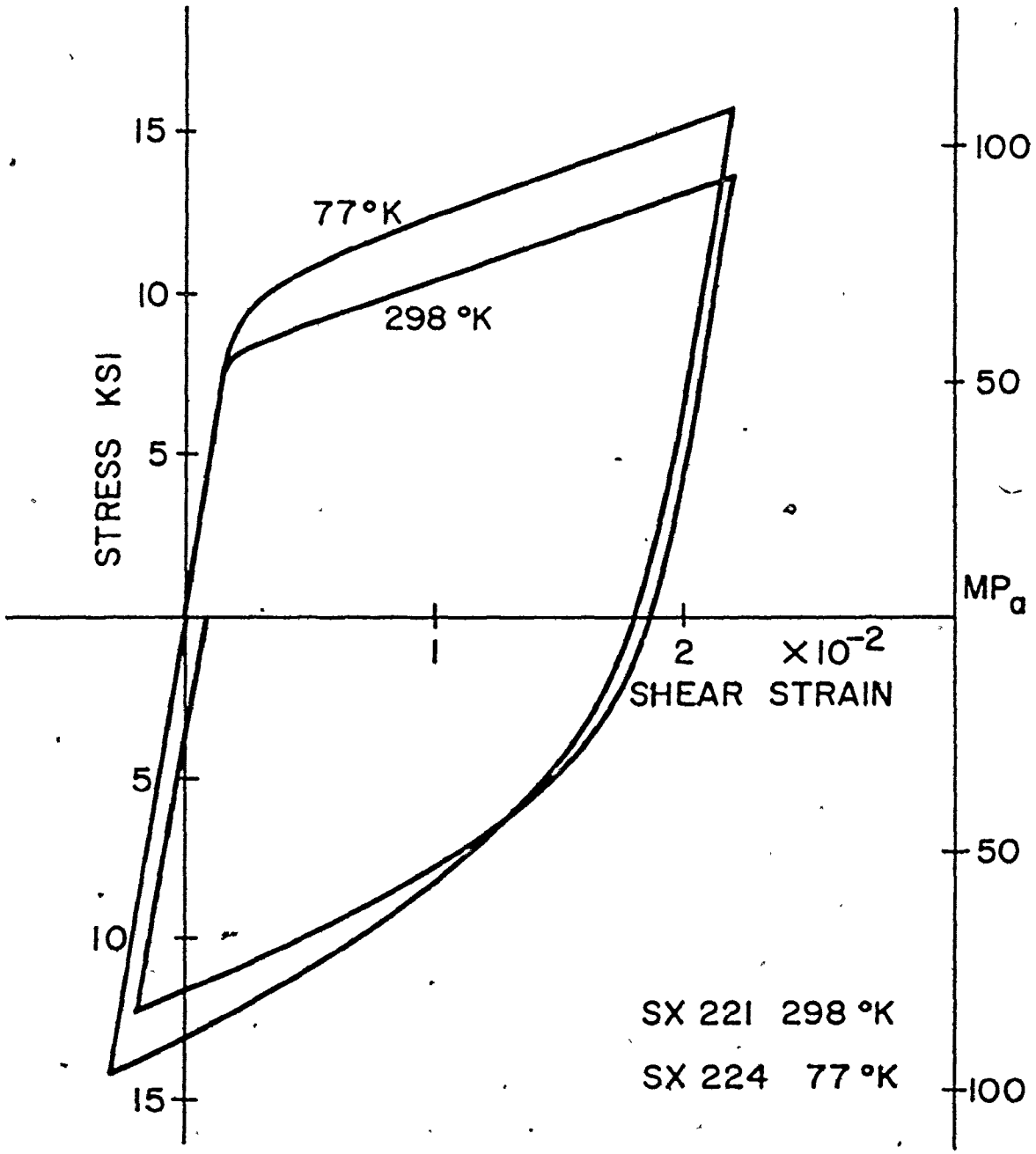
15
10
5
STRESS KSI
77°K
298 °K
1
2
×10⁻²
SHEAR STRAIN
100
50
MPa
50
100
5
10
15
SX 221 298 °K
SX 224 77 °K

FIG 4.5

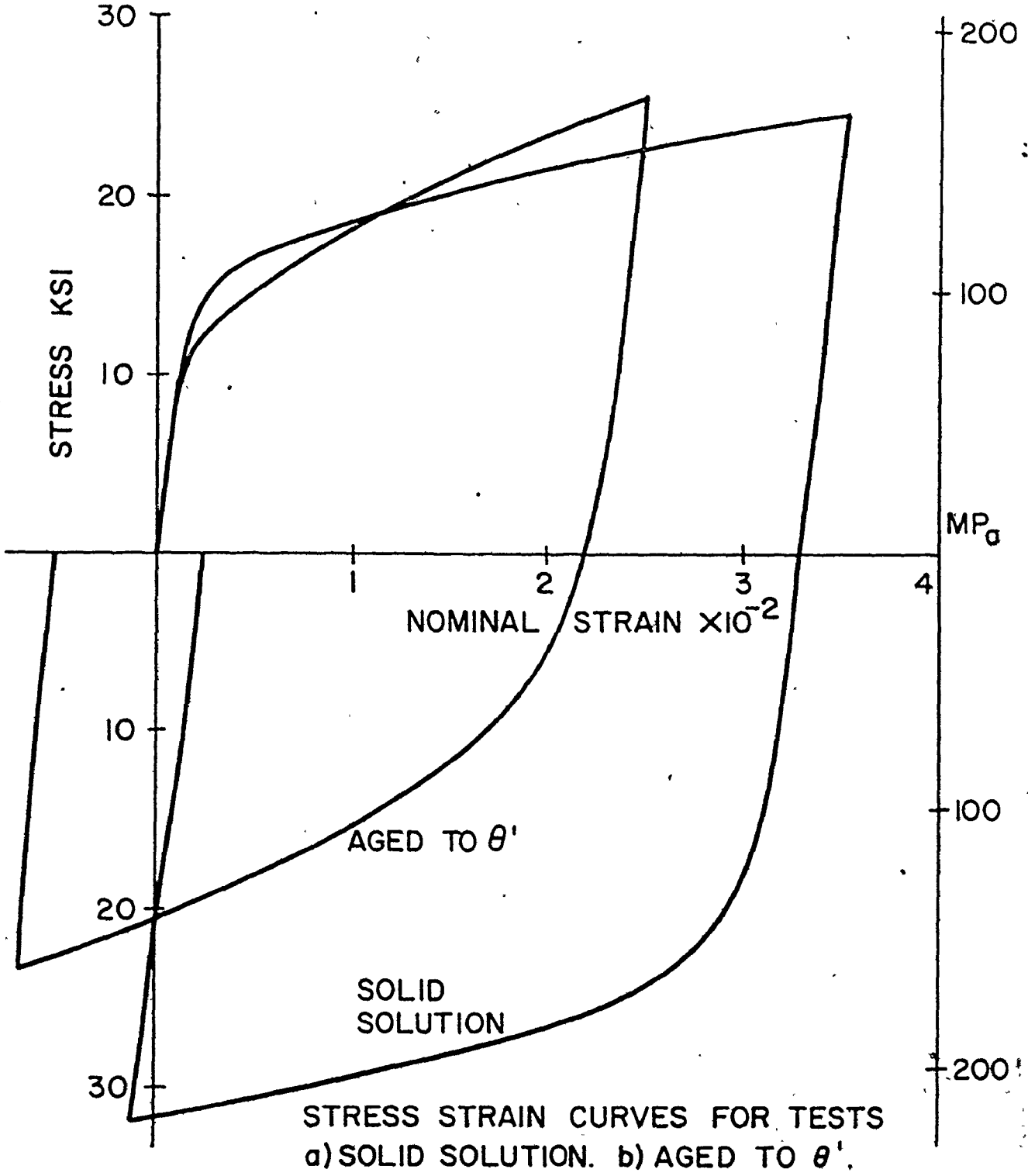
30
20
10
STRESS KSI
10
20
30
200
100
MPa
100
200
1
2
3
4
NOMINAL STRAIN X10⁻²
AGED TO θ'
SOLID
SOLUTION
STRESS STRAIN CURVES FOR TESTS
a) SOLID SOLUTION. b) AGED TO θ'.

FIG 4.6

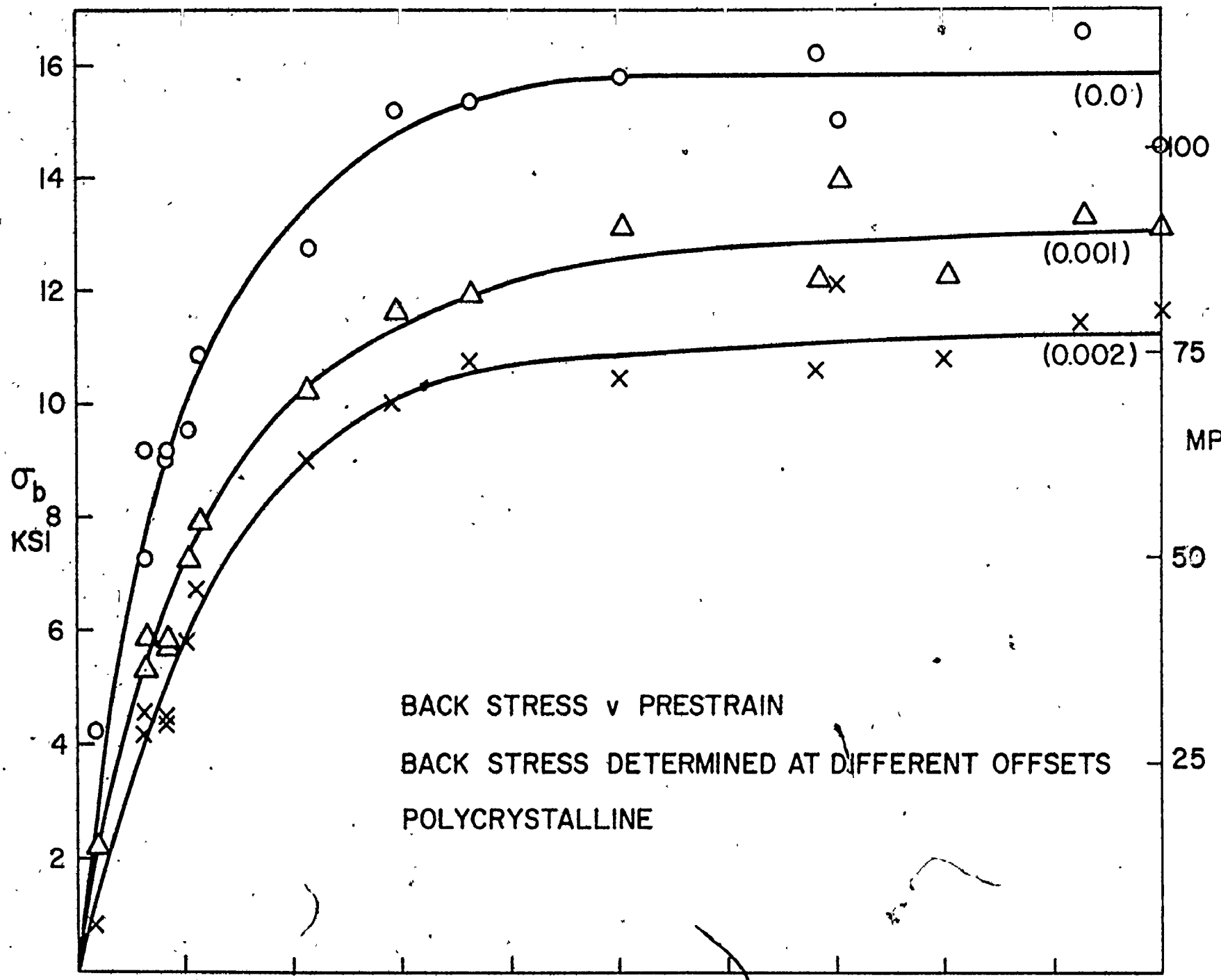
16
14
12
10
8
6
4
2
σ_b
KSI
100
75
50
25
MPa
(0.0)
(0.001)
(0.002)
BACK STRESS v PRESTRAIN
BACK STRESS DETERMINED AT DIFFERENT OFFSETS
POLYCRYSTALLINE
1
2
3
4
5
6
7
8
9
10
X 10^{-2} STRAIN

FIG. 4.7

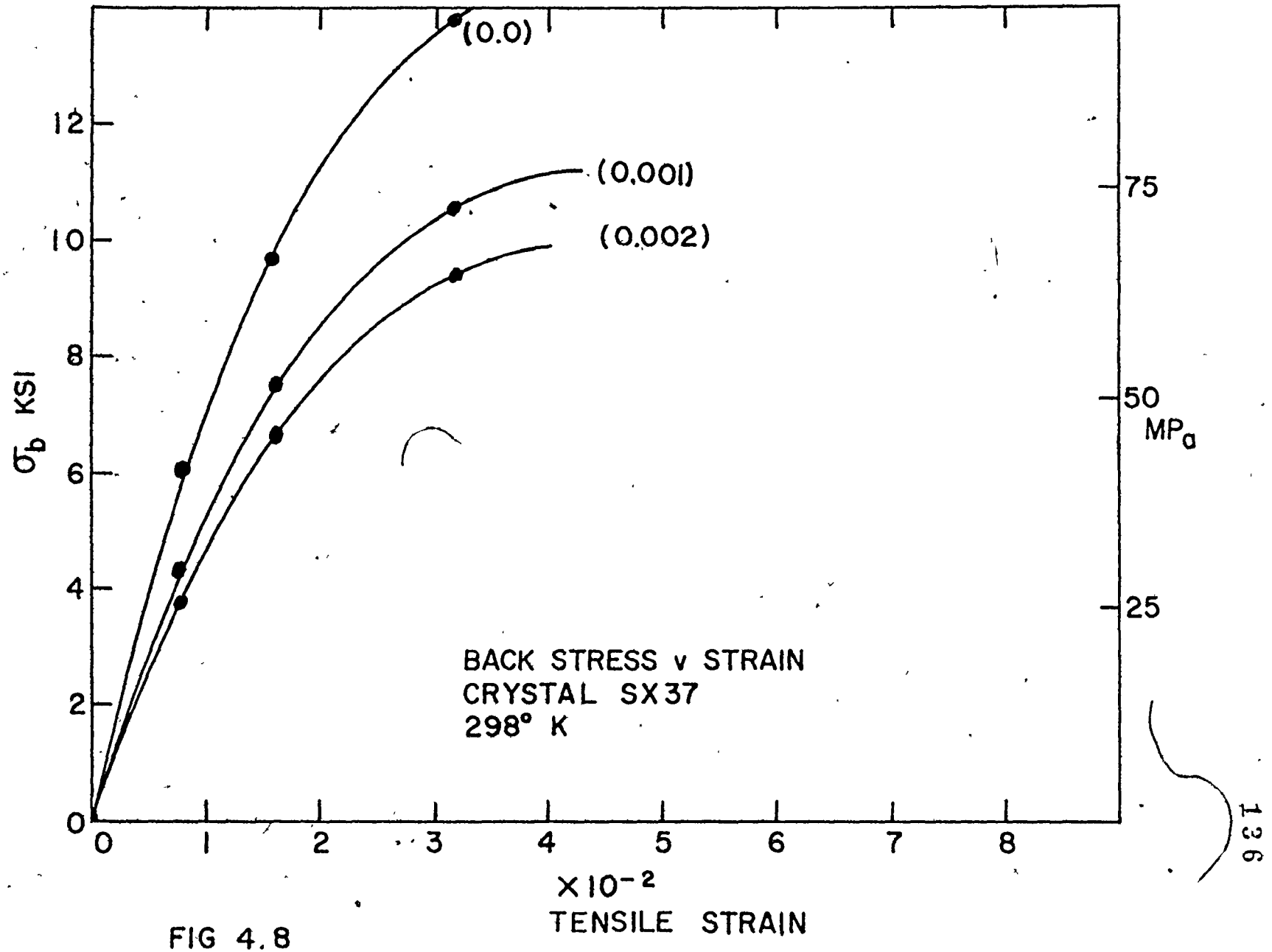
(0.0)
(0.001)
(0.002)
σ_b KSI
MPa
BACK STRESS v STRAIN
CRYSTAL SX37
298° K
$\times 10^{-2}$
TENSILE STRAIN

FIG 4.8

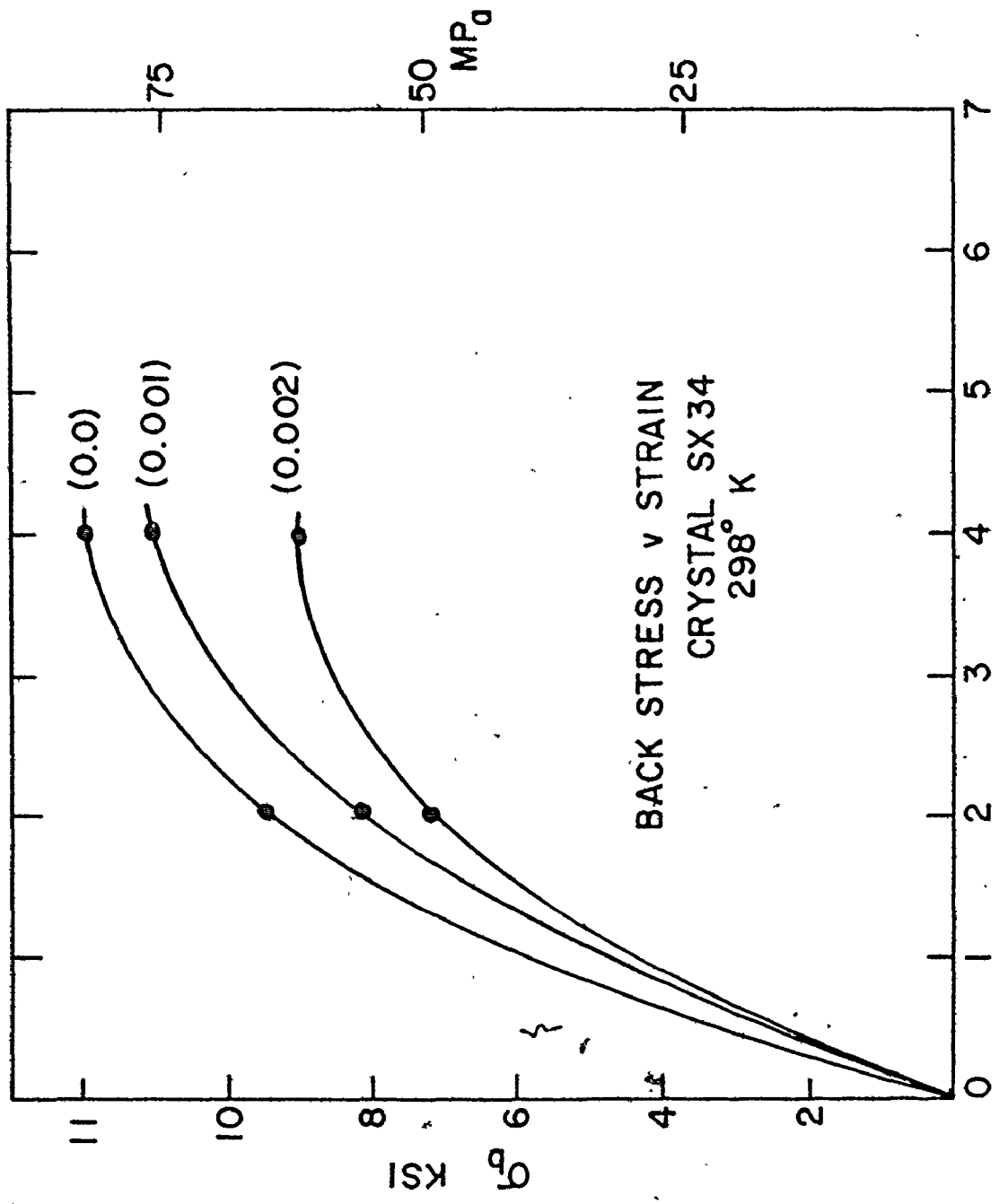
BACK STRESS v STRAIN
CRYSTAL SX34
298° K
(0.0)
(0.001)
(0.002)
σb ksi
MPa
X10-2 TENSILE STRAIN

FIG 4.9

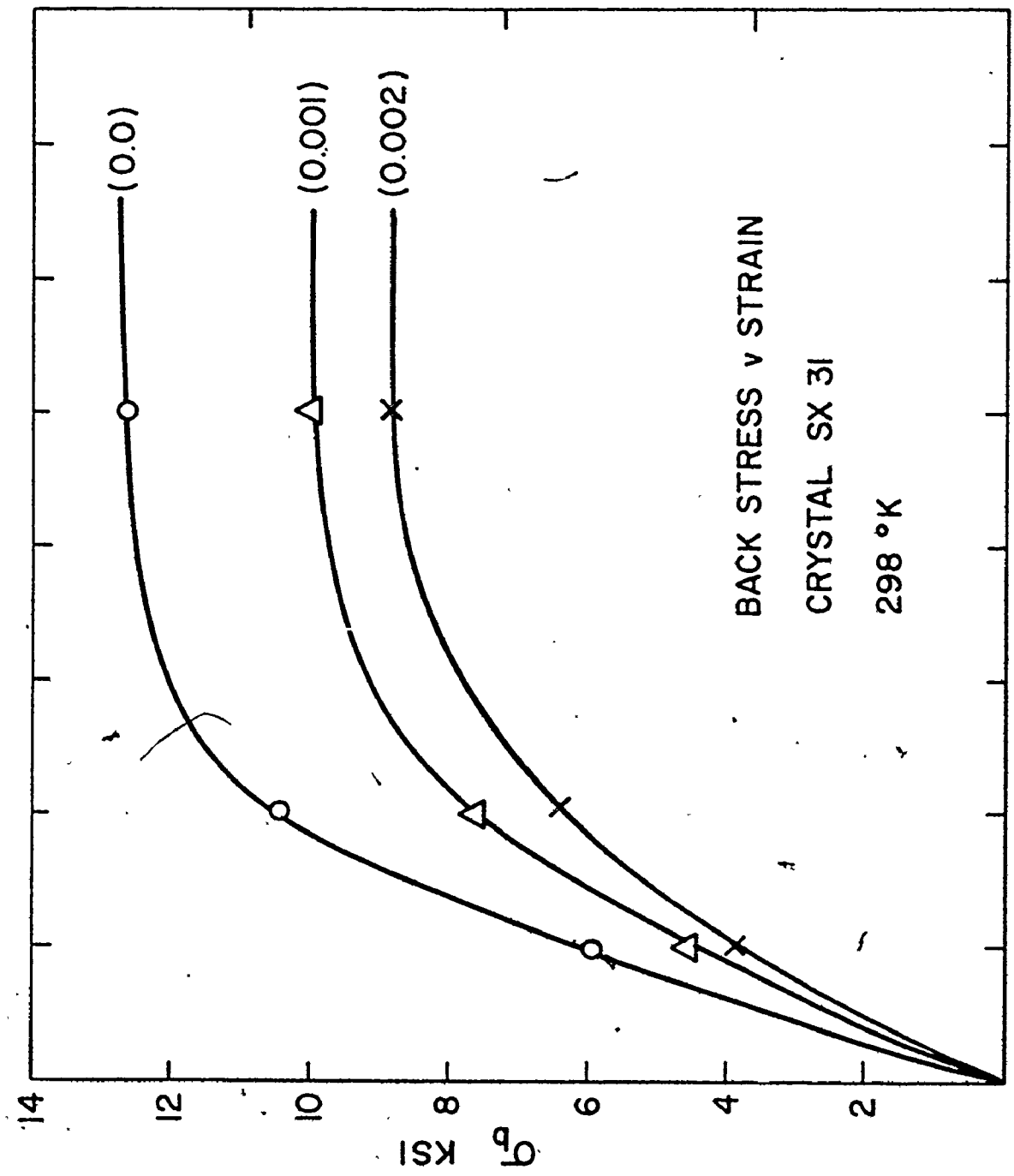
BACK STRESS v STRAIN
CRYSTAL SX 31
298 °K
(0.0)
(0.001)
(0.002)
σ_b KSI
STRAIN $\times 10^{-2}$
2
4
6
8
10
12
14
1
2
3
4
5
6
7
8

FIG 4.10

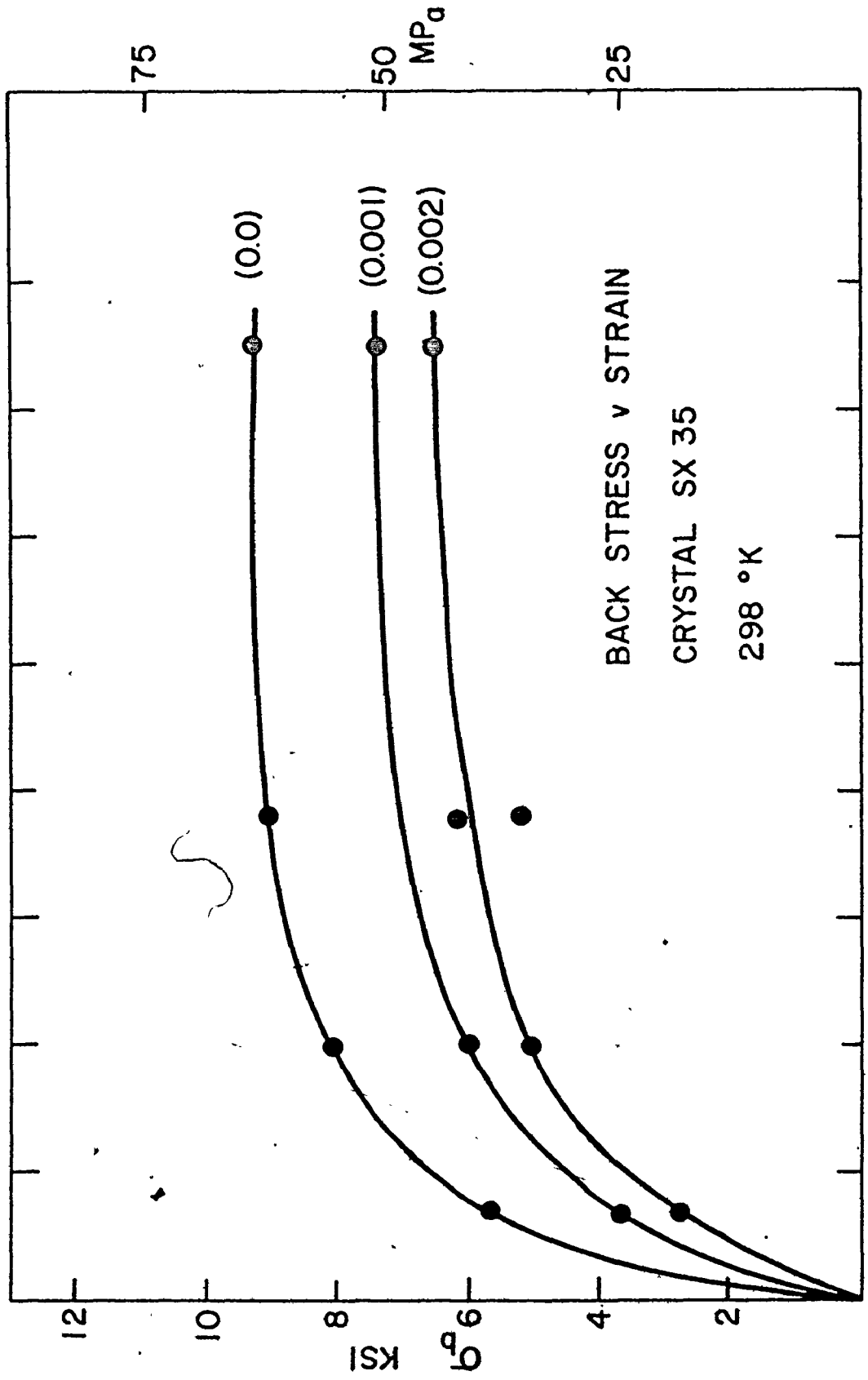
BACK STRESS v STRAIN
CRYSTAL SX 35
298 °K
(0.0)
(0.001)
(0.002)
σ_b KSI
MPa
X 10^{-2}
NOMINAL STRAIN
0
2
4
6
8
10
12
25
50
75
1
3
5
7

FIG 4.11

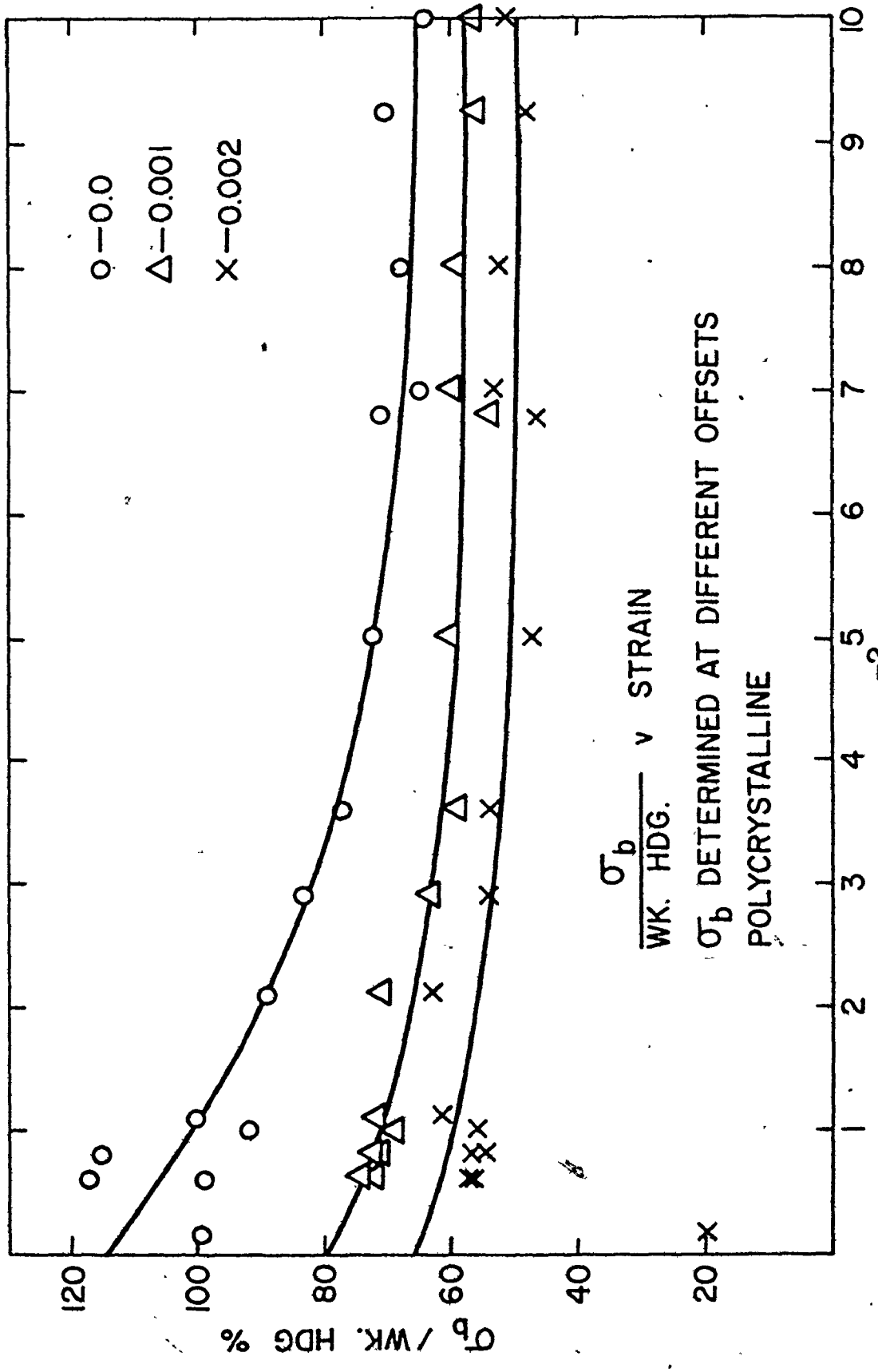
o—0.0
Δ—0.001
x—0.002
$\frac{\sigma_b}{\text{WK. HDG.}}$ v STRAIN
σ_b DETERMINED AT DIFFERENT OFFSETS
POLYCRYSTALLINE
σ_b / WK. HDG %
120
100
80
60
40
20
1
2
3
4
5
6
7
8
9
10
$\times 10^{-2}$ STRAIN

FIG 4.12

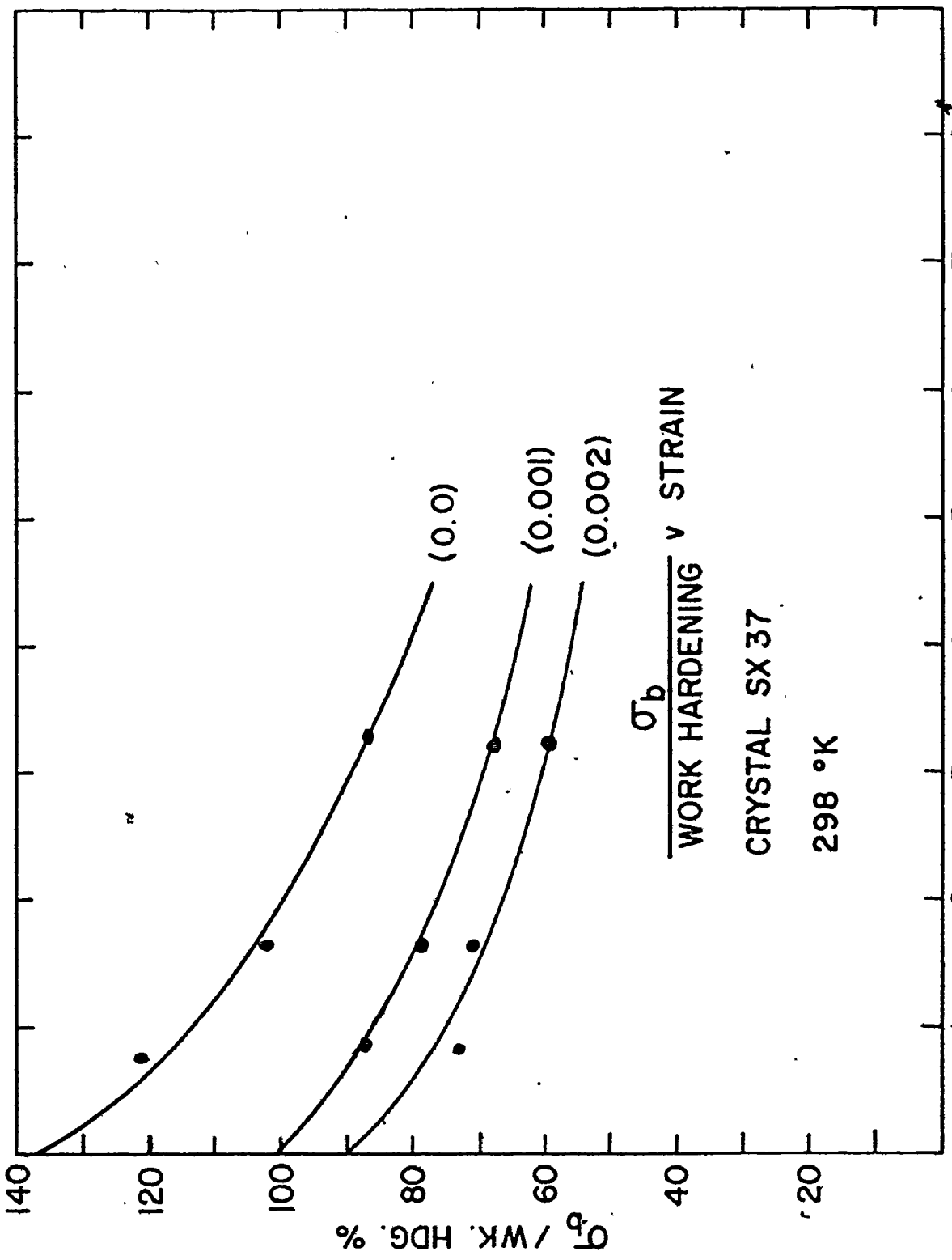
140
120
100
80
60
40
20
σ_b / WK. HDG. %
1
2
3
4
5
6
7
8
TENSILE STRAIN $\times 10^{-2}$
(0.0)
(0.001)
(0.002)
$\frac{\sigma_b}{\text{WORK HARDENING}}$ v STRAIN
CRYSTAL SX 37
298 °K

FIG 4.13

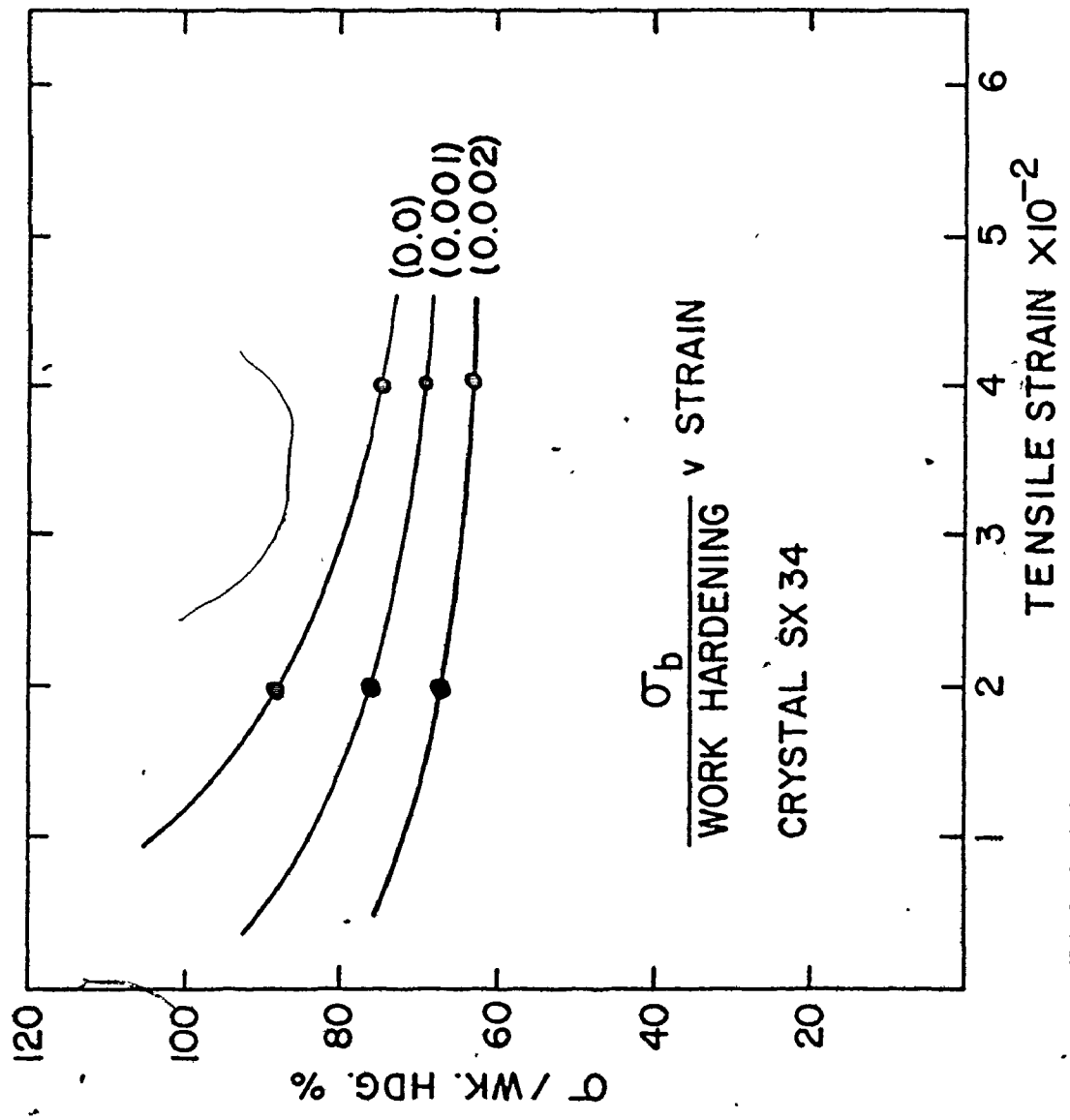
σ / WK. HDG. %
120
100
80
60
40
20
1
2
3
4
5
6
TENSILE STRAIN X10⁻²
(0.0)
(0.0011)
(0.002)
σb / WORK HARDENING v STRAIN
CRYSTAL SX 34

FIG 4.14

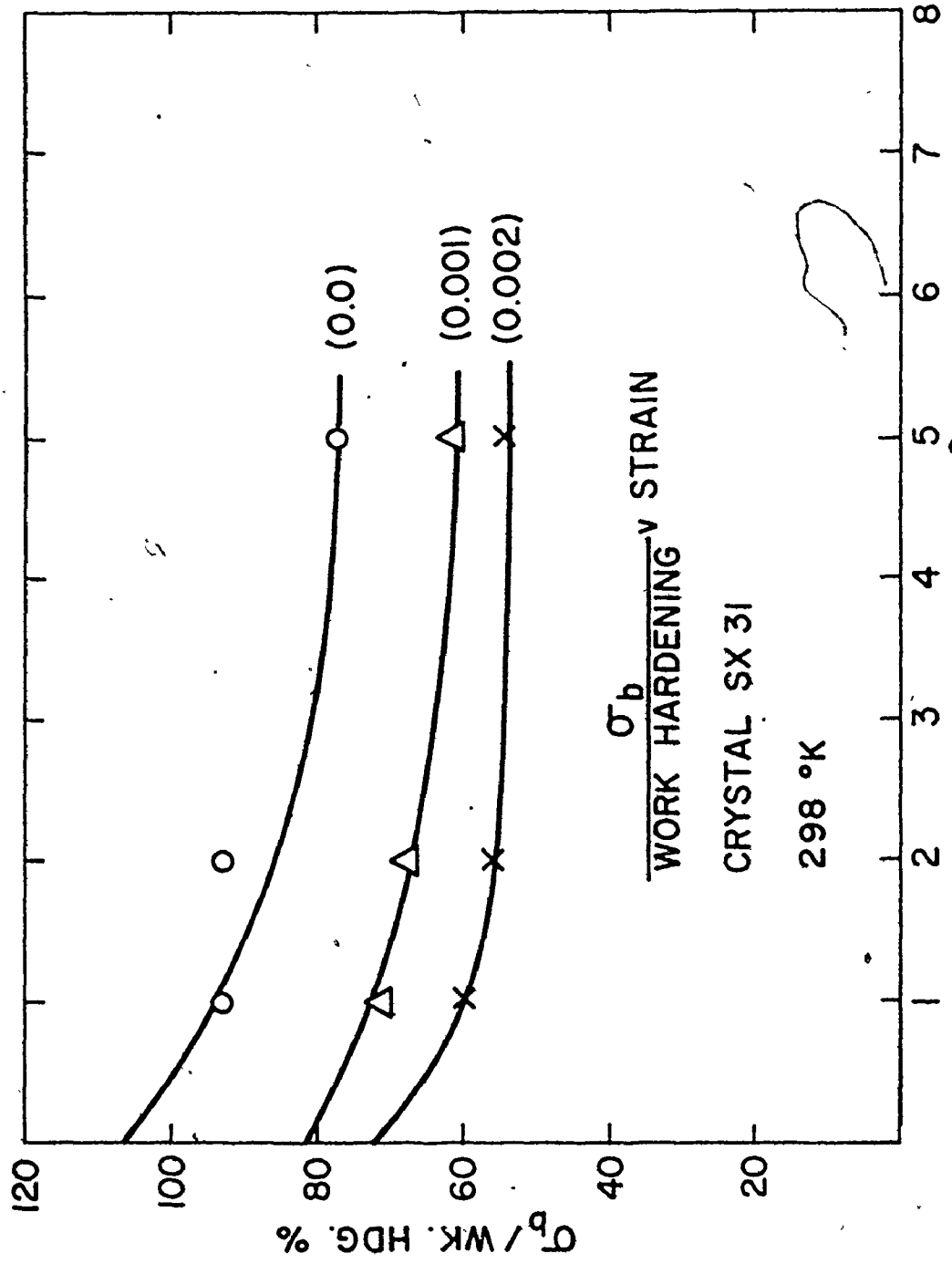
(0.0)
(0.001)
(0.002)
$\frac{\sigma_b}{\text{WORK HARDENING}}$ v STRAIN
CRYSTAL SX 31
298 °K
σ_b / WK. HDG. %
120
100
80
60
40
20
1
2
3
4
5
6
7
8
STRAIN X10^{-2}

FIG 4.15

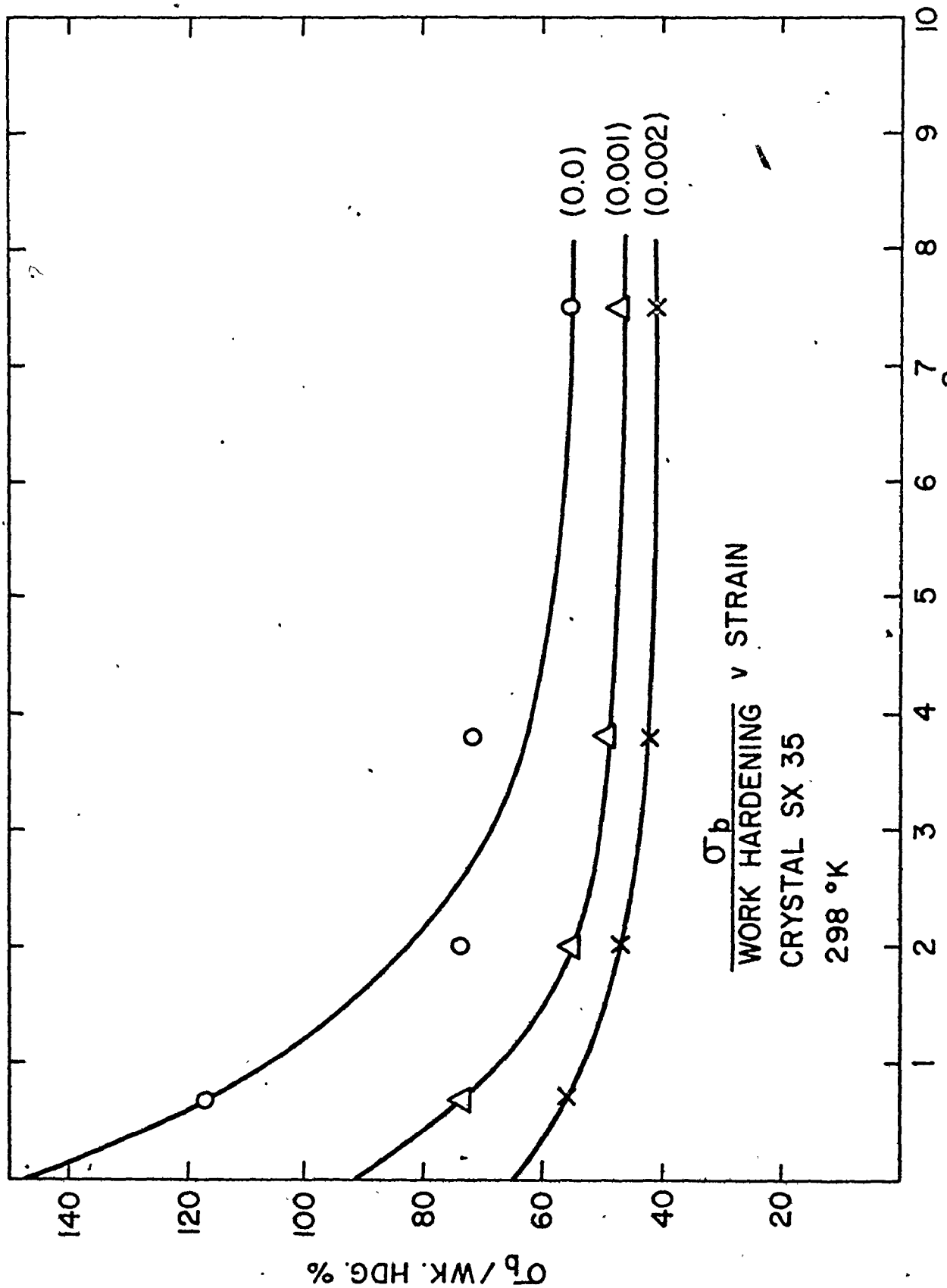
(0.0)
(0.001)
(0.002)
$\frac{\sigma_b}{\text{WORK HARDENING}}$ v STRAIN
CRYSTAL SX 35
298 °K
NOMINAL STRAIN $\times 10^{-2}$
σ_b / WK. HDG. %

FIG 4.16

use of the .001 reverse offset in the measurement of the reverse yield stress. The first of these is contained in the plots of σ_b/wk hdg v ε_p. Examination of these plots leads to Table 4.4.

Values of σ_b/wk hdg Extrapolated to Zero Prestrain

Reverse offset strain used for $\sigma_{reverse}$	zero	.001	.002
1. SX 37	1.35	1.00	.88
2. SX 34	1.30	1.00	.80
3. SX 31	1.05	.75	.63
4. SX 35	1.15-1.40	.92	.65
5. polycrystals	1.05	.79	.70

TABLE 4.4

It can be seen in this table that the values of σ_b/wk hdg extrapolated to zero prestrain are unacceptable if they are based on the zero offset method of determining the reverse yield stress. They are unacceptable because they imply that the back stress is greater than the work hardening, even though it is only a part of it.

The second set of values taken at the reverse offset of .001 are more acceptable in that they do not exceed

unity. The values obtained from the .002 reverse offset method do not exceed unity, but they do lead to problems at small prestrains. At these small prestrains, the .002 reverse strain has greatly reduced the back stress built up during the prestrain, so that it is not surprising that the σ_b/wk hdg data points should be about .2 - .4 instead of the .8 - .95 as expected from the extrapolation. This problem does not arise with the .001 reverse offset method.

The second piece of evidence to support the use of the .001 reverse offset method comes from the work of Wilson. It could be argued that the .001 reverse offset method will greatly overestimate the back stress when compared with the experimental results obtained by Wilson in his X-ray study. A very careful study of Wilson's results shows that this is not correct; in fact, the .001 reverse offset method leads to results which are smaller than Wilson's. The details of the calculations are as follows.

In Wilson's work there are two pieces of experimental data of direct relevance to this thesis.

a) Wilson's Table 2 gives $\tau_{xray} = 6.3$ ksi and $\tau_{wk\ hdg} = 8.0$ ksi for the alloy Duralumin. The τ_{xray} is a stress of the same type as that studied in this work. Then it follows that

$$\frac{\tau_b}{wk\ hdg} = \frac{\tau_{xray}}{wk\ hdg} = \frac{6.3}{8.0} = .79$$

b) Wilson's Figure 3 gives stress-strain curves for the alloy Al-4.1% Cu, aged at 190°C for 300 hours to have a precipitate similar to that used in this study. Analysis of the graphs as presented leads to τ_y = 9.6 ksi, τ_{S3} = 10.2 ksi, τ_{f9} = 18.5 ksi from which using Wilson's Figure

$$\frac{\tau_{xray}}{\tau_{wk\ hdg}} = \frac{.53\ \tau_{S3}}{\tau_{f9}-\tau_y} = \frac{.53 \times 10.2}{18.5-9.6} = .61.$$

It must be remembered that the prestrain in both these experiments was 9% torsion. This can be approximated to a tensile strain by dividing by $\sqrt{3}$, to give 5.2%. When these two data points are plotted with the polycrystalline data from this study, it is seen that the reverse offset method using .001 gives good agreement with the results of Wilson's work on Al-4.1Cu. At the same strain the results from the polycrystals have

$$\frac{\sigma_b}{wk\ hdg} = .57.$$

The difference between this value and Wilson's is smaller than the scatter in the experimental data.

For the reasons given above, the consistency of the results using the .001 reverse offset method and the good agreement with Wilson's data has led to the use of the .001 reverse offset method in the comparison of the experimental results with those of the different theories.

Results are also presented for the back stress σ_b and $\sigma_b/wk\ hdg$ for the tests carried out at 77°K and 373°K on aluminum-copper aged to θ'. These show the temperature dependence of the back stress. It was not possible to obtain a complete set of data at the different temperatures as the maximum number of test pieces available at any orientation was four. A further set of results is given for a test carried out on a polycrystalline test piece that had not been aged to θ'; it was tested in the as-quenched condition, a single phase solid solution. This test confirms that the θ' particles were responsible for the large back stress observed. In Figure 4.3, it can be seen that the reverse deformation curve for the unaged alloy has a much larger reverse yield stress when compared with the test on the material aged to θ'.

Figure 4.17 shows a stress strain curve for a test on pure polycrystalline aluminum. This material again shows a large reverse yield stress, and the Bauschinger Effect is small. The results for the back stress in this material are shown in Figure 4.18 and it is clear that the back stress is small, and that it represents a very small fraction of the work hardening.

Several tests were carried out on a 2024-T6 alloy, which is similar to the Al-4% Cu alloy. Stoltz and Pelloux (1974), using this alloy, obtained reverse stress-strain

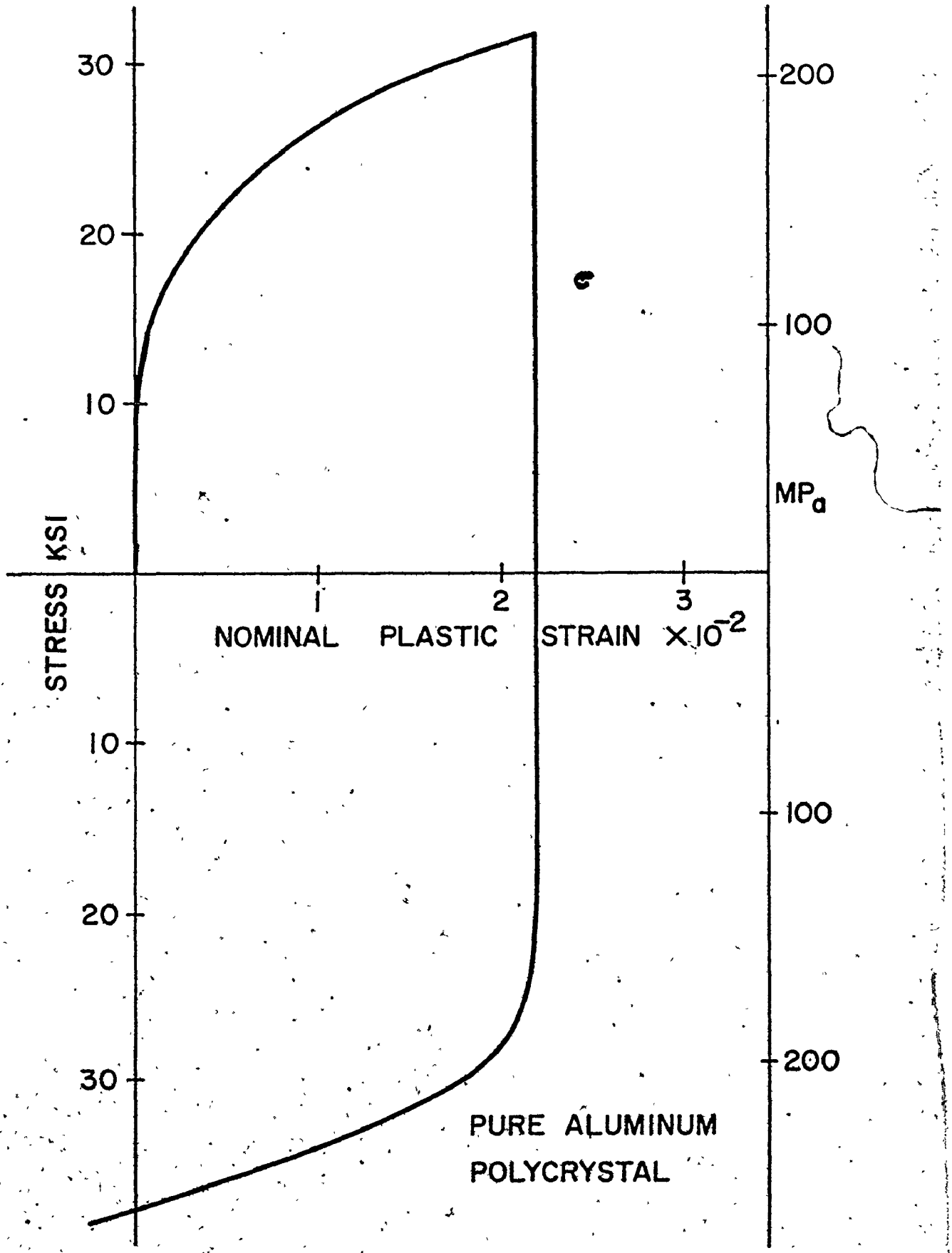
30
20
10
STRESS KSI
10
20
30
200
100
MPa
100
200
1
2
3
NOMINAL PLASTIC STRAIN X10^{-2}
PURE ALUMINUM
POLYCRYSTAL

FIG 4.17

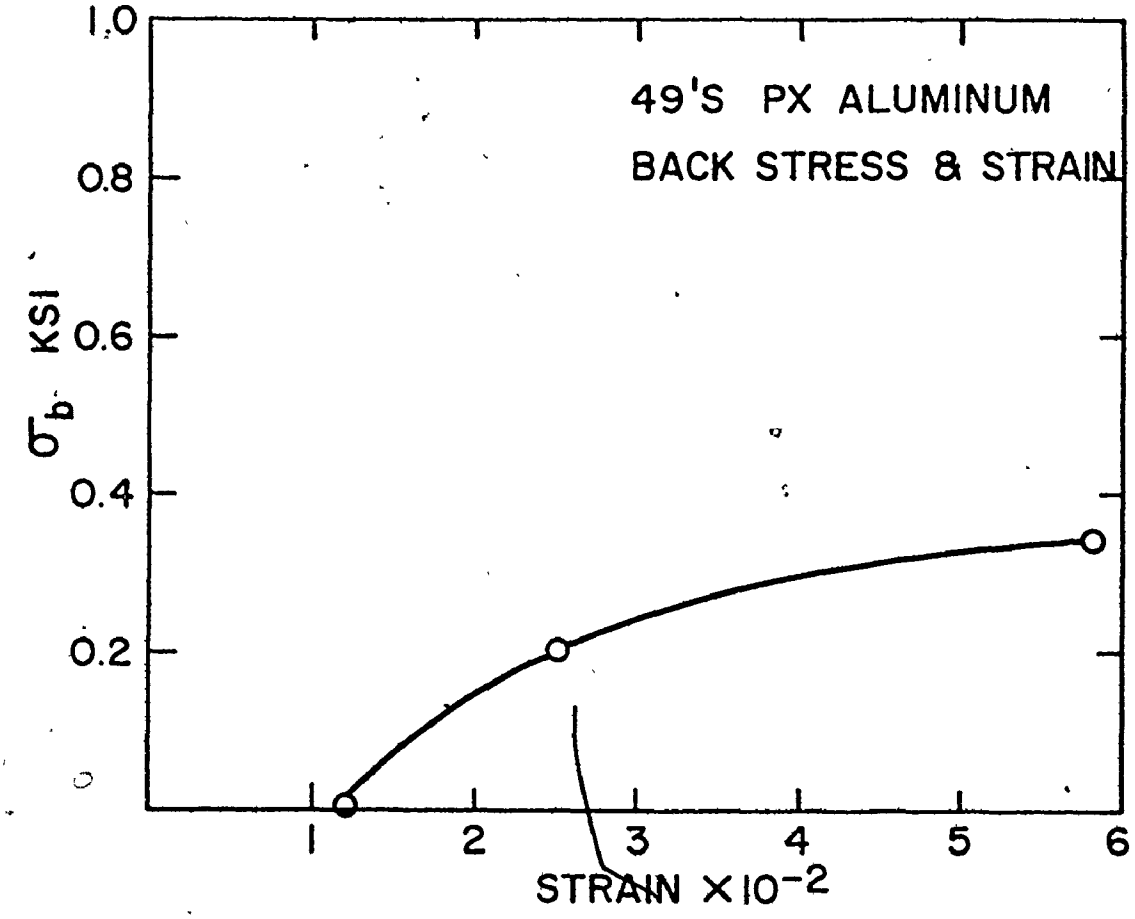
49'S PX ALUMINUM
BACK STRESS & STRAIN
σ_b KSI
1.0
0.8
0.6
0.4
0.2
1
2
3
4
5
6
STRAIN $\times 10^{-2}$

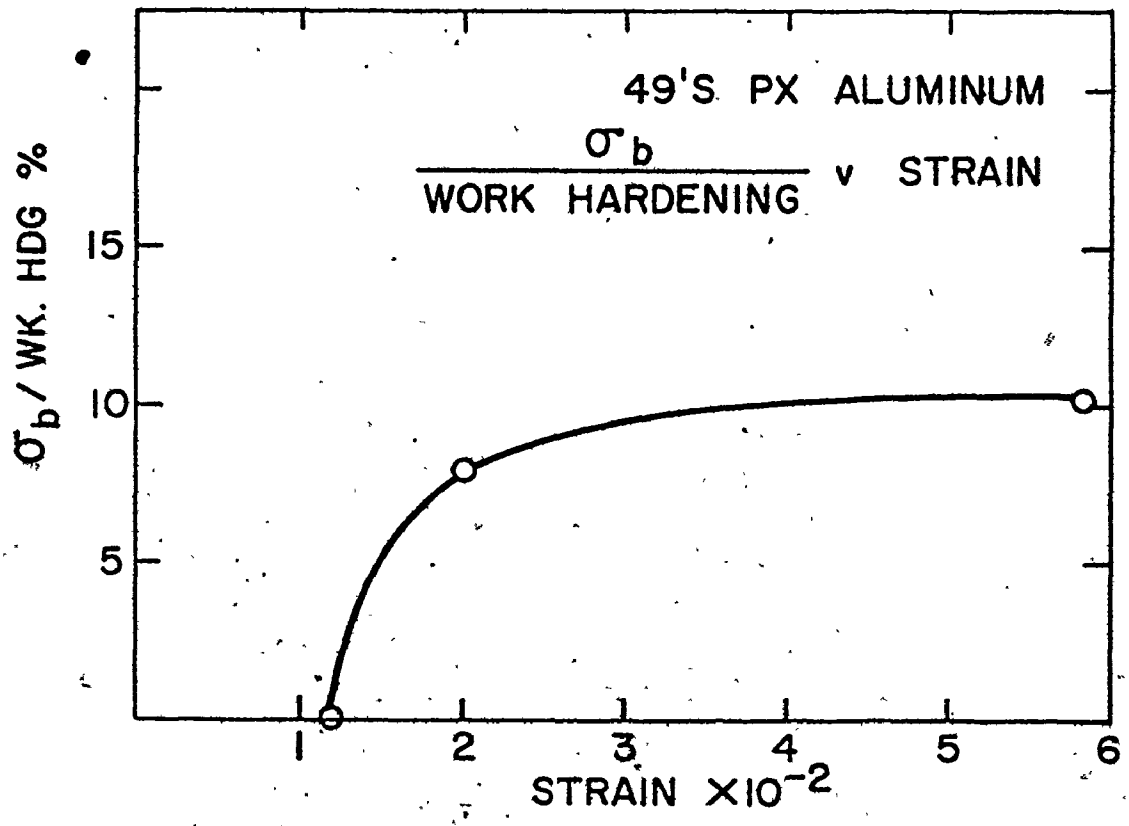
49'S PX ALUMINUM
$\frac{\sigma_b}{\text{WORK HARDENING}}$ v STRAIN
σ_b / WK. HDG %
15
10
5
1
2
3
4
5
6
STRAIN $\times 10^{-2}$

FIG 4.18

curves which showed a concave section. Similar concave sections were claimed by these authors for the Al-4% Cu aged to θ'. These had not been observed in the present work and it was felt necessary to establish that their non-occurrence was not due to the experimental method. It was decided to repeat the 2024-T6 tests. At small prestrains the concave sections were observed as shown in Figure 4.19. When the corresponding tests were carried out at similar small strains on the Al Cu θ' alloy, the concave sections were not observed. Two such tests are shown in Figure 4.1, with prestrains 0.6×10^{-2} and 0.15×10^{-2} and it can be seen that the curves are convex.

4.2 X-Ray Studies

The results of the X-ray studies were obtained as sets of Laue patterns, Figures 4.20 - 4.22. In these, the main interest was in the development of the asterism of the spots, as the deformation history of the test pieces was changed. Thus, as far as possible, each set of Laue patterns contains one each from

a) a virgin specimen

b) the specimen after a strain in tension

c) the specimen from b) given an equal strain in compression so that the net strain is zero

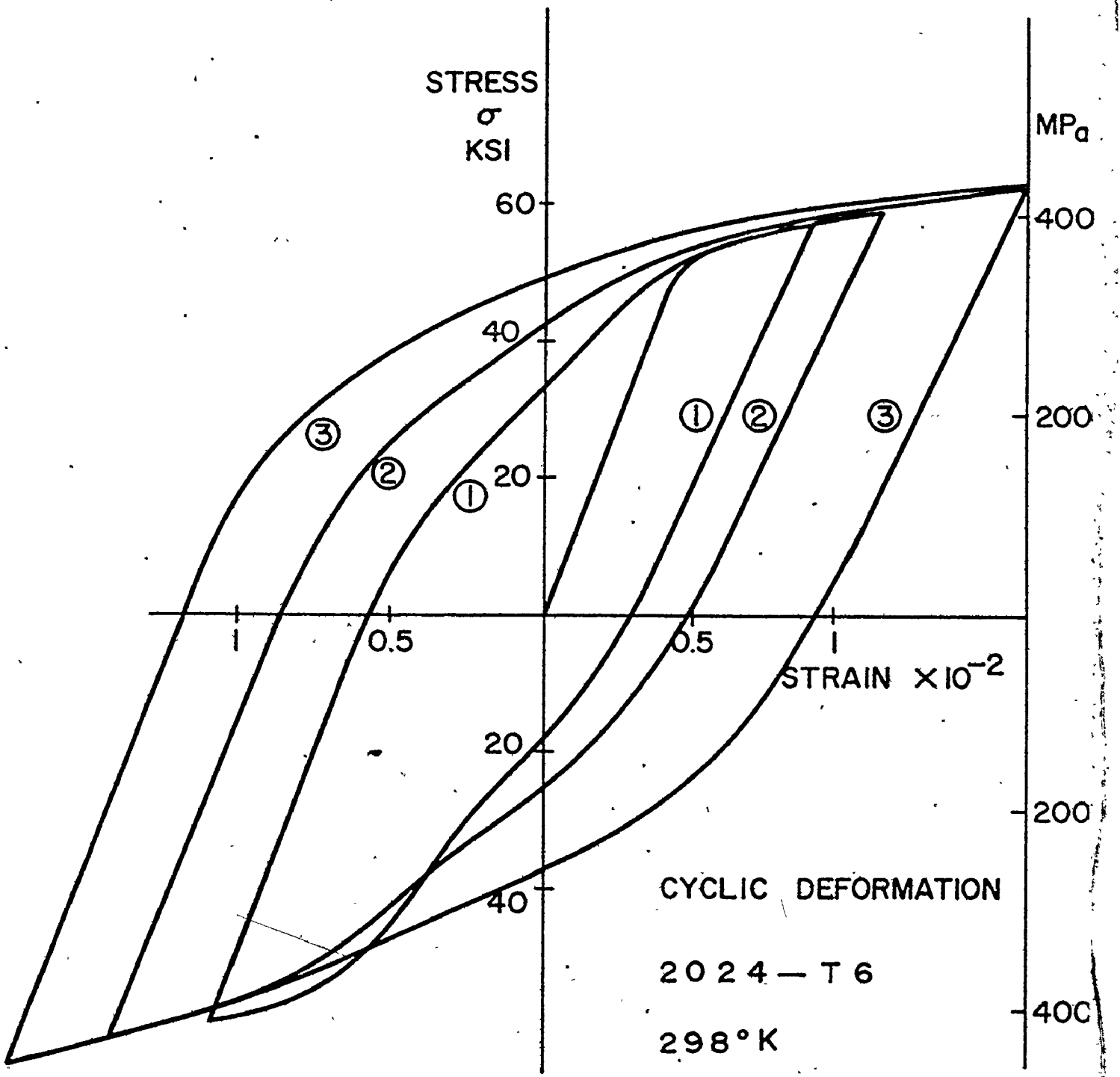
STRESS
σ
KSI
MPa
60
40
20
20
40
400
200
200
400
1
0.5
0.5
1
STRAIN X10⁻²
①
②
③
CYCLIC DEFORMATION
2024 — T6
298°K

FIG 4.19

d) in some cases c) was given a further strain in compression.

The sets of Laue patterns show that asterism was developed by the deformation in tension. This result is in agreement with the Laue patterns shown by Russell and Ashby. The extent of the asterism increased as the deformation increased. The asterism on some of the Laue patterns was analysed to determine the axis about which it developed. In these cases the result agreed with that of Russell and Ashby. The axis about which the lattice bending took place in the crystals oriented for single slip was [1$\bar{2}$1].

The asterism was found to decrease when the sense of the deformation was reversed. In the patterns shown at zero net strain, the asterism was effectively removed especially for the spots with low indices. Some spots with high indices do not show the removal as convincingly as those with low indices. On increasing the reverse deformation, the asterism again increases.

The decrease of the asterism is shown in more detail in Figure 4.20. As stated, it is easier to see the effect in low index spots, eg. the (111) spot in the first set of patterns. Here the (1$\bar{1}$1) spot is magnified in each case. Its initial circular shape is clearly elongated in the second pattern, (at 4% shear strain), and then circular again at zero net strain. There is a second spot in the magnified

BACK REFLECTION LAUE PHOTOGRAPHS

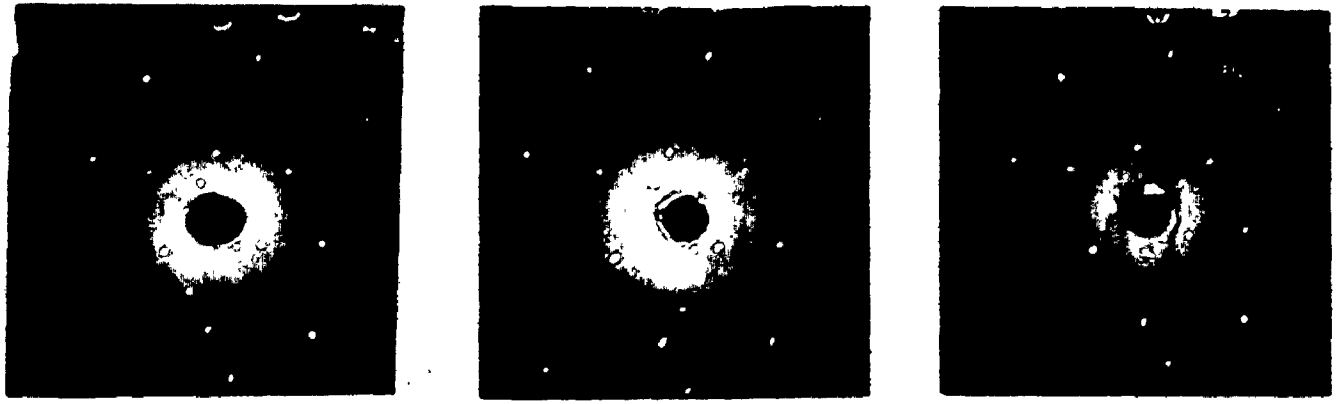

UNDEFORMED | SHEAR STRAIN | TENSILE STRAIN

FIG 4.20

MAGNIFIED (111) STEREOGRAM LAUE BACK REFLECTIONS

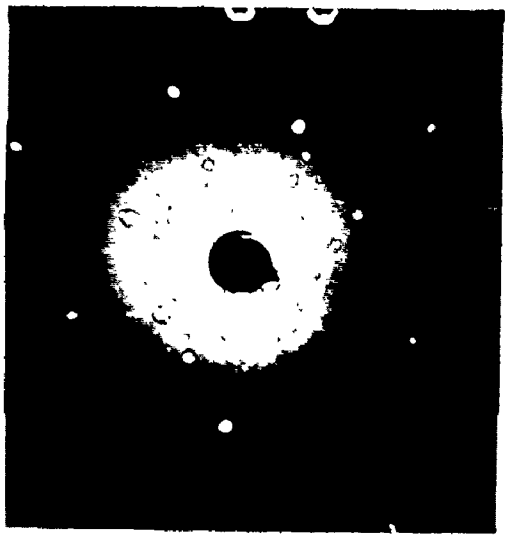

(a)

(b)

(c)

LAUE PATTERNS FROM SIDE FACES SX243

a) UNDEFORMED TEST PIECE

b) 0.04 SHEAR STRAIN IN TENSION

c) 0.04 IN COMPRESSION – NET ZERO

FIG 4.21

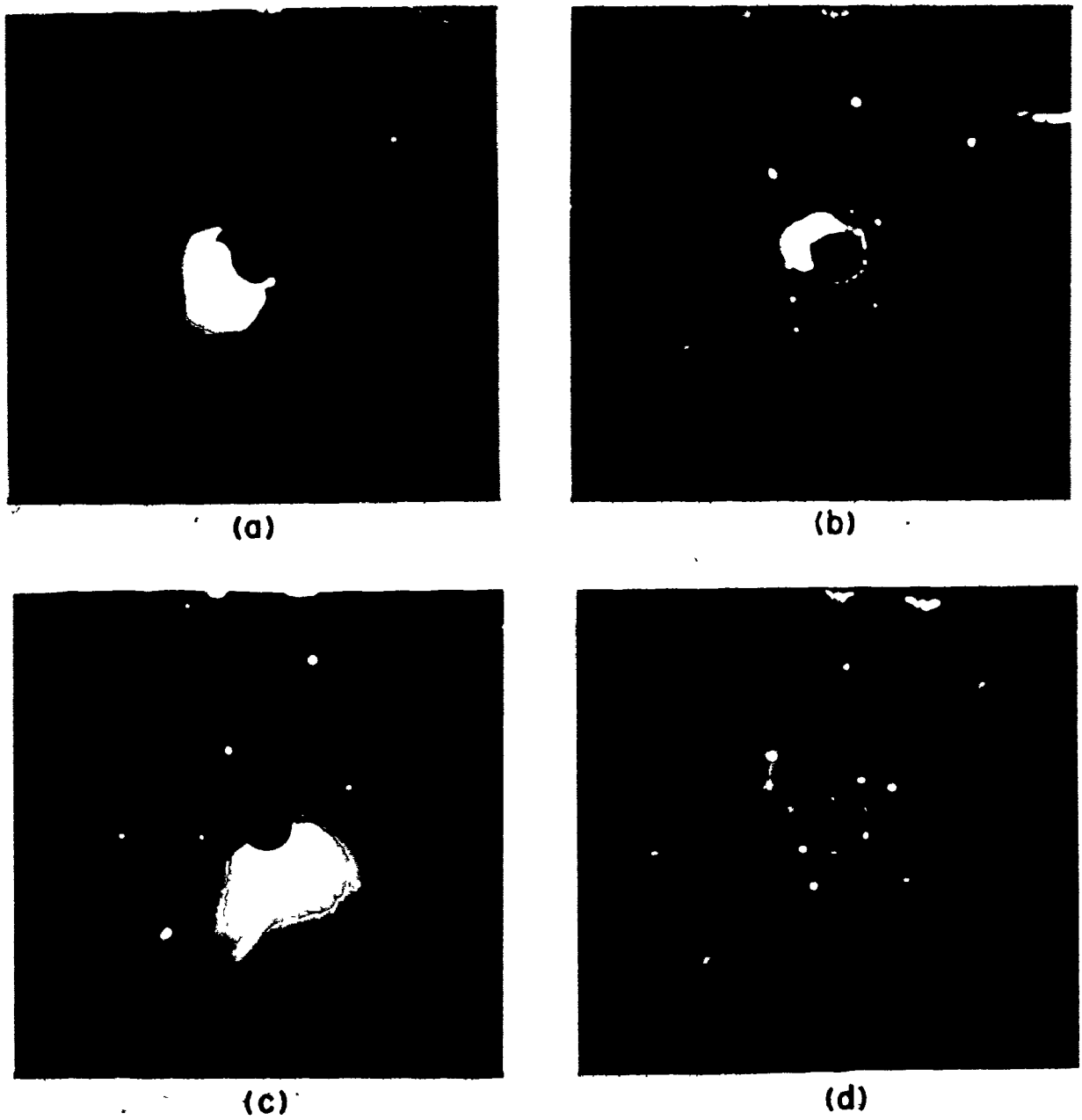

LAUE PATTERNS FROM SIDE FACES SX 342.

a) UNDEFORMED TEST PIECE

b) 0.04 SHEAR STRAIN IN TENSION

c) 0.04 IN COMPRESSION – NET ZERO

d) FURTHER 0.04 IN COMPRESSION

FIG 4.22

photographs in the top right corner. In the case of the 4% shear strain, the asterism has caused this spot to be almost invisible, whilst at zero net strain it is again visible.

It is only in the case of the test pieces oriented for single slip that the asterism was developed extensively. In the test piece oriented at [100], deforming by multiple slip, the asterism did not develop at small strains. Here it is necessary to use some results from the work on the fracture of the [100] test piece. (Figures 5.7 and 5.8) As shown in the composite photograph, the asterism is developed when the X-ray beam was incident .1" away from the fracture surface, but when the pattern from a region 1" away from the fracture is examined, some asterism is observed. This Laue pattern was taken after the test piece had necked and broken. The point of maximum load, which indicates the strain at which necking can commence, is at some 10% strain; this means that the Laue pattern at 1" from the fracture surface comes from a region which had undergone at least 10% strain. The asterism shown in this photograph is less than that from the single slip test piece.

4.3 Transmission Electron Microscopy

Transmission Electron Microscopy was used to

characterise the alloy before testing. Two aspects of the structure were investigated:

(a) it was important to ascertain that the distribution of the θ' particles was uniform on a micro- and on a macro-scale. The first of these was carried out by examining micrographs containing some 400 particles each, representing an area approximately 15μ x 15μ in the material. It was easy to see that the particle distribution was uniform. Figure 4.24 contains an example of such a micrograph.

To establish that the distribution was uniform on a macroscale required that several foils be made from the same crystal.

(b) it was necessary to determine the particle size and spacing. These were measured using micrographs obtained from foils whose normals, [100] and [111], were parallel to the incident beam. The particle diameter was determined using the method reported by Boyd (1966) modified from the work of Scheil (1935). The particle size distribution was measured and a correction applied for the effect of the particles which fell out during electropolishing. The mean particle size was 1.5 ± .4μm.

The important interparticle spacing measured was that in the slip direction on the slip plane; i.e. in the [100] direction on the (111) plane. The result obtained here was 0.7 ±0.3μm, which is similar to the result of

Fig. 4.23. Transmission Electron Micrograph, typical region, showing 3 sets of θ^1 particles on {100} planes.

Russell and Ashby. Thus the particles were much larger than their average interparticle spacing.

It was hoped to carry out a Burgers vector analysis of the dislocations present during the forward and reverse deformation of the three different types of single crystal orientations: single slip, double slip and multiple slip. Much trouble was experienced in the foil preparation from the deformed test pieces, and only in one case was the Burgers vector analysis possible. The problem that arose in the foil preparation was the formation of an etched structure on the foil surface; this made it difficult to image the dislocations. Several other authors have experienced similar problems and only incomplete Burgers vector analyses were made. (Calabrese and Laird, 1973). It was possible to show that after a prestrain of 0.01 in tension in a test piece oriented for single slip the Burgers vector of the dislocations present was $\frac{a}{2}[110]$; (Figure 4.24).

The contrast adjacent to many of the particles was also examined. This contrast was shown by Russell and Ashby to be due to strain gradients close to the particles. There were two effects:

a) adjacent to individual particles

b) in the space (box-like) between some closely spaced particles.

The contrast close to individual particles was commonly

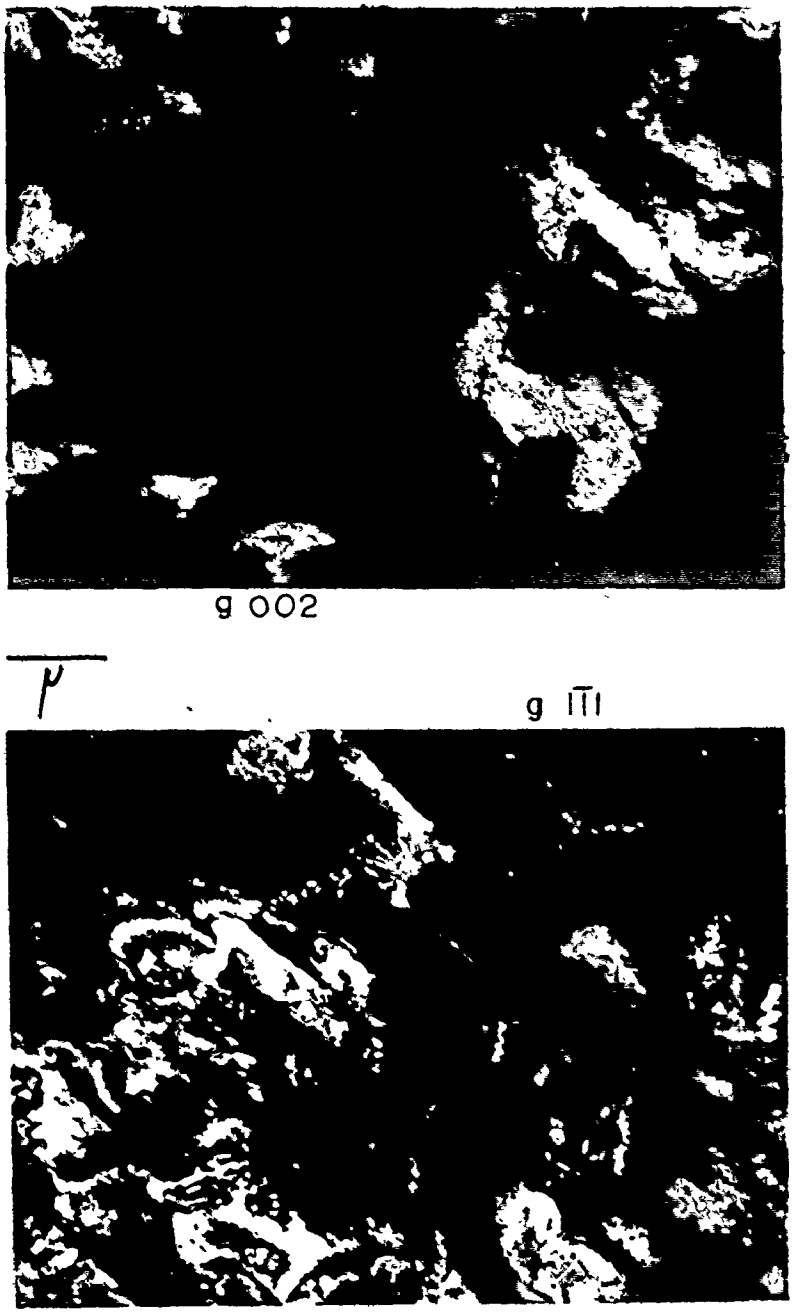

Fig. 4.24. Burgers vector analysis. SX341, shear strain 0.01, section cut // (111), tilted to [110]. Burgers vector of type $\frac{a}{2}$ [110].

observed. It was found to disappear in a matrix $(2\bar{4}2)$ reflection, and can thus be considered a true contrast effect, not arising merely from variations in foil thickness.

The second type of contrast effect, sometimes referred to as "checker board", was not seen very often except in small regions. It was common to see that the contrast on different sides of a particle was of opposite sign. The most common place to observe the effect was at the edge of an extinction contour. In the example shown in Figure 4.25 the regions labelled 3, 4 and 5 have different contrast, and there are small regions of checker board contrast nearby. The small orientation differences between the areas 3, 4 and 5 have been studied using Kikuchi Line techniques. The misorientations are small, approximately 0.1°, whereas the strain in specimen was a shear strain of 0.02. In some other cases studied the contrast disappeared in the matrix $(2\bar{4}2)$ reflection. It should be pointed out here that these contrast effects indicate the presence of strain gradients in the material. These are to be expected in materials which show a large Bauschinger Effect.

In the test pieces examined, the dislocation arrangements can be summarised as:

a) foils after tensile strain - dislocations were observed to lie close to the particles, with some bowing between them,

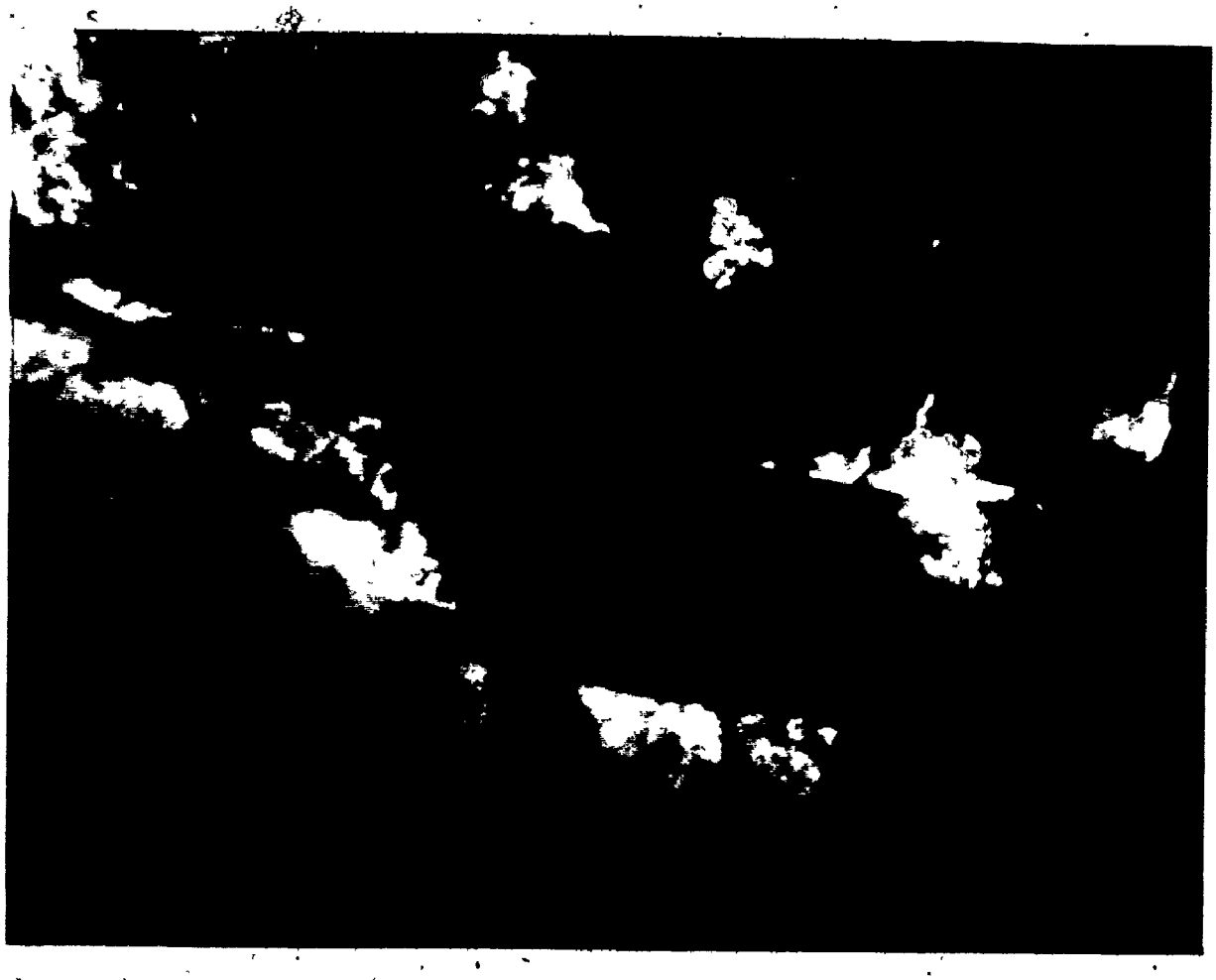

FIG. 4.25 SINGLE SLIP, STRAIN 0.02.

b) foils after strain in tension and compression to zero net strain - the dislocations occupy the space between the particles, and appear to have moved away from them. This motion of the dislocations away from the particles will contribute to the reverse strain.

Comparison of these arrangements can be seen in Figure 4.26.

It was necessary in this study to determine the nature of the processes causing the constant value of the long range back stress at tensile strains greater than 0.05. It has been indicated earlier that several processes can limit the magnitude of the back stress by causing plastic relaxation. The aluminum-copper alloy aged to θ' contains large particles and possible relaxation processes could be

a) breakdown of the interface between the particles and matrix, as reported by Atkinson et al. (1974) in Cu-SiO_2.

b) fracture of the particles, as seen in Al-13% Si. (Tetelman and McEvily (1967), from J. Gurland and J. Plateau, (1963)).

c) the plastic deformation of the particles.

Processes a) and b) involving the formation of voids adjacent to the particles have important implications in this work. The voids would cause the Orowan loops to disappear and the long range back stress would be reduced to zero. If the relaxation occurs by the plastic deformation of the particles the number of Orowan loops would remain almost

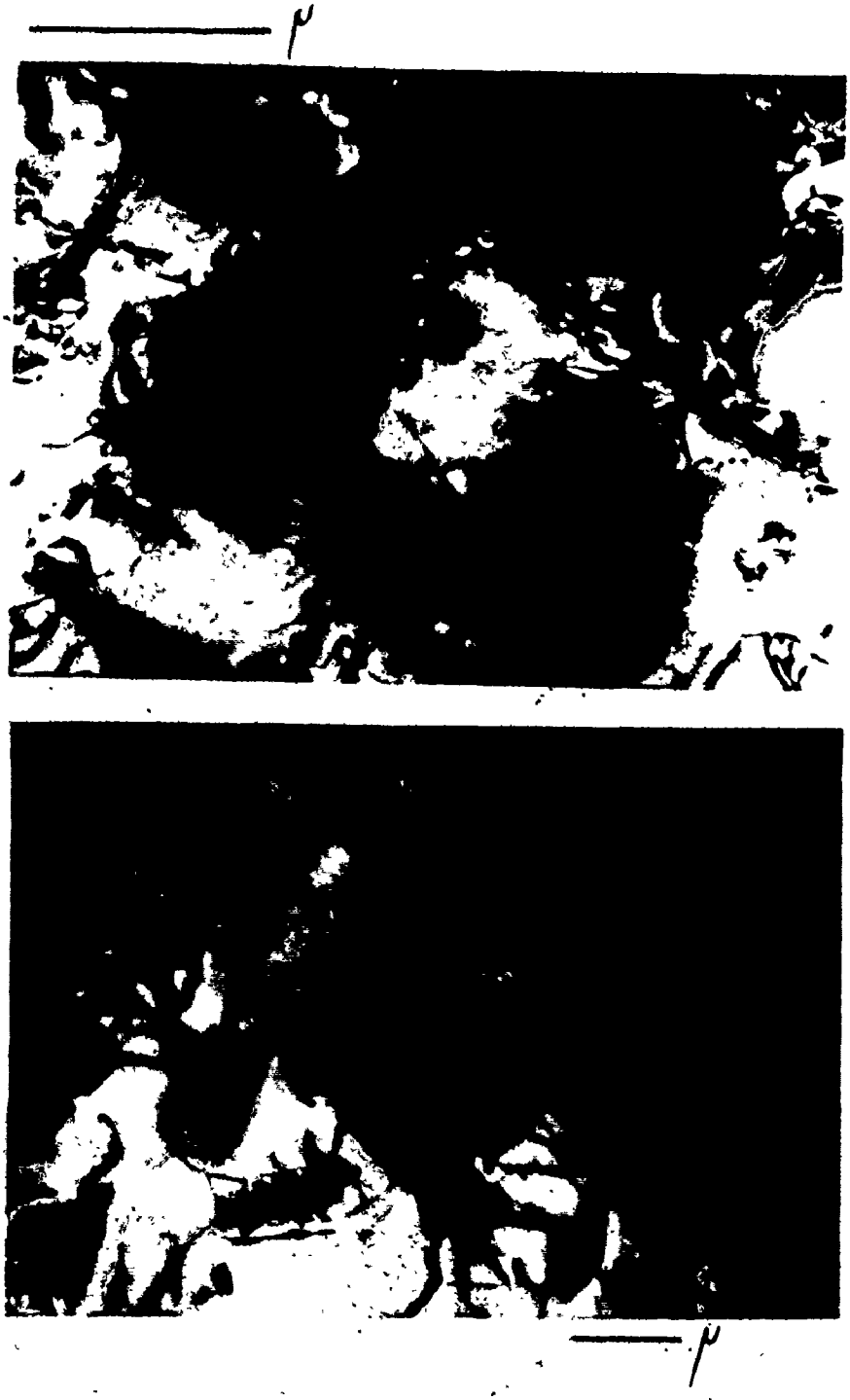

Fig. 4.26. a) Dislocations close to particles after Shear Strain .01.
b) Dislocations uniformly arranged after shear strain .01 in tension followed by .01 compression.

constant with increasing deformation, and the back stress would remain close to the value it had before the onset of particle deformation. Experiments were carried out to distinguish between the different processes.

In one set of experiments a piece of alloy aged to θ' was deformed by cold rolling 50% in one pass. The subsequent examination in transmission electron microscopy showed that the particles were no longer straight, but had assumed a sigmoidal shape, with no shape discontinuities (Figure 4.27). The particles were being plastically deformed, but not broken. The voids present from the electropolishing make it difficult to rule out the possibility of breakdown of the particle-matrix interface, but the voids were not observed in a second set of experiments.

In the second set of experiments, test pieces which had been tested to fracture in tension were sliced, and prepared for examination in the transmission electron microscope. The majority of the slices were taken outside the necked region, and had undergone approximately 10% tensile strain. The particles were found again to have undergone plastic deformation. Many of them were bent uniformly, but some showed discontinuities. On examination of the bent particles in dark field microscopy, using a θ' reflection (101), the black and white line contrast showed that the particles had been cut by matrix dislocations. Further

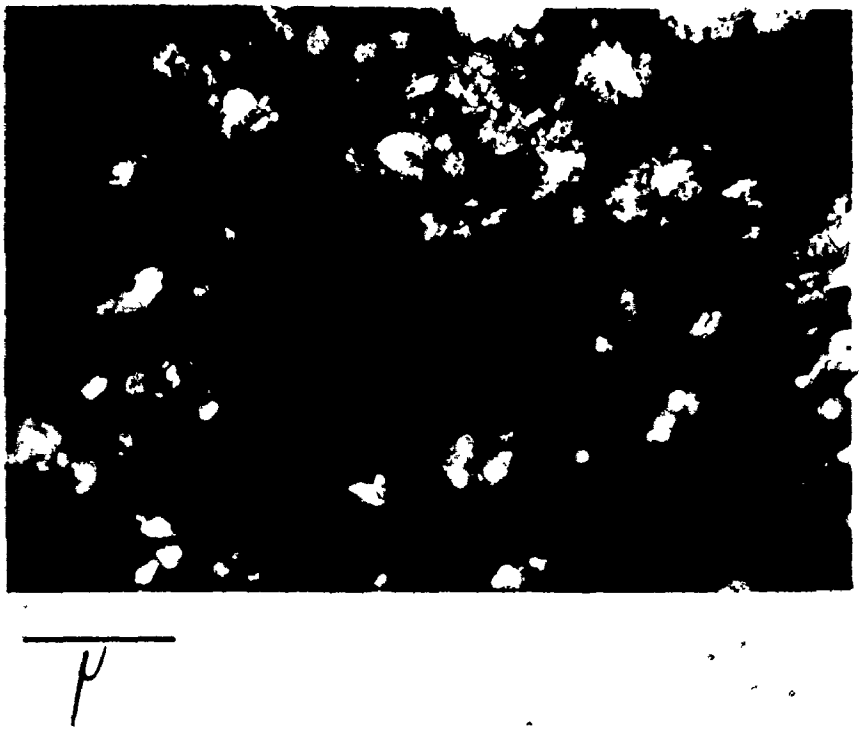

Fig. 4.27. Microstructure obtained after cold rolling 50%. The θ^1 particles have been plastically deformed into a sigmoidal shape.

evidence of the cutting came from the offsets observed in some of the anti phase boundaries. No evidence was detected for voiding at the particle-matrix interface. This work will be reported more fully in Chapter V, together with the electron micrographs (Figure 5.10 ff).

Thus the particles were found to undergo plastic deformation by being cut by the matrix dislocations. They were not found to have undergone fracture nor did the interface appear to break down. These results are consistent with the reported constant back stress at strains in excess of 0.05.

4.4 Errors

Although the load cell and strain gauge and their accompanying amplifiers were calibrated in the prescribed manner to the limits of 0.5%, it is realised that large errors must be present in the measurements made during the tests and in the material parameters used.

The important errors that may arise in the material parameters can be listed

a) variations in copper content along the length of the single crystals

b) variations in the density of θ' particles resulting from a).

The first of these involving the variation of copper is by far the most important since the concentration of the second phase particles is directly dependent on the copper content. It was for this reaon that the chemical analysis was carried out on 0.25" slices cut from the as grown crystals about 1" from the tops and bottoms. This chemical analysis showed that there was a loss of copper of some 0.5% during the single crystal preparation (when compared with the chemical analysis of the starting material). The results for 10 crystals shows that the average copper content is 3.08 $\pm$.15% at the bottom and 2.96 $\pm$.04% at the top. The crystals with the most differences were not used in the subsequent mechanical tests. The crystals which were used had a copper difference of less than 0.2 wt% between the top and bottom. This difference will be reflected in a greater θ' volume fraction in some of the test pieces and will lead to differences in their mechanical behaviour. The copper content in the calculations is taken as 3.0 wt% in the single crystals, and 3.6 wt% in the polycrystals.

The orientation of the single crystals was determined from back reflection Laue patterns. The accuracy is limited to 2°, and affects the calculated Schmid factor leading to a 5% error. There are other effects which are likely to have a greater effect.

In the mechanical testing, the testing rig and

specimen were carefully aligned, and the sources of error from other factors can be described as:

a) pen width and pen noise in the load measuring system. In the worst cases, at the highest load range, these were equivalent to a 10 pound uncertainty on the load scale, and for the test this represents a stress uncertainty of 0.15 ksi (1.03 MPa);

b) a small amount of backlash in the strain gauge, which was traced to the gear system of the chart drive. This represented a strain uncertainty of 0.03%;

c) the values of the yield stresses for the forward and reverse deformation had some uncertainty

(i) the initial yielding was well defined and the values obtained were subject to the noise (mentioned above) of 0.15 ksi (1.03 MPa).

(ii) the reverse yield stress taken at the 0.1% reverse offset is subject to a greater uncertainty because of the high work hardening rates at the small reverse strains. Pen noise and pen width combine here to lead to a maximum uncertainty of some 0.3 ksi (2.07 MPa).

It was necessary, in the mechanical testing, to ensure that buckling did not occur during the compression. This was prevented by the careful aligning procedure and by checking the test pieces after the tests for signs of buckling. Watt (1967) described a very detailed check on

his test pieces to show they were not buckled; those test pieces were cylindrical. The test pieces used in this study had square cross sections and a different check was used involving reflected light. Data from test pieces found to be buckled were discarded.

There were also difficulties associated with the measurement and meaning of strain for the single crystal test pieces oriented for single slip. The chief problems arose from (1) the effect of shoulders of the test pieces and (2) the effect of the grips in constraining the test piece.

Since slip in the test pieces took place along well defined slip planes, this would have been restricted in the early stages of the deformation so that both ends of the slip plane were in the gauge length. In this case dead zones existed at the top and bottom of the gauge length; as the material deformed and work hardened the size of the dead zones would decrease. In many cases slip lines were observed to penetrate into the shoulders of the fractured test pieces. The presence of the dead zones causes the measured strain based on a gauge length of 0.5" to be an underestimate of the strain that took place in the central portion of the gauge length. As the magnitude of the strain increased, the real strain and the measured strain would be closer.

The plastic deformation of the single crystal, oriented for single slip, leads to the displacement of the top of the test piece with respect to the bottom in a plane at right angles to the tensile axis. The testing rig prevented this displacement and a grip constraint effect resulted. This effect has been discussed by Hauser and Jackson (1961). It was considered to promote the onset of slip on some secondary slip systems and to cause the Schmid factor to be in error. The effective Schmid factor will be smaller than that determined for deformation with respect to the (111)[$\bar{1}$01] slip system. If a [213] orientation is considered, an estimate of the effect of the grip constraint on the Schmid factor may be obtained from the following

Slip system	Schmid Factor
primary	.47
conjugate	.29

The effective Schmid factor will be a complex combination of these values, plus others if other slip systems are forced to operate. The value will be smaller than that for primary slip. No attempt was made to determine the extent of the slip on the secondary slip systems.

The grip constraint cannot have a large effect on the onset of yielding in the reverse deformation. The tests carried out on the crystals oriented for single, double and

multiple slip show stress strain curves that are qualitatively similar to each other and to those from tests on polycrystalline materials. It is known that the polycrystalline and multiple slip test pieces are not subject to the grip constraint.

An analysis can be made of the experimental scatter found in the many tests carried out on polycrystalline test pieces. These tests indicate that at strains in excess of 0.04, the back stress values are constant, and independent of strain. It is the intention to use this scatter as a measure of the experimental error.

The data from these tests can be analysed to give

mean: 13.0 ksi (89.6 MPa)

standard deviation: 0.64 ksi (4.4 MPa).

This represents a standard deviation of about 5% of the mean value. A corresponding analysis cannot be made for the other tests on single crystals as the number of tests carried out on a given orientation was limited by the size of the crystal grown. For these tests the 5% value will be used for the standard deviation.

CHAPTER V

THE FRACTURE BEHAVIOUR

5.1 Introduction

The study of the fracture behaviour of the aluminum-copper alloys was considered separately from the principal area of investigation. However some of the experimental results obtained were necessary in the development of a comprehensive model for the deformation of the alloy. In particular the structural aspects of the fracture study contributed important data to the overall understanding of the mechanical behaviour of the material. The X-ray study of the side faces of the fractured test pieces and the Transmission Electron Microscopy of material from close to the fracture surfaces both help to determine the role of the second phase particles at large strains.

This Chapter will be divided into two parts. In the first a brief review of the literature will be presented covering the earlier experimental work on the fracture of precipitation hardened Al-Cu alloys, and indicating the criteria which have been developed to describe the observations. The second part will be devoted to an account of the experimental results obtained in the present study. The discussion and interpretation of these results will

be given in Chapter VI.

5.2 Review of Fracture Studies on Al-Cu Alloys

The principal studies reported in the literature, of the fracture behaviour of the Al-Cu alloys will be examined in this section. The attention will be restricted principally to the alloy containing 5 wt% or less of copper. Of particular interest will be the criteria proposed for the onset of the observed phenomena.

In most tensile tests the occurrence of necking prevents analysis of the load elongation data at large strains. It was reported, however, by Elam (1925, 1927) that aluminum-zinc crystals with more than 10% Zn failed by sudden shear along a {111} plane. Karnop and Sachs (1928) working with Al-5% Cu crystals reported a similar behaviour, with some orientation dependence of the tensile fracture stress.

Beevers and Honeycombe (1962) studied the fracture of Al-5.5% copper crystals in more detail and attempted to define a possible failure condition. All the crystals used were oriented for single slip and were aged to one of the following conditions:

a) solution treated, single phase; the only strengthening effect came from the solid solution.

b) GP Zones, so that strength was produced principally by the small copper rich zones which were cut by matrix dislocations from the start of plastic deformation.

c) θ" particles, in which the strengthening resulted from small coherent particles of composition approximately $CuAl_{1.8}$. These particles were also considered to be cut by the matrix dislocations early in the plastic deformation.

The crystals in the single phase solid solution condition showed large elongations with coarse slip bands parallel to the primary and secondary slip systems, closely parallel to the final fracture surface. Those crystals aged to contain GP zones showed less ductility, failing suddenly after some necking with little drop in load. Some slip markings were observed close to the fracture surface; only one crystal showed visible secondary slip. The alloys aged to contain θ" showed sudden failure without appreciable necking. The elongation was smaller than that for the other two ageing conditions. Slip lines were visible with coarse slip bands close to the fracture surface.

In all the crystals tested - all oriented for single slip - the fracture occurred on a {111} plane, parallel to the slip system operating at the time of fracture. The fracture surface contained many shallow dimples. The stresses at fracture were calculated from the measured load,

area and Schmid Factor (at fracture): a marked orientation dependence was found, and the author considered that the condition for fracture was a constant resolved shear stress. However they were not able to determine the event which occurred in the material to cause the fracture at a constant shear stress.

Price and Kelly (1964) argued that the critical process in the deformation was the formation of the shear bands, which they said occurred at a constant resolved shear stress for the material. They worked with superpure aluminum based single crystals containing 3.7% Cu, or 20% Ag or 15% Zn. The alloys were aged in different ways to produce a variety of precipitates. In two papers the deformation in tension and fracture of the crystals were discussed. The major portion of the work was devoted to alloys containing GP zones; the copper alloy aged to θ' was not extensively studied as it was reported to have necked and fractured on a 45° plane, not parallel to the active slip systems.

In the alloys aged to contain θ" there were different distinct processes in the deformation history. Coarse bands formed, followed by strain localisation, and then fracture took place. The stresses at which the bands formed were determined during interrupted tests. It was argued that the resolved shear stress was constant for the formation of the bands. The values obtained were similar to those reported

by Beevers and Honeycombe and by Karnop and Sachs - but these other values were for fracture, not shear band formation.

Price and Kelly attempted to determine a critical event to coincide with the observed shear stress criterion. Their discussion indicates that they were not able to determine such an event. Also, that the constant, resolved shear stress should be applicable to a wide range of materials, some containing different precipitates, and some tested in the single phase condition presents a further problem of interpretation. Likewise it is not clear if the proposed constant value is to apply to all orientations; the tests reported so far have all been carried out on crystals oriented for single slip.

In this present work it is desired to study the effect of the particles on the work hardening process, and at larger strains to determine how the processes occurring at the particles influence the stability of the deformation, and lead to continued uniform deformation or to its localisation. Even in some cases in which the strain is localised the processes leading to failure are of importance.

To study the onset of failure at large strains and the effect that the local events occurring at the particles have on the process a short series of experiments was carried out. In them it was desired to determine how the

fracture behaviour was affected by the orientation, and dimensions of the test piece, and the temperature at which the test was carried out.

5.3 Results of Fracture Studies

In this section, a brief account of the results obtained in the fracture studies will be given. Single crystals of aluminum 3% copper alloy aged to contain θ' particles were used for most of the tests carried out at 25°C. In some cases the tests were conducted at 77°K, or on crystals which had not been aged, but were in the solid solution condition obtained by quenching from 550°C, and storing for a short time at 77°K.

The major observations are given below. Some of the shear stress shear strain curves are shown in Figure 5.1, together with the curve for the Al-3% Cu alloy from Russell and Ashby, which was tested in compression. The crystals after yielding work hardened and gave a uniform shear strain of some 0.20 before a maximum was reached on the load-elongation curve. Necking commenced, and in most of the tests there was a slow decrease in the load level (Figure 5.2). Sudden small load drops were seen to coincide with the appearance on the sides of the test piece of coarse slip bands. In one such case, the load drops were equivalent to a stress drop of 0.3 ksi (2.07 MPa) at a load at which the

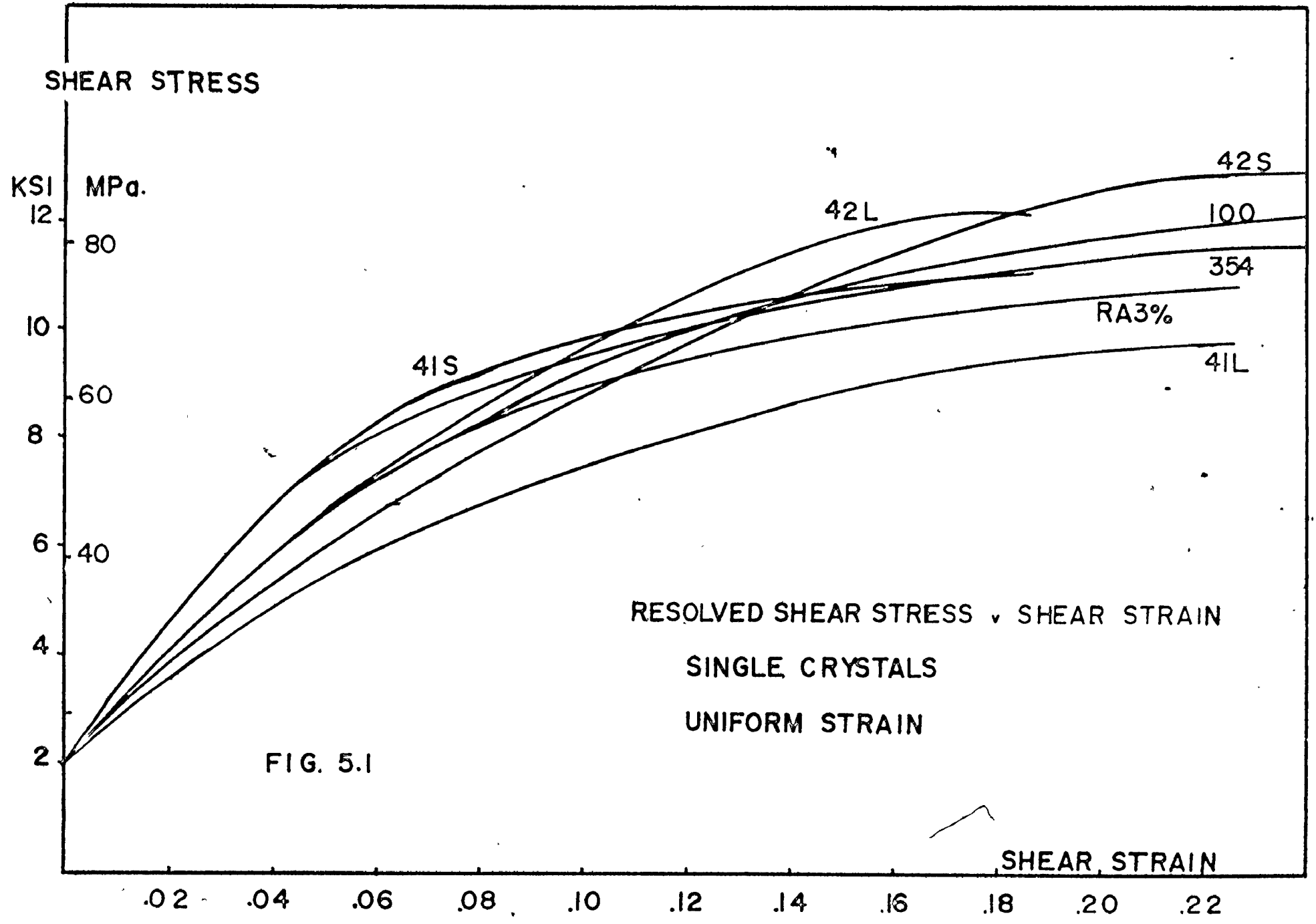
SHEAR STRESS
KSI
MPa.
12
80
10
60
8
6
40
4
2
42S
42L
100
354
RA3%
41S
41L
RESOLVED SHEAR STRESS v SHEAR STRAIN
SINGLE CRYSTALS
UNIFORM STRAIN
SHEAR STRAIN
.02
.04
.06
.08
.10
.12
.14
.16
.18
.20
.22

FIG. 5.1

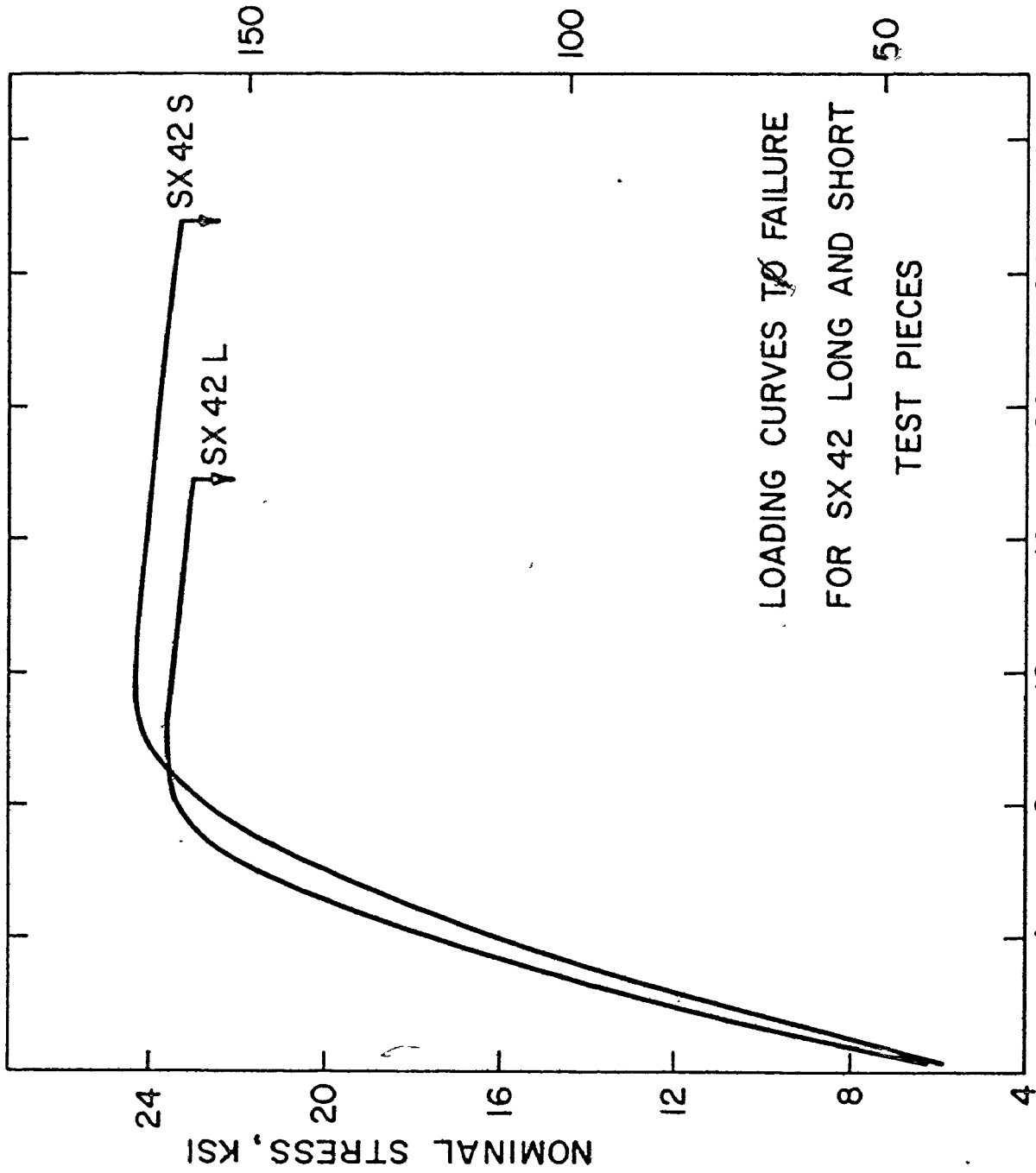
NOMINAL STRESS, KSI
24
20
16
12
8
4
150
100
50
SX 42 S
SX 42 L
LOADING CURVES TO FAILURE
FOR SX 42 LONG AND SHORT
TEST PIECES
4
8
12
16
20
24
28
ELONGATION %

FIG. 5.2

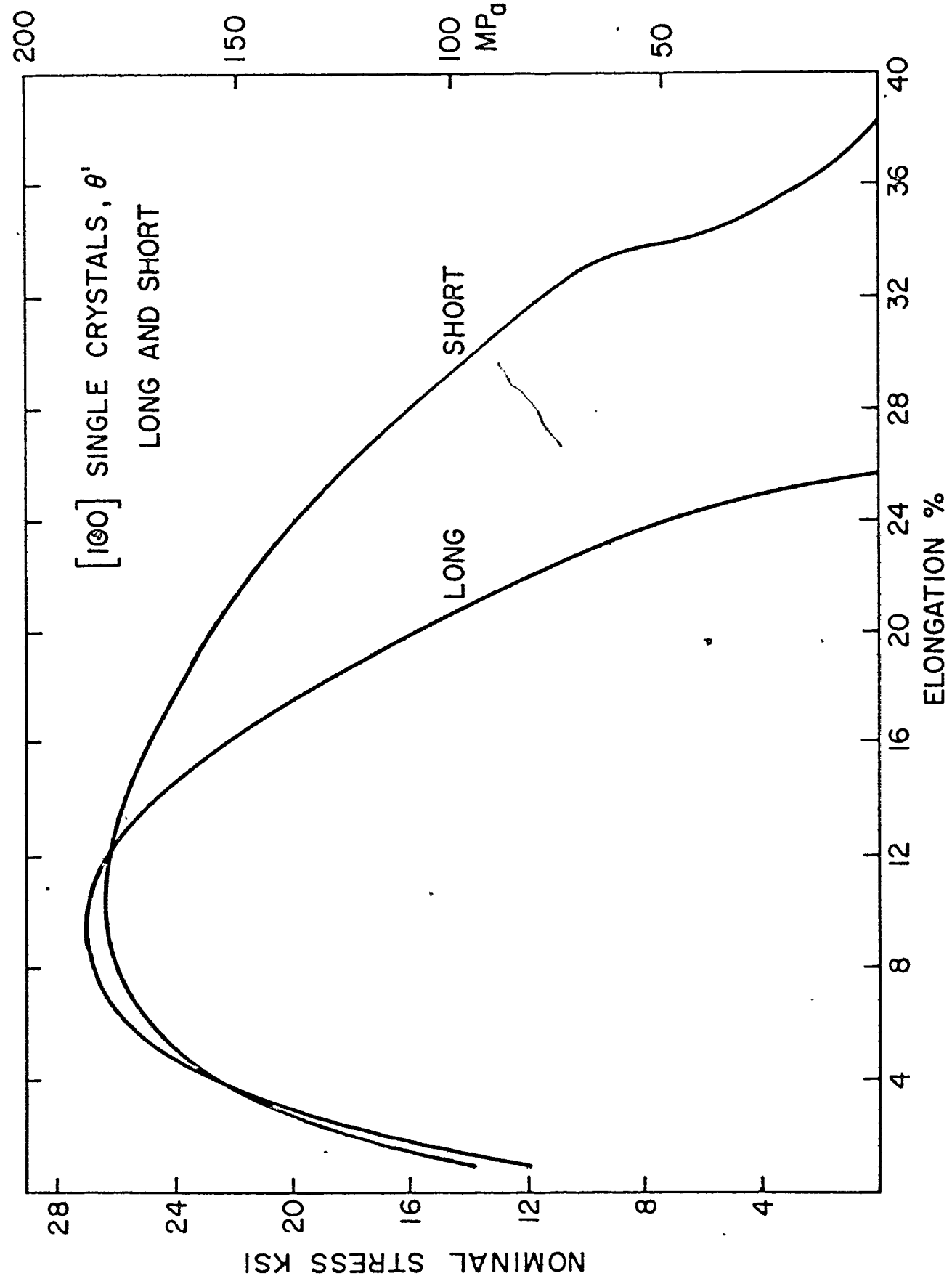
[100] SINGLE CRYSTALS, θ'
LONG AND SHORT
SHORT
LONG
NOMINAL STRESS KSI
ELONGATION %
MPa
200
150
100
50
28
24
20
16
12
8
4
4
8
12
16
20
24
28
32
36
40

tensile stress was approximately 34 ksi (234 MPa). The load drops were transient in form, and the load elongation curve returned to its original shape. Many such bands were observed on some test pieces. As indicated on the photographs, they were well separated.

Sudden failure often followed the formation of the bands. The final fracture occurred as shown in Figures 5.3-4, sometimes a) parallel to the primary slip system

b) parallel to a secondary slip system

c) parallel to two slip systems.

The final fracture surface was not heavily dimpled; such dimples as were observed after the sudden fractures were shallow (Figure 5.5).

There was an orientation dependence of the fracture behaviour. Test pieces oriented for slip on one or two slip systems failed in a sudden manner, with little necking, and with little reduction in the load level from its maximum. The test pieces maintained their square cross section. Those oriented for slip on many systems at [100] showed quite a different behaviour (Figure 5.6). They did not fail in a sudden manner, but ruptured only after extensive necking and at a greatly reduced load. The square cross section was not maintained, but became cross shaped. The fracture surface showed larger dimples than the unstable fractures.

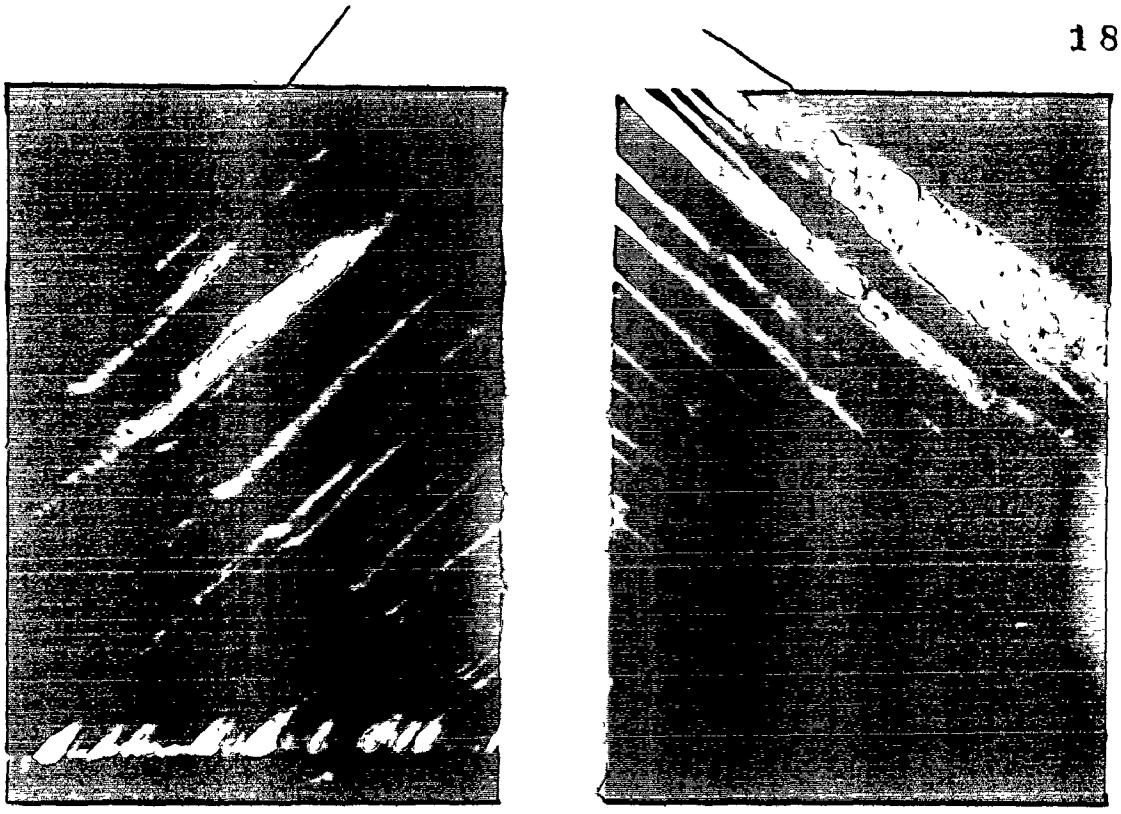

FRACTURE PARALLEL TO PRIMARY SLIP PLANE.

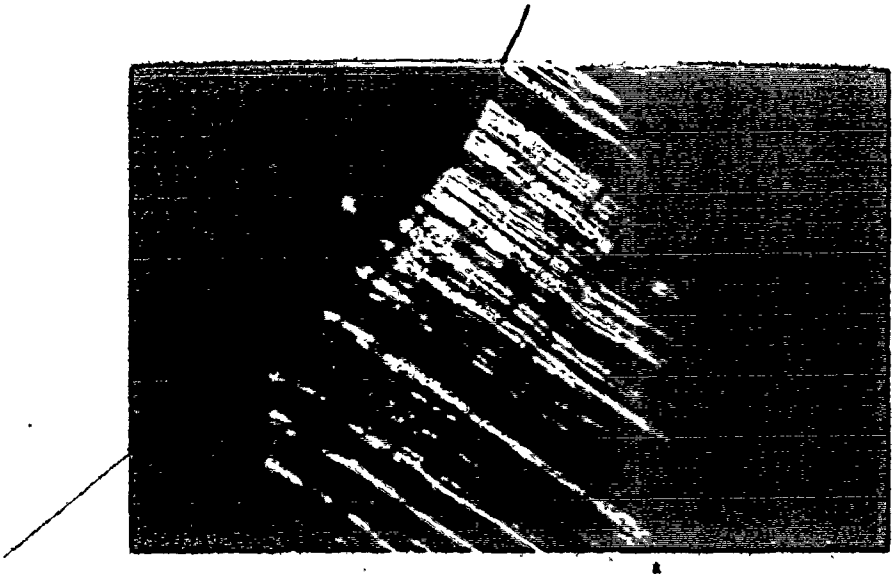

FRACTURE PARALLEL TO SECONDARY SLIP PLANE.

FIG 5.3

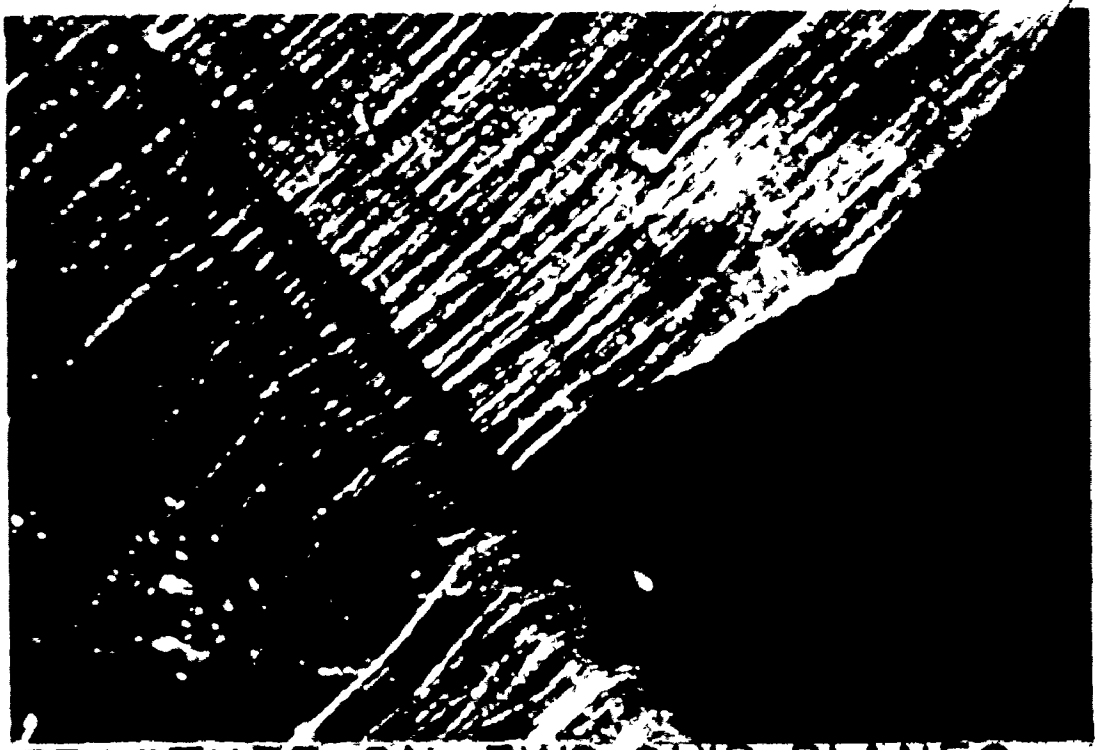

FRACTURE ON TWO SLIP PLANES

10μ (A)

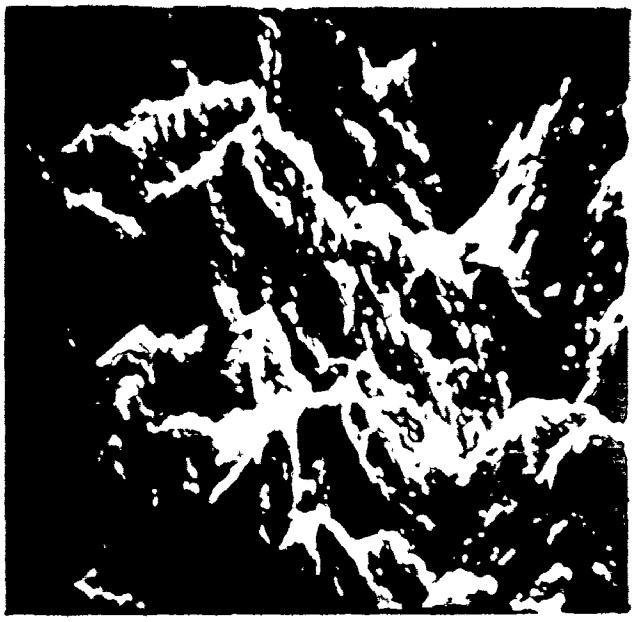

10μ (B)

(A) 100

(B) SX 382 DOUBLE SLIP

(C) SX 43L SINGLE SLIP

10μ (C)

FIG 5.5

SEM MICROGRAPHS FROM FRACTURE SURFACES OF SINGLE CRYSTALS

SIDES OF FRACTURED [100] SINGLE CRYSTAL

FIG. 5.6

Tests at 77°K showed that the sudden failures were still obtained, at higher stress levels and at larger strains.

Laue patterns were obtained at different points along the sides of the test pieces. They showed two different effects:

a) specimens oriented for single slip showed extensive asterism; in the region close to the fracture surface the pattern gave way to Debye Rings (Figure 5.7).

b) test pieces oriented for multiple slip did not show the same extensive asterism. It was less pronounced, and only in the region close to the fracture did it become extensive. Very close to the fracture surface, the spots became parts of Debye Rings; away from the neck, they showed very little asterism (Figure 5.8).

The major portion of the tests were carried out on single crystal specimens with a gage length of 0.5", (1.25 cm). Additional tests were carried out on other specimens cut from the same crystal, one with a short gage length, the other with a gage length in excess of 2.5", (6.25 cm). Similar effects, necking, sudden load drops, coarse slip, sudden failures were obtained, together with the necking to zero cross section in the [100] orientation.

A further set of tests was carried out on test pieces, prepared from the same crystal, oriented for single

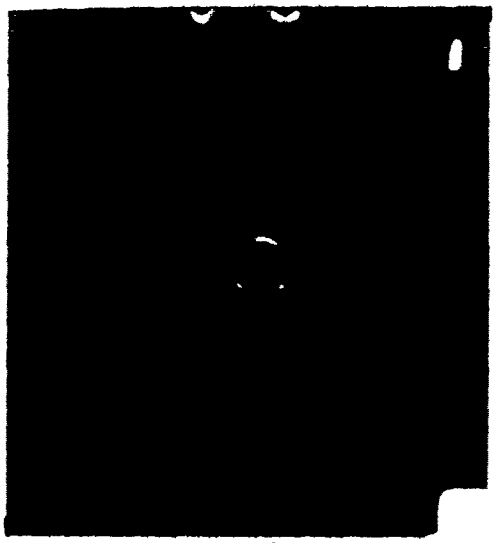

(a)

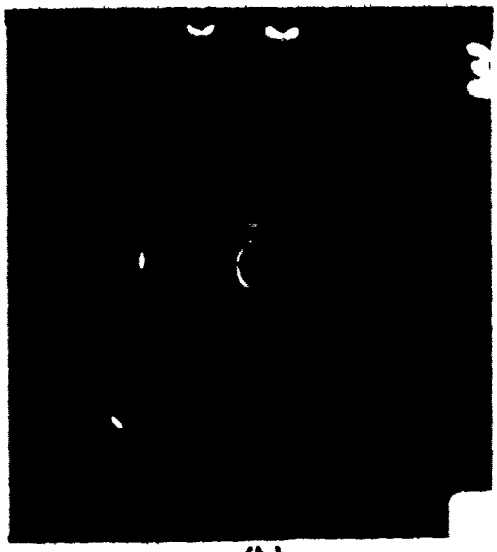

(b)

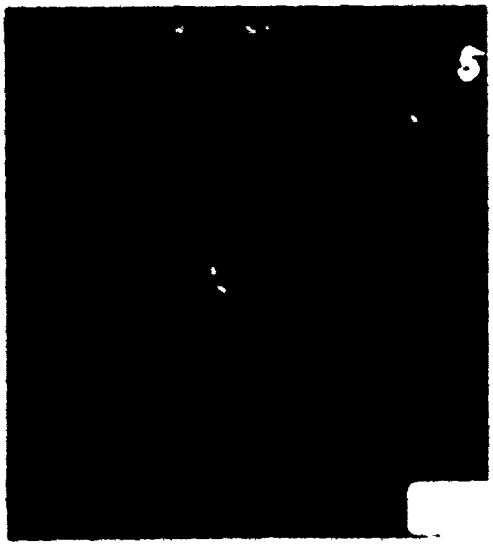

(c)

LAUE PATTERNS FROM SIDE FACE
SX-43L, θ'

a) 0.1"

b) 0.25"

c) 1"

FROM FRACTURE SURFACE

FIG 5.7

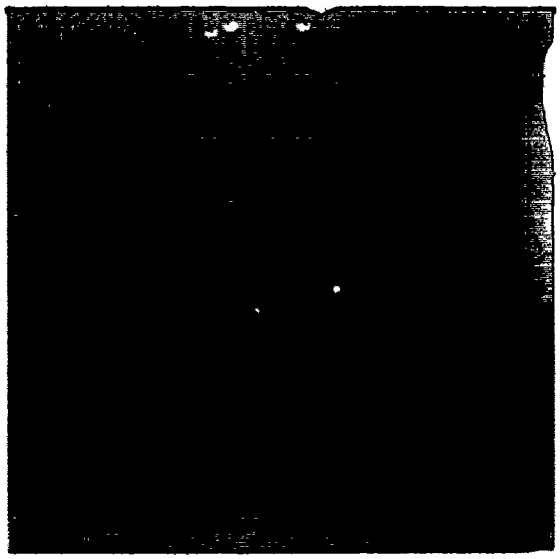

(a)

(b)

(c)

[100] SINGLE CRYSTAL, θ'

LAUE PATTERNS FROM SIDE FACES

a) 1"

b) 0.25"

c) 0.1"

FROM FRACTURE SURFACE

FIG 5.7

slip. One of these was aged to the θ' condition; it showed the effects mentioned above. The other was tested in the solid solution state. Its fracture behaviour was quite different in that it necked down and its fracture surface was chisel shaped (Figure 5.9). It failed at close to zero load.

A series of compression tests were carried out using small cylindrical test pieces, whose size was chosen to minimise the buckling. At large strains the coarse slip was observed. In tests carried out at different strain rates, a slightly positive strain rate dependence was obtained; this result agrees with that reported by Byrne et al. (1964).

Samples cut from the fractured test pieces were examined using Transmission Electron Microscopy. The evidence from this study was that the particles were cut by the matrix dislocations. There are two types of evidence for the cutting:

a) on some micrographs, it could be seen that the θ' particles were not straight, but were bent. (Figure 5.10)

b) examination in dark field microscopy using a precipitate reflection gave a black and white line contrast at the precipitates. This sort of contrast is typical of that obtained from antiphase domain boundaries formed when matrix dislocations cut ordered precipitates, such as θ'. (Figures 5.11, 12 and 13).

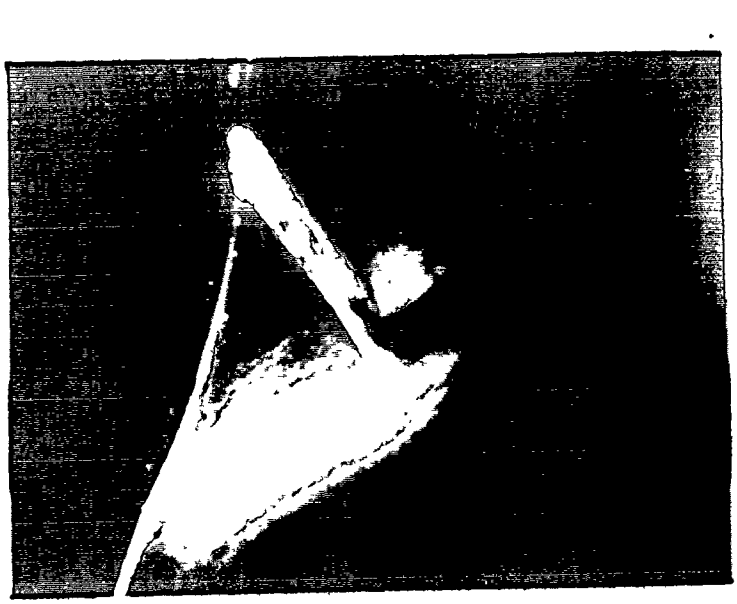

AGED TO θ'

UNAGED

FIG 5.9

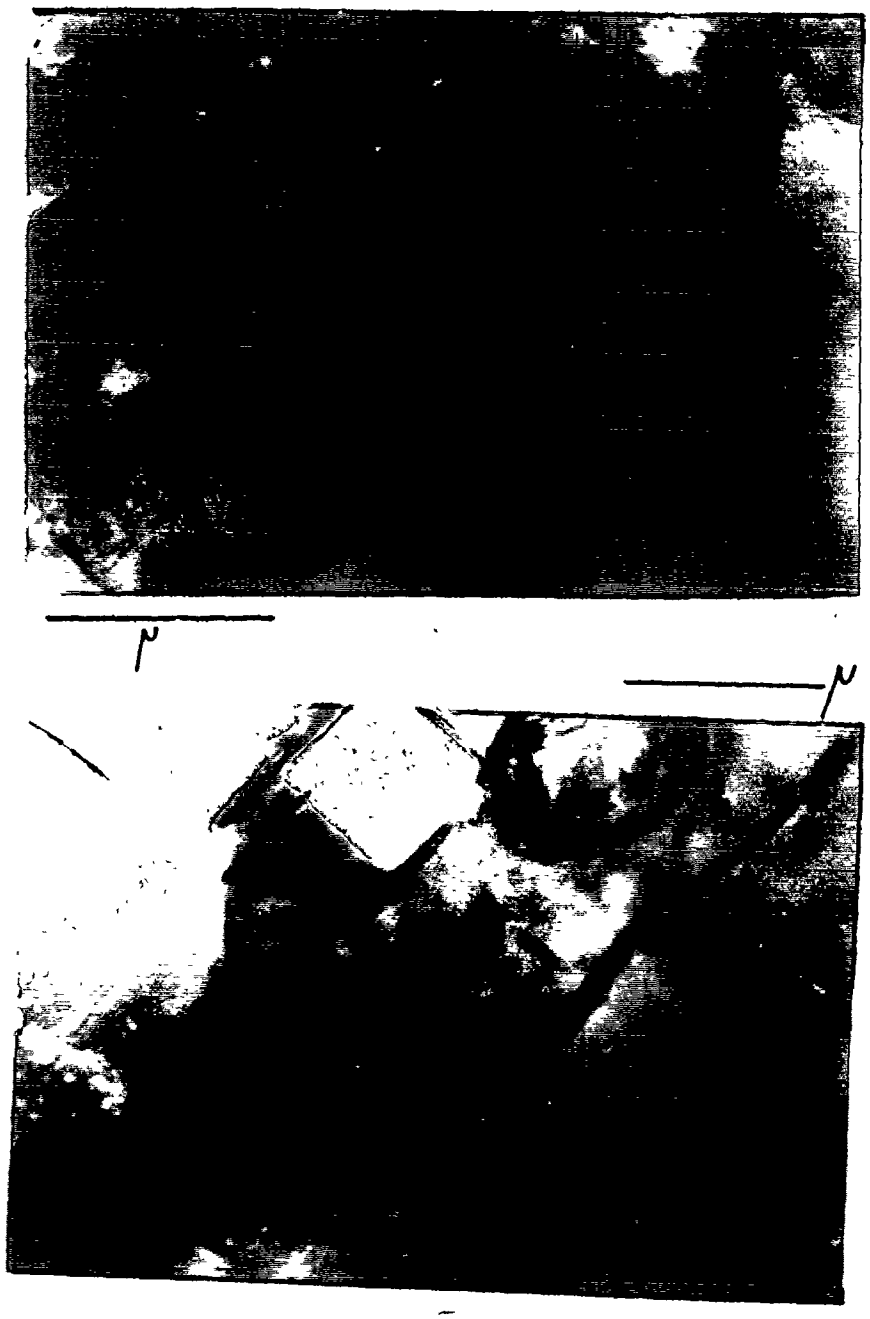

Fig. 5.10. Transmission Electron Micrographs showing deformed particles. Foil taken about 5 mm from fracture surface, [110] crystal, tilted to [100].

FIG 5.11

DARKFIELD MICROGRAPHS OF θ' PARTICLES SHOWING THE ANTIPHASE BOUNDARIES FORMED WHEN THEY ARE CUT BY MATRIX DISLOCATIONS. REFLECTION USED θ'_{101}

FIG 5.12

DARKFIELD MICROGRAPHS OF θ' PARTICLES SHOWING THE ANTIPHASE BOUNDARIES FORMED WHEN THEY ARE CUT BY MATRIX DISLOCATIONS. REFLECTION USED θ'_{101}.

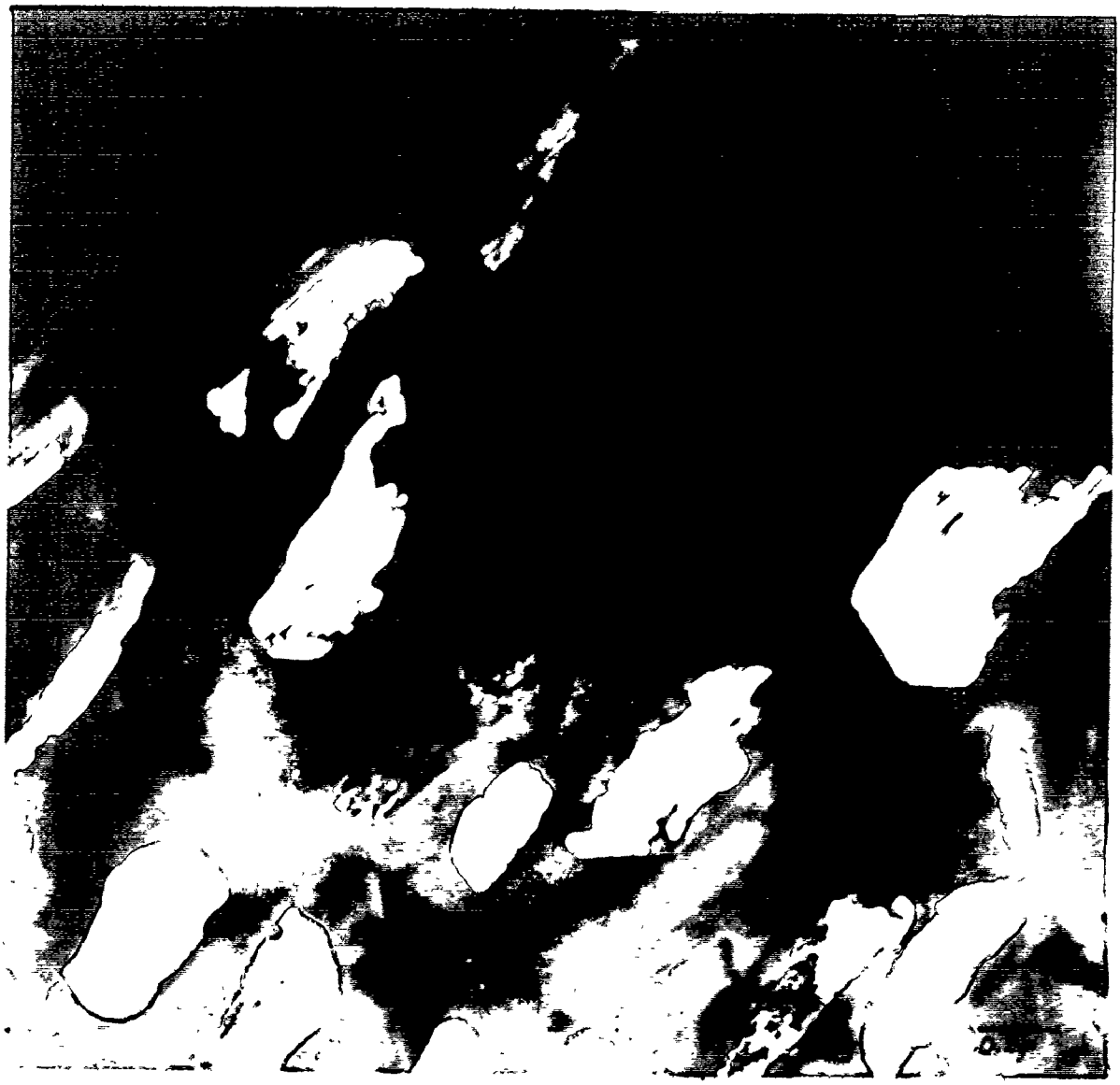

FIG 5.13.
DARKFIELD MICROGRAPHS OF θ' PARTICLES SHOWING THE ANTIPHASE BOUNDARIES FORMED WHEN THEY ARE CUT BY MATRIX DISLOCATIONS. REFLECTION USED θ'_{101}.

The fracture behaviour of polycrystalline samples of the alloy aged to θ' was dominated by the grain boundaries. All the tests carried out on such material showed the fracture occurring by the slow growth of cracks in the grain boundaries.

The results of these fracture studies will be discussed in Chapter VI. There it will be necessary to include an examination of the conditions leading to necking, the formation of the shear bands and the final fracture in either an unstable or a stable manner. The discussion will also include an account of the processes occurring in the material which lead to the above tests.

CHAPTER VI

DISCUSSION

INTRODUCTION

The important feature of the experimental results obtained in this study is the large long range back stress. This back stress is the same as that investigated by Wilson (1965), and it represents a large fraction of the work hardening at small strains in the alloy studied. That its magnitude is large suggests there is a polarisation in the dislocation accumulation at the particles. Then any attempt to devise a theoretical model must include the degree of polarisation, the magnitude of the back stress and its dependence on temperature and orientation. In addition it is necessary to consider the other experimental evidence (that obtained in X-ray and Transmission Electron Microscopy) that there is a removal of the dislocation structure during reverse straining.

It has been indicated in the literature survey that there are several possible models to describe the work hardening behaviour of two phase materials during unidirectional deformation. To distinguish between these models, it has been necessary to consider the evidence from

the reverse deformation studies. The results of this study will be compared with some of the theoretical models. Of importance also is the need to re-examine critically some of the data in the literature. Good agreement was obtained between some of the models and uni-directional tests. The agreement casts doubt on the attempt made in this study to explain the work hardening in terms of long range back stresses. This problem is the more important when these long range back stresses were explicitly excluded from the development of the models reported in the literature.

In comparing the experimental results with the models, it is necessary to make use of some material constants. These are given here for reference.

a) Shear Modulus of Aluminum

The shear modulus used is that given by Russell and Ashby (1970), with the values at different temperatures obtained using the formulation in Kaye and Laby (1962).

Temperature	Shear Modulus kg/mm^2	Shear Modulus psi	Shear Modulus MPa
77°K	$2.82 \cdot 10^3$	$4.01 \cdot 10^6$	$27.69 \cdot 10^3$
298°K	$2.55 \cdot 10^3$	$3.62 \cdot 10^6$	$25.00 \cdot 10^3$
373°K	$2.44 \cdot 10^3$	$3.47 \cdot 10^6$	$23.96 \cdot 10^3$

b) Volume fraction f of θ' particles

The volume fraction is calculated in a manner similar to that used by Boyd (1966). This is a calculation based on the phase diagram and leads to the following:

i) Polycrystalline material, containing 3.6 wt% Cu, f=3.7%

ii) Single crystal material, containing 3.0 wt% Cu, f=3%

The difference in copper content represents the loss of copper which occurred during the preparation of the single crystals.

c) The particles are large, and closely spaced;

diameter 1.5 $\pm$0.4 μm

spacing 0.7 $\pm$0.3 μm

d) The elastic moduli of the particles and of the solid solution are obtained from studies on the eutectic Al-$CuAl_2$ by Pattnaik and Lawley (1971), so that

$$\mu_{\theta'}/\mu_\alpha \approx \mu_\theta/\mu_\alpha = 1.32$$

e) Burgers vector

$$b = 2.86 \text{ Å}$$

6.1 Discussion of the Formula Used For the Flow Stress in Chapter IV

Before commencing any discussion of the results obtained in this study, some attention has to be given to

the formula used for the flow stress during the mechanical testing of the test pieces. This more detailed consideration is necessary as the method used to obtain the long range back stress depends on the applicability of the formula.

Many different terms can be included in a formula for the flow stress of an alloy at some strain ε_p. Atkinson et al. (1974) considered carefully how to add these different terms to determine the flow stress σ_f in the Cu-SiO_2 system. The terms were the lattice friction σ_L, the long range back stress σ_b, the source shortening σ_{ss}, the Orowan stress σ_{OR}, and the forest hardening stress σ_d. The lattice friction and the long range back stress were added linearly: the Orowan stress and the source shortening were also linearly added, but they were derived from strong obstacles among many weak ones (forest). These had to be added according to the addition law of the square root of the sum of squares. The overall result was:

$$\sigma_f = \sigma_L + \sigma_b + \sqrt{(\sigma_{OR} + \sigma_{ss})^2 + \sigma_d^2}$$

A more detailed account of the addition laws is given by Brown and Ham (1971).

In the Al-Cu-θ' alloy the source shortening can be considered small because the slip is well distributed, and then the forward flow stress approximates to

$$\sigma_f = \sigma_L + \sigma_b + \sqrt{\sigma_{OR}^2 + \sigma_d^2} \qquad A$$

This is different from the formula used in Chapter IV, but it will be shown that the difference is not great.

When the reverse deformation is examined, it is necessary to consider carefully the sense in which the different components of the forward flow stress will act. The lattice friction is independent of the sense of the deformation; so also is the forest hardening. The forest hardening is assumed to remain unchanged during the early part of the reverse deformation. The back stress aids the reverse deformation, and its value will decrease as the reverse strain increases. The Orowan stress presents an uncertainty. If the slip is exactly reversible, so that each dislocation moves back along the same slip plane on which it advanced, the Orowan stress will have no contribution to the reverse flow stress. The dislocations moving back will not see the array of obstacles. At the other extreme, if the reverse slip is completely independent of the forward slip so that no "forward" dislocation moves back and new sources have to be activated for the reverse deformation, the Orowan stress will have to be added to the formula for the reverse flow stress.

There are then two extreme possibilities for the reverse yield stress

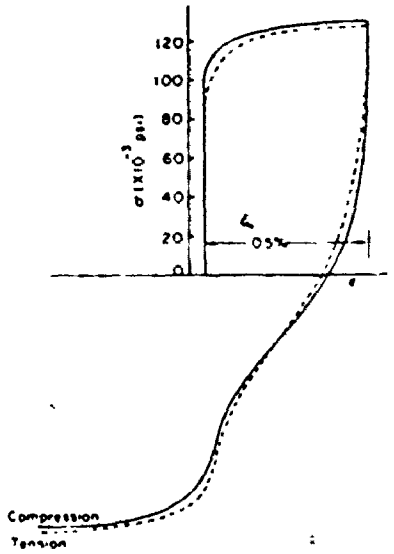

Fig. 6 A comparison between reverse and forward straining in compression first and tension first tests

Fig. 6.1. Stress Strain curve obtained at small strains, in dispersion hardened Nimonic 80 A. (After Asaro 1975)

a) for exactly reversible dislocation motion

$$\sigma_{rev} = \sigma_L - \sigma_b + \sigma_d \qquad B$$

b) for completely independent dislocation motion

$$\sigma_{rev} = \sigma_L - \sigma_b + \sqrt{\sigma_{OR}^2 + \sigma_d^2} \qquad C$$

and their applicability as indicated depends on the nature of the reverse slip in the alloy.

Some examples have been given in recent literature of the cyclic deformation of materials which deform by planar slip from the start of plastic deformation. Two such examples are

i) aluminum alloys - Stoltz and Pelloux (1974)

ii) Nimonic alloys and Fe-10%Al - Asaro (1975)

in which the planar slip was achieved by the cutting of the second phase particles. The important detail in the cyclic stress strain curves for these materials is that they show sections which are concave. An example from the work of Asaro is shown in Figure 6.1 . The concave parts are due to the almost exact reversibility of slip which can occur under these circumstances. As other processes occur to render the slip non-planar, the shape of the stress strain curves becomes more convex.

The aluminum copper alloy aged to θ' did not show any concave sections in its stress strain curve and it is

concluded that its slip is not exactly reversible. A further hint that the slip is more complex in this alloy can be found in the work of Russell and Ashby who showed that there were many cusps and jogs on the dislocations near the particles. The cross slip which caused these means that the dislocations would not use the same slip planes for the reverse deformation. However, the reverse slip planes will be close to the forward slip planes, and some form of favourable interaction must be expected during the reverse flow. The reverse flow in the aluminum copper alloy aged to θ' must be somewhere between the extremes.

From the equations A and B:

$$\sigma_f - \sigma_{rev} = 2\sigma_b \qquad D$$

and from A and C:

$$\sigma_f - \sigma_{rev} = 2\sigma_b + \sqrt{\sigma_{OR}^2 + \sigma_d^2} - \sigma_d \qquad E$$

whilst the correct result lies between these two expressions. In this study the Orowan stress can be estimated by comparison with Figure 3 in Russell and Ashby.

$$\tau \approx \frac{\mu b}{2L} \sim 0.7 \text{ ksi } (4.8 \text{ MPa})$$

For the polycrystalline material, this represents a tensile stress of approximately 2 ksi (13.78 MPa).

At strains larger than 2%, the estimated forest hardening contribution is more than 4 times this value (~9 ksi, 62 MPa). The difference between equations D and E is of the order of 0.22 ksi (1.5 MPa) at stress levels where

$$\sigma_f - \sigma_{rev} \approx 20 \text{ ksi (138 MPa)}$$

Thus, if the difference between D and E is ignored, it is likely to introduce an error of 1%. This 1% error will be found only if slip is exactly reversible; for slip which is not exactly reversible, the error will be less. The sense of the error can be determined. The desired quantity is the true long range back stress. The approximate value obtained from the use of equation D (the equation used in Chapter IV) will be slightly larger than the true back stress if the slip were exactly reversible. If the slip is completely independent, the values obtained from Chapter IV will be the true back stress.

At small strains, the effect of the Orowan stress can be estimated by approximating the forest hardening term to zero. Then equations A, B and C can be rearranged to give

$$\sigma_f - \sigma_{rev} = 2\sigma_b + \sigma_{OR} \quad \text{for exactly reversible slip} \quad F$$

$$\text{or} \quad \sigma_f - \sigma_{rev} = 2\sigma_b \quad \text{for completely independent slip} \quad G$$

In Chapter IV equation G was used to determine the back stress. If the slip were exactly reversible, equation F should have been used. The error then is $\sigma_{OR}/2\sigma_b$ which represents 2/2.2·16 in the case of test 502. The estimated error is about 45%, if the slip had been exactly reversible. It has been discussed earlier that the slip is not exactly reversible and the error must then be much less than this 45%.

It is useful to end this section with two points which indicate that the equation used in Chapter IV to determine the back stress was not too much in error.

a) Wilson determined σ_b/wk hdg for Duralumin by X-ray techniques, and for Al-Cu-θ' from his τ_{SN}. The values are 79% and 61% respectively. At the same strain the value for σ_b/wk hdg obtained in this study is 58% by the use of equation D.

b) The value of the back stress at a strain of 1% agrees very well with that determined from the use of the Brown and Clarke formula. This calculation will be given in a later section.

Some attention was given to the possibility that there were other methods that could be used to derive the long range back stress from the experimental load-elongation data. The methods used by Atkinson et al. (1974) were not suitable:

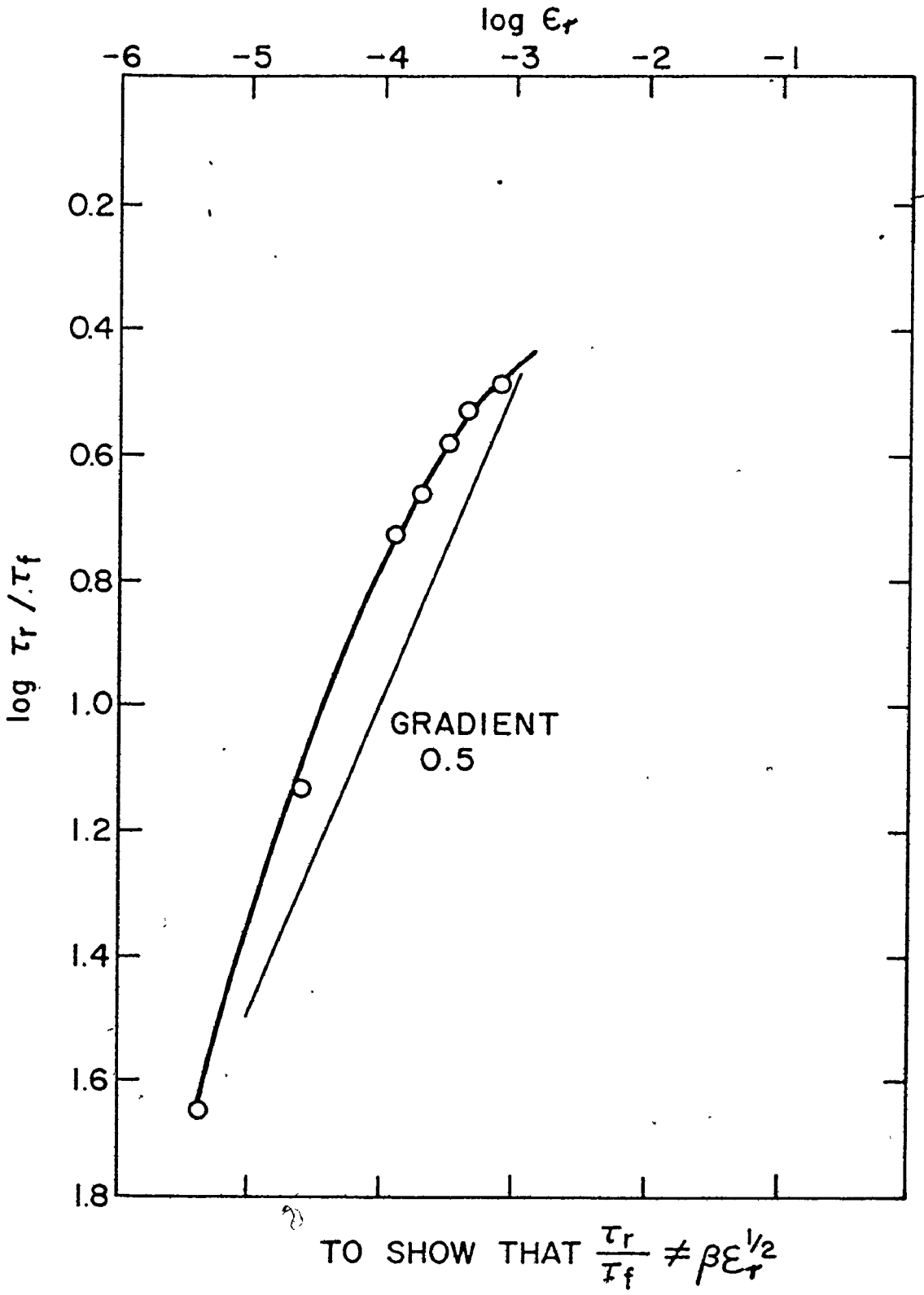
log ϵ_r
-6
-5
-4
-3
-2
-1
0.2
0.4
0.6
0.8
1.0
1.2
1.4
1.6
1.8
log τ_r / τ_f
GRADIENT
0.5
TO SHOW THAT $\frac{\tau_r}{\tau_f} \neq \beta \epsilon_r^{1/2}$

FIG. 6.2

(i) the forward and reverse deformation curves in the Al-Cu-θ' did not show the permanent softening of the type predicted by Orowan.

(ii) the reverse deformation curves in Wilson's work were found to satisfy $\tau_r/\tau_f = \beta\varepsilon_r^{1/2}$, and Atkinson was able to determine the mean stress in the matrix for the Cu-SiO_2 alloys by using a master plot derived from the many different tests of Wilson. The Al-Cu-θ' alloy did not obey this empirical relationship as shown in Figure 6.2, and when the Atkinson analysis was carried out on the Al-Cu-θ' alloy, inconsistent results were obtained.

6.2 Discussion of the Experimental Results

The principal experimental results obtained in this study show that the back stress increases rapidly with pre-strain, up to strains of the order of 0.03, after which the value approaches saturation. This is seen more clearly in the case of the tests carried out on the polycrystalline material, as many tests were performed to establish the dependence on strain. At the same strains, σ_b/wk hdg is decreasing and approaching a constant value. It is necessary to discuss the following aspects of the experimental results:

a) the initial dependence at small strains.

b) the dependence at larger strains.

c) the orientation dependence.

d) the temperature dependence.

For clarity, these will be discussed in sequence:

a) the dependence of σ_b and σ_b/wk hdg at small strains.

The initial rapid increase of σ_b with strain is similar to that observed in other work, and is considered to be due to unrelaxed deformation. The dislocations responsible for the unrelaxed plastic deformation, leave Orowan (or shear) loops on particles when the particles intersect the active slip planes. The number of the loops does not decrease due to relaxation and is related to the imposed strain. In other work reported in the literature, the deformation became relaxed so that the number of Orowan loops was not maintained and was reduced due to the operation of secondary slip, especially in the Cu-SiO_2 system, (Atkinson et al. 1974, Gould et al. 1974). In the Al-Cu alloy used in this study, the particle size is much larger and less equiaxed than the SiO_2 particles, and the particles are much closer together so that the cross slip mechanism will have unsuitable conditions to operate. There will still be some cross slip occurring at the perimeter of the particles, but geometric considerations indicate that the effect will be much smaller than that observed in the Cu-SiO_2 alloys.

At small strains the curve for σ_b/wk hdg can be extrapolated to zero strain to indicate the fraction of the early work hardening caused by the increasing back stress. These values, together with the values at large strains

(in excess of strains of .05) are tabulated in Table 6.1. The values at small strains are large and indicate that nearly all the work hardening is caused by the back stress. This is an important consideration, since it conflicts with the model used by Russell and Ashby (1970). The polycrystal tests of which a large number was carried out, indicate that about 80% of the early work hardening is derived from the back stress. It is important that there be other independent experimental evidence to support this result. The major piece of evidence comes from the X-ray measurements of Wilson (1965). From the work on Duralumin it can be shown that the ratio $\frac{\sigma_b}{\text{wk hdg}}$ at 9% torsion strain (~5.2% tensile) was greater than 79%. The trend established in this study is that $\frac{\sigma_b}{\text{wk hdg}}$ decreases as the strain increases. It could then be expected that at very small strains $\frac{\sigma_b}{\text{wk hdg}}$ would be close to unity.

b) Dependence of σ_b and σ_b/wk hdg at large strains.

In all the tests carried out, σ_b increases rapidly at small prestrains, and then, after some 3% strain, it tends towards a saturation value. These values are tabulated in Table 6.2. At the same strains it is also found that σ_b/wk hdg is approaching a constant value, as shown in Table 6.1.

The dependence of σ_b and σ_b/wk hdg on strain are

σ_b/wk hdg AT ZERO STRAIN AND AT LARGE STRAIN

TESTS	ZERO STRAIN	LARGE STRAIN (> .05)
SX 37 SS	~1.00	.55
SX 34 SS	~1.00	~.67
SX 31 DS	.75	.63
SX 35 MS	.92	.45
PX	.80	.55

TABLE 6.1

SATURATION VALUES OF σ_b

TEST	SATURATION σ_b ksi TENSILE	σ_b ksi SHEAR
PX	13.2	4.3
SX 37	>11	>4.8
SX 34	>11	>4.8
SX 31	11	4.8
SX 35	7.4	3.6

TABLE 6.2

both consistent with a relaxation mechanism dominating the work hardening process after some 3% strain. The cross slip mechanism responsible for the relaxation in Cu-SiO_2 can be ruled out as the major factor, as the geometrical constraints on the cross slip mechanism make it likely to operate only close to the perimeter of the θ' particles. The evidence presented in Figures 5.10 - 5.13 indicates that the relaxation process is the cutting of the particles by the matrix dislocations. The fracture of the particles and the voiding that accompanies it can be excluded for two reasons:

(i) the back stress does not decrease to zero; it would be zero if the particle matrix interface separated

(ii) the rolling experiment did not reveal broken particles, but rather the θ' particles were severely bent.

c) The orientation dependence

The tests on the polycrystal test pieces at strains larger than 5% show that σ_b has a constant value. The scatter in the results has been used to estimate a standard deviation of ± 0.6 ksi which represents a standard deviation of $\pm 5\%$. The small number of tests carried out on each single crystal orientation does not permit such an estimate;

the same percentage standard deviation is taken to apply for these tests.

Examination of the saturation values of the back stress indicates that those oriented for single slip are in excess of 11 ksi, whilst the double and multiple slip orientations are smaller. There is a significant difference between the multiple slip orientation and the other orientations, based on the difference in their saturation stresses exceeding twice the standard deviation.

$$|\sigma_{b\ max} - \sigma_{b\ max}^{SX\ 35}| > 2 \cdot \text{STANDARD DEVIATION}$$

But the data as obtained does not permit the determination of a significant difference between the single slip and the double slip orientations.

The values of σ_b/wk hdg can be examined in a similar way. The standard deviation of the back stress leads to a standard deviation of the ratio σ_b/wk hdg of about 7%. There is a significant difference between the multiple slip orientation and the other orientations, but it is not possible to establish that there is a significant difference between the single slip and the double slip orientations. The orientation dependence of the tensile back stress and the functions of the work hardening can be summarised:

The results for the multiple slip orientation SX 35, at [100] are significantly different from those for the

other orientations. The Schmid Factors can be used to convert the tensile stresses to shear stresses. When this is carried out the shear stresses are as shown in Table 6.2. The differences still have the same significance.

d) Temperature dependence

The temperature dependence of the back stress σ_b and σ_b/wk hdg can be seen in Table 4.3, which gives results for tests carried out at different temperatures on single crystal test pieces. In all cases the prestrain was close to 0.01 tensile strain, and the results show that the back stress and σ_b/wk hdg decrease as the temperature is increased from 77°K.

The temperature dependence of the mechanical behaviour could be due to the temperature dependence of the elastic modulus. The results, when normalised with respect to the temperature dependent modulus, are shown in Table 6.3. The majority of the results are close to unity, indicating that the temperature dependence of the results is largely due to the effect of temperature on the modulus. However, there is one set of results for each crystal which shows the largest departure - in each case it is the quantity

$$\sigma_{b\ 77}\ \mu_T/\sigma_{bT}\ \mu_{77}$$

	SX 22	SX 25
$\frac{\sigma_{077}\ \mu_{298}}{\sigma_{0298}\ \mu_{77}}$	1.1	1.02
$\frac{\sigma_{f77}\ \mu_{298}}{\sigma_{f298}\ \mu_{77}}$	1.06	1
$\frac{\sigma_{b77}\ \mu_{298}}{\sigma_{b298}\ \mu_{77}}$	1.13	1.08
$\frac{\sigma_{077}\ \mu_{373}}{\sigma_{0373}\ \mu_{77}}$		.99
$\frac{\sigma_{f77}\ \mu_{373}}{\sigma_{f373}\ \mu_{77}}$		.95
$\frac{\sigma_{b77}\ \mu_{373}}{\sigma_{b373}\ \mu_{77}}$		1.07

TABLE 6.3 THE DEPENDENCE OF THE PROPERTIES OF SINGLE CRYSTALS OF Al-Cu-θ' ON THE TESTING TEMPERATURE

where σ_{bT} is the measured long range back stress at temperature T°K. The discussion of the result can be carried out most easily with the help of some data from Atkinson et al. (1974). For the Cu-SiO_2 alloy, the values of the back stress obtained are shown in Table 6.4.

It is well established by Atkinson et al. (1974) and by Gould et al. (1974) that the deformation of Cu-SiO_2 is unrelaxed at shear strains up to 0.06 at 77°K, and .015 at 293°K. Beyond these strains the extent of the relaxation increases. The process of relaxation reduces the long range back stress, so that it is to be expected that, as the temperature is increased from 77°K, the back stress will decrease. For example, the ratio from Atkinson et al.

$$\sigma_{b\ 77}/\sigma_{b\ 293} = .87/.54 = 1.6$$

is an indication of a large relaxation. The values for the other temperature ratios increase rapidly, and a little care is needed as the ratio of unity for the result at 77°K does not suggest that no relaxation is taking place.

The results in Table 6.3 show that there is some relaxation occurring at the test temperatures to give the ratio

$$\sigma_{b\ 77}\ \mu_T/\sigma_{bT}\ \mu_{77} > 1.$$

However, the ratios remain close to unity, indicating that

TEMPERATURE T °K	BACK STRESS σ_b kg/mm^2	σ_{b77}/σ_{bT}
77	.87	1.0
293	.54	1.6
343	.31	2.8
400	.11	7.9

These results are obtained from Atkinson et al. (1974) Table 2. Care was taken to ensure that the crystals Cu-SiO_2-I-925 were used for all above results and that the prestrain and volume fraction were the same. The values of σ_b are corrected for modulus variation.

TABLE 6.4 RESULTS FOR Cu-SiO_2

the extent of the relaxation at the test temperatures and at the imposed strains is not great. The cause for this small relaxation must be found in the aspect ratio of the space between the particles; it is unfavourable to the cross slip process. Even at 100°C the deformation process is mostly unrelaxed.

6.3 Dislocation Model Used to Rationalise Observations

The interpretation of the above experimental results must be related to the structural evidence revealed by the X-ray and TEM studies. The X-ray evidence shows that extensive asterism was developed during prestraining and that it decreased during reverse deformation. It was observed in the crystals oriented for single slip, but not for those crystals which, oriented at [100], deformed by multiple slip. The TEM evidence is that dislocations accumulate at the particles during the prestrain, and during the reverse strain they move away from the particles and occupy the centres of the boxes between them. At larger strains the particles are cut by the matrix dislocations.

The model appropriate to describe the results is similar to that developed by Russell and Ashby (1970) based on the work of Ashby. In this model, the plastic deformation occurs by the movement of primary dislocations on the slip plane until they are stopped by the particles. It

has been explained earlier how the model calculates the flow stress by using the average dislocation density and the formula derived earlier by Nabarro et al. (1964). In this study the large Bauschinger Effect must be accounted for, and the model of Russell and Ashby will have to be developed further.

It is necessary to examine the model in two stages: these consider the crystals oriented for single slip and multiple slip. The single slip case will be considered first.

The alloy aged to θ' contains 3 sets of θ' particles with average diameter about 1.5μ and interparticle spacing about .7μ. The alloy is oriented for single slip, and at a critical resolved shear stress (which will match the value obtained by Russell and Ashby), dislocations can commence to move in the matrix. The stress necessary is the matrix friction stress. They move towards the first array of particles and will be stopped there until an additional stress of

$$\tau \approx \frac{\mu b}{2L}$$

is applied to cause the dislocations to bow between the particles. The factor of 2 is based on a comparison with Russell and Ashby, figure 3. Here L is the spacing between the particles in the [110] direction on the (111) slip

plane. This additional stress is the Orowan stress. For the alloy it is about .7 ksi (4.8 MPa), and it enables the dislocations to bow between the particles, leaving at them Orowan loops, with primary Burgers vector.

Continued deformation leads to the further bowing of dislocations between the particles and the accumulation of Orowan loops. The arrangement of these loops as the strain increases has been examined by Russell and Ashby. The loops accumulate close to the particles at small strains. At larger strains ($\gamma > .02$) the dislocations seem to stand off from the particle in an edge wall, similar to a low angle grain boundary. The edge of the wall is perpendicular to the Burgers vector, so that it is a (110) plane.

Ashby was able to estimate the dislocation density in terms of the applied strain using simple geometry. He was able also to show that the angle ϕ through which the plates were rotated was equal to the shear strain γ, and that the lattice acquired a curvature whose mean was $2\gamma/L$.

In the development of the model for other types of precipitate particles, especially SiO_2, Ashby introduced the formation of prismatic loops by the cross slip process or by a punching process. This could happen easily in the Cu-SiO_2 alloy system with equiaxed particles. However, in the Al-Cu-θ' alloy it is not likely, as the aspect ratio of the space between the particles is unfavourable. In the

Al-Cu-θ' alloy only glide loops are found, except perhaps close to the perimeter of the particles where some cross slip can occur. There is evidence in the TEM results of Russell and Ashby which showed that at shear strains up to 0.05 almost all (95%) of the dislocations at the particles had primary Burgers vector. The few secondary dislocations were not significantly arranged or positioned.

No assumption has been made about the distribution of slip planes. The evidence indicates that the slip is uniformly distributed, and that it is not planar, as has been observed in many alloys containing cutable precipitates. The observations that the dislocations stack as edge walls at the particles, and that there are many cusps and kinks, can only be accounted for by the dislocations having to cross slip to form the walls. The coplanar Orowan loops at the particles, of the type proposed by Hazzledine and Hirsch in the Cu-Al_2O_3 alloy, have not been observed in the Al-Cu-θ' alloy. The cross slip will have an important influence on the reverse deformation characteristics of the alloy.

The accumulation of Orowan loops at the particles leads to development of asterism on Laue X-ray photographs. This can be accounted for using the Ashby model. The accumulated dislocations indicate that the lattice has been curved in the regions close to the particles because of the rotation of the platelets. The mean curvature increases

as the strain increases, so that the asterism must also increase.

Also, during the reverse strain, the asterism is reduced and is built up again as the strain increases in reverse. This requires that some or all of the dislocations move back along their slip planes. To have the dislocations behave in an exactly reversible manner demands that the slip be planar. The many cusps observed, indicating that some cross slip has occurred, will render exact reversible slip impossible. The reduction of asterism must be obtained by some of the dislocations moving back on their own slip plane or on adjacent slip planes (leaving some debris close to the particles). The TEM evidence supports this idea. The dislocations during the reverse flow occupy the centres of the boxes, whilst during the forward strain they were close to the particles.

The matrix has been deforming plastically, whilst the particles have been undergoing only elastic deformation, and the dislocations have accumulated at the particles. The particles have caused inhomogeneity in the plastic deformation and their elastic deformation causes a long range back stress to be developed. Ashby, in his model, considered that this back stress would be negligible and did not include it in the formulation of the equation for the work hardening increment. However, it has been shown that

the back stress is appreciable and, at small strains, accounts for nearly all the work hardening. The magnitude of the back stress obtained in the present experiments will be compared with the values predicted on the basis of the Brown and Clark model.

At larger strains, the particles begin to undergo plastic deformation. The process occurs because the stress on the particles, approximated by σ_b/f, exceeds their yield stress. When this happens, there is not an avalanche of dislocations, but rather there is a one to one process. One dislocation arriving at the particle leads to a dislocation on the same or on a nearby slip plane to pass through the particle. The reason why all the dislocations on a given slip plane do not rush through the particle is because the particles still have strength; their yielding is not like the cracking and voiding process experienced with some particles in steels. When these particles crack or void, there is nothing to support the dislocation loops and they collapse into the void. In the alloy with θ' particles this does not happen: the number of dislocation loops, and hence the elastic strain on the particles, remains constant. The significance of the quantity σ_b/f will be discussed later.

When cutting of the particles takes place, the back stress remains constant. Then the work hardening rate is

dominated by the matrix and it will not have a contribution from the back stress. A change in the work hardening rate is observed. In the tension tests this is difficult to detect because the onset of necking obscures the effect. However, in compression tests there is a marked change in the work hardening rate at some 10% shear strain. The almost constant back stress, and the slowly increasing flow stress lead to an almost constant value of σ_b/wk hdg at shear strains greater than 10%.

When the crystals oriented for multiple slip at [100] are considered, not all of the above discussion is applicable. The important differences are:

a) the asterism is not developed until larger strains ($\gamma \gtrsim .10$)

b) the back stress is smaller

c) the back stress contribution to the work hardening is smaller.

These three results can be included in the proposed model, if multiple slip is allowed to take place.

Plastic deformation of the [100] crystal occurred by the operation of at least four slip systems. These will intersect at the particles and there the possibility exists for dislocation interactions which can either

a) reduce the lattice rotation

b) reduce the displacement at the particles

or c) reduce both the displacement and the rotation. When the lattice rotation is reduced the asterism is reduced, and the reduction of the displacement at the particles causes the long range back stress to be reduced.

Bonar (1962), in an investigation of line contrast at θ' particles after plastic deformation in Al-Cu alloys, showed that interactions of the above type take place. Many other explanations for the line contrast, including Moiré fringes and antiphase domain boundaries, were excluded on account of experimental observations that the lines lay parallel to <110> and were invisible when a matrix $(\bar{2}20)$ reflection was used.

One example of a reaction will be given. Consider the intersecting slip planes (111) and $(11\bar{1})$; Burgers vectors of dislocations moving on these planes are:

$$\frac{a}{2}[10\bar{1}] \quad \text{and} \quad \frac{a}{2}[011]$$

They intersect along $[1\bar{1}0]$, and along the line of intersection the two dislocations react to produce the dislocation with Burgers vector $\frac{a}{2}[110]$. This is a pure edge dislocation, and the glide plane available to it is (001), which is not a normal slip plane in the fcc materials. The reaction is energetically favourable according to Frank's Rule (1949). This dislocation has been known for some time as a Lomer Lock (1951). It is a prismatic dislocation, and

the displacement at the particle is smaller than that obtained if either of the two dislocations $\frac{a}{2}[10\bar{1}]$ or $\frac{a}{2}[011]$ had collected at the interface. It can also be argued that the lattice bending has been reduced.

Not every dislocation of the type $\frac{a}{2}[10\bar{1}]$ and $\frac{a}{2}[011]$ arriving at the particle interface will undergo the reaction; to do so would require that every plane was an active slip plane. In fact, these slip planes are at least 40 atomic spacings apart, so there is a finite probability that the reaction will not take place for all dislocations. However this probability increases if multiple slip is considered to take place.

The reverse deformation of the crystals oriented at [100] must take place less readily than that for the single slip crystals. The reason for this is found in the way that the dislocation reaction to form Lomer Locks has pinned the two dislocations so that they cannot move. The reverse plastic deformation must use the dislocations which had not interacted to form the Lomer Locks or produce some additional ones by the operation of some sources. The experimental results show that the long range back stress is smaller for the [100] crystals than for the crystals deforming by single slip. The second way to consider this reduction of the back stress is that the prismatic dislocations produced by the dislocation interactions have a much

smaller displacement at the particle interface. Both Atkinson et al. (1974) and Gould et al. (1974) have shown a similar result, that the Bauschinger Effect is reduced when prismatic loops are formed. Gould et al. showed that the

$$\frac{\text{back stress from one Orowan loop}}{\text{back stress from one prismatic loop}} = \frac{12}{7} .$$

The model described is very similar to that of Ashby (1970). However Ashby calculated the work hardening by assuming that it depended only on the average dislocation density; the back stress contribution was considered negligible. The chief experimental result of the present study is that there is a large Bauschinger Effect in the Al-Cu-θ' alloy, implying that there is a large long range back stress. Ashby's model gave a good agreement with the experiments carried out by Russell and Ashby. These experiments were unidirectional only, being conducted in compression. There is a need to examine further this agreement and to determine if the results can also be explained using another model which includes the back stress hardening. The next section will discuss the details.

6.4 More Detailed Discussion of the Ashby, and Russell and Ashby Model

The good agreement between Ashby's model and their experimental data for unidirectional tests is shown in

Figure 6.3 from the paper by Russell and Ashby. In this figure the work hardening increment $\frac{\tau-\tau_o}{\mu}$ is plotted against $\sqrt{\frac{\gamma b}{D}}$, where τ is the flow stress at a shear strain γ, τ_o is the initial yield stress, μ the shear modulus and D the interparticle spacing in the [110] direction on the (111) slip plane. The graph was obtained by calculating these quantities for the 2, 3 and 4% Cu alloys at shear strains of .05, .10, .15 and .20. The earlier data from Dew-Hughes and Robertson was also included. The agreement between the data points and the line is good, and the slope of the line is very close to the slope predicted by Ashby's model. The authors concluded that the work hardening in the alloys could be satisfactorily accounted for by the model.

The Russell and Ashby calculations must be examined in more detail. The model used a relationship between flow stress and dislocation density similar to that of Nabarro, Holt and Basinski (1964),

$$\tau = \alpha G b \sqrt{\rho}$$

where ρ is the dislocation density. In the formulation of the model, Russell and Ashby attempted to prove this parabolic relationship between flow stress and dislocation density. Figure 13RA shows the measured dislocation density as a function of shear strain, and also as a function of work hardening increment. The model depends critically on

this plot. The dislocation density determinations were carried out at shear strains of less than 0.025, but, in the formulation of the model, these data were extended to shear strains of 0.2. Again, the plot of dislocation density v work hardening increment appears parabolic, but closer inspection shows that it can be argued that there are really two different sets of data for the aged materials. One set is for the 4% Cu alloy, and the other for the 3% alloy; straight lines can be drawn through the origin and the data points for each alloy, and the linear fit is more convincing than the parabolic curve. This new linear fit implies that:

a) there is a linear relationship between the dislocation density and the work hardening increment
b) some dependence of the work hardening increment on the volume fraction of the second phase.

This is not too surprising since the plot of dislocation density against shear strain (Figure 13aRA) does show a strong dependence on volume fraction (or copper content).

The data presented by Russell and Ashby in Figure 3RA and used in Figure 14RA has been recalculated and replotted. The data of Dew-Hughes and Robertson has not been included on this plot as their interparticle spacing was not measured in the same way. For this calculation the following were used:

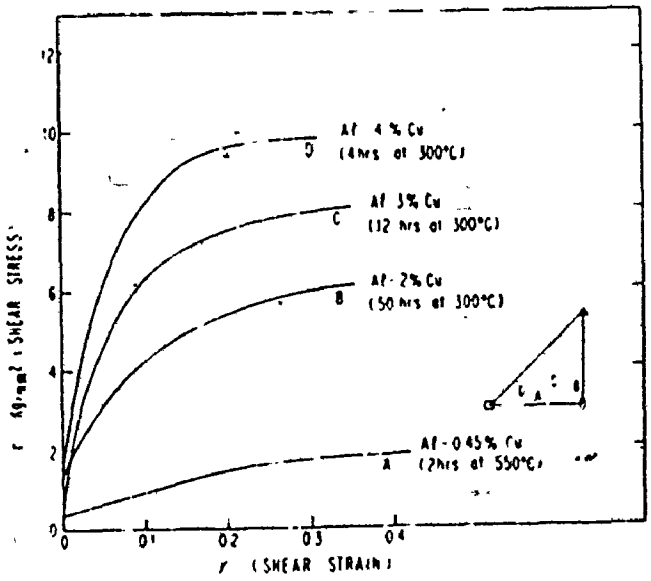

Fig. 3. Shear stress-shear strain curves of the solid solution, and of the three aged alloys.

Note alternate linear relationship in Figure 13b.

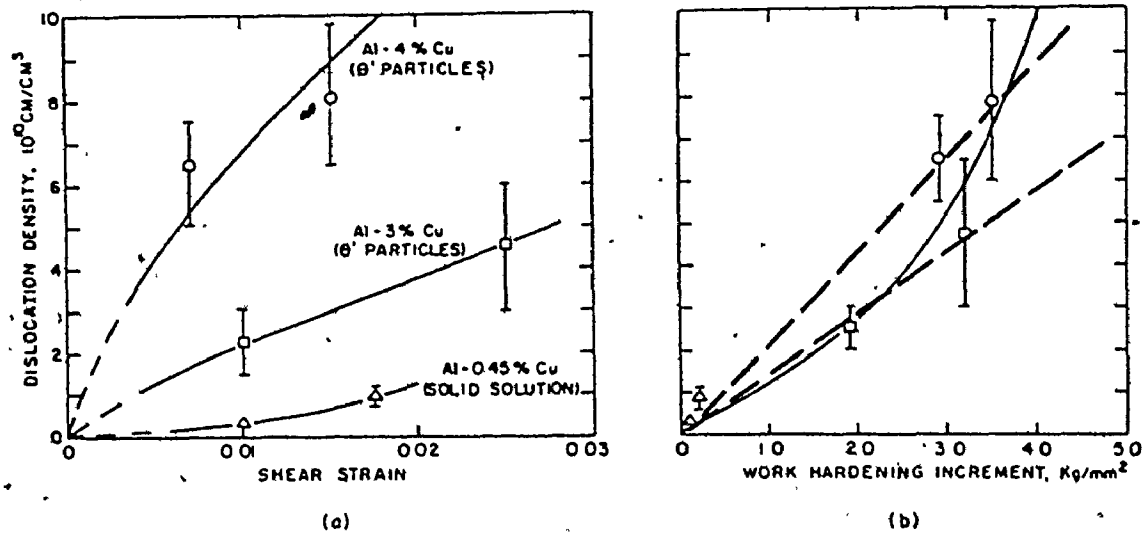

Fig. 13. Dislocation densities in crystals with and without particles, plotted against strain (left) and stress increment above the initial yield stress (right).

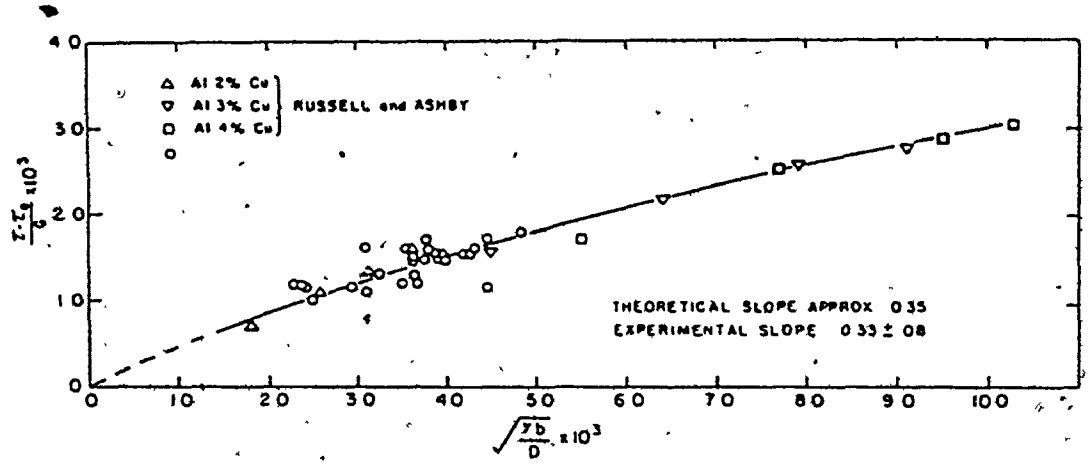

Fig. 14. The work hardening increment, plotted according to equation (3) for our crystals (triangles and squares, and for the crystals of Dow Hughes and Robertson[8] (circles).

Fig. 6.3. Results from Russell and Ashby (1970)

a) Russell and Ashby Figure 3RA together with the plotted yield stresses;

b) their quoted values of modulus and interparticle spacing;

c) data at each 0.02 strain increment, instead of 0.05 as used by Russell and Ashby;

d) the full range of the strains shown in Figure 3RA.

The replotted data is shown in Figure 6.4. It indicates that the Russell and Ashby formulation does not lead to the reported good agreement with the experiments; it is clear that their choice of 5, 10, 15 and 20% data points for the original plots was fortuitous in that it led to the linear relationship shown in Figure 14RA. The three different curves for the 2, 3 and 4% alloys can not be considered as one line. There is an obvious volume fraction dependence, but its exact formulation in terms of the quantity $\sqrt{\frac{Yb}{D}}$ is difficult since D is not constant for the alloys. Also, the plots as extrapolated do not go through the origin, and estimates of the gradients of the individual lines (approximating the early portions as linear) show they are in excess of 0.5, considerably larger than the 0.33 obtained by Russell and Ashby. It could be argued that Russell and Ashby took an average gradient of the series of lines, and not the average of the gradients. This will lead to a reduction in the quantity, as the

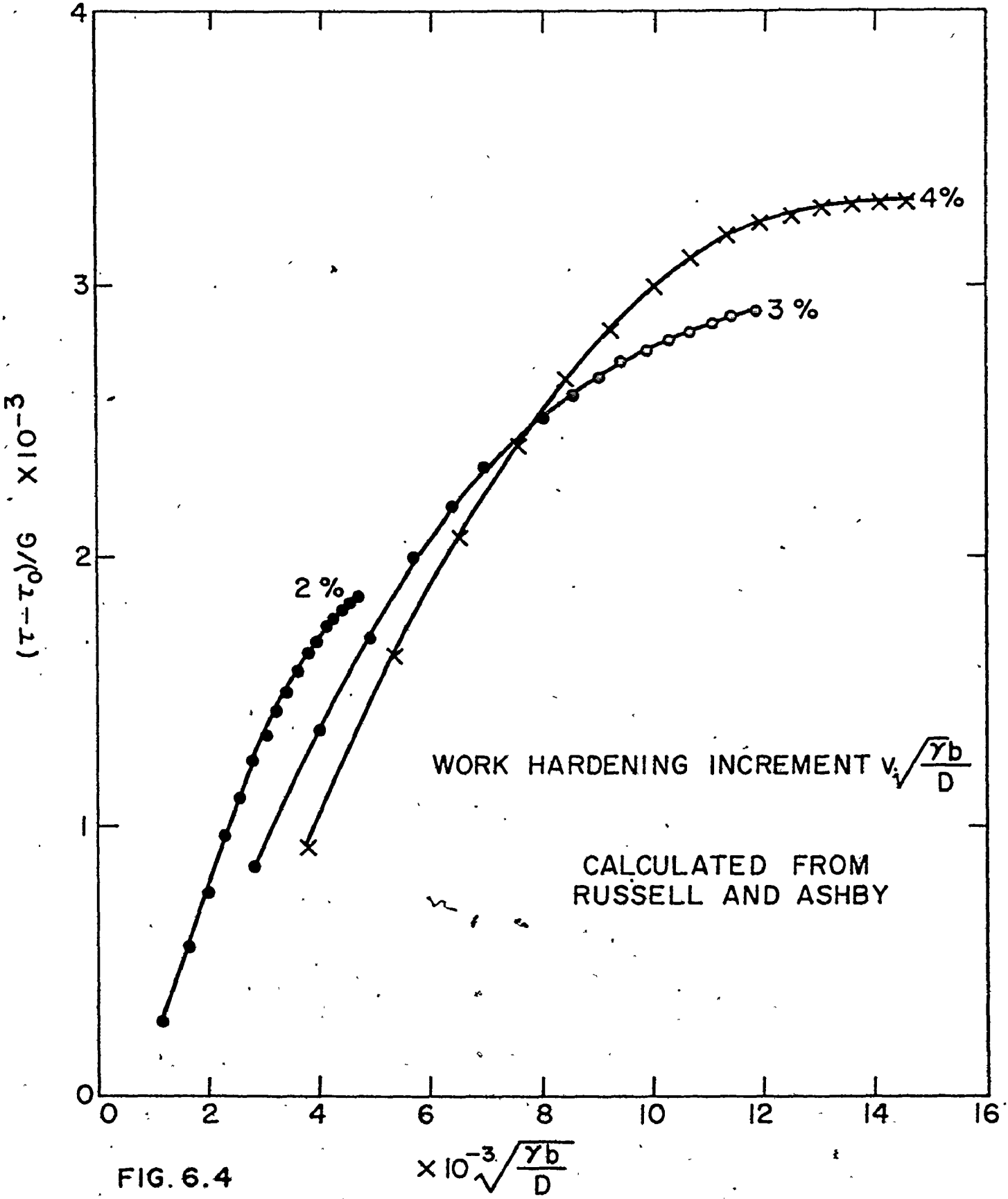
4
3
2
1
0
0
2
4
6
8
10
12
14
16
$(\tau-\tau_0)/G \times 10^{-3}$
$\times 10^{-3}\sqrt{\frac{\gamma b}{D}}$
2 %
3 %
4%
WORK HARDENING INCREMENT $v_i\sqrt{\frac{\gamma b}{D}}$
CALCULATED FROM
RUSSELL AND ASHBY

FIG. 6.4

gradients of the 3 and 4% alloys reduce rapidly at large strains. Nevertheless, if the Russell and Ashby analysis is to be applicable, it must be so at small strains, as it was at these strains that they determined the dislocation densities on which their formulation depends . As indicated, at these small strains, the gradient is in excess of 0.5.

This detailed discussion of the Ashby model and the Russell and Ashby analysis was necessary because of the good agreement reported for the model with the experimental data from their compression tests. The exclusion of a long range back stress and the Bauschinger Effect in the Ashby formulation resulted in the model being not only unsuitable to explain the results of this study, but in fact being contradictory to them. The contribution of the long range back stress is a major part of the work hardening, but the Ashby model attempted to calculate the work hardening on the basis of an average dislocation density using the formula of Nabarro et al. (1964). The Nabarro et al. model used a forest hardening model to calculate the work hardening. This study has shown that the maximum forest hardening contribution is only about 50% of the work hardening in this alloy. It is not clear that Ashby calculated this quantity, as the dislocation content measured in the Al-Cu alloy was that for the primary dislocations - not secondary.

In the next section of this discussion, it will be shown how the Russell and Ashby data can be fitted to an analysis proposed by Brown and Clarke to describe the work hardening in materials containing non deforming particles, discs or fibres. This model is a long range back stress model.

6.5 The Re-examination of Russell and Ashby's Data in Terms of the Brown and Clarke Analysis

The calculations and analysis carried out for the previous section show that the data of Russell and Ashby do not support the position that the Ashby model satisfactorily accounts for the work hardening in two phase alloys. The model is also deficient in the way it excludes any consideration of the long range back stress and Bauschinger Effect. The analysis of Brown and Clarke, which does include these considerations, will be examined and it will be shown how the data from Russell and Ashby, Figure 3RA fits this analysis.

Brown and Clarke have shown how to calculate the mean stress in the matrix, (or in the terminology used in this work, the long range back stress) at a given plastic strain ε_p:

$$\tau = 2\gamma.D\mu f\varepsilon_p$$

where τ is the mean shear stress on the active slip plane

γ is an accommodation factor, determined from Eshelby's work

D is a modulus correction factor

μ is the shear modulus of the matrix

f is the volume fraction of the hard second phase

ϵ_p is the unrelaxed symmetrical plastic shear strain (equal to 0.5 of the resolved shear strain).

For the Al-Cu alloys used by Russell and Ashby, the following constants can be determined:

a) $\gamma(\text{SINGLE SLIP}) = \frac{2-\nu}{3(1-\nu)} = \frac{5}{6}$ for $\nu = \frac{1}{3}$

b) The ratio of shear moduli, $\frac{\mu^*}{\mu} = 1.3$, based on the work of Pattniak and Lawley (1971), μ^* is the modulus of the hard phase.

c) $D = 1.2$ for disc shaped particles on {100} planes (Brown and Clarke, 1975).

d) The volume fraction f of θ' in the three alloys used by Russell and Ashby are a little difficult to establish since only the nominal copper content before the preparation of the single crystals is reported. The actual copper content can vary from that reported. It is known from this work that there is a loss of copper during the remelting, (.6% loss in 3.6%). The volume fractions are calculated using the method employed by Boyd (1966), and lead to the

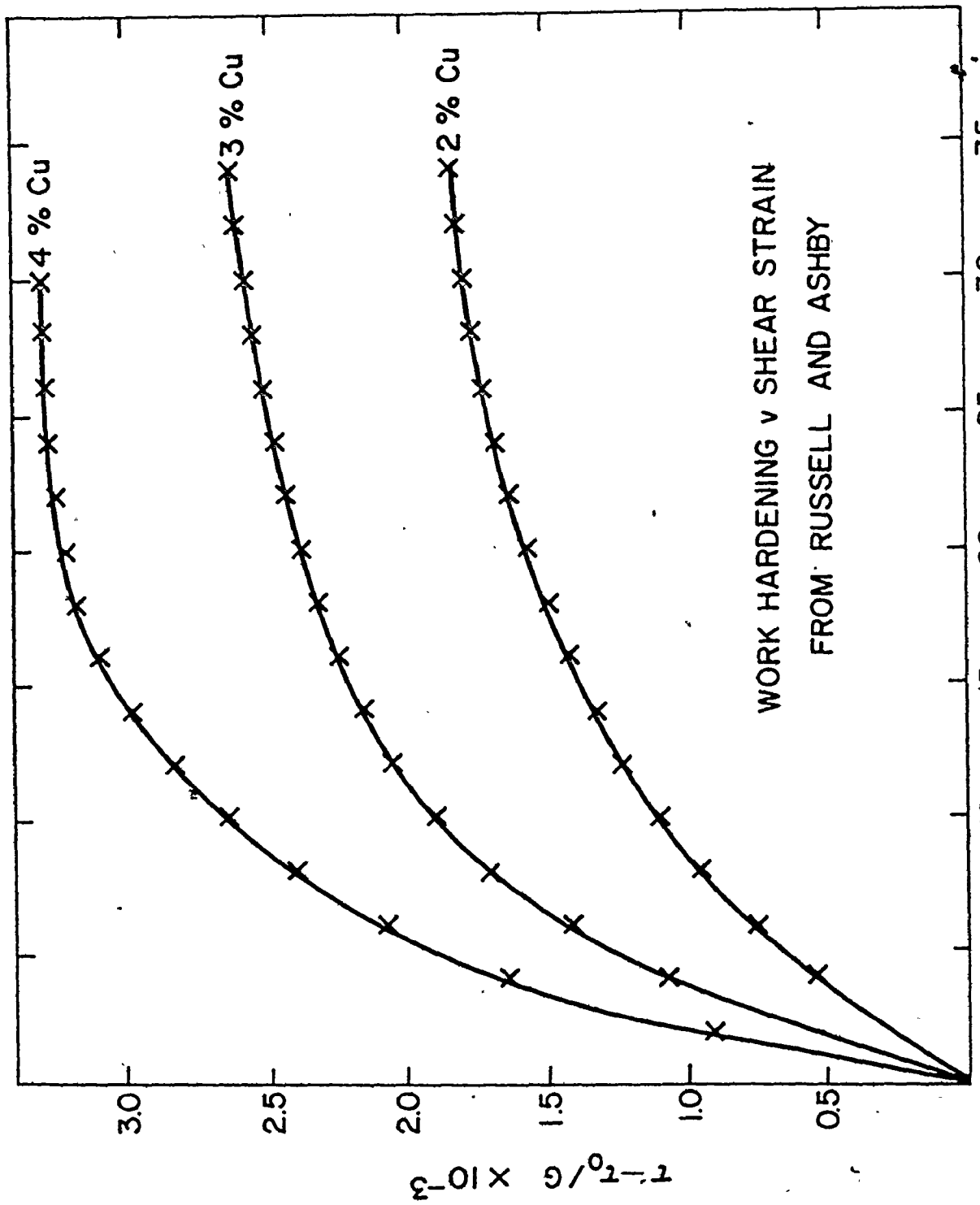
4 % Cu
3 % Cu
2 % Cu
WORK HARDENING v SHEAR STRAIN
FROM RUSSELL AND ASHBY
$\tau - \tau_0/G \times 10^{-3}$
$\times 10^{-2}\ \gamma$
0.5
1.0
1.5
2.0
2.5
3.0
5
10
15
20
25
30
35

FIG. 6.5

values shown in Table 6.5, for final heat treatments at 300°C.

The minimum additional shear stress which must be applied to the material for continued plastic deformation is the back stress at that strain. This is the quantity

$$\tau = 2\gamma D\mu f\varepsilon_p$$

calculated by Brown and Clarke. For comparison purposes this formula will be used to calculate the expected hardening over the yield stress as

$$\frac{\tau}{\mu} = 2\gamma Df\varepsilon_p$$

at a symmetrical shear strain of 0.01 forward (resolved shear strain 0.02). The results from the work of Russell and Ashby will be obtained at the same strain from Figure 3RA.

These results have been plotted, Figure 6.6 and it can be seen that the agreement between the calculated and experimental values is good, and well within the 15% expected accuracy of the Brown and Clarke formulation. The one experimental result for the 3% copper alloy seems to be considerably higher than it might be, and examination of the original data reveals that this alloy has an initial yield stress much lower than might be expected.

It must be pointed out that any uncertainties in the copper content and subsequent volume fractions of θ'

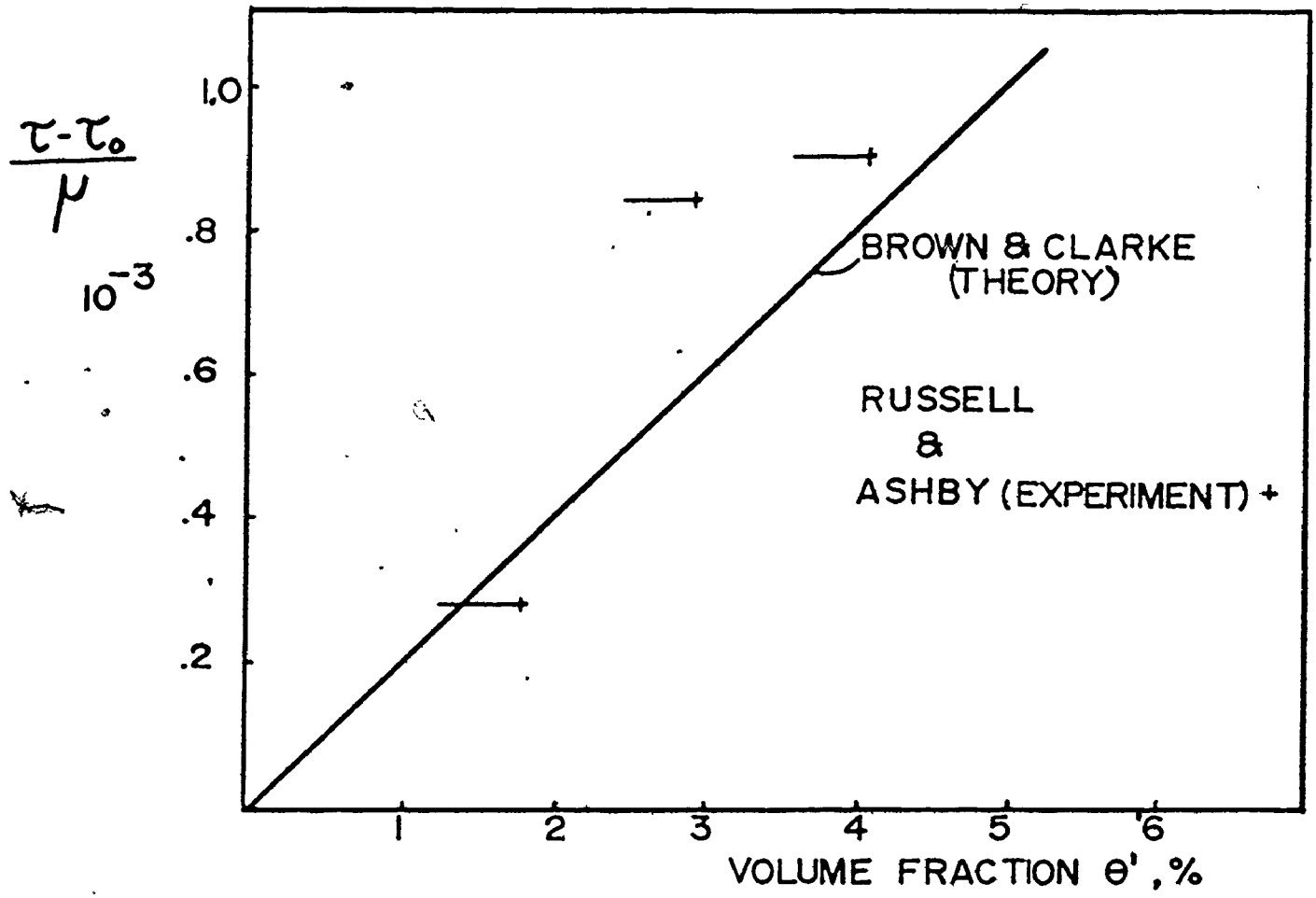

NOTE — POSSIBLE ERROR FROM LOSS OF Cu. DURING CRYSTAL PREPARATION ——

WORK HARDENING INCREMENT v VOLUME FRACTION θ'

FIG 6.6

COPPER WT%	VOLUME FRACTION θ' %	BROWN AND CLARKE $\frac{\tau}{\mu} \cdot 10^3$ THEORY	RUSSELL AND ASHBY $\frac{\tau-\tau_o}{\mu} \cdot 10^3$ EXPERIMENT
2	1.55	.31	.28
3	2.95	.59	.84
4	4.1	.82	.90

TABLE 6.5 TABLE TO SHOW COMPARISON OF WORK HARDENING INCREMENTS AT SYMMETRIC SHEAR STRAIN 0.01; RUSSELL AND ASHBY EXPERIMENT, BROWN AND CLARKE THEORETICAL

will not affect the position of the theoretical line; its gradient will remain unchanged. They will, however, affect the plotting of the Russell and Ashby results and might be expected to introduce some additional scatter. The re-melting of the alloys during single crystal preparation will tend to reduce the copper content and to move the experimental points to lower volume fractions. The possible error bars resulting from this loss of copper are marked on Figure 6.6.

In this section it has been shown that the Russell and Ashby experimental data gives a good agreement with the work hardening increments calculated from the Brown and Clarke formulation. This is important as it shows that the formulation which includes the mean stress in the matrix (or the long range back stress) leads to a satisfactory description of the forward work hardening process, in addition to describing the Bauschinger Effect. In the following section, the results from the present study will be compared with the Brown and Clarke formulation; in this case, however, the flow stress will not be compared, but rather the long range back stress as determined from the reverse deformation studies.

6.6 Comparison of Experimental Values of Back Stress From This Study With the Brown and Clarke Formulation

In this section the values of the long range back

stresses σ_b obtained from the experimental work in this study will be compared with the work of Brown and Clarke. As in the earlier section, the comparison will be made at a symmetric shear strain of 0.01 (resolved shear strain of 0.02). However, considerable care is necessary as the Brown and Clarke mean matrix stress is a shear stress, whilst the back stresses calculated in this study are tensile stresses. The appropriate Schmid and Taylor factors will be used.

As before, the Brown and Clarke mean shear stress in the matrix acting against increasing deformation is given by

$$\frac{\tau}{\mu} = 2f\gamma D\varepsilon_p$$

Here ε_p is the symmetrical shear strain; in these calculations it is taken as being approximately equal to the tensile strain. For the Al-Cu alloy system, with thin discs on the {100} planes, $\gamma = \frac{5}{6}$ and $D = 1.2$.

The calculation for SX37 is as follows. The volume fraction for this alloy is $f = 3.0\%$, and then

$$\frac{\tau}{\mu} = 2 \cdot 0.03 \cdot \frac{5}{6} \cdot 1.2 \cdot 0.01$$
$$= 0.60 \times 10^{-3}$$

The experimental results giving σ_b as a function of prestrain, using the 0.001 reverse offset to calculate the reverse yield stress, gives at a prestrain of 0.01

$$\sigma_{b\ TENSILE} = 5.2 \text{ ksi} = 35.8 \text{ MPa}$$

This is converted to a shear stress by multiplying by the Schmid factor;

$$\sigma_{b\ SHEAR} = 5.2 \times .43$$
$$= 2.24 \text{ ksi} = 15.4 \text{ MPa}$$

and then

$$\frac{\sigma_{b\ SHEAR}}{\mu} = \frac{2.29}{3.62} \times 10^{-3}$$
$$= 0.62 \times 10^{-3}$$

This has to be compared with the value of 0.60×10^{-3} from the Brown and Clarke formulation.

For SX35, oriented at [100] for multiple slip, $\gamma = \frac{2-\nu}{4(1-\nu)} = \frac{5}{8}$, Schmid Factor = .40 and

$$\frac{\tau}{\mu} = 2f\gamma D\varepsilon_p$$
$$= 2 \cdot 0.03 \cdot \frac{5}{8} \cdot 1.2 \cdot 0.01$$
$$= 0.45 \cdot 10^{-3}$$

For this crystal the experimental value is

$$\sigma_{b\ tensile} = 4.4 \text{ ksi} = 30.3 \text{ MPa}$$

and leads to

$$\frac{\sigma_{b\ shear}}{\mu} = \frac{4.4 \times .40}{3.62} \times 10^{-3}$$
$$= 0.49 \times 10^{-3}.$$

The data for the polycrystalline tests can also be compared with the theory. The deformation is by multiple slip so that $\gamma = 5/8$. To convert the tensile stress to a shear stress the Taylor Factor $M = 3.1$ is used. The Taylor Factor was not determined experimentally. The experimental tensile back stress at a strain of 0.01 is 7.0 ksi = 48.2 MPa. This converts to

$$\sigma_{b\ shear} = \frac{7.0}{3.1} = 2.26 \text{ ksi} = 15.8 \text{ MPa}$$

and

$$\frac{\sigma_{b\ shear}}{\mu} = \frac{2.26}{3.62} \times 10^{-3} = 0.62 \cdot 10^{-3}.$$

The Brown and Clarke formulation leads to

$$\frac{\tau}{\mu} = 2 \cdot 0.037 \cdot \frac{5}{8} \cdot 0.01 \cdot 1.2$$

$$= 0.56 \times 10^{-3}.$$

In this last calculation, the volume fraction, f, is slightly higher than that used for the single crystal material. This has the original copper content, 3.6 wt%, whereas the single crystals had been found to have a copper content of 3%.

These values are tabulated, together with the values for SX34 which was also oriented for single slip. Included also is the data for SX31 oriented for slip on two slip systems. The calculated value of the hardening increment

has not been carried out for this orientation as the Brown and Clarke formulation is completed for single slip and multiple slip only. However, the values calculated for single slip and multiple slip do provide upper and lower bounds for the double slip case. It can be seen that the experimental value is between these extremes. Also tabulated are the calculated and experimental values for tests at 77°K and 373°K.

Table 6.6 shows the comparison between the experimental results for $\sigma_{b\ SHEAR}/\mu$ and the calculated τ/μ for tests in series SX3N, polycrystals, and SX2N. The values for the series SX3N and polycrystals were determined at $\varepsilon_p = .01$ from the graphs which show the relationship between σ_b and prestrain. The values for series SX2N were obtained from the individual tests which were carried out to prestrains close to 0.01. The actual values are shown in Table 4.3. These prestrains were the values of ε_p used in the calculation of the theoretical values.

There is very good agreement for the tests in series SX3N and polycrystals. The magnitudes are well within the 15% estimated error in the Brown and Clarke formulation, and the effect of the crystal orientation can be seen in the comparison of:

SX 37 - single slip

SX 31 - double slip

SX 35 and polycrystals - multiple slip.

TEMP °K	TESTS	EXPERIMENTAL $\frac{\sigma_b}{\mu}$ SHEAR $\times 10^3$	CALCULATED $\frac{\tau}{\mu} \times 10^3$
298	SX 37	0.62	0.60
298	SX 34	0.66	0.60
298	SX 31	0.52	(0.45-0.60)
298	SX 35	0.49	0.45
298	POLYCRYSTALS	0.62	0.56
298	SX 251	0.70	0.72
77	SX 252	0.75	0.72
373	SX 253	0.71	0.72
77	SX 221	0.74	0.66
298	SX 224	0.66	0.66
298	SX 231	0.97	0.66
373	SX 233	0.80	0.66
298	SX 244	.79	0.66
298	SX 241	1.0	0.72

TABLE 6.6 COMPARISON OF EXPERIMENTAL VALUES OF σ_b SHEAR/μ AND THEORETICAL VALUES CALCULATED USING THE BROWN AND CLARKE MODEL.

The temperature dependence can be seen in a comparison of the tests in series SX25M and SX22M. These tests show close agreement between the observed and calculated values at the temperatures 77, 298 and 373°K. The results for SX23M and 24M are less satisfactory in that some of the differences are of the order of 50%.

The good agreement between the experimental and calculated values shown in Table 6.6, including the

a) orientation dependence and

b) temperature dependence of the back stress

is confirmation that the Brown and Clarke model is a good description of the work hardening process in the Al-Cu alloy aged to θ'. It confirms that the major portion of the work hardening at small strains is due to the back stress. At small strains (~1%) the deformation is unrelaxed; the extent of the relaxation increases at larger strains.

6.7 Comparison of the Results of This Study With The Model Proposed by Tanaka and Mori

The experimental results for the back stress determination presented earlier can also be compared with the values predicted by the model proposed by Tanaka and Mori. Their formulation predicts that the uniaxial tensile strain σ_{33} is given at a tensile strain ε by

$$\sigma_{33} = \frac{\sigma_o}{1 - B} + \frac{A\ E\ \varepsilon}{1 - B}$$

where A and B are constants which depend on particle modulus shape and volume fraction. Of greater interest in this work is the hardening increment over the yield stress of the material.

$$\Delta\sigma_{33} = \frac{A\ E\ \varepsilon}{1 - B}$$

For the material tested, the particles are disc shaped, and lie on {100}, such that, for the [100] orientation single crystal, there are 2 sets parallel to the tensile axis, whilst one set is perpendicular to it. Under these conditions Tanaka and Mori average the contributions, and the work hardening increment becomes

$$\sigma_{33} = \frac{1}{3}\left[\frac{2A_1}{1-B_1} + \frac{A_2}{1-B_2}\right] E\ \varepsilon$$

where the subscripts 1 and 2 refer to particles parallel to and perpendicular to the tensile axis.

The constants A_1, B_1 etc. are given by Tanaka and Mori, (their equations 5 and 6) and for crystal SX35 they can be calculated using

$$\nu = \nu^* = \frac{1}{3}$$

$$E^* = 14.4 \times 10^6 \text{ psi} = 99.2 \times 10^3 \text{ MPa}$$

$$E = 10.9 \times 10^6 \text{ psi} = 75.1 \times 10^3 \text{ MPa}$$

$$f = 3\%$$

The values obtained are

$$A_1 = .041 \qquad A_2 = .030$$
$$B_1 = .040 \qquad B_2 = .035$$

from which

$$\Delta\sigma_{33} = \frac{1}{3} \cdot 0.117 \cdot E \cdot \varepsilon$$

At a tensile strain of $\varepsilon = 0.01$,

$$\Delta\sigma_{33} = 4.23 \text{ ksi} = 29.1 \text{ MPa.}$$

The experimental result is

$$\sigma_{b \text{ tensile}} = 4.5 \text{ ksi}$$
$$= 31.0 \text{ MPa}$$

Here there seems to be reasonable agreement between the calculated work hardening increment and the experimentally determined back stress.

The corresponding calculation carried out for the polycrystalline material, with f = 3.65%, gives at $\varepsilon = 0.01$,

$$\Delta\sigma_{33} = 5.1 \text{ ksi} = 35.1 \text{ MPa.}$$

This is considerably smaller than the experimental value of $\sigma_{b \text{ tensile}}$ obtained for the polycrystalline material. This value is

$$\sigma_{b \text{ tensile}} = 7.0 \text{ ksi} = 48.2 \text{ MPa}$$

It seems that the Tanaka and Mori formulation underestimates the long range back stress. A further check on this can be made by calculating the hardening increment possible if all the precipitates in the polycrystalline material were parallel to the tensile axis, and calculating $\Delta\sigma_{33}$ as

$$\Delta\sigma_{33} = 5.6 \text{ ksi} = 38.6 \text{ MPa}$$

This is still considerably smaller than the experimental value. The difference 1.9 ksi (13.1 MPa) represents a difference of some 27% which is much larger than the expected error in the measurements.

Thus it seems that the Tanaka and Mori formulation leads to close agreement with the experimental back stress in the [100] single crystal. For this material the model fits the crystal and particles closely. However, for the polycrystalline case, in which the averaging process and assumed uniform multiple slip may not be completely accurate, there is considerable difference. The Tanaka and Mori formulation does not permit the calculation of the effect for the other single crystals oriented for single slip; in these cases the angle between the slip direction and the particle normals can not be included in their formulation.

6.8 The Value of σ_b Maximum

It was shown in Chapter IV that the back stress σ_b

increases at small strains, and reaches a constant value after a strain of some 5%. The meaning of the maximum value of the back stress must now be examined, and rationalised with the microstructural events.

The values of the saturation back stresses are given in Table 6.1; the values of greatest interest are the shear stress values. They are all of the order of 4 ksi (28 MPa). The back stress can be considered to represent a shear stress on the individual particles. In this calculation, the inverse of the operation employed by Brown and Stobbs is used. The magnitude

$$\tau_{\text{max local}} = \frac{\tau_b}{f}$$

where f is the volume fraction.
This stress represents a local shear stress of 133 ksi (919 MPa).

The significance of the stress, $\tau_{\text{max local}}$, must be established. The fracture studies have shown that the particles at larger strains are cut by matrix dislocations. This cutting is shown by the dark field micrographs and it was discussed earlier how the saturation back stress is due to the cutting of the particles taking place on a large scale, so that no further increment of back stress is possible. The saturation value of the back stress is then to be taken as the local stress required to cause cutting of

the particles on a large scale by the matrix dislocations.

There is an alternative method available to estimate the local stress at the particle to cause the cutting by matrix dislocations. The method is based on the common observation that the shear stress of a material is often close to

shear modulus/30.

This estimate of the shear stress is intended for fcc materials; the estimate for a complex structure like θ' is not clear. However, the use of μ/30 for θ' leads to an estimated shear stress

$$\mu/30 = 120 \text{ ksi} = 827 \text{ MPa}.$$

which is close to the value obtained from the use of the experimental value of the saturated back stress. Here the value of μ is that for the θ phase in the eutectic alloy as determined by Pattniak and Lawley (1971). So far, no experimental determination of the yield stress for θ' particles has been carried out.

The agreement between these two values for the stress necessary to cause cutting of the θ' particles lends support to the model in which the saturation of the long range back stress is considered to be due to the particles undergoing plastic deformation. There is experimental

evidence from Transmission Electron Microscopy that the particles are cut, but the foils which were examined had been subjected to tensile strains greater than 10%. The above agreement indicates that the particle deformation is well established at tensile strains of approximately 5%. One other piece of evidence confirms this value of 5% (or approximately 10% shear strain). The compression tests of Russell and Ashby show the work hardening rate in the material becomes almost constant at shear strains larger than 10%.

6.9 Removal of the Long Range Back Stress

A problem which has caused some concern in this study is the magnitude of the reverse strain required to remove the long range back stress resulting from an imposed prestrain.

Wilson (1965) showed that, in many polycrystalline materials, the long range back stress after 9% torsion prestrain was removed by reverse strains which did not exceed 5%, and were sometimes ~2%.

Atkinson et al. (1974) studied the reverse strain needed to remove the back stress in Cu-SiO_2. Crystals were deformed at 77°K to 8% prestrain and interrupted after different reverse strains for an anneal at room temperature. This anneal was found to reduce the long range back stress

and to lead to an increased yield stress in reverse. However, a 4% reverse strain was found to lead to no change between the reverse curves before and after the anneal. It was argued that the 4% reverse strain removed the long range back stress resulting from the 8% prestrain.

These experimental results are not the same as those obtained in this study which showed that, after a 4% prestrain, a 4% reverse strain removed the back stress. The back stress was built up again in the opposite sense by further reverse deformation. The work of Atkinson et al. and of Wilson indicates that a reverse strain much smaller than the forward strain will remove the back stress. This present study shows the forward and reverse strains should be equal.

The difference between these results is to be found in the way that the plastic deformation was obtained in the different materials.

a) in the Cu-SiO_2 the crystals were oriented for single slip, but, after some 6% forward strain at 77°K, the single slip at the particle gave way to slip on other systems as the deformation became relaxed. The result of this process was to reduce the number of Orowan loops on the particles, and to produce prismatic loops. The contribution to the back stress from an unrelaxed dislocation is much larger than that from a prismatic loop. Gould et al. obtain the ratio:

$$\frac{\text{back stress from unrelaxed loop}}{\text{back stress from relaxed loop}} = \frac{12}{7}$$

During the reverse deformation, the glide dislocations interacting with the original loops at the particle will reduce the long range back stress in such a way that:

1 reverse dislocation will remove the back stress from 1 forward Orowan loop

and 7 reverse dislocations will remove the back stress from 12 forward prismatic loops.

It is not surprising then that the required reverse strain is smaller than the prestrain.

b) the materials used by Wilson were all polycrystalline, and most of the deformation took place by slip on many systems, with the dislocation interactions leading to the formation of prismatic loops. Again it must be expected that the long range interactions from these loops will be removed by a few reverse dislocations.

c) in the present work, the study of the asterism was carried out on single crystals in which the deformation took place by single slip. The forward prestrain to 4 or 8% shear strain was still an unrelaxed deformation, with the Orowan loops accumulating at the particles with little formation of prismatic dislocations. It has already been discussed how some cross slip might be expected to take place near the perimeter of the particles. The dislocations

responsible for the reverse deformation will cause a reduction in the number of Orowan loops on the particles and the asterism will be removed when the reverse deformation has removed or counteracted all the forward Orowan loops. The non-exact reversibility of slip will lead to the accumulation of some debris at the particles. This debris will contribute to the forest hardening of the material.

There is a further piece of work which can be discussed here; it shows that, in an alloy similar to that used in this study, the effect of the prestrain is removed when the material has undergone a reverse strain equal to the prestrain. The work is that of Liu and Sachs (1949) in which the deformation and fracture of an aluminum alloy 24ST was studied after different strain histories. The experiments of particular interest are reported in their Figures 2 and 3.

In their Figure 2, the effect of unbalanced strain cycles on the strain to fracture is studied. The test piece was subjected to a strain ε_1 in tension, and then to ε_2 in compression, after which it was pulled to failure and the retained tensile ductility ε_f was measured. It was found that ε_f was greatest when

$$|\varepsilon_1| = |\varepsilon_2|,$$

but that its maximum value decreased as the magnitude of ε_1

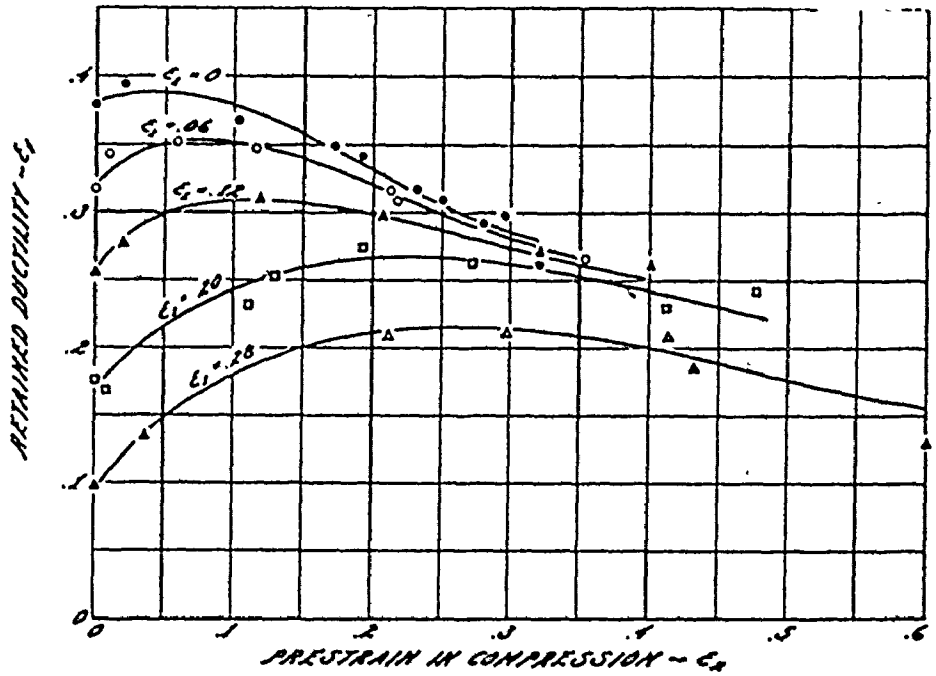

FIG 2—EFFECT OF COMPRESSION SUBSEQUENT TO VARIOUS STRAINS IN TENSION ON THE FRACTURE CHARACTERISTICS OF THE ALUMINUM ALLOY 24ST.

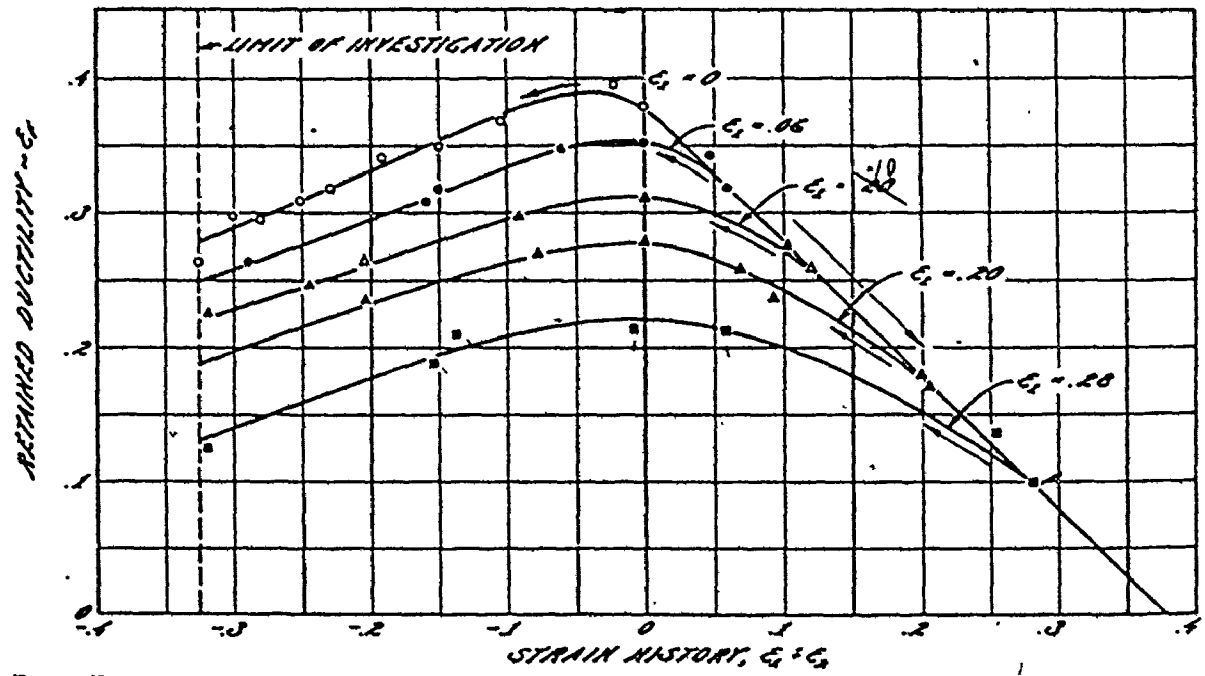

FIG 3—EFFECT OF THE STRAIN HISTORY COMPOSED OF VARIOUS TENSION AND COMPRESSIVE STRAINS ON THE RETAINED DUCTILITY OF THE ALUMINUM ALLOY 24ST.

Fig. 6.7. Results taken from Liu and Sachs (1948). 24ST is an Aluminum Alloy, corresponding to 2024-T6

increased.

These results are plotted in a different way in their Figure 3. Again the retained ductility ε_f is a maximum when

$$|\varepsilon_1| = |\varepsilon_2|$$

so that, at the start of the tensile test, the material had a net strain of zero. Again the maximum value of the retained ductility decreases as the prestrain increased.

Two points can be mentioned here:

1. The maximum retained ductility occurring at zero net strain is consistent with the model described in Section 6.3. In materials which have undergone little relaxation, the reverse strain needed to remove the effect of the prestrain must be equal to the prestrain.

2. The decreasing retained ductility, as the total strain is increased, confirms that there is not exact reversibility of slip in the Al-Cu alloy, and that there is accumulation of dislocation debris.

The discussion in this section has shown that the magnitude of the reverse strain required to remove the effect of the prestrain depends on the extent of the relaxation during the prestrain. The work of Liu and Sachs has confirmed the results of the present study. There is no conflict between the results of the work of Wilson and of Atkinson et al. and of the present study.

6.10 Work Hardening Behaviour At Large Strains

The tests carried out on single crystals, in the present study, together with the reported work of Beevers and Honeycombe (1964) and of Price and Kelly (1962) indicate that the work hardening behaviour of the aluminum-copper precipitation hardened alloys is complex. There are three principal events which need to be discussed, and criteria obtained to determine the conditions under which they are observed. The events are

i onset of necking

ii formation of coarse slip bands or shear bands

iii final fracture and its dependence on orientation.

These events must be considered separately as the experimental evidence indicates they are different. For example, Price and Kelly reported the occurrence of shear bands on their single crystals just before fracture; they reported no necking in θ" crystals. In the present study, coarse slip bands formed, but only after necking was established. In other work, shear bands were observed in tests carried out in compression. In all the tests carried out in tension, the final fracture occurred after the formation of the shear bands.

The discussion will be carried out with the help of Figures 6.8 and 6.9. These show the work hardening rates plotted against shear stress for the following tests:

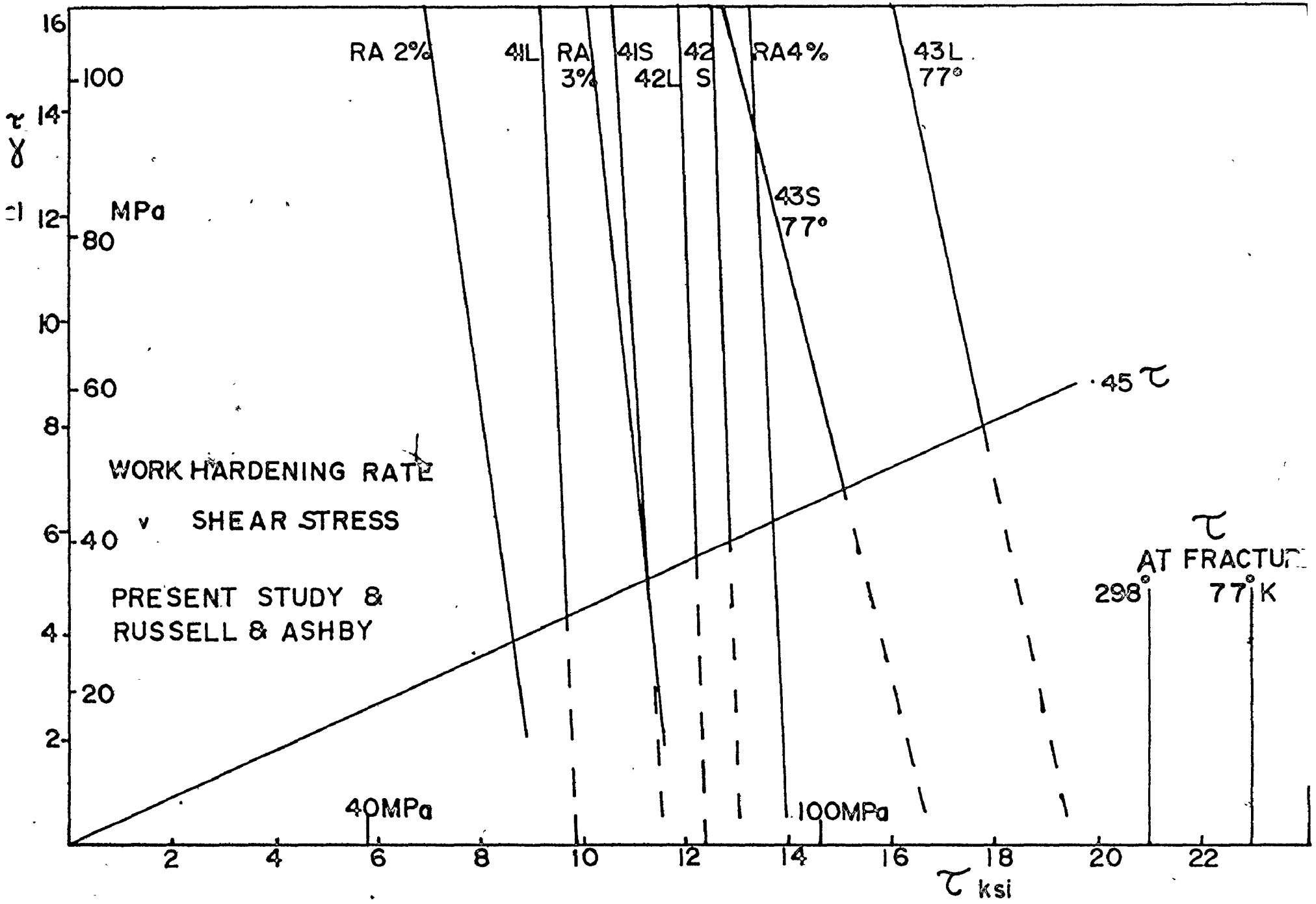
RA 2%
41L
RA 3%
41S
42L
42 S
RA4%
43L 77°
43S 77°
16
100
14
τ/γ
MPa
12
80
10
60
8
40
6
20
4
2
WORK HARDENING RATE
v SHEAR STRESS
PRESENT STUDY &
RUSSELL & ASHBY
.45 τ
τ AT FRACTURE
298°
77°K
40MPa
100MPa
2
4
6
8
10
12
14
16
18
20
22
τ ksi

FIG 6.8

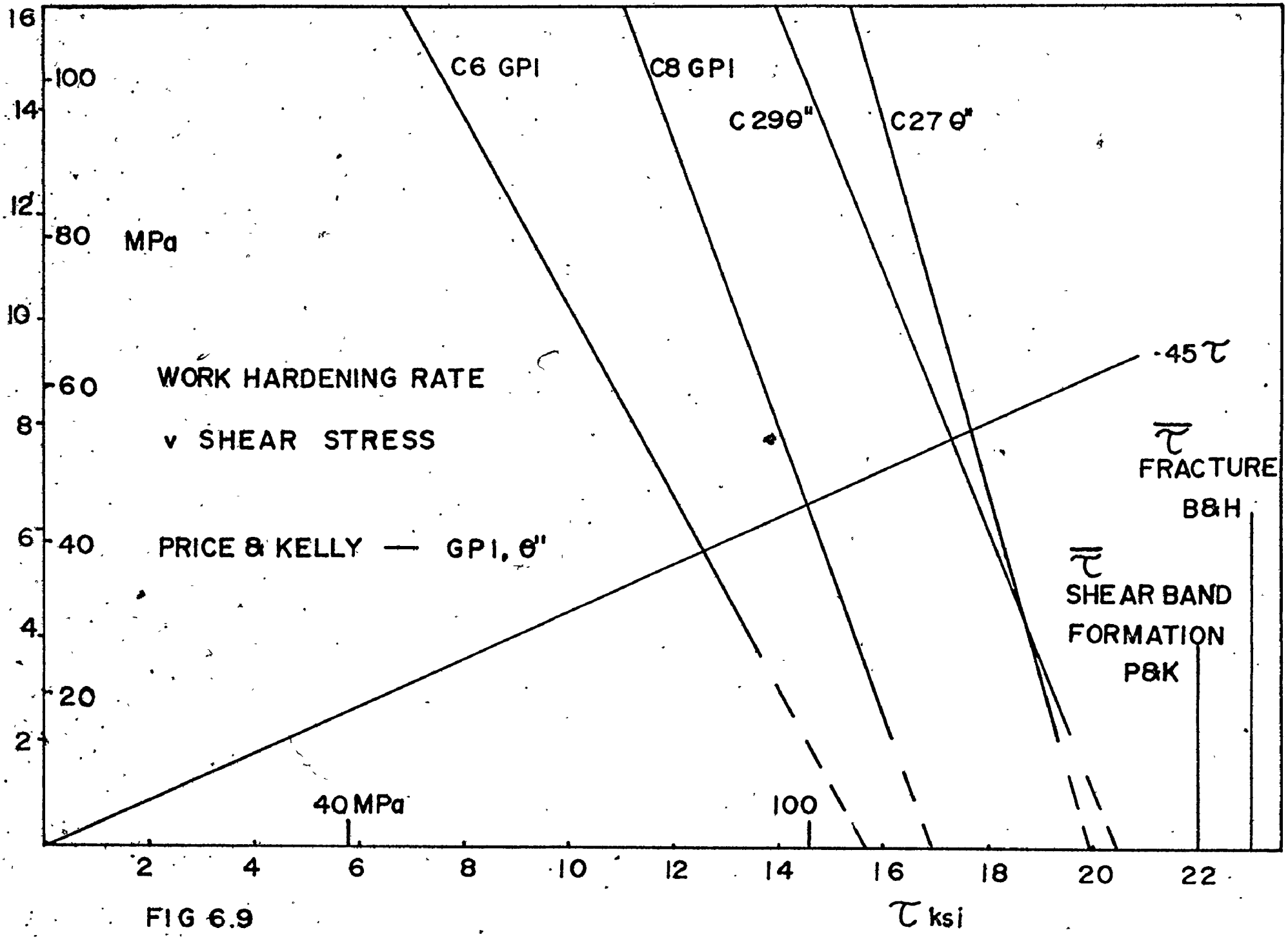
C6 GPI
C8 GPI
C29θ"
C27θ"
MPa
WORK HARDENING RATE
v SHEAR STRESS
PRICE & KELLY — GPI, θ"
·45τ
τ̄ FRACTURE B&H
τ̄ SHEAR BAND FORMATION P&K
40MPa
100
τ ksi

FIG 6.9

a) crystals SX41 and SX42 tested at 298°K.

b) crystals SX43 tested at 77°K. For all these plots, the stresses were calculated up to the load maximum.

c) compression tests by Russell and Ashby on Al-Cu containing 2, 3 and 4 wt% copper. These tests were not subject to necking, and the data was processed to much lower work hardening rates.

d) crystals C6 and C8 containing GP zones.

e) crystals C27 and C29 containing θ" precipitates, from the work of Price and Kelly. These tests were reported not to be subject to necking; this point will have to be discussed later.

All the data plotted appears linear. Only the lower part of the $d\tau/d\gamma$ results are shown on the Figures. Also shown on the graphs is the line 0.45τ. The reason for this line will be indicated later.

(i) Onset of Necking

An attempt was made to establish the condition for the onset of necking. In polycrystalline materials, necking commences after

$$\frac{d\sigma}{d\varepsilon} \leq \sigma$$

where σ and ε are the true stress and true strain. The deformation of single crystals is more difficult to analyse

as the angle λ between the slip direction and the tensile axis changes during the deformation. Also, the development of a neck requires the activation of slip on at least two slip systems, and, under these conditions, formulae derived for single slip deformation are not strictly applicable.

The relationships between τ, σ, ε and γ are complex and an expression for $d\tau/d\gamma$ is unmanageable. A simpler expression can be obtained if it is assumed that

a) $\tau = \sigma.SF$ where SF is the Schmid Factor at strains ε and γ.

b) $\gamma \approx \varepsilon/SF$

Then

$$\frac{d\sigma}{d\varepsilon} \approx \frac{d\tau}{d\gamma} \cdot \frac{1}{SF^2} \leq \sigma \approx \frac{\tau}{SF}$$

so that

$$\frac{d\tau}{d\gamma} \leq SF \cdot \tau$$

becomes the approximate condition for the onset of necking. The value of the Schmid Factor to be used should be that for the crystal being tested. However, since most of the crystals tested have Schmid Factors close to 0.45, this value will be used. This is the origin of the line $\frac{d\tau}{d\gamma} = .45\tau$ on the Figures 6.8 - 6.9. According to the condition, necking can be expected at work hardening rates below the line $.45\tau$. This condition is very close to that which determines the onset of necking in tests on rolled sheet. The

linear graphs obtained from the work of Russell and Ashby indicate the line which would be followed in the other crystals, if necking had not occurred.

There are two sets of data to be mentioned here. The first set contains the results of the present study. The conditions for the onset of necking in crystals SX41, 42 and 43 were known from the load maxima. The intersection of the $d\tau/d\gamma$ and $.45\tau$ lines occur at positions very close to those corresponding to the load maxima. The agreement with the proposed criterion can be seen in Table 6.7, which shows the values of $\frac{1}{\tau}\frac{d\tau}{d\gamma}$ at the load maxima. There is a small range of strains over which there is an uncertainty about the position of the load maxima: these are indicated in the Table. Examination of the Table shows that the range of values for the quantity $\frac{1}{\tau}\frac{d\tau}{d\gamma}$ includes the estimated Schmid Factor at the onset of necking. These Schmid Factors were estimated from the stereographic plots of Calnan and Clews (1951). The approximate criterion gives a good description of the condition for the onset of necking.

From the work of Price and Kelly it is not possible to determine which test pieces showed necking. It is reported that a small amount of necking was observed occasionally, particularly in the Al-Cu crystals containing GPI zones. None of those containing θ" (or GPII) precipitates

TEST	41S	41L	42L	42S	43SN2	43LN2	354	100
SHEAR STRAIN γ	.18-.20	.22-.23	.17-.18	.225	.66-.67	.46-.47	.23-.24	.25-.26
τ ksi	11.2	9.7	12.1-12.2	12.7	15.2-15.3	18.2-18.4	11.5	12.2
MPa	77.2	66.8	83.4	87.5	104.7	125.4	79.2	84.1
$\frac{d\tau}{d\gamma}$ ksi	7.5-5.5	5.2-3.5	8.0-4.5	6.0	6.8-6.5	8.2-8.0	4.7-3.5	6.0-5.0
$\frac{d\tau}{d\gamma}$ MPa	52-38	36-24	55-31	41	47-45	56-55	32-24	41-34
$\frac{1}{\tau}\frac{d\tau}{d\gamma}$	.67-.48	.54-.36	.66-.37	.47	.45-.42	.45-.43	.41-.3	.49-.41
Schmid Factor at Start	.48	.48	.50	.50	.50	.50	.41	.41
Estimated Schmid Factor at Strain γ	.46	.46	.47	.47	.47	.47	.41	.41

TABLE 6.7 COMPARISON OF SHEAR STRESS AND WORK HARDENING RATE AT MAXIMUM LOAD, TO SHOW THE CONDITIONS AT THE ONSET OF NECKING.

were said to have necked. Some of the shear stress shear strain curves have been analysed to test the quantity

$$\frac{1}{\tau}\frac{d\tau}{d\gamma}$$

as a criterion for the onset of necking. The graphs in Figure 6.9 show the comparison. The value of .45 for the average Schmid Factor is here based on the estimated values which range from .42 to .46, at large strains.

It is clear that the crystals aged to GPI condition could have necked commencing at a shear stress of approximately 14 ksi (96 MPa) which might agree with the experimental stresses. However, the crystals aged to GPII (or θ"), which were reported to have not undergone necking, are indicated to have suitable conditions for necking at stresses of approximately 17 ksi (117 MPa). It seems unlikely that the crystals aged to contain GPI and θ' would undergo necking whilst crystals containing θ" would not.

A further indication that necking might have occurred in the θ" alloys can be obtained from some of the stress levels reported by Price and Kelly for the formation of coarse shear bands. These stresses were obtained from direct measurement of the area of the test pieces, and were in excess of 15 kg/mm^2 (21 ksi, 146 MPa), whilst the highest shear stress plotted is close to 14 kg/mm^2 (20 ksi, 137 MPa). The values shown on their graphs are obtained using the

assumption of uniform strain on a single slip system. Slip on a second system to produce a neck would reduce the cross section below that obtained from a uniform strain calculation. The corresponding stress would be higher.

(ii) Formation of Shear Bands

Kelly and Nicholson (1963) discussed the conditions leading to the load drop often observed at yielding in tensile tests on single crystals. For a crystal subjected to a load P at a shear stress τ and shear strain γ, Kelly and Nicholson wrote

$$\frac{dP}{d\ell} = \frac{A_o}{\ell_o \cos \phi_o} \left[\frac{1}{\cos^2\lambda \cos \phi_o} \frac{d\tau}{d\gamma} - \frac{\tau \tan^3 \lambda}{\sin\lambda_o}\right]$$

where ℓ is the length of the test piece.

Since it has been shown experimentally (Price and Kelly, and present study) that the formation of shear bands in the Al-Cu alloys is accompanied by a load drop, the analysis of Kelly and Nicholson will be examined to determine if it can predict the conditions for the formation of the shear bands. To obtain a load drop

$$\frac{dP}{d\ell} \leq 0$$

which requires that

$$\frac{d\tau}{d\gamma} \leq \tau \frac{\tan^3\lambda}{\sin \lambda_o} \cos^2\lambda \cos \phi_o$$

This equation is not the same as that obtained by Kelly and Nicholson; their equation cannot be correct as it does not contain the shear stress τ on the right hand side. If the angles $\lambda = \lambda_0$ then the trigonometric factors are the same as those of Kelly and Nicholson.

It is clear that the possibility of a load drop depends on the two quantities $\frac{d\tau}{d\gamma}$ and τ, and the likelihood of obtaining it increases at larger strains. Under these conditions $\frac{d}{d\gamma}$ decreases whilst τ increases.

The trigonometric factor is dependent on the current angle between the slip direction and the tensile axis. The angle decreases during the deformation. Kelly and Nicholson consider the trigonometric factor to be about 0.5 for face centred cubic materials, so that the condition to obtain a load drop - and by inference, a shear band - is that

$$\frac{d\tau}{d\gamma} < .5\tau.$$

However, it has been calculated in the present study that possible values for the trigonometric factor range from 0.14 to 1.23, depending on orientation.

If the discussion of the previous section dealing with the onset of necking is considered with the above condition, it is seen that the shear bands will form before necking if the trigonometric factor is less than .45. However, if the θ" crystals of Price and Kelly are all to show shear band formation before necking, as reported

experimentally, the criterion as derived cannot be correct. The trigonometric factor is not less than [illegible] for all of the orientations tested by Price and Kelly in the [illegible] direction.

A further indication that the criterion as derived is not applicable can be obtained from a closer examination of [illegible] [illegible] [illegible] [illegible] Figure [illegible] the work hardening [illegible] at the [illegible] stresses to be very low and [illegible] to be less than 1.5 kg/mm², 2.1 ksi, 14 MPa). The low work hardening rates close to these stresses is confirmed by the shear stress shear strain curves, which are very flat. Then the quantity $\frac{1}{\tau}\frac{d\tau}{d\gamma}$ [illegible] .1 which is even smaller than the minimum value of the trigonometric factor. The condition as obtained from the equation of Kelly and Nicholson can then be excluded as a criterion for the formation of the shear bands.

Price and Kelly argued that their results showed there was a critical resolved shear stress condition for the formation of the first shear band. The meaning of such a condition is not clear since a critical stress condition implies that some event occurs at the critical stress and is directly responsible for the shear bands. In the aluminum-copper alloys, the "critical" stresses are almost independent of the type of precipitate present. It is not explained what the important event might be. A better

correlation might be obtained with the help of Figures 6.8 and 6.9.

These figures show that the work hardening rate is decreasing rapidly as the applied shear stress is increased. At stresses close to those reported as "critical", the work hardening rates are very small. Then a very large strain excursion is required in a matrix element if some inhomogeneity in the material causes a local reduction. As the stress increases the work hardening rate decreases further, demanding even larger strain excursions.

In the present study, the tests were not stopped after the formation of the shear bands to determine the current cross section. The values of the stresses at the shear band formation can be estimated as being greater than 12 ksi (83 MPa); in most cases necking commenced close to 11 ksi (76 MPa). The work hardening rates were then small.

The mechanism for the formation of the shear bands will be discussed later.

(iii) Criteria for Fracture in Single Crystals

Beevers and Honeycombe, on the basis of their experimental results, considered that fracture occurred in the single crystals of the Al-Cu alloy when the resolved shear stress reached a critical value. This value depended on the condition to which the alloy had been heat treated. Their

figures 8, 9 and 10 show the values of the tensile, shear and normal stresses at fracture for the different ageing conditions.

The constant shear stress criterion suggests there is some event which occurs at the critical stress and leads to the unstable fracture. If some such event occurred in the tensile tests conducted by Beevers and Honeycombe and by Price and Kelly, and in some of the tensile tests in the present study, to cause the unstable fracture at a critical resolved shear stress, it did not occur in all tests. The tensile tests carried out on crystals oriented at [100], deforming by multiple slip, did not show the unstable fracture. Instead they necked down to almost zero cross section. The crystals compressed by Russell and Ashby did not show any special event at high stresses. The plane strain compression tests of Hosford and Zeisloft (1972) again did not show any special event at high stresses.

The common denominator in the tests which revealed unstable fracture was that the crystals were all oriented for slip on one or two slip systems. If the top and bottom of the test piece were not constrained by the rigid grip system, there would have been a lateral displacement of the top relative to the bottom. The grip constraint must cause a bending moment on the test piece. The magnitude of this bending moment will increase as the imposed strain

increases. The bending moment will increase the normal stress on the active slip planes, and promote slip on a secondary slip system. It will also promote crack nucleation and growth. Any criterion derived to describe the onset of fracture should include the normal stress on the active slip planes. The data from Beevers and Honeycombe and from the present study will be examined to test the applicability of one of these possible criteria. The experimental evidence of crack shape, obtained from an interrupted test, indicates that the crack was oriented parallel to the active slip plane, but the displacement of the sides had a component perpendicular to the crack plane.

Priestner and Louat (1963) examined a similar problem. They were interested in the conditions to produce unstable crack growth in a material which was subjected to a shear stress τ, in addition to the stress σ_N normal to the crack (as in the usual Griffith case). They argued that the presence of both stresses contributes to the total energy available to do the work necessary for the crack propagation. By examining the total energy and establishing a critical crack length, they showed that for crack growth

$$\tau^2 + \sigma_N^2 = \text{constant} = \Sigma$$

This equation was derived for a material in which the fracture process was governed by the surface energy. The fracture

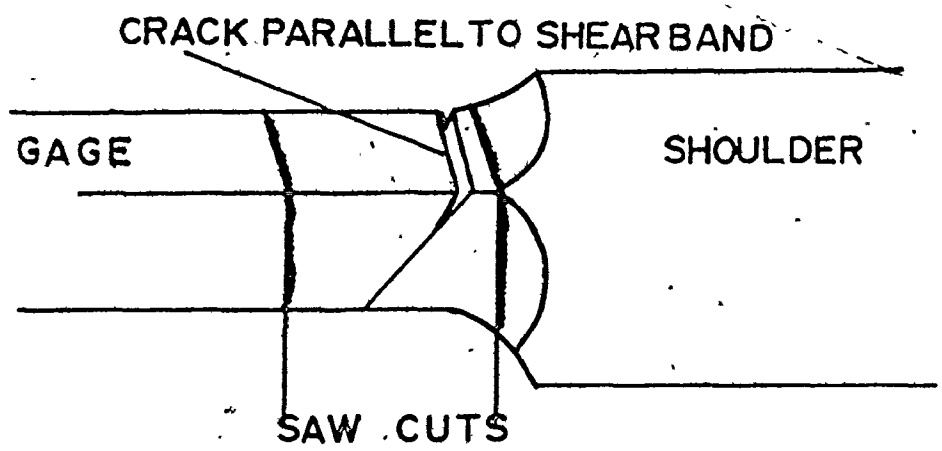

FIG. 6.10 ARRESTED FRACTURE IN SINGLE CRYSTAL

of Al-Cu alloys produces dimples, and the work necessary to form them should be included in the magnitude of the constant. However, a criterion to describe the fracture of the Al-Cu alloys based on Σ can be tested against the experimental results.

The data reported by Beevers and Honeycombe have been analysed to determine if the quantity

$$\Sigma = \tau^2 + \sigma_N^2$$

is constant at fracture. The standard error in the measurements of Σ will be compared with the standard errors in the values of τ and σ_N. The values for the age hardened alloys are:

$$\Delta\tau \leq \pm 4\%$$

$$\Delta\sigma \leq \pm 7\%$$

$$\Delta\Sigma \leq \pm 4\%$$

The larger standard error for the normal stress is thus almost double that of the other two. Then a criterion based on the quantity Σ or on the shear stress could be considered equally applicable, based on the statistics. However, the quantity Σ, which includes the effect of the normal stress, represents the physical process more closely than a criterion based only on the shear stress.

The results of the present fracture study, containing

Material	τ	σ_N	$\Sigma = \tau^2 + \sigma_N^2$
1. solution treated, single phase	ksi 18.8 ±.6 MPa 130 ±4	10.4 ±.7 72 ±5	466 ±29 ksi^2 22122 MPa^2
2. GPI alloy	ksi 23.5 ±1.0 MPa 162 ±7	12.8 ±.5 88 ±3	721 ±30 34227
3. θ" alloy	ksi 21.0 ±.4 MPa 145 ±3	12.7 ±.5 88 ± 3	608 ±21 28863

TABLE 6.8 COMPARISON OF REPORTED SHEAR STRESS, NORMAL STRESS AND THE SUM Σ FOR THE FRACTURE OF Al-Cu CRYSTALS - AFTER BEEVERS AND HONEYCOMBE.

Test Piece SX	Schmid Factor	cos φ	σ_F ksi	τ ksi	σ_N ksi	τ^2 ksi^2	σ_N^2 ksi^2	Σ ksi^2
41S	.46	.81	45.2	20.8	29.7	432	882	1315
41L			43.1	19.8	28.3	392	801	1193
42S	.47	.72	43.5	20.4	22.6	416	511	927
42L			44.1	20.7	22.9	429	524	953
43SN2	.47	.64	50.7	23.8	21.0	568	439	1007
43LN2			54.8	25.8	22.5	666	506	1172

TABLE 6.9 TENSILE, SHEAR AND NORMAL STRESSES AT FRACTURE OF SINGLE CRYSTAL TEST PIECES - PRESENT STUDY.

fewer test pieces, have the following standard errors:

$$\Delta\tau \sim \pm 2\%$$

$$\Delta\sigma_N \sim \pm 7\%$$

$$\Delta\Sigma \sim \pm 7\%$$

and as such seem to support the constancy of shear stress as a criterion. However, as indicated above, this criterion does not include the effect of the stress normal to the crack on the crack propagation.

The discussion of this section can be summarised as follows:

a) necking occurs in the single crystal tensile tests when

$$\frac{d\tau}{d\gamma} \lesssim .45\tau$$

b) the shear bands are formed when the magnitude of the work hardening rate is smaller.

c) the fracture occurs when the work hardening rate is close to zero.

The observations are correlated then with the work hardening rate rather than with the criterion proposed by Price and Kelly (and by Beevers and Honeycombe). This was a constant resolved shear stress criterion.

6.11 Mechanism Leading to Shear Fracture in Single Crystals

The results of the previous section have shown that the single crystals of Al-Cu alloys were subject to necking, shear band formation and, in most cases, unstable shear fracture. The conditions that seem to describe the first two of these are directly related to a rate of work hardening $\frac{d\tau}{d\gamma}$ which decreases as the flow stress is increased. First necking starts when the condition $\frac{d\tau}{d\gamma} \leq .45\tau$ is satisfied, and the shear bands are formed when the work hardening has been reduced further. The extrapolated work hardening rate is then close to zero. At larger strains the crystals finally break; the work hardening rate will have been reduced again.

In this section it is necessary to discuss how decreasing the work hardening rate leads to the observed events, and how the [100] crystals, although they undergo necking and shear band formation do not fail in an unstable manner.

It was discussed earlier how the θ' particles were responsible for the increasing back stress at small strains, and how at larger strains the back stress remained constant. The cause of this constant value was attributed to the cutting of the particles by the matrix dislocations. Before cutting took place each increment of strain led to an

increase in the back stress and also in the forest hardening. After cutting the strain increments produced only an increment in the forest hardening - the back stress contribution was constant at the value it had before cutting. It was not reduced to zero by the particle cutting. If particle fracture or breakdown of the particle matrix interface had occurred the back stress would have been reduced to zero.

It is possible to write down the flow stress and work hardening rates for an element of volume in the alloy

a) before cutting of the particles:

$$\sigma_f = \sigma_o + \sigma_b + \sigma_d$$

and

$$\frac{d\sigma_f}{d\varepsilon} = \text{local work hardening rate} = \frac{d\sigma_b}{d\varepsilon} + \frac{d\sigma_d}{d\varepsilon}$$

b) immediately after cutting:

$$\sigma_f = \sigma_o + \sigma_b + \sigma_d$$

$$\frac{d\sigma_f}{d\varepsilon} = \frac{d\sigma_d}{d\varepsilon} \qquad \sigma_b = \text{constant}$$

c) immediately after particle fracture or breakdown of interface:

$$\sigma_b = 0$$

$$\sigma_f = \sigma_o + \sigma_d$$

$$\frac{d\sigma_f}{d\varepsilon} = \frac{d\sigma_d}{d\varepsilon} - \frac{\sigma_b}{d\varepsilon}$$

where $d\varepsilon$ is the strain increment over which the event took place.

When some particles were cut the local work hardening rate was reduced, and to restore the load carrying ability of the material the volume element had to undergo an additional strain. This strain caused additional work hardening of the matrix and an increased back stress in the elements not subject to cutting. In turn then there was an increased stress on the neighbouring particles and they were closer to undergoing plastic deformation. The most likely place for the next particles to be cut was on the same slip plane, (or closely parallel to it) as that on which the previous particles were cut.

The process of particle cutting continued on a local scale until many particles on a given slip plane had been cut and the neighbouring particles and matrix subjected to the additional strain necessary for the extra work hardening. As the imposed strain increased, the work hardening rate decreased. The magnitudes of the additional local strains then increased rapidly. Eventually the situation was reached such that a further strain increment led to the cutting of the particles on a large scale on a given slip plane. Then the band of material which had undergone a large strain extended across the test piece. The band was subjected to a large strain and increased the load carrying

ability of all the elements in it.

Further strain increments tended to concentrate in this element because its work hardening rate was lower than that of the rest of the test piece. However the flow stress everywhere was increasing slowly, so that the possibility of a second or third shear band forming existed. Each succeeding shear band was strained just sufficient to raise its flow stress to that of the surrounding elements. But the work hardening rate at successive shear bands was reducing so that the strain increments had to be greater.

When the work hardening rate was very close to zero, the very large strain increment raised the possibility of void nucleation close to some of the particles in the active shear band. When this voiding occurred the back stress contribution from the affected particles was reduced to zero and there was an immediate reduction in the work hardening rate by the amount $\sigma_b/\Delta\varepsilon$ where $\Delta\varepsilon$ is the strain increment over which the voiding occurred. This reduction of the work hardening rate had the effect of greatly localising the plastic deformation in the active shear band. It may even have reduced the work hardening rate to a negative quantity. Rapid additional void growth could occur and accelerated failure then resulted. Since the volume undergoing the large deformation in the shear band was small the dimples produced from the fracture process were shallow.

The evidence from some interrupted tests indicated that there was a stress component perpendicular to the final crack, and it caused the crack to open up as a wedge. The stress normal to the active slip plane promoted fracture, and prevented the possibility of the specimen failure occurring by shear all across the slip plane. It also influenced the shape of the dimples produced on the fracture surface.

The [100] crystal deformation must be examined. These crystals deformed by slip on at least 4 active slip systems. The back stress increased and led to particle cutting. However the intersecting slip systems then dominated the work hardening process; the matrix work hardening rate was higher at this orientation than at the single slip orientations. The result of the higher work hardening rate was that a small strain was sufficient to raise the local flow stress after particle cutting. However, eventually, all the particles on a given slip plane were cut and the shear band formed. Since the work hardening rate was high the strain in the shear band was small, and further bands were formed.

An important consideration in the deformation of the [100] crystals is that the symmetric slip caused no change in the angles between the tensile axis and the many slip directions. There was no lateral displacement of the top and bottom of the crystal and the bending moment present

in the other single crystal tests was absent. The deformation of the crystal then continued, with the many slip systems leading to extensive necking. Eventually the test piece failed after the nucleation and growth of voids in the neck. Measurements have shown that the true strain at fracture in the [100] crystals was an order of magnitude larger than that in the other crystals.

The observed asterism in the [100] crystals was consistent with this model. The Laue photograph taken about 1" from the fracture surface did not show extensive asterism even though the deformation was about 0.1 tensile strain. As indicated earlier the multiple slip led to the production of many prismatic loops and a reduction of the lattice bending close to the particles. In the neck, the extensive slip on intersecting slip systems following particle cutting caused the material to deform almost as a single phase alloy. It is well established that such crystals show extensive asterism at large strains. A good example is shown by Russell and Ashby (1970) in which Laue photographs were obtained from their single crystal single phase control samples.

This section has discussed the processes leading to shear band formation and fracture of the single crystals. The emphasis has been placed on the work hardening rates when the observations occurred. In this the approach has been different from that followed by Price and Kelly who

considered that there was a critical shear stress criterion. Such a criterion suggests that an event occurs at the given stress causing the shear bands to form or leading to fracture. Price and Kelly were not able to establish the nature of the event. In the present study it has been shown that the work hardening rate decreases as the flow stress increases, and the shear band formation and fracture were explained in terms of the low work hardening rates.

CHAPTER VII

APPENDIX

A Review of "The Bauschinger Effect in Precipitation Strengthened Aluminum Alloys" R.E. Stoltz and R.M. Pelloux (1976).

Since the content of the work reported by Stoltz and Pelloux (1974, 1976) was very close to that of the present study, and because there were considerable differences in the approach taken to analyse the cyclic stress strain curves and in the numerical results obtained from them, it was decided to review their work separately.

Stoltz and Pelloux studied the Bauschinger Effect in several polycrystalline aluminum precipitation strengthened alloys. Some were aged to contain precipitates which were cut by the matrix dislocations from the start of plastic deformation. Others contained precipitates which were considered not to be cut by the matrix dislocations. The cyclic stress strain curves obtained from the alloys containing cutable precipitates were similar to those reported earlier for single phase alloys, and were considered to confirm that the alloys with cutable precipitates do not build up large long range back stresses during plastic deformation. The curves obtained for the alloys with hard

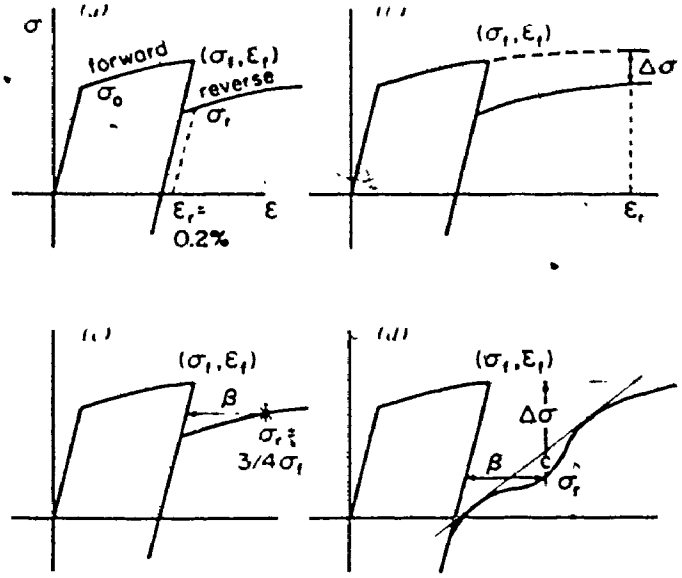

Fig. 1—Graphical constructions for measuring the Bauschinger effect

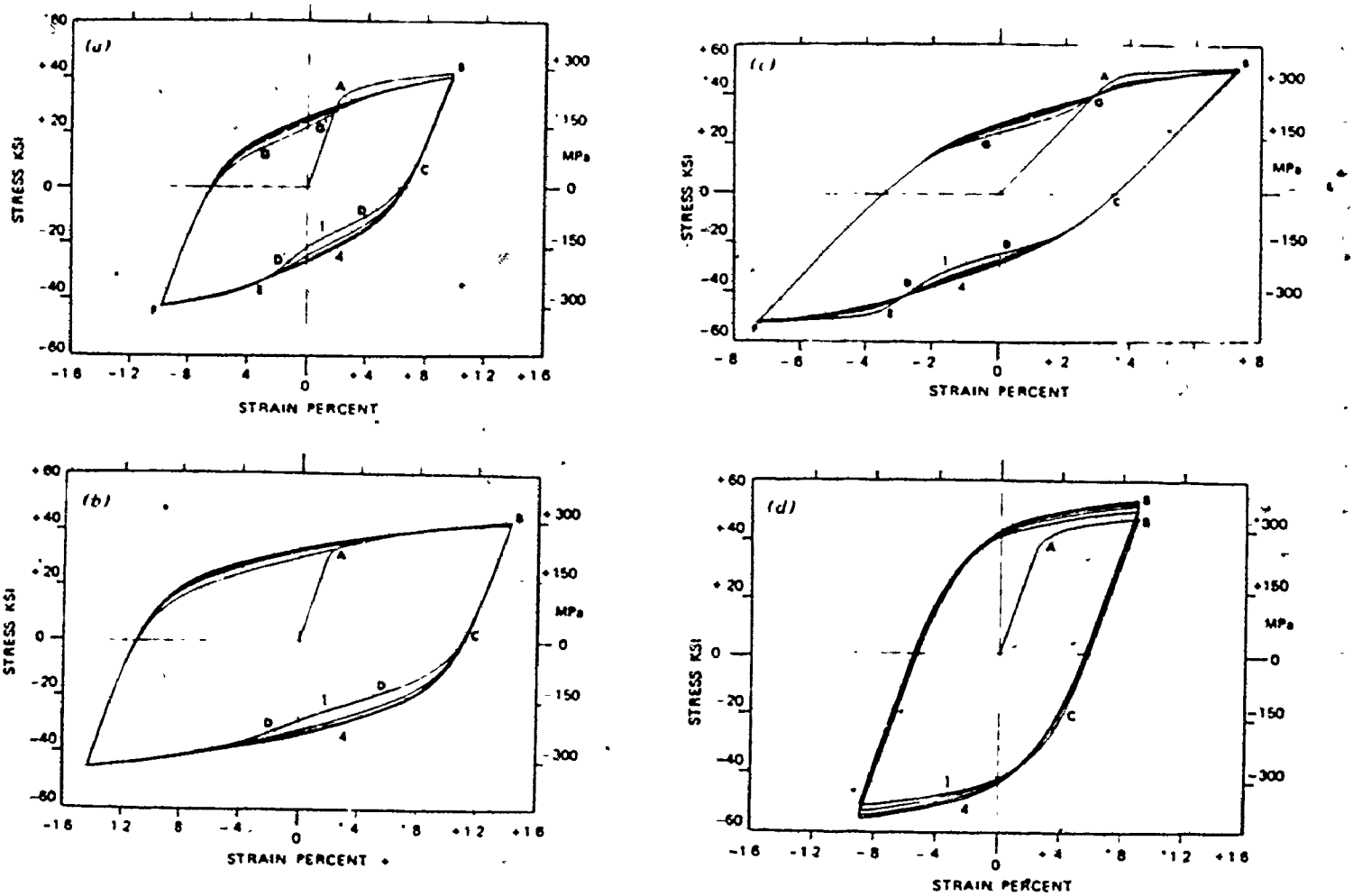

Fig. 3—Initial stress-strain hysteresis loops: (*a*) Al-Cu-Mg-T6 (nonshearable), ϵ_p = 0.72 pct, (*b*) Al-Cu-Mg-T6 (nonshearable), ϵ_p = 1.16 pct, (*c*) 7075-T73 (nonshearable), ϵ_p = 0.34 pct, (*d*) 2024-T4 (shearable), ϵ_p = 0.60 pct.

Fig. 7.1. Figures taken from Stoltz and Pelloux (1976)

particles demonstrated a unique effect, shown in their Figure 3. However, it is felt that the description of the effect as convex is erroneous. The curves for the alloys with cutable precipitates when compared with an optical lens are convex; the curves from the hard precipitates are concave.

Because a new shape was obtained for the cyclic stress strain curve, a different method was devised to measure the long range back stress in the alloys. The analysis used is identical to that used by Moan et al. (1973) and discussed in Chapter IV of the present study. Where the two methods differ is shown in their Figure 1; a tangent was drawn to the two parts of the reverse curve and the point of maximum deviation from the tangent was taken as their reverse yield stress. The Bauschinger Strain was measured to this same point. The precise meaning of this point will have to be discussed later.

One of the alloys used in the study was Al-Cu, (4.5% Cu) aged to θ' and tested in tension-compression to small prestrains ($\leq$.68%). The θ' particles were 0.7μ diameter and .46μ apart, and their estimated volume fraction was 7%. A comparison with the work of Russell and Ashby indicates that the Orowan stress for such an alloy is

$$\sigma_{OR} \approx \frac{\mu b}{2L} \approx 3.5 \cdot 10^3 \text{ ksi} \quad (24 \text{ MPa})$$

which is nearly half of the initial yield stress.

Two areas of importance which must be discussed are

a) the interpretation of the new stress strain curve

b) its applicability to the Al-Cu-θ' alloy.

The interpretation of the new stress strain curve can be carried out most easily with the help of a simplified model. It is assumed initially that the forest hardening and source shortening terms do not exist at small strains in the age hardened alloys, that the deformation is unrelaxed, and that the only contribution to the work hardening comes from the back stress which has been shown to increase almost linearly at small strains. The model is shown in Figure 7.2.

At yielding the flow stress is the sum of two terms: σ_L the lattice friction and σ_{OR} the Orowan stress. As the plastic strain is increased from zero, the back stress σ_{bl} increases and then

$$\sigma_f = \sigma_L + \sigma_{OR} + \sigma_{bl}$$

During unloading, the back stress will aid the reverse deformation, and the lattice friction will oppose all dislocation motion. The Orowan stress must be examined carefully.

If slip is exactly reversible, the dislocations moving in reverse will not see the array of obstacles. In fact, the interaction with the Orowan loops on the particles

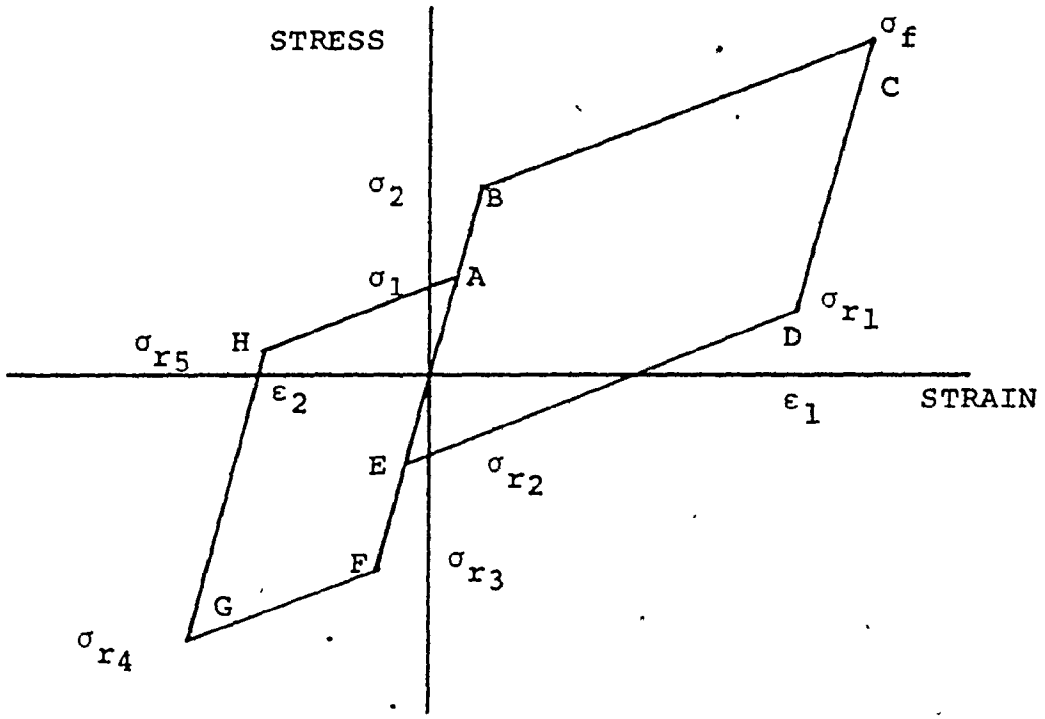

σ_L = Lattice friction

σ_{OR} = Orowan Stress

σ_b = Long range back stress

$$\sigma_1 = \sigma_L$$

$$\sigma_2 = \sigma_L + \sigma_{OR}$$

$$\sigma_f = \sigma_L + \sigma_{OR} + \sigma_{b_1}$$

$$\sigma_{r_1} = -\sigma_L + \sigma_b$$

$$\sigma_{r_2} = -\sigma_L$$

$$\sigma_{r_3} = -\sigma_L - \sigma_{OR}$$

$$\sigma_{r_4} = -\sigma_L - \sigma_{OR} - \sigma_{b_2}$$

$$\sigma_{r_5} = \sigma_L - \sigma_{b_2}$$

Fig. 7.2 Schematic diagram of cyclic stress strain curve for model material, deformed ε_1 in tension and ε_2 in compression

will result in the 'reverse' dislocations being aided as they move past the particles. The line tension will straighten out the dislocations after the interaction with the Orowan loops. Then the Orowan stress cannot enter the equation for the reverse yield stress. Reverse yielding occurs at σ_{r1}.

$$|\sigma_{r1}| = \sigma_L - \sigma_{b1}$$

As the reverse strain is increased from zero, the magnitude of the current back stress must decrease as the number of Orowan loops is decreased and the elastic strain on the particles is reduced. The magnitude of the applied stress needed to continue reverse deformation is

$$\sigma_r(\varepsilon) = \sigma_L - \sigma_{b1}(\varepsilon)$$

At zero net strain, the magnitude of σ_{b1} will be zero; all the forward Orowan loops will have been removed, and

$$|\sigma_{r2}| = \sigma_L$$

The next increment of plastic deformation can occur if the reverse dislocations are able to bow between the obstacles. A stress increment in reverse equal to the Orowan stress is required. The reverse flow stress is then

$$|\sigma_{r3}| = \sigma_L + \sigma_{OR}$$

Continued plastic deformation in reverse leads to the build up of a new back stress σ_{b2} (whose sense is opposite to that built up during the forward strain). Then

$$|\sigma_{r4}| = \sigma_L + \sigma_{OR} + \sigma_{b2}$$

The magnitude of σ_{b2} will depend on the magnitude of the reverse strain.

Unloading from reverse stress σ_{r4} will lead to forward plastic flow when the applied flow stress is σ_{r5},

$$\sigma_{r5} = \sigma_L - \sigma_{b2}$$

and as the strain decreases towards zero the magnitude of σ_{b2} is reduced and the flow stress increases. At zero net strain the flow stress is again

$$\sigma_1 = \sigma_L$$

At this strain all the reverse Orowan loops will have been removed from the particles and continued forward deformation requires a stress increment equal to the Orowan stress so that

$$\sigma_2 = \sigma_L + \sigma_{OR} \quad \text{as before.}$$

This model is very simplified, but it is necessary to demonstrate that if slip is exactly reversible a new type of stress strain is obtained for cyclic deformation. Some modifications must be made to the model if it is to be

compared with real materials:

1. slip is not exactly reversible so that some fraction of the Orowan stress will have to be included in the terms for σ_{r1} and σ_{r2}. The line DE will move closer to the line FG, and HA will move closer to BC.

2. the deformation might not be unrelaxed. In that case, the magnitude of the back stress will not increase linearly with strain, and dislocation debris will lead to a forest hardening contribution.

3. forest hardening will play a role and increase the stress necessary for plastic deformation. Then DE will move closer to FG, and HA even closer to BC.

4. dislocation sources do not all require the same applied stress for activation. There is a distribution of strengths, and the corners at D, E, F, H and A will become rounded.

Including these modifications into the model leads to a cyclic stress strain curve similar to those shown by Stoltz and Pelloux for the alloys with hard particles. As the magnitude of the forest hardening increases with repeated cycling, the steps at EF and AB disappear.

There are two important differences in the interpretation of the curves presented here from that proposed by Stoltz and Pelloux:

1. they do not include the effect of the Orowan stress on the shape of the cyclic stress strain curve.

2. they obtain the magnitude of the back stress by considering the difference between the flow stress σ_f and the stress σ_r at the point C in their Figure 1. This difference is equated to $2\sigma_b$. Examination of the experimental curves shows that the point C is closer to zero strain than it is to the forward prestrain. Then the magnitude of the difference is not equal to $2\sigma_b$, but is closer to σ_b. All the results for σ_b in their Table V should be considerably larger; also, σ_d will be correspondingly smaller.

The shape of the cyclic stress strain curve for Al-Cu-θ' must be considered. Stoltz (1974a) attempted to analyse the curves and considered them to be shallow double inflected curves at strains less than 0.2%, with a straight line reverse loading path present up to strains of 1%. A careful examination of the literature (1974a, 1974b, 1976) failed to uncover curves for the Al-Cu-θ' alloy, so that the precise meaning of this description is not clear. Figure 4.1 in the present study shows cyclic curves obtained at small strains after the initial report by Stoltz (1974b) of the new curve shapes. The reverse curve is rounded, and shows no sign of the "new" shape. It seems that Stoltz has made the Al-Cu-θ' alloy fit the same method of analysis used for the other alloys, even though the curves do not show the

new shape. A problem then arises as to which tangent was drawn on the reverse curve. The evidence suggests that Stoltz has underestimated the back stress in the Al-Cu-θ' alloy by at least a factor of 2.

The back stress reported by Stoltz and Pelloux represents some 30% or less of the work hardening in the Al-Cu-θ' alloy at small strains (up to 0.68%). This obviously conflicts with the results reported in Chapter IV in the present study, where at small strains in the polycrystalline alloy the quantity

$$\sigma_b/\text{wk hdg} \sim 80\%,$$

and then decreases at large strains to 60%. Stoltz' result at a prestrain of 0.68% shows that

$$\sigma_b/\text{wk hdg} \sim 20\%$$

The difference between these results arises from the different methods used to determine the back stress.

There is independent evidence that the magnitude of the back stress in the Al-Cu-θ' alloy must be greater than that reported by Stoltz. Wilson in his X-ray study on Duralumin and his τ_{SN} study on Al-Cu-θ' show that σ_b/wk hdg for these alloys was 80% and 60% respectively, at 9% torsion prestrain (~5% tensile). As indicated in Chapter IV these are close to the values obtained in the present study and indicate that the results of Stoltz and Pelloux should be

increased by at least a factor of 2.

The reason why the Al-Cu-θ' alloy does not show the new curve shape for cyclic deformation can be found in the difference between the precipitates found in the alloys. The Al-Cu-θ' has only one type of precipitate, θ', which is not cut by the matrix dislocations at small strains. The other alloys have two sets of precipitates, eg. S' and GPB in 2024-T6 and Al-Cu-Mg-T6. The S' are not sheared during the plastic deformation, but the GPB zones are sheared from the onset of yielding. Under these circumstances, the slip pattern in the 2024 and Al-Cu-Mg will be more planar than in the Al-Cu-θ'. Planar slip is more exactly reversible. It has already been indicated that local cross slip near θ' particles will cause the dislocation array to form cusps and jogs which will reduce the exact reversibility of slip.

The dislocation arrangements reported by Stoltz and Pelloux are more complex than those given in the present study. The structures in the present study were obtained for single crystals, deforming by single slip. Stoltz' study was made on polycrystalline materials which deformed by multiple slip, and with more complex dislocation interactions.

CHAPTER VIII

CONCLUSIONS

The principal conclusions arising from the present study are:

1. In the Al-Cu alloy aged to contain θ' particles, the long range back stress increases with the imposed strain, reaching a saturation after 5% strain. In the single phase alloy, and in pure aluminum, the back stress is very small.
2. The back stress accounts for the major portion of the work hardening at small strains.
3. There is an orientation dependence of the back stress σ_b, and also of σ_b/wk hdg.
4. Ashby's model for the work hardening of two phase alloys attempts to calculate the work hardening in terms of the dislocation density. It excludes the long range back stress as a contribution. A good agreement was reported between the model and the results of compression tests carried out by Russell and Ashby. Such good agreement conflicts with the large long range back stress observed in the present study. It has been necessary to re-examine the data of Russell and Ashby and to show that the agreement is not as good as that

reported. The data was further analysed and shown to agree with the model proposed by Brown and Clarke.

5. At tensile strains of 1%, the magnitude of the back stress obtained in the present study has been shown to be in agreement with the model of Brown and Clarke; the agreement includes
   a) orientation dependence
   b) temperature dependence
6. At small strains, little plastic relaxation occurs even at 100°C.
7. At large strains, the major plastic relaxation process was the cutting of the particles by matrix dislocations. The saturation value of the back stress agrees reasonably with the yield stress of the θ' particles estimated from $\mu/30$.
8. The asterism obtained during prestraining in tension was found to decrease during compressive straining to zero net strain, and to increase during further compressive straining.
9. The Al-Cu-θ' alloy did not show the concave stress strain curve of the type obtained by Stoltz for other alloys. Evidence is presented to show that the method used by Stoltz to determine the long range back stress leads to results which are too small by at least a factor of 2.

10. A dislocation model has been used to account for the shape of the concave cyclic stress strain curves reported by Stoltz.

11. The maximum on the load elongation curve occurred close to the condition

$$\frac{d\tau}{d\gamma} = \tau \text{ . (Schmid Factor)}$$

Using this criterion, the crystals aged to θ" used by Price and Kelly should have shown some necking.

12. The formation of coarse slip bands in the aged alloys was shown to commence when the work hardening rate was low.

13. An orientation dependence of the fracture behaviour was found. Crystals oriented for single slip failed in an unstable manner; those oriented for multiple slip at [100] necked down to zero cross section.

PROPOSALS FOR FURTHER WORK

1. A Burgers vector analysis of the dislocations present as a function of forward and reverse strain in the single crystals oriented for single, double and multiple slip.
2. A study of the dimensional stability of the deformation of single and polycrystal test pieces.
3. A study of the microstrain effects observed after unloading to zero load from a prestrain in tension or compression.
4. A determination of the strain at which the θ' particles are cut by the matrix dislocations.
5. Further study of the work hardening rate at large strains through the use of tests carried out in tension and in compression on crystals with the same orientation. The work hardening rate at the formation of the shear bands could then be determined.

REFERENCES

Abel, A., 1965, M.Sc. Thesis, McMaster University.

Abel, A. and Ham, R.K., 1966, Acta Met., 14, 1489.

Abel, A. and Muir, H., 1972, Metals Australia, 267; 1973, Phil. Mag., 25, 489.

Asaro, R.J., 1975, Acta Met., 23, 1255.

Ashby, M.F., 1966a, Oxide Dispersion Strengthening; Bolton Landing Conference, Gordon and Breach, N.Y.; 1966b, Phil. Mag., 14, 1157; 1969, Physics of Strength and Plasticity; Ed. A. Argon, MIT Press, Cambridge; 1970, Phil. Mag., 21, 399; 1971, Strengthening Methods in Crystals, Ed. A. Kelly and R.B. Nicholson, Wiley, N.Y.

Atkinson, J.D., Brown, L.M., and Stobbs, W.M., 1973, Proceedings 3rd Int. Conference on The Strength of Metals and Alloys, Cambridge; 1974, Phil. Mag., 26, 1274.

Bauschinger, J., 1881, Civiling. N.F., 27, 289; 1886, Min. Proc. Inst. Civ. Eng., London, 87, 463.

Beton, R.H. and Rollason, E.C., 1957, J. Inst. Met., 86, 77.

Borelius, G., Andersson, J., and Gullberg, K., 1943, Ing. Vetenskaps Akad., 169.

Boyd, J.D., 1966, Ph.D. Thesis, University of Cambridge.

Brown, L.M., 1973, Acta Met., 21, 879.

Brown, L.M. and Clarke, D.R., 1975, Acta Met., 23, 821.

Brown, L.M. and Ham, R.K., 1971, Strengthening Methods in Crystals, Ed. A. Kelly and R.B. Nicholson, Wiley, N.Y.

Brown, L.M. and Stobbs, W.M., 1971, Phil. Mag., 23, 1185 and 1201; 1977, Phil. Mag., to be published.

Buckley, S.N. and Entwistle, R.N., 1956, Acta Met., 4, 352.

Byrne, J.G., Fine, M.E., Kelly, A., 1961, Phil. Mag., 6, 1119.

Calabrese, C., and Laird, C., 1970, Mat. Sci. and Eng., 13, 159.

Calnan, E.A. and Clews, C.J.B., 1951, Phil. Mag., 42, 616.

Clarke, D.R. and Lilholt, H., 1975, Scripta Met., 9, 93.

Dew-Hughes, D. and Robertson, W.D., 1960, Acta Met., 8, 147 and 156.

Elam, C.F., 1925, Proc. Roy. Soc., A 109, 143; 1927, Proc. Roy. Soc., A 115, 133.

Eshelby, J.D., 1957, Proc. Roy. Soc., A 241, 376; 1959, Proc. Roy. Soc., A 252, 561; 1961, Prog. Solid Mech., 2, 89.

Fisher, J.C., Hart, E.W. and Pry, R.H., 1953, Acta Met., 1, 336.

Fleischer, R.L. and Chalmers, B., 1958, J. Mech. Phys. Solid, 6, 307.

Frank, F.C., 1949, Physica, 15, 131.

Gould, D., Hirsch, P.B., Humphreys, F.J., 1973, Proceedings 3rd Int. Conference on the Strength of Metals and Alloys, Cambridge; 1974, Phil. Mag., 26, 1353.

Gupta, S.P., and Kodali, S.P., 1976, Scripta Met., 10, 111.

Hart, E.W., 1972, Acta Met., 20, 275.

Hauser, J.J., and Jackson, K.A., 1961, Acta Met., 9, 1.

Hazzledine, P.M. and Hirsch, P.B., 1974, Phil. Mag., 30, 1331.

Hertzberg, R.W., Lemky, F.D. and Ford, J.A., 1965, Tr. AIME, 233, 342.

Hirsch, P.B., 1957, J. Inst. Met., 86, 7; 1962, Phil. Mag., 7, 67.

Hirsch, P.B., Howie, A., Nicholson, R.B., Pashley, D.W., Whelan, M.J., 1965, Transmission Electron Microscopy of Crystals, Butterworths, London.

Hirsch, P.B., and Humphreys, F.J., 1969, Physics of Strength and Plasticity, Ed. A. Argon, MIT Press, Cambridge; 1970, Proc. Roy. Soc., A 318, 45.

Hosford, W.F., and Zeisloft, R.H., 1972, Met. Trans., 3, 113.

Humphreys, F.J., and Hirsch, P.B., 1970, Proc. Roy. Soc., A 318, 73.

Ibrahim, N., 1974, Ph.D. Thesis, McMaster University.

Ibrahim, N., and Embury, J.D., 1975, Mat. Sci. Eng., 19, 147.

Karnop, R. and Sachs, G., 1928, Z. Phys., 49, 480.

Kaye, G.W.C., and Laby, T.H., 1962, Tables of Physical and Chemical Constants, Longmans, London.

Kelly, A. and Nicholson, R.B., 1963, Prog. Mat. Sci., 10, 151.

Kishi, T. and Tanabe, T.T., 1973, J. Mech. Phys. Solids, 21, 303.

Kroupa, F., 1962, Phil. Mag., 7, 783.

Lasalmonie, A. and Martin, J.W., 1974, Scripta Met., 8, 377; 1975, Scripta Met., 9, 99.

Lin, S.C., Mura, T., Shibata, M., Mori, T., 1973, Acta Met., 21, 505.

Lomer, W.M., 1951, Phil. Mag., 42, 1327.

Lui, S.I., and Sachs, G., 1949, AIME, 180, 193.

Mader, S., 1963, Electron Microscopy and the Strength of Crystals, Ed. G. Thomas and J. Washburn, Interscience.

Masing, G., 1927, Wiss. Veroff. Siemens-Konzern, III Band.

Moan, G.D., Sargent, C.M., and Embury, J.D., 1973, Proceedings 3rd International Conference on the Strength of Metals and Alloys, Cambridge.

Mori, T. and Narita, K., 1975, Acta Met., 23, 85.

Mori, T. and Tanaka, K., 1970, Acta Met., 18, 931; 1973, Acta Met., 21, 571.

Morrison, J., 1975, Ph.D. Thesis, McMaster University.

Nabarro, F.R.N., Holt, D.B., Basinski, Z.S., 1964, Adv. Phys., 13, 193.

Orowan, E., 1947, Symposium on Internal Stresses, Inst. of Metals, London; 1959, Internal Stresses and Fatigue in Metals; Ed. G.M. Rassweiler and W.L. Grube, Elsevier, N.Y.

Priestner, K. and Louat, N., 1963, Acta Met., 11, 195.

Palmer, I.G. and Smith, G.C., 1968, 2nd Bolton Conference on Oxide Dispersion Strengthening, Gordon and Breach.

Park, B.K., Greenhut, V., Lutjering, G., Weissman, S., 1970, Tech. Report, AFML-TR-70-195.

Price, R.J. and Kelly, A., 1962, Acta Met., 10, 980; 1963, Acta Met., 11, 915; 1964, Acta Met., 12, 979.

Rogers, H.C., 1960, Tr. AIME, 218, 498.

Russell, K.C. and Ashby, M.F., 1970, Acta Met., 18, 891.

Stoltz, R.E., 1974, Ph.D. Thesis, M.I.T.

Stoltz, R.E. and Pelloux, R.M., 1974, Scripta Met., 8, 269; 1976, Met. Trans., 7A, 1295.

Tanaka, K., 1974, Scripta Met., 8, 101.

Tanaka, K., and Mori, T., 1970, Acta Met., 18, 931.

Tanaka, K., Mori, T., Nakamura, T., 1970, Phil. Mag., 21, 267.

Watt, D.F., 1967, Ph.D. Thesis, McMaster University.

Weatherly, G.C., 1970, Acta Met., 18, 15.

Weatherly, G.C. and Sargent, C.M., 1970, Phil. Mag., 22, 1049.

Wilson, D.V., 1965, Acta Met., 13, 807.

Wilson, D.V. and Konnen, Y.A., 1964, Acta Met., 12, 617.

Woolley, R.L., 1953, Phil. Mag., 44, 597.